Classical and quantum integrability out of equilibrium

Miao, Y.

Publication date
2021
Document Version
Final published version

Classical and Quantum Integrability out of equilibrium

Yuan Miao

Classical and Quantum Integrability out of Equilibrium

Yuan Miao

Cover design by Yuan Miao
Printed by Gildeprint

ISBN: 978-94-6419-276-6

The research presented in this thesis was carried out at the Institute for Theoretical Physics, University of Amsterdam. The research of this doctoral thesis received financial support from the European Research Council (ERC) under the ERC Advanced grant 743032 DYNAMINT.

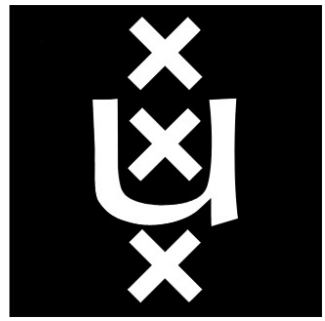

Classical and Quantum Integrability out of Equilibrium

ACADEMISCH PROEFSCHRIFT

ter verkrijging van de graad van doctor
aan de Universiteit van Amsterdam
op gezag van de Rector Magnificus
prof. dr. ir. K.I.J. Maex
ten overstaan van een door het College voor Promoties ingestelde commissie,
in het openbaar te verdedigen in de Aula der Universiteit
op woensdag 15 september 2021, te 11.00 uur

door Yuan Miao
geboren te Shandong

Promotiecommissie

Promotor:	prof. dr. J.S. Caux	Universiteit van Amsterdam
Copromotor:	prof. dr. C.J.M. Schoutens	Universiteit van Amsterdam
Overige leden:	prof. dr. J. de Boer	Universiteit van Amsterdam
	prof. dr. J.V. Stokman	Universiteit van Amsterdam
	dr. V. Gritsev	Universiteit van Amsterdam
	dr. P.R. Corboz	Universiteit van Amsterdam
	prof. dr. P. Fendley	University of Oxford
	prof. dr. B. Doyon	King's College London
	dr. E. Ilievski	University of Ljubljana

Faculteit der Natuurwetenschappen, Wiskunde en Informatica

List of Publications

This thesis is based on the following publications:

[1] O. Gamayun, Y. Miao and E. Ilievski, *Domain-wall dynamics in the Landau-Lifshitz magnet and the classical-quantum correspondence for spin transport*, Phys. Rev. B **99**, 140301 (2019).

[2] Y. Miao, E. Ilievski and O. Gamayun, *Semi-classical quantisation of magnetic solitons in the anisotropic Heisenberg quantum chain*, SciPost Phys. **10**, 86 (2021).

[3] Y. Miao, *An exact solution to asymptotic Bethe equation*, J. Phys. A **54**(19), 194001 (2020).

[4] Y. Miao, J. Lamers and V. Pasquier, *On the Q operator and the spectrum of the XXZ model at root of unity*, arXiv:2012.10224 (2020).

[5] Y. Miao, *Conjectures on Hidden Onsager Algebra Symmetries in Interacting Quantum Lattice Models*, arXiv:2103.14569 (2020).

Other publications by the author of this thesis:

[6] Y. Miao, E. Ilievski and O. Gamayun, *Interplay of solitons and radiation in one-dimensional Bose gases*, Phys. Rev. A **99**, 023605 (2019).

Contributions:

[1] I contributed to the consideration of the concept of the domain-wall quench and the analytical and numerical calculations. Specifically, I studied the hydrodynamic description of the ballistic transport in the easy-plane regime, numerical simulations in the isotropic regime and the analytic solutions to the soliton solutions in the easy-plane regime. I also participated in the writing process and the creation of all the figures.

[2] I contributed to the initial concepts of the semi-classical quantisation and the analytical and numerical calculations. Specifically, I contributed to the construction of the finite-gap solutions and the semi-classical quantisation of them. I performed the numerical solutions to the Bethe ansatz equations. I participated in the writing process and all the creation of the figures.

[3] I performed this work by myself, including all the analytic and numerical calculations, the writing of the article and the creation of the figures.

[4] I initiated the research project. I contributed to the analytic construction of the transfer matrices with highest-weight and semi-cyclic representations. I constructed the proof of the "RTT relation" for the semi-cyclic transfer matrices. I performed the numerical calculations that lead to the various examples in the article. I participated in the writing process and the creation of some figures.

[5] I performed this work by myself, including all the analytic and numerical calculations, the writing of the article and the creation of the figures.

to my grandparents

Contents

Chapter 1

Introduction

> L'homme est né libre, et
> partout il est dans les fers.
>
> Jean-Jacques Rousseau

Quantum many-body systems have been at the core of many studies in condensed matter physics, through combining the principles of quantum mechanics and of statistical mechanics. Large-scale behaviours of quantum many-body systems are particularly rich and intricate, and at the core of theoretical physics. Even though people have studied the quantum many-body systems in equilibrium thoroughly, especially on the classification of phases of matters and their phase transitions, there are many aspects of quantum many-body systems in the non-equilibrium regime that are still under scrutiny. The reasons are twofold: first, the enormous amount of particles involved makes it difficult to study the problem both analytically and numerically; second, the interactions between particles have to be treated non-perturbatively, especially in the low-dimensional regime. However, out-of-equilibrium phenomena are ubiquitous, and it is of vital importance to understand the physical properties of various quantum many-body systems.

In this thesis, we aim to present analytical and numerical results on a specific type of many-body systems, integrable models, out of equilibrium. We study the one-dimensional systems with strong interaction. By virtue of the exact solvability of the integrable models, we obtained exact

solutions in the non-perturbative regime. In this chapter, we will present several examples of the physical systems that we are interested in, and they will serve as a gentle introduction and motivation to the results in the rest of the thesis.

1.1 Integrable models

Looking for the exact mathematical language to describe the physical world has always been the pursuit of theoretical physicists. Integrability allows us to solve strongly interacting systems non-perturbatively in a mathematically accurate manner.

We start with classical integrable models. Even though our goal in this thesis is to elucidate the non-equilibrium properties of quantum many-body systems, classical integrable models are still crucial, because many quantum many-body phenomena remain the same in the semi-classical limit which enables their study using classical integrability. Some of the most notable examples are the classical-quantum correspondence in spin transport [2] and hydrodynamics [7, 8]. Therefore, it is useful to study the classical integrable models which reveal similar features as in their quantum counterpart. Classical integrability used in this thesis focuses on the theory of exactly solvable partial differential equations [9, 10, 11]. It has played an instrumental role in a broad range of physics applications, ranging from experimentally relevant setups with ultracold atoms, Josephson junctions and nonlinear optics, and many theoretical concepts including the AdS/CFT correspondence [12, 13], Gromov-Witten theory [14], Painlevé transcendents [15, 16] and random matrix theory [17]. The techniques developed for the classical integrable models will be used extensively in Chapters 4 and 5.

Not all quantum many-body systems are semi-classical, where a fully quantum approach is needed. In that case, we make use of the theory of quantum integrability. The quantum integrable models under our consideration are solved by Bethe ansatz, an ingenious construction of solutions to one-dimensional Heisenberg model that was proposed by Hans Bethe in 1931 [18]. The anisotropic version of the one-dimensional Heisenberg model, the spin-1/2 XXZ model, plays a central role in this thesis. Moreover, those quantum integrable models satisfy the Yang-Baxter re-

lation [19, 20]. The Yang-Baxter relations are obtained with the observation that the one-dimensional quantum integrable lattice models can be mapped into two-dimensional classical statistical mechanical models, usually vertex models. For instance, the quantum XXZ model is mapped into the 6-vertex model [21, 22, 19]. The transfer matrix formalism of the latter allows us to obtain exact results using Yang-Baxter relations. This approach is used extensively in Chapters 6 and 7.

Both classical and quantum integrable models give us the opportunity to exploit the exact solvability. Most importantly, integrable models are not merely a theoretical mirage, but are in fact captured in many recent experiments with ultracold atoms [23].

For example, the bright soliton solution in non-linear Schrödinger equation [9], a classical integrable field theory, has been observed in ultracold atom experiment [24]. In addition, one of the most celebrated experiments, which eventually led to a full development of the modern ideas on thermalisation in quantum many-body systems, is that of the motion of one-dimensional Bose gases in a confining potential [25]. The absence of thermalisation in the one-dimensional Bose gases, well approximated by quantum integrable model called Lieb-Liniger model [26], motivated the study of quantum quench 1.2. The advances in experimental ultracold atom physics, which turn the theoretical models into tunable experimental set-ups with often unexpected discoveries of new physical phenomena, have provided an enormous boost to the applications of integrability to describe quantum many-body systems far from equilibrium, which is our aim.

1.2 Quantum quench

We are particularly interested in the out-of-equilibrium properties of quantum many-body systems. One of the simplest yet most influential approaches is the *quantum quench* [27, 28]. Quantum quench studies the scenario when an initial state $|\psi\rangle$, which is not an eigenstate of the Hamiltonian H_f, evolves under H_f. Typically, $|\psi\rangle$ is a ground state of an initial Hamiltonian H_i. In that case quantum quench is subject to a sudden change of the Hamiltonian, $H_i \to H_f$. For instance, we are interested in the time evolution of correlation functions that reveals the relaxation of

the quantum quench,

$$\langle\psi(t)|\hat{O}|\psi(t)\rangle = \sum_{n,m} \frac{\langle\psi|n\rangle\langle n|\hat{O}|m\rangle\langle m|\psi\rangle}{\langle n|n\rangle\langle m|m\rangle} e^{\mathrm{i}(E_n - E_m)t}, \tag{1.1}$$

where $|n\rangle$ is a eigenstate of H_f with eigenvalue E_n. In principle, we would like to have the knowledge of the full spectrum of H_f to study the time evolution of correlation functions. For quantum integrable models, it is possible and we study the full spectrum of XXZ model in Chapter 6.

We first consider the initial state $|\psi\rangle$ to be homogeneous. Specialised to quantum integrable models, it is hypothesised that after a quantum quench, the time averaged correlation functions of local operator will relax to value described by a Generalised Gibbs Ensemble (GGE),

$$\lim_{t\to\infty} \int_0^t \mathrm{d}\tau \langle\psi(\tau)|\hat{O}|\psi(\tau)\rangle = \mathrm{tr}\left(\hat{O}\varrho_{\mathrm{GGE}}\right), \tag{1.2}$$

where the GGE is obtained with preserving all conserved charges of integrable model Q_j while maximising the entropy,

$$\varrho_{\mathrm{GGE}} = \frac{1}{\mathcal{Z}} e^{-\sum_j \mu_j Q_j}, \quad \mathcal{Z} = \mathrm{tr}\left(e^{-\sum_j \mu_j Q_j}\right). \tag{1.3}$$

μ_j are Lagrange multipliers fixed by the initial state $|\psi\rangle$. In fact, we could obtain much more information about the non-equilibrium dynamics knowing the overlaps between the initial states and the eigenstates of the quantum integrable Hamiltonian. This method is dubbed Quench Action [29, 30], and it leads to numerous studies such as the interaction quench in Lieb-Liniger model [31] and Néel quench in XXZ model [32, 33, 34].

When the initial state is inhomogeneous, we can use Generalised Hydrodynamics (GHD) [35, 36], which has been developed in recent years. GHD uses the approximation of the local relaxation in the mesoscopic scale, and it has been extremely successful in describing the dynamics of an inhomogeneous initial profile in integrable models (both classical and quantum), as well as the correlation functions [37, 38], which has been demonstrated in the atomic chip experiment [39] too. GHD is able to capture the ballistic transport of physical quantities [40, 41], and the corrections are diffusive, which is deciphered in [42]. Interestingly, a superdiffusive regime in quantum integrable models is studied in [43, 44, 45]

that is beyond the paradigm of GHD. We encounter a similar scenario for the classical counterpart in Chapter 4, where we use classical inverse scattering method to demonstrate the superdiffusion.

1.3 Outline

The outline of this thesis is as follows. In Chapter 2 we give a detailed introduction on the classical integrability on the classical Landau–Lifshitz model, which is the model we use in latter chapters. We present both the classical inverse scattering method, applied to the infinite system size, and finite-gap integration method, applied to systems with periodic boundary condition.

In Chapter 3 we introduce the basic notions of quantum integrability, with an emphasis on the transfer matrix formalism and algebraic Bethe ansatz. These two methods are of vital significance when constructing eigenstates for quantum integrable models.

The first result about the domain-wall quench in classical Landau–Lifshitz model is presented in Chapter 4. We use the classical inverse scattering method introduced in Chapter 2 to study the spin transport problem with domain-wall profile. We obtain three different regimes of spin transport and find a remarkable classical-quantum correspondence with the quantum counterpart, spin-1/2 XXZ model.

Chapter 5 is devoted to the semi-classical quantisation of finite-gap solutions of Landau–Lifshitz model. In order to find a quantitative description of the classical-quantum correspondence found in Chapter 4, we use the finite-gap integration method to construct the semi-classical eigenstates of the quantum XXZ model, whose Bethe root density is well described using classical theory. This allows us to treat the problems concerning quantum out-of-equilibrium properties with methods developed for the classical integrable models.

We switch the focus from the regime with semi-classical limit of quantum models to the regime where a fully quantum description is needed in Chapter 6. To begin with, we construct Baxter's Q operator of quantum XXZ model. Specialised to the anisotropic parameter at root of unity, we obtain the full spectrum and elucidate the exponential degeneracies in the spectrum. Eventually, the structure of the spectrum helps us under-

stand the out-of-equilibrium properties such as non-vanishing spin Drude weight in XXZ model at root of unity.

We continue the investigation on the spectrum of XXZ model at root of unity in Chapter 7, where we conjecture the existence of hidden Onsager algebra symmetries. Onsager algebra symmetry implies two sets of conserved charges that do not commute with each other, and the out-of-equilibrium properties of XXZ model at root of unity should be influenced tremendously due to the non-Abelian nature of the conserved charges.

In the concluding chapter 8, we summarise the results presented in previous chapters and give an outlook over the open problems that are intriguing and have the potential to be solved using methods introduced in this thesis.

Chapter 2

Classical integrability

Tous pour un, un pour tous.

Les Trois Mousquetaires,
Alexandre Dumas, père

In this chapter we introduce the important concepts and techniques of classical integrability using classical Landau–Lifshitz model as an example, which will be used extensively in Chapters 4 and 5. We start with the definition of the physical model and derivations of some basic physical properties of the model. This is followed by a pedagogical introduction to classical inverse scattering method, the central method behind the results in Chapter 4. Furthermore, we move to the finite-gap integration method, a well-established method of algebraic geometry, which will play a pivotal rôle in the semi-classical quantisation of the classical Landau–Lifshitz model in Chapter 5.

2.1 Classical Landau–Lifshitz model

We start with introducing the Landau–Lifshitz (LL) model, a classical field theory which governs the precessional motion of spin field defined on a unit sphere S^2. The equation of motion of the spin field

$\vec{S} = (S^{\mathrm{x}}, S^{\mathrm{y}}, S^{\mathrm{z}})^{\mathrm{T}}$ is

$$\vec{S}_t = \vec{S} \times \vec{S}_{xx} + \vec{S} \times \left(\mathbf{J}\vec{S}\right), \quad \vec{S} \cdot \vec{S} = 1, \tag{2.1}$$

with derivative denoted as $\frac{\mathrm{d}}{\mathrm{d}a} f := f_a$. The anisotropy tensor $\mathbf{J}$ can be parametrised by three parameters

$$\mathbf{J} = \mathrm{diag}(J_x, J_y, J_z), \quad J_x, J_y, J_z \in \mathbb{R}. \tag{2.2}$$

In fact, for arbitrary anisotropy tensor $\mathbf{J}$, the model is classically integrable [9]. We focus on a specific regime when $J_x = J_y = 0$, $J_z = \delta$, i.e. $\mathbf{J}$ is uniaxial. Sometimes we use another parametrisation of the anisotropy parameter

$$\delta = \epsilon^2 \in \mathbb{R}. \tag{2.3}$$

When $\delta > 0$ ($\epsilon \in \mathbb{R}$), we are in *easy-axis* regime. When $\delta < 0$ ($\epsilon \in \mathrm{i}\mathbb{R}$), the regime is called as *easy-plane*. We also denote the regime with $\delta = \epsilon = 0$ as the isotropic regime.

As we will explain in Chapter 4, the classical LL model with uniaxial anisotropy can be considered as the semi-classical limit of a ferromagnetic spin-1/2 XXZ model, which is the main focus of the latter chapters.

The Hamiltonian of the classical LL model is

$$H = \int_0^\ell \mathrm{d}x \left[\vec{S}_x(x) \cdot \vec{S}_x(x) - \delta(S^{\mathrm{z}}(x))^2\right], \tag{2.4}$$

with classical system size ℓ. We will consider different boundary conditions later. Even though the Hamiltonian looks like a "free" Hamiltonian with only quadratic terms, classical LL model is interacting because of the constraint $|\vec{S}(x)|^2 = 1$, which can be seen as a non-relativistic sigma model.

The equation of motion (2.1) can be obtained through the Poisson structure

$$\{S^a(x), S^b(y)\} = -\epsilon_{abc} S^c(x) \delta(x - y). \tag{2.5}$$

ϵ_{abc} is the antisymmetric Levi-Civita symbol and $\delta(x)$ denotes the delta function.

2.2 Classical inverse scattering method

Classical LL model is a classical integrable field theory, permitting an auxiliary linear description that transforms the non-linear equation of motion in terms of spin field $\vec{S}(x,t)$ to a linear problem of auxiliary (matrix) function $\Psi(x,t)$. The auxiliary linear problem reads

$$\Psi_x(\mu;x,t) = \mathbf{U}(\mu;x,t)\Psi(\mu;x,t), \quad \Psi_t(\mu;x,t) = \mathbf{V}(\mu;x,t)\Psi(\mu;x,t), \tag{2.6}$$

where the Lax connections $\mathbf{U}(\mu;x,t)$ (spatial component) and $\mathbf{V}(\mu;x,t)$ (temporal component) satisfy the *zero-curvature condition*,

$$\mathbf{U}_t(\mu;x,t) - \mathbf{V}_x(\mu;x,t) + [\mathbf{U}(\mu;x,t), \mathbf{V}(\mu;x,t)] = 0. \tag{2.7}$$

The spectral parameter $\mu \in \mathbb{C}$ is introduced in order to obtain the spectral properties of the model. The existence of UV pair and zero-curvature condition in auxiliary linear problem (2.6) is universal for all classical integrable field theories. Specifically for classical LL model, the Lax connections are expressed in terms of spin field, i.e.

$$\mathbf{U}(\mu;x,t) = \frac{1}{2\mathrm{i}} \begin{pmatrix} \mu\, S^{\mathrm{z}} & \sqrt{\mu^2+\delta}\, S^- \\ \sqrt{\mu^2+\delta}\, S^+ & -\mu\, S^{\mathrm{z}} \end{pmatrix}, \tag{2.8}$$

$$\begin{aligned} \mathbf{V}(\mu;x,t) =& \frac{\mathrm{i}}{2} \begin{pmatrix} (\mu^2+\delta)S^{\mathrm{z}} & \mu\sqrt{\mu^2+\delta}S^- \\ \mu\sqrt{\mu^2+\delta}S^+ & -(\mu^2+\delta)S^{\mathrm{z}} \end{pmatrix} \\ & - \frac{1}{2\mathrm{i}} \begin{pmatrix} \mu\, J_0^{\mathrm{z}} & \sqrt{\mu^2+\delta}\, J_0^- \\ \sqrt{\mu^2+\delta}\, J_0^+ & -\mu\, J_0^{\mathrm{z}} \end{pmatrix}, \end{aligned} \tag{2.9}$$

with

$$J_0 \equiv \vec{S}_x \times \vec{S}, \tag{2.10}$$

denoting the spin current density at $\delta = 0$. From the definitions of Lax connections, it is easy to show that zero-curvature condition (2.7) is equivalent to the equation of motion for spin field (2.1).

2.2.1 Spectral problem of domain-wall initial conditions

We consider the system size $\ell \to \infty$ and with boundary condition $S(\pm\infty) = \pm 1$, i.e. domain-wall initial condition. We demonstrate the classical in-

verse scattering method using this example, and the results will become important in Chapter 4. More specifically, we study the following initial conditions

$$S^{\mathrm{z}}(x,t=0)=\tanh(x),\quad S^{-}(x,t=0)=S^{+}(x,t=0)=\operatorname{sech}(x),\tag{2.11}$$

satisfying $S^{+}S^{-}+(S^{\mathrm{z}})^{2}=1$.

The direct scattering problem of auxiliary linear problem can be written as

$$\partial_x T(x,y)=\mathbf{U}(\mu,x)T(x,y),\tag{2.12}$$

with transition matrix $T(x,y)=\mathcal{P}\exp\int_x^y \mathbf{U}(\mu,x')\mathrm{d}x'$ satisfying $T(y,y)=1$ and $\det T(x,y)=1$. $\mathcal{P}$ denotes the path ordering. Equivalently, from the definition of the transition matrix we have

$$\partial_y T(x,y)=-\mathbf{U}(\mu,y)T(x,y).\tag{2.13}$$

Further differentiating (2.12) and taking into account the zero-curvature condition (2.7), we have (omitting the dependence on the variables for simplicity)

$$\partial_x\partial_t T=\mathbf{U}\partial T+\partial_t\mathbf{U}T=\partial_x(\mathbf{V}T)+\mathbf{U}(\partial_t T-\mathbf{V}T),\tag{2.14}$$

or equivalently

$$\partial_x(\partial_t T-\mathbf{V}T)=\mathbf{U}(\partial_t T-\mathbf{V}T).\tag{2.15}$$

Together with the property that $T(y,y)=1$, we write down the time evolution of the transition matrix which is of vital importance,

$$\partial_t T(x,y)=\mathbf{V}(\mu,x)T(x,y)-T(x,y)\mathbf{V}(\mu,y).\tag{2.16}$$

Asymptotically, we have two Jost solutions labelled as $T_{\pm}(x)$

$$T_{+}(x\to+\infty)=\exp\left(\frac{\mu x\sigma^{\mathrm{z}}}{2\mathrm{i}}\right),\tag{2.17}$$

and

$$T_{-}(x\to-\infty)=\exp\left(-\frac{\mu x\sigma^{\mathrm{z}}}{2\mathrm{i}}\right)\mathrm{i}\sigma^{\mathrm{x}}.\tag{2.18}$$

These two Jost solutions can be obtained by taking into account $\mathbf{U}(\mu, x \to \infty\pm) = \pm\frac{\mu}{2\mathrm{i}}\sigma^{\mathrm{z}}$.

According to the definition of transition matrix, two Jost solutions are expressed as

$$\begin{aligned} T_+(x) &= \lim_{y\to+\infty} T(x,y)\exp\left(\frac{\mu y\sigma^{\mathrm{z}}}{2\mathrm{i}}\right), \\ T_-(x) &= \lim_{y\to-\infty} T(x,y)\exp\left(\frac{-\mu y\sigma^{\mathrm{z}}}{2\mathrm{i}}\right)\mathrm{i}\sigma^{\mathrm{x}}. \end{aligned} \tag{2.19}$$

Taking the appropriate limit of the time evolution (2.16), we obtain the time evolution of the Jost solutions, i.e.

$$\partial_t T_\pm(x) = \mathbf{V}(\mu,x)T_\pm(x) - T_\pm(x)\frac{\mathrm{i}\sigma^{\mathrm{z}}(\mu^2+\epsilon^2)}{2}. \tag{2.20}$$

Therefore, we introduce the classical monodromy matrix $T(\mu)$ as

$$T_-(\mu,x) = T_+(\mu,x)T(\mu), \tag{2.21}$$

satisfying simple time evolution

$$\partial_t T(\mu) = \frac{\mathrm{i}(\mu^2+\delta)}{2}\left[\sigma^{\mathrm{z}}, T(\mu)\right]. \tag{2.22}$$

From the time evolution of $T(\mu)$, we have

$$\partial_t \mathrm{tr}T(\mu) = \mathrm{tr}\partial_t T(\mu) = 0, \tag{2.23}$$

i.e. the trace of the classical monodromy matrix is time-invariant (conserved). We can define the transfer function

$$\tau(\mu) = \mathrm{tr}T(\mu) \tag{2.24}$$

as the generating function for the local conserved charges. A detailed analysis is postponed to the periodic case in Sec. 2.3.2.

With the initial profile (2.11), the classical monodromy matrix $T(\mu)$ is written as

$$T(\mu) = \begin{pmatrix} a(\mu) & -\bar{b}(\mu) \\ b(\mu) & a(\mu) \end{pmatrix}, \quad \det T(\mu) = |a(\mu)|^2 + |b(\mu)|^2 = 1. \tag{2.25}$$

The scattering data reads

$$\begin{aligned} a(\mu, t=0) &= \frac{\sqrt{\mu^2+\epsilon^2}\mathbf{\Gamma}^2\left(\frac{1}{2}-\frac{\mathrm{i}}{2}\mu\right)}{2\mathbf{\Gamma}\left(1-\frac{\mathrm{i}}{2}(\mu+\mathrm{i}\epsilon)\right)\mathbf{\Gamma}\left(1-\frac{\mathrm{i}}{2}(\mu-\mathrm{i}\epsilon)\right)}, \\ b(\mu, t=0) &= \mathrm{i}\frac{\cos(\frac{\pi}{2}\epsilon)}{\cosh(\frac{\pi}{2}\mu)}, \end{aligned} \tag{2.26}$$

where $\mathbf{\Gamma}(x)$ is the Gamma function.

From the time evolution (2.22), we obtain the time evolution of the components in a simple manner

$$a(\mu, t) = a(\mu, 0), \quad b(\mu, t) = b(\mu, 0)e^{\mathrm{i}(\mu^2+\epsilon^2)t}. \tag{2.27}$$

The detailed analysis of the scattering data for different regimes (different values of δ or ϵ) is postponed to Chapter 4.

2.2.2 Inverse scattering

After obtaining the scattering data, we convert the (non-linear) time evolution of the spin field to the simple time evolution of the scattering data $a(\mu)$ and $b(\mu)$. However, eventually we are interested in the spin field after time evolution $\vec{S}(x,t)$ itself. What is needed now is to find the transformation that maps the scattering data back to the time-evolved spin field $\vec{S}(x,t)$. This procedure is called "inverse scattering".

To begin with, we introduce the uniformisation parameter z, such that

$$\mu = \frac{1}{2}\left(z - \frac{\epsilon^2}{z}\right), \quad \sqrt{\mu^2+\epsilon^2} = \frac{1}{2}\left(z + \frac{\epsilon^2}{z}\right). \tag{2.28}$$

The auxiliary linear problem (2.6) can then be expressed in terms of z,

$$\partial_x \Psi = \left(\frac{z}{4\mathrm{i}}S - \frac{\varepsilon^2}{4\mathrm{i}z}\tilde{S}\right)\Psi, \tag{2.29}$$

where $\tilde{S} = \sigma^{\mathrm{z}} S \sigma^{\mathrm{z}}$. Let us rewrite the equation above in integral form. More specifically, for Jost solution $T_+(x)$ we have

$$\begin{aligned} T_+(x) = E(x) &+ \frac{z}{4\mathrm{i}}\int_x^\infty \mathrm{d}y \Gamma_+(x,y)E(y) + \frac{1}{4\mathrm{i}}\int_x^\infty \mathrm{d}y \Gamma_0(x,y)E(y) \\ &+ \frac{z^{-1}}{4\mathrm{i}}\int_x^\infty \mathrm{d}y \Gamma_-(x,y)E(y), \end{aligned} \tag{2.30}$$

where the matrix

$$E(x) = \exp\left(\frac{\mu x \sigma^{\mathrm{z}}}{2\mathrm{i}}\right) = \exp\left(\frac{(z-\epsilon^2/z)x\sigma^{\mathrm{z}}}{4\mathrm{i}}\right). \tag{2.31}$$

The kernels $\Gamma_i(x,y)$ do not depend on the spectral parameter z.

Since T_+ satisfies the auxiliary linear problem (2.29), the kernels $\Gamma_i(x,y)$ satisfy the following Goursat equations,

$$\partial_x \Gamma_+(x,y) = -S(x)\partial_y \Gamma_+(x,y)\sigma^{\mathrm{z}} + S(x)\Gamma_0(x,y), \tag{2.32}$$

$$\partial_x \Gamma_-(x,y) = -\tilde{S}(x)\partial_y \Gamma_-(x,y)\sigma^{\mathrm{z}} - \epsilon^2 \tilde{S}(x)\Gamma_0(x,y), \tag{2.33}$$

$$\partial_x \Gamma_0(x,y) = \frac{S(x)-\tilde{S}(x)}{4\mathrm{i}}\Gamma_-(x,y) + \epsilon^2 \frac{S(x)-\tilde{S}(x)}{4\mathrm{i}}\Gamma_+(x,y). \tag{2.34}$$

Integrating by parts, we obtain the following equations for the Landau–Lifshitz model,

$$\begin{aligned}
&\frac{z}{4\mathrm{i}}\partial_x \int_x^\infty \mathrm{d}y \Gamma_+(x,y)E(y) = \frac{z}{4\mathrm{i}}\left[S\Gamma_+(x,x)\sigma^{\mathrm{z}} - \Gamma_+(x,x)\right]E(x) \\
&+ \frac{z}{4\mathrm{i}}\frac{z-\epsilon^2/z}{4\mathrm{i}} S \int_x^\infty \mathrm{d}y \Gamma_+(x,y)E(y) + \frac{z}{4\mathrm{i}} S \int_x^\infty \mathrm{d}y \Gamma_0(x,y)E(y),
\end{aligned} \tag{2.35}$$

$$\begin{aligned}
&\frac{z}{4\mathrm{i}}\partial_x \int_x^\infty \mathrm{d}y \Gamma_-(x,y)E(y) = \frac{z^{-1}}{4\mathrm{i}}\left[\tilde{S}\Gamma_-(x,x)\sigma^{\mathrm{z}} - \Gamma_-(x,x)\right]E(x) \\
&+ \frac{z^{-1}}{4\mathrm{i}}\frac{z-\epsilon^2/z}{4\mathrm{i}} \tilde{S} \int_x^\infty \mathrm{d}y \Gamma_-(x,y)E(y) \\
&+ \frac{z^{-1}\epsilon^2}{4\mathrm{i}} \tilde{S} \int_x^\infty \mathrm{d}y \Gamma_0(x,y)E(y),
\end{aligned} \tag{2.36}$$

$$\begin{aligned}
&\partial_x \int_x^\infty \mathrm{d}y \Gamma_0(x,y)E(y) = -\Gamma_0(x,x)E(x) \\
&+ \frac{S-\tilde{S}}{4\mathrm{i}} \int_x^\infty \mathrm{d}y \Gamma_-(x,y)E(y) + \epsilon^2 \frac{S-\tilde{S}}{4\mathrm{i}} \int_x^\infty \mathrm{d}y \Gamma_+(x,y)E(y).
\end{aligned} \tag{2.37}$$

As for the boundary values of the Goursat problem, we have

$$\begin{aligned}
&\sigma^{\mathrm{z}} + S(x)\Gamma_+(x,x)\sigma^{\mathrm{z}} - \Gamma_+(x,x) = S(x), \\
&\epsilon^2\sigma^{\mathrm{z}} - \tilde{S}(x)\Gamma_+(x,x)\sigma^{\mathrm{z}} - \Gamma_-(x,x) = \epsilon^2 S(x), \\
&\Gamma_0(x,x) = 0.
\end{aligned} \tag{2.38}$$

We parametrise the kernels Γ_i as

$$\Gamma_+ = \begin{pmatrix} \gamma_1 & \bar{\gamma}_2 \\ \gamma_2 & -\bar{\gamma}_1 \end{pmatrix}, \quad \Gamma_- = -\epsilon^2 \begin{pmatrix} \gamma_1 & -\bar{\gamma}_2 \\ -\gamma_2 & -\bar{\gamma}_1 \end{pmatrix}, \quad \Gamma_0 = \gamma_0 \sigma^{\mathrm{z}}. \tag{2.39}$$

Once obtaining the values of the kernels, we can reconstruct the spin field via (2.38),

$$\begin{aligned} S^z(x,t) &= \frac{|\gamma_1(x,x,t)-1|^2 - |\gamma_2(x,x,t)|^2}{|\gamma_1(x,x,t)-1|^2 + |\gamma_2(x,x,t)|^2}, \\ S^- &= \frac{2[\gamma_1(x,x,t)-1]\bar{\gamma}_2(x,x,t)}{|\gamma_1(x,x,t)-1|^2 + |\gamma_2(x,x,t)|^2}. \end{aligned} \tag{2.40}$$

The numerical and analytic results in Chapter 4 are obtained via numerically or analytically solving equations above.

GLM equation with $\delta = 0$

In principle, solving the Goursat equations (2.32), (2.33) and (2.34) and using reconstruction formulae (2.40), we are able to obtain analytic solutions to the time-evolved spin field. However, sometimes it is difficult to obtain the solutions analytically. In order to study the transport properties, which typically need to perform numerical simulations for a relatively long time scale, we rewrite the Goursat equations into integral equations, i.e. Gelfand–Levitan–Marchenko (GLM) equations that are efficient for numerical simulations.

For the domain-wall profile that we are interested in, the GLM equations are especially needed in the isotropic regime ($\delta = 0$). In that regime, we can express the one of Jost solutions as

$$T_+(x) = E(x) + \frac{\mu}{4\mathrm{i}} \int_x^\infty \mathrm{d}y \Gamma(x,y) E(y). \tag{2.41}$$

By integrating the auxiliary linear problem, we obtain the GLM equation

$$\Gamma(x,y) - K_1(x+y) + \int_x^\infty \mathrm{d}s \Gamma(x,s) K_2(s+y) = 0, \tag{2.42}$$

with kernels defined as

$$K_1(x) = \begin{pmatrix} 0 & \bar{k}(x) \\ k(x) & 0 \end{pmatrix}, \quad K_2(x) = \begin{pmatrix} 0 & -\partial_x \bar{k}(x) \\ \partial_x k(x) & 0 \end{pmatrix}, \tag{2.43}$$

$$k(x) = \frac{1}{2\pi \mathrm{i}} \int_{-\infty}^{\infty} \mathrm{d}\mu \frac{\tilde{r}(\mu)}{(\mu + \mathrm{i}0)^2} e^{\mathrm{i}\mu x/2 - \mathrm{i}\mu^2 t}, \tag{2.44}$$

$$\tilde{r}(\mu) = \lim_{\epsilon \to 0} \frac{b(\mu)}{a(\mu)} = \frac{2}{\cosh(\pi\mu/2)} \frac{\mathbf{\Gamma}^2(1 - \mathrm{i}\mu/2)}{\mathbf{\Gamma}^2(1/2 - \mathrm{i}\mu/2)}. \tag{2.45}$$

The integral equations above can be solved numerically in an efficient manner, forming the basis for the numerical evaluation of the spin transport properties with domain wall profile in the isotropic regime.

Similar to the anisotropic case above, we can parametrise the matrix $\Gamma(x, y)$ as

$$\Gamma(x, y) = \mathbb{1} + \begin{pmatrix} \gamma_1(x, y) & \bar{\gamma}_2(x, y) \\ \gamma_2(x, y) & -\bar{\gamma}_1(x, y) \end{pmatrix}. \tag{2.46}$$

Using the reconstruction formulae (2.40), we could obtain the numerical results for the time-evolved spin field, thus spin transport properties.

2.2.3 Solitons and radiation modes

Before proceeding with the finite-gap integration for the periodic case, we would like to mention types of solutions to the classical inverse scattering method, i.e. solitons and radiation modes. Solitons are the non-dispersive modes of the classical integrable models, while radiation modes are dispersive. In general, the spectrum of a generic initial state might contain both. They are directly related to the analytic structure of the scattering data $a(\mu)$ and $b(\mu)$.

More specifically, the soliton part of the spectrum is given by the zeros of $a(z)$ in the upper half plane (or the poles in the lower half plane) [1], while the radiative part is given by the regular part of $a(z)$ in $\mathbb{C}$, i.e.

$$a(z) = \prod_j \frac{z - z_j}{z - \bar{z}_j} a_{\mathrm{reg}}(z). \tag{2.47}$$

When $b(z) = 0$, and $|a_{\mathrm{reg}}(z)| = 1$, the spectrum only contains the solitons. In this case, the GLM equations become algebraic, leading to exact analytic solutions to the non-linear equations of motion. We will demonstrate this point in Chapter 4 in the easy-axis regime.

[1] here we use uniformisation parameter z

2.3 Finite-gap integration

In this section we consider the periodic boundary condition, i.e. system size $\ell \in \mathcal{O}(1)$ and $\vec{S}(x=0) = \vec{S}(x=\ell)$. In this circumstance we can no longer use the classical inverse scattering method introduced in Sec. 2.2. Furthermore, the periodicity induces a constraint on possible modes in the spectrum, different from the $\ell \to \infty$ case. We need to use finite-gap integration method to obtain exact solutions of classical Landau–Lifshitz model with periodic boundary condition.

2.3.1 Adjoint linear problem

We begin with rewriting the auxiliary linear problem in the adjoint form. The advantage of doing so is to avoid the ambiguity of normalisation in the usual construction of Baker–Akhiezer vectors.

The solution to the auxiliary linear problem (2.6) can be written as

$$\boldsymbol{\psi}(\mu; x) = \mathscr{P} \exp\left(\int_{x_0}^{x} \mathrm{d}x' \mathbf{U}(\mu; x')\right) \equiv \mathbf{T}_{\mathrm{cl}}(x, x_0), \tag{2.48}$$

by formally integrating along the spatial direction with fixed time. $\mathscr{P}$ stands for the path ordering. With the periodic boundary condition $\vec{S}(x=0) = \vec{S}(x=\ell)$, we define the (classical) monodromy matrix

$$\mathbf{M}_{\mathrm{cl}}(\mu) = \mathbf{T}_{\mathrm{cl}}(x_0 + \ell, x_0), \tag{2.49}$$

which does not depend on the initial starting point. Therefore, we have

$$\boldsymbol{\psi}(\mu; x + \ell) = \boldsymbol{\mu}(\mu)\boldsymbol{\psi}(\mu; x), \tag{2.50}$$

where $\boldsymbol{\mu}(\mu) = \mathrm{diag}(\mu_+(\mu), \mu_-(\mu))$ is given by the eigenvalues of $\mathbf{M}_{\mathrm{cl}}(\mu)$, i.e. $\mu_\pm(\mu)$. The eigenvalues are time-invariant and unimodular because of the zero-curvature condition (2.7) and $\mathrm{Tr}\mathbf{U}(\mu) = 0$. We can parametrise the eigenvalues as

$$\mu_\pm(\mu) = \exp\left(\pm \mathrm{i}\mathfrak{p}(\mu)\right), \tag{2.51}$$

where quasi-momentum $\mathfrak{p}(\mu)$ encodes the information about the conserved charges as we will see. Subsequently, we express the monodromy matrix as

$$\mathbf{M}_{\mathrm{cl}}(\mu) = \cos(\mathfrak{p}(\mu)) + \mathrm{i}\sin(\mathfrak{p}(\mu))\boldsymbol{\Psi}(\mu; x), \tag{2.52}$$

where the *squared eigenfunction* can be written as

$$\mathbf{\Psi}(\mu;x) = \boldsymbol{\psi}(\mu;x)\sigma^z\boldsymbol{\psi}^{-1}(\mu;x). \tag{2.53}$$

From the definition, $\det \mathbf{\Psi} = -1$.

The squared wavefunction is periodic, $\mathbf{\Psi}(\mu;x+\ell) = \mathbf{\Psi}(\mu;x)$ and it satisfies the adjoint linear problem

$$\begin{aligned} \mathbf{\Psi}_x(\mu;x,t) &= [\mathbf{U}(\mu;x,t), \mathbf{\Psi}(\mu;x,t)]\,, \\ \mathbf{\Psi}_t(\mu;x,t) &= [\mathbf{V}(\mu;x,t), \mathbf{\Psi}(\mu;x,t)]\,. \end{aligned} \tag{2.54}$$

2.3.2 Local conserved charges

We introduce the uniformisation of the spectral parameter μ,

$$\mu = \frac{1}{2}\left(z - \frac{\delta}{z}\right), \quad \sqrt{\mu^2+\delta} = \frac{1}{2}\left(z + \frac{\delta}{z}\right), \tag{2.55}$$

the same as in (2.28). The squared eigenfunction, i.e. solution to the adjoint linear problem, can be expressed in terms of a formal Laurent series of z,

$$\mathbf{\Psi}(z) = \sum_{n=0}^{\infty} \frac{\mathbf{\Psi}_n}{z^n}. \tag{2.56}$$

We define two matrices,

$$\mathbf{S} = \vec{S}\cdot\vec{\sigma} = \begin{pmatrix} S^{\mathrm{z}} & S^- \\ S^+ & -S^{\mathrm{z}} \end{pmatrix}, \quad \tilde{\mathbf{S}} = \sigma^z\mathbf{S}\sigma^z. \tag{2.57}$$

The expansions in $\mathbf{\Psi}$ read

$$\begin{aligned} &\mathbf{\Psi}_0 = \mathbf{S}, \quad \mathbf{\Psi}_1 = \mathrm{i}[\mathbf{S},\mathbf{S}_x], \\ &\mathbf{\Psi}_2 = -\mathrm{tr}(\mathbf{S}_x)^2\mathbf{S} - \big[\mathbf{S},[\mathbf{S},\mathbf{S}_{xx}]\big] + \frac{\delta}{4}\big[\mathbf{S},[\tilde{\mathbf{S}},\mathbf{S}]\big], \end{aligned} \tag{2.58}$$

and so forth.

As for the local conserved charges, we start from the quasi-momentum,

$$\mathfrak{p}(z) = -\mathrm{i}\int_0^\ell \mathrm{tr}\big[\mathbf{U}(\mathbf{\Psi}+\sigma^z)\big] = -\frac{z\ell}{4} + \sum_{n=0}^{\infty}\frac{Q_n}{z^n}, \tag{2.59}$$

where Q_n are the local conserved charges that do not evolve with respect to time. For example, the first two with local density are essentially momentum and Hamiltonian,

$$\begin{aligned} Q_0 &= \frac{\mathrm{i}}{4}\int_0^\ell \mathrm{d}x \frac{S^- S_x^+ - S^+ S_x^-}{1+S^{\mathrm{z}}} = -\frac{P}{2}, \\ Q_1 &= -\frac{1}{2}\int_0^\ell \mathrm{d}x \left[\vec{S}_x^2 + \delta\big(1-(S^{\mathrm{z}})^2\big) - \frac{\delta}{2}\right] = -H + \frac{\delta\ell}{4}, \end{aligned} \tag{2.60}$$

and in spectral parameter μ we have

$$\mathfrak{p}(\mu) = -\frac{\mu\ell}{2} - \frac{P}{2} - \frac{H}{\mu} + \mathcal{O}(\mu^{-2}). \tag{2.61}$$

2.3.3 Finite-gap solutions

We focus on a special class of solutions, i.e. finite-gap solutions, parametrised by finite-many branch cuts in the Riemann surface. Most notable examples are the elliptic solutions that become magnetic soliton in the soliton limit. We start with parametrising the squared eigenfunction as

$$\mathbf{\Psi}_{\mathfrak{g}}(\mu) = \frac{1}{\sqrt{\mathcal{R}_{2\mathfrak{g}+2}(\mu)}} \begin{pmatrix} a_{\mathfrak{g}+1}(\mu) & \sqrt{\mu^2+\epsilon^2}\, b_{\mathfrak{g}}(\mu) \\ \sqrt{\mu^2+\epsilon^2}\, \bar{b}_{\mathfrak{g}}(\mu) & -a_{\mathfrak{g}+1}(\mu) \end{pmatrix}, \tag{2.62}$$

where functions $a_d(\mu)$, $b_d(\mu)$ and $\mathcal{R}_d(\mu)$ are *polynomials* in variable μ of degree d. In particular, $\mathcal{R}_{2\mathfrak{g}+2}(\mu)$ is a polynomial of degree $2\mathfrak{g}+2$,

$$\mathcal{R}_{2\mathfrak{g}+2}(\mu) = \prod_{j=1}^{\mathfrak{g}+1}(\mu-\mu_j)(\mu-\bar{\mu}_j) = \sum_{k=0}^{2\mathfrak{g}+2}(-1)^k r_{2\mathfrak{g}+2-k}\mu^k, \tag{2.63}$$

which specifies a hyperelliptic algebraic curve in $\mathbb{C}^2$,

$$\Sigma: \qquad y^2(\mu) = \mathcal{R}_{2\mathfrak{g}+2}(\mu). \tag{2.64}$$

The curve is fully characterised by $2(\mathfrak{g}+1)$ branch points μ_j (or, equivalently, symmetric polynomials r_k thereof, with $r_{2\mathfrak{g}+2}=1$). Because $\det \mathbf{\Psi}_{\mathfrak{g}} = -1$, functions $a(\mu)$ and $b(\mu)$ are not independent but satisfy

$$a_{\mathfrak{g}+1}^2(\mu) + \big(\mu^2+\delta\big)\, b_{\mathfrak{g}}(\mu)\bar{b}_{\mathfrak{g}}(\mu) = \mathcal{R}_{2\mathfrak{g}+2}(\mu). \tag{2.65}$$

From the trace identity (2.59) we obtain the following compact expression for the quasi-momentum

$$\mathfrak{p}(\mu) = -\frac{\mu}{2}\int_0^\ell \mathrm{d}x\, S^{\mathrm{z}}(x) - \frac{\mu^2+\delta}{4}\int_0^\ell \mathrm{d}x\, \frac{S^-\bar{b}_{\mathfrak{g}}(\mu) + S^+ b_{\mathfrak{g}}(\mu)}{\sqrt{\mathcal{R}_{2\mathfrak{g}+2}(\mu)} + a_{\mathfrak{g}+1}(\mu)}. \quad (2.66)$$

This form is compatible with the correct asymptotic expansion about $\mu \to \infty$. A series expansion of $\mathfrak{p}(\mu)$ will involve only $(\mathfrak{g}+1)$ functionally independent integrals of motion Q_n. They can be expressed as certain functions of coefficients r_j of $\mathcal{R}_{2\mathfrak{g}+2}(\mu)$. Moreover, the total filling fraction ν with respect to the ferromagnetic vacuum $S^{\mathrm{z}}_{\mathrm{vac}} = 1$,

$$\nu \equiv \frac{1}{2\ell}\int_0^\ell \mathrm{d}x\, (1 - S^{\mathrm{z}}(x)), \quad (2.67)$$

can be obtained as

$$\mathfrak{p}(\mu = \pm \mathrm{i}\epsilon) = \mp\frac{\mathrm{i}\epsilon}{2}\int_0^\ell \mathrm{d}x\, S^{\mathrm{z}}(x) = \mp\frac{\mathrm{i}\epsilon\ell}{2}(1-2\nu). \quad (2.68)$$

2.3.4 Dynamical divisor and Dubrovin equations

As we see from above, the diagonal part of $\mathbf{\Psi}$ contains the information of the quasi-momentum $\mathfrak{p}$, equivalent to the conserved charges. We would like to know about the dynamical degrees of freedom too, which are the dynamical zeros of the off-diagonal elements of $\mathbf{\Psi}$.

To satisfy (2.65), we have

$$b_{\mathfrak{g}}(\mu; x, t) = S^-(x,t)\prod_{j=1}^{\mathfrak{g}}\big(\mu - \gamma_j(x,t)\big). \quad (2.69)$$

The set $\mathcal{D} = \{\gamma_j\}_{j=1}^{g}$ is known as the *dynamical divisor* of the Riemann surface Σ. Since $S^-(x,t)$ should also be regarded as an independent dynamical variable, we have in total $(\mathfrak{g}+1)$ dynamical degrees of freedom. This number exactly matches the number of action variables and corresponds to the number of forbidden zones in the finite-gap spectrum.

We employ an extended dynamical divisor $\mathcal{D}_{\mathrm{ext}}$ by adjoining it two extra non-dynamical variables $\gamma_\pm \equiv \pm\mathrm{i}\epsilon$ which we label by $\gamma_{\mathfrak{g}+1}$ and

$\gamma_{\mathfrak{g}+2}$, respectively. Using the Lagrange interpolation formula, we restore $a_{\mathfrak{g}+1}(\mu)$ from (2.65), yielding

$$a_{\mathfrak{g}+1}(\mu;x,t)=\sum_{j=1}^{\mathfrak{g}+2}\sqrt{\mathcal{R}_{2\mathfrak{g}+2}(\gamma_j(x,t))}\prod_{k\neq j}^{\mathfrak{g}+2}\frac{\mu-\gamma_k(x,t)}{\gamma_j(x,t)-\gamma_k(x,t)}. \tag{2.70}$$

From the adjoint linear problem (2.54), we obtain the equations of motion for the dynamical divisor,

$$\begin{aligned}\partial_x\gamma_j(x,t)&=\mathrm{i}\sqrt{\mathcal{R}_{2\mathfrak{g}+2}(\gamma_j(x,t))}\prod_{k\neq j}^{\mathfrak{g}}(\gamma_j(x,t)-\gamma_k(x,t))^{-1},\\ \partial_t\gamma_j(x,t)&=\mathrm{i}\,G(x,t)\sqrt{\mathcal{R}_{2\mathfrak{g}+2}(\gamma_j(x,t))}\prod_{k\neq j}^{\mathfrak{g}}(\gamma_j(x,t)-\gamma_k(x,t))^{-1},\end{aligned} \tag{2.71}$$

where

$$G(x,t)\equiv\frac{r_1}{2}-\sum_{k\neq j}^{\mathfrak{g}}\gamma_k(x,t),\qquad r_1=\sum_{j=1}^{\mathfrak{g}+1}(\mu_j+\bar{\mu}_j). \tag{2.72}$$

We have obtained a system of differential equations that governs the motion of the dynamical divisor of a Riemann surface, commonly known in the literature under the name of *Dubrovin equations* [46, 47, 48]. The form of these equations is universal, not depending on the model under consideration. The reconstruction formulae, i.e. how γ-variables relate to physical fields, are model-dependent. A spin field can be described by two degrees of freedom, e.g. the S^{z} and S^{-} components. These can be restored from (2.54), which yields

$$S^{\mathrm{z}}(x,t)=\sum_{j=1}^{\mathfrak{g}+2}\frac{\sqrt{\mathcal{R}_{2\mathfrak{g}+2}(\gamma_j(x,t))}}{\prod_{k\neq j}^{\mathfrak{g}+2}(\gamma_j(x,t)-\gamma_k(x,t))}, \tag{2.73}$$

and

$$\mathrm{i}\frac{S^{-}_x(x,t)}{S^{-}(x,t)}=\sum_{j=1}^{\mathfrak{g}+2}\frac{\gamma_j\sqrt{\mathcal{R}_{2\mathfrak{g}+2}(\gamma_j(x,t))}}{\prod_{k\neq j}^{\mathfrak{g}+2}(\gamma_j(x,t)-\gamma_k(x,t))}, \tag{2.74}$$

$$\mathrm{i}\frac{S^{-}_t(x,t)}{S^{-}(x,t)}=\mathrm{i}\frac{r_1}{2}\frac{S^{-}_x(x,t)}{S^{-}(x,t)}-\sum_{j=1}^{\mathfrak{g}+2}\frac{\gamma_j\sqrt{\mathcal{R}_{2\mathfrak{g}+2}(\gamma_j)}\left(\sum_{k\neq j}^{\mathfrak{g}+2}\gamma_k(x,t)\right)}{\prod_{k\neq j}^{\mathfrak{g}+2}(\gamma_j(x,t)-\gamma_k(x,t))}. \tag{2.75}$$

2.3.5 Abel–Jacobi transformation

The Dubrovin equations (2.71) allow for exact integration. We define the standard basis of $2\mathfrak{g}$ closed cycles on Riemann surface Σ. They are $\mathfrak{g}$-many $\mathcal{A}$-cycles and their conjugate $\mathcal{B}$-cycles according to the following prescription: $\mathcal{A}_j$-cycle encircles the the jth branch cut $\mathcal{C}_j$ on the upper Riemann sheet of Σ, whereas $\mathcal{B}_{jk}$ denotes a cycle that passes through cut $\mathcal{C}_j$ on the upper sheet and closes back to itself through $\mathcal{C}_k$, as shown in Fig. 2.1.

Dubrovin equations for the dynamical divisor on Σ can be integrated with aid of the Abel–Jacobi transformation,

$$\varphi_j = 2\pi \sum_{k=1}^{\mathfrak{g}} \int_{\gamma_k(0,0)}^{\gamma_k(x,t)} \omega_j, \tag{2.76}$$

where ω_j form the basis of holomorphic differentials of the Riemann surface. The above mapping provides a variable transformation from γ-variables to angle variables φ, $\{\gamma_j(x,t)\} \mapsto \{\varphi_j(x,t)\}$.

The holomorphic differentials ω_j are expressed as

$$\omega_j = \sum_{k=1}^{\mathfrak{g}} \frac{C_{jk}\mu^{\mathfrak{g}-k}\mathrm{d}\mu}{\sqrt{\mathcal{R}_{2\mathfrak{g}+2}(\mu)}}, \qquad j = 1, 2, \ldots \mathfrak{g}. \tag{2.77}$$

Coefficients C_{jk} are determined by requiring canonical normalisation with respect to $\mathcal{A}$-cycles

$$\oint_{\mathcal{A}_j} \omega_k = \delta_{jk}. \tag{2.78}$$

Taking into account Eq. (2.76), equations of motion of the dynamical divisor (2.71) linearise. Using the Lagrange interpolation formula, we obtain

$$\partial_x\varphi(x,t) = 2\pi\mathrm{i}\, C_{j1}, \quad \partial_t\varphi(x,t) = 2\pi\mathrm{i}\left[\frac{r_1}{2}C_{j1} + C_{j2}\right], \tag{2.79}$$

implying

$$\varphi_j(x,t) = k_j\, x + w_j\, t + \varphi_j(0,0), \tag{2.80}$$

with wave numbers k_j and frequencies w_j

$$k_j = 2\pi\mathrm{i}C_{j1}, \quad w_j = 2\pi\mathrm{i}\Big[\frac{r_1}{2}C_{j1} + C_{j2}\Big]. \tag{2.81}$$

Phases $\varphi_j(x,t)$ satisfy linear evolution in both space and time, executing quasiperiodic motion on a Liouville torus $\mathbb{T}^{2\mathfrak{g}}$ of real dimension $2\mathfrak{g}$. γ-variables evolve along closed trajectories which are equivalent to $\mathcal{A}$-cycles $\mathcal{A}_j$.

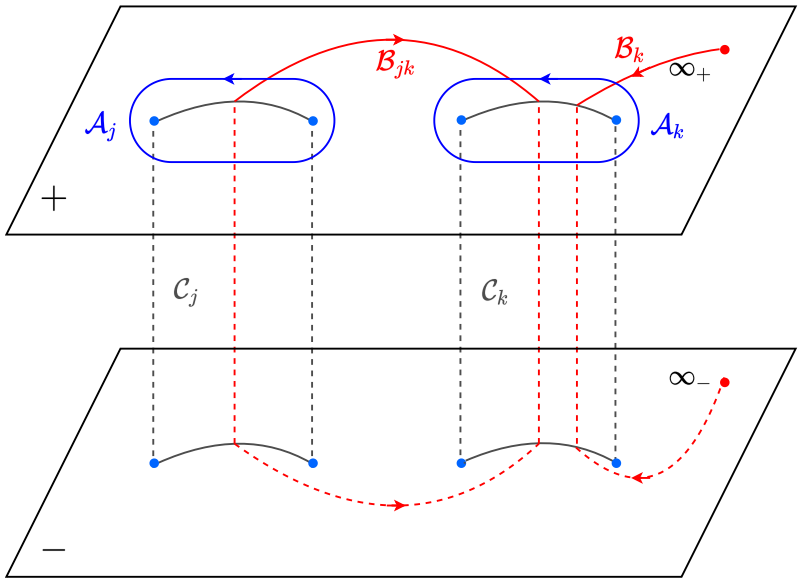

Figure 2.1: Cycles on a two-sheeted Riemann surface, illustrated on an example of two cuts $\mathcal{C}_j$ and $\mathcal{C}_k$. Upon tunnelling to the other Riemann sheet, the integration orientation is reversed [13].

In order to obtain physical solutions, we need to impose another constraint, namely periodicity of the spin field. We would like to consider a family of periodic solutions $\vec{S}(x) = \vec{S}(x+\ell)$. They can be achieved by demanding the periodicity of angles, $\varphi_j(x+\ell,t) = \varphi_j(x,t) + 2\pi\, n_j$ where integers $n_j \in \mathbb{Z}$ specify the mode numbers assigned to each branch cut. Similarly, invariance under translation for a temporal period T implies quantisation of frequencies w_j. Under these extra conditions, coefficients C_{j1} and $(r_1/2)C_{j1} + C_{j2}$ become integer-valued, imposing a non-trivial restriction on the admissible algebraic curves.

Chapter 3

Quantum integrability

> Algebra is generous; she often
> gives more than is asked of her.
>
> Jean-Baptiste de Rond
> d'Alembert

In this chapter we introduce the algebraic Bethe ansatz technique to solve the quantum spin-1/2 XXZ model, a paradigmatic quantum integrable model. The generalisation of the method introduced here will be of vital importance in Chapter 6. Instead of introducing the coordinate Bethe ansatz technique (à la Bethe [18]) first, we construct the transfer matrix formalism of 6-vertex model, a two-dimensional classical statistical mechanical model. In fact, the quantum spin-1/2 XXZ model can be considered as the Hamiltonian limit of 6-vertex model, which will be explained later in this chapter. This is the reminiscence of the correspondence between D-dimensional quantum system and $(D+1)$-dimensional classical system. The transfer matrix constructed for 6-vertex model will play the central rôle in constructing the conserved charges of XXZ model [20].

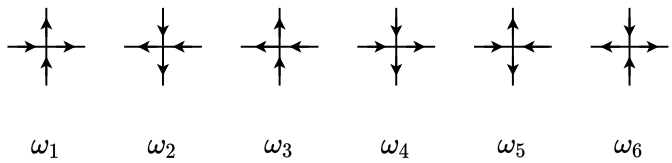

Figure 3.1: Six possible configurations satisfying the ice rule. The weight of each configure is denoted as ω_j, $j = 1, 2 \cdots 6$.

3.1 6-vertex model

We start by defining a statistical mechanical model on a square lattice imposing the so-called "ice rule":
For each vertex, there are two arrows of the edges pointing toward the vertex and the other two arrows of the edges pointing away from the vertex.

This leaves us six possible configurations on each vertex, shown in Fig. 3.1.

In principle, the weights of different types of vertices might differ. We only consider the case when $\omega_1 = \omega_2 = a$, $\omega_3 = \omega_4 = b$, $\omega_5 = \omega_6 = c$, i.e. symmetric 6-vertex model. When all weights are different, i.e. asymmetric 6-vertex model, which can be achieved by acting horizontal and vertical "electric fields" on the vertices. We will not use asymmetric 6-vertex model in the rest of the thesis.

The partition function of the 6-vertex model is written as

$$\mathcal{Z} = \sum_{\text{configurations}} \prod_{\text{vertex}} \omega_{\text{vertex}}. \tag{3.1}$$

Equivalently, we could define the partition function on a $L \times N$ torus as

$$\mathcal{Z} = \text{tr}\mathbf{T}^L, \tag{3.2}$$

where $\mathbf{T}$ is the $2^N \times 2^N$ matrix which corresponds to a periodic strip of N sites, demonstrated in Fig. 3.2.

From the weight configurations in Fig. 3.1, we express the transfer matrix $\mathbf{T}$ as

$$\mathbf{T} = \text{tr}_0(\mathbf{R}_{0N} \cdots \mathbf{R}_{02}\mathbf{R}_{01}), \tag{3.3}$$

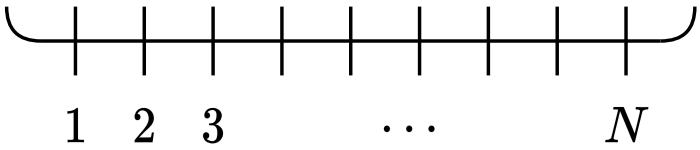

Figure 3.2: A demonstration of transfer matrix of 6-vertex model. It is defined on a periodic strip of N sites.

where $\mathbf{R}_{ij}$ is defined on $(\mathbb{C}^2)^{\otimes(N+1)}$ and acts on the tensor product of i-th and j-th spaces. Matrix $\mathbf{R}$ in terms of the weights reads

$$\mathbf{R} = \begin{pmatrix} a & 0 & 0 & 0 \\ 0 & b & c & 0 \\ 0 & c & b & 0 \\ 0 & 0 & 0 & a \end{pmatrix}. \tag{3.4}$$

3.1.1 Integrability: Yang–Baxter relation

We choose a specific parametrisation of the weights, i.e.

$$a = \sinh(\lambda + \eta), \quad b = \sinh\lambda, \quad c = \sinh\eta. \tag{3.5}$$

Two parameters λ and η are enough to parametrise three different weights up to a global scaling factor. We also define two additional parameters independent of λ for later convenience,

$$q = \exp\eta, \quad \Delta = \frac{a^2 + b^2 - c^2}{2ab} = \cosh\eta. \tag{3.6}$$

Remarkably, matrix $\mathbf{R}$ satisfies the renowned *Yang-Baxter relation* [20],

$$\mathbf{R}_{ij}(\lambda - \mu)\mathbf{R}_{ik}(\lambda)\mathbf{R}_{jk}(\mu) = \mathbf{R}_{jk}(\mu)\mathbf{R}_{ik}(\lambda)\mathbf{R}_{ij}(\lambda - \mu), \quad \lambda, \mu \in \mathbb{C}. \tag{3.7}$$

From the Yang–Baxter relation, we apply the "train argument" and obtain the relation

$$[\mathbf{T}(\lambda), \mathbf{T}(\mu)] = 0, \tag{3.8}$$

i.e. we obtain infinitely many commuting operators. We define a set of conserved charges in the 6-vertex model as the logarithmic derivatives of the transfer matrix $\mathbf{T}$, i.e.

$$\mathbf{I}^{(n)} = -\mathrm{i}\,\frac{\mathrm{d}^j}{\mathrm{d}\lambda^j}\log\mathbf{T}(\lambda)\bigg|_{\lambda=0}, \quad n\in\mathbb{N}. \tag{3.9}$$

From the commuting property of transfer matrices (3.8), it is easy to observe that the conserved charges are in involution,

$$\left[\mathbf{I}^{(n)},\mathbf{I}^{(m)}\right] = 0, \quad \forall n,m\in\mathbb{N}. \tag{3.10}$$

3.1.2 Relation to spin-1/2 XXZ model

To begin with, we first define the spin-1/2 XXZ model with periodic boundary condition, a one-dimensional quantum spin chain, as

$$\mathbf{H} = \sum_{j=1}^{N}\left[\frac{1}{2}\left(\sigma_j^+\sigma_{j+1}^- + \sigma_j^-\sigma_{j+1}^+\right) + \frac{\Delta}{4}\left(\sigma_j^z\sigma_{j+1}^z - 1\right)\right], \tag{3.11}$$

where $\sigma_j^\alpha = \mathbb{1}^{\otimes(j-1)}\otimes\sigma_j^z\otimes\mathbb{1}^{\otimes(N-j)}$ are Pauli matrices and $\sigma_{N+1}^\alpha = \sigma_1^\alpha$.

The relation between 6-vertex model and spin-1/2 XXZ model can be readily seen, since

$$\mathbf{I}^{(1)} = -\mathrm{i}\mathbf{T}^{-1}(0)\partial_\lambda\mathbf{T}(0) = \frac{2}{\mathrm{i}\sinh\eta}\left(\mathbf{H} + \frac{\Delta N}{2}\right), \tag{3.12}$$

after identifying that $\Delta = \cosh\eta$ are the same in both models.

From (3.10), we readily identify infinitely many conserved charges in the spin-1/2 XXZ model associated to the transfer matrix $\mathbf{T}(u)$ of 6-vertex model to XXZ model. Furthermore, we define the $2^{N+1}\times 2^{N+1}$-dimensional monodromy matrix $\mathbf{M}$ such that

$$\mathbf{M}_0(\lambda) = \mathbf{R}_{0N}(\lambda)\cdots\mathbf{R}_{02}(\lambda)\mathbf{R}_{01}(\lambda) = \begin{pmatrix}\mathbf{A}(\lambda) & \mathbf{B}(\lambda)\\ \mathbf{C}(\lambda) & \mathbf{D}(\lambda)\end{pmatrix}_0, \tag{3.13}$$

where the transfer matrix (3.3) is the partial trace of monodromy matrix

$$\mathbf{T}(\lambda) = \mathrm{tr}_0\mathbf{M}_0(\lambda) = \mathbf{A}(\lambda) + \mathbf{D}(\lambda). \tag{3.14}$$

The reason why we introduce the monodromy matrix is as follows. The transfer matrix $\mathbf{T}(\lambda)$ contains the information about the spectrum, namely the conserved quantities, which is the diagonal part of the monodromy matrix. As we will show in the next section, the off-diagonal part of the monodromy matrix can actually be used to construct the eigenvectors of the transfer matrix.

3.2 Algebraic Bethe ansatz

From Yang–Baxter relation (3.7), we obtain the "RMM relation", i.e.

$$\mathbf{R}_{ab}(\lambda-\mu)\mathbf{M}_a(\lambda)\mathbf{M}_b(\mu)=\mathbf{M}_b(\mu)\mathbf{M}_a(\lambda)\mathbf{R}_{ab}(\lambda-\mu),\quad \lambda,\mu\in\mathbb{C}. \tag{3.15}$$

This relation essentially guarantees the commuting property of the transfer matrix. Hence, (3.15) ensures the quantum integrability of spin-1/2 XXZ model.

Moreover, from RMM relation (3.15), we can derive the relation between the diagonal and off-diagonal terms, the central object of algebraic Bethe ansatz (ABA),

$$[\mathbf{A}(\lambda),\mathbf{A}(\mu)]=[\mathbf{B}(\lambda),\mathbf{B}(\mu)]=[\mathbf{C}(\lambda),\mathbf{C}(\mu)]=[\mathbf{D}(\lambda),\mathbf{D}(\mu)]=0, \tag{3.16}$$

$$\mathbf{A}(\lambda)\mathbf{B}(\mu)=\frac{\sinh(\lambda-\mu-\eta)}{\sinh(\lambda-\mu)}\mathbf{B}(\mu)\mathbf{A}(\lambda)+\frac{\sinh\eta}{\sinh(\lambda-\mu)}\mathbf{B}(\lambda)\mathbf{A}(\mu), \tag{3.17}$$

$$\mathbf{B}(\lambda)\mathbf{A}(\mu)=\frac{\sinh(\lambda-\mu-\eta)}{\sinh(\lambda-\mu)}\mathbf{A}(\mu)\mathbf{B}(\lambda)+\frac{\sinh\eta}{\sinh(\lambda-\mu)}\mathbf{A}(\lambda)\mathbf{B}(\mu), \tag{3.18}$$

$$\mathbf{B}(\lambda)\mathbf{D}(\mu)=\frac{\sinh(\lambda-\mu+\eta)}{\sinh(\lambda-\mu)}\mathbf{D}(\mu)\mathbf{B}(\lambda)-\frac{\sinh\eta}{\sinh(\lambda-\mu)}\mathbf{D}(\lambda)\mathbf{B}(\mu), \tag{3.19}$$

$$\mathbf{D}(\lambda)\mathbf{B}(\mu)=\frac{\sinh(\lambda-\mu+\eta)}{\sinh(\lambda-\mu)}\mathbf{B}(\mu)\mathbf{D}(\lambda)-\frac{\sinh\eta}{\sinh(\lambda-\mu)}\mathbf{B}(\lambda)\mathbf{D}(\mu), \tag{3.20}$$

and the other relations are not listed here, since we will not use them in most parts of the thesis. They can be found in Ref. [49, 20].

In order to construct the eigenvalues of the transfer matrix, we start with a pseudo vacuum state $|\varnothing\rangle=|\uparrow\uparrow\cdots\uparrow\rangle$ which is an eigenstate of both A and D operators, i.e.

$$\mathbf{A}(\lambda)|\varnothing\rangle=\sinh^N(\lambda+\eta)|\varnothing\rangle,\quad \mathbf{D}(\lambda)|\varnothing\rangle=\sinh^N(\lambda)|\varnothing\rangle. \tag{3.21}$$

In the meantime, $|\varnothing\rangle$ is annihilated by C operator $\mathbf{C}(\lambda)|\varnothing\rangle = 0$. (C operator change the magnetisation by $+1$, and B operator change the magnetisation by -1.) We assume that all eigenstates of XXZ model with M down spins can be written as

$$|\{\lambda_1, \lambda_2, \cdots, \lambda_M\}\rangle := \prod_{j=1}^{M} \mathbf{B}(\lambda_j)|\varnothing\rangle, \tag{3.22}$$

and from the commutation relations above, we can infer the relation that λ_j has to satisfy.

We focus on the following equation,

$$\begin{aligned}[\mathbf{A}(\lambda) + \mathbf{D}(\lambda)] \prod_{j=1}^{M} \mathbf{B}(\lambda_j)|\varnothing\rangle =& \Lambda(\lambda) \prod_{j=1}^{M} \mathbf{B}(\lambda_j)|\varnothing\rangle \\ &+ \sum_{j=1}^{M} \Lambda'_j \mathbf{B}(\lambda) \prod_{k\neq j}^{M} \mathbf{B}(\lambda_k)|\varnothing\rangle,\end{aligned} \tag{3.23}$$

and Λ'_j are the unwanted terms, when $\prod_{j=1}^{M} \mathbf{B}(\lambda_j)|\varnothing\rangle$ is an eigenstate of transfer matrix. By demanding $\Lambda'_j = 0$, we obtain

$$\left(\frac{\sinh(\lambda_j + \eta)}{\sinh \lambda_j}\right)^N = \prod_{k\neq j}^{M} \frac{\sinh(\lambda_j - \lambda_k + \eta)}{\sinh(\lambda_j - \lambda_k - \eta)}. \tag{3.24}$$

We reparametrise the spectral parameter, i.e. $u = \lambda + \eta/2$, and all the arguments in equations above are shifted by $\eta/2$. We obtain

$$\left(\frac{\sinh(u_j + \eta/2)}{\sinh(u_j - \eta/2)}\right)^N = \prod_{k\neq j}^{M} \frac{\sinh(u_j - u_k + \eta)}{\sinh(u_j - u_k - \eta)}. \tag{3.25}$$

The scattering phase between two Bethe roots is thus

$$S(u_j, u_k) = \frac{\sinh(u_j - u_k - \eta)}{\sinh(u_j - u_k + \eta)}, \tag{3.26}$$

by rewriting (3.25) as

$$e^{\mathrm{i}p_j L} \prod_{k\neq j}^{M} S(u_j, u_k) = 1. \tag{3.27}$$

These coupled non-linear equations are known as the *Bethe ansatz equations* for XXZ model, with solution u_j called *Bethe roots*. The (quasi-)energy and (quasi-)momentum of each magnon with Bethe root u_j are

$$\begin{aligned} p_j &= \mathrm{i}\,\log\frac{\sinh(u_j-\eta/2)}{\sinh(u_j+\eta/2)}, \\ E_j &= \cos(p_j)-\Delta = \frac{\sinh^2\eta}{2\,\sinh(u_j+\eta/2)\,\sinh(u_j-\eta/2)}. \end{aligned} \tag{3.28}$$

The total momentum and energy of the eigenstate $|\{u_j\}_{j=1}^M\rangle$ are thus

$$p=\sum_{j=1}^M p_j, \quad E=\sum_{j=1}^M E_j. \tag{3.29}$$

This construction of eigenstates has caveats when $q=\exp\eta$ is at root of unity value. We devote the entire Chapter 6 to study the complete spectrum of XXZ model at root of unity. As we shall show in Chapter 6, Bethe equations are equivalent to Baxter's TQ relation, which is a linear matrix equation, in principle easier to solve compared to (3.25).

The ABA is a very powerful tool to study quantum integrable systems. Notably it can be used to calculate the norm and overlaps between Bethe states $|\{u_j\}\rangle$ in terms of determinants. This allows us to obtain analytical and numerical results for the form factors or correlation functions in the realm of quantum integrable systems. We will not expand on this here. One can find extensive results and discussions in Refs. [20, 49].

Chapter 4

Domain wall quench in the Landau–Lifshitz ferromagnet

The contents of this chapter were published in [1].

In this chapter we aim to study an inhomogeneous quench problem in the classical Landau–Lifshitz model. In general it is rare to obtain exact results on the out-of-equilibrium properties of soliton systems (classical integrable systems) due to the fact that the formal integration scheme cannot be implemented analytically except for a few exceptions. Specifically, we consider the time evolution of the domain-wall initial condition in the Landau–Lifshitz ferromagnet, which enables us to analytically explore the non-equilibrium transport properties using methods developed in Chapter 2. Another motivation lies in the results obtained in the quantum spin-1/2 Heisenberg XXZ ferromagnet, where the time evolution of domain-wall initial state $|\cdots\uparrow\uparrow\downarrow\downarrow\cdots\rangle$ has been investigated. Landau–Lifshitz ferromagnet can be considered as the semi-classical (long-wavelength) limit of the quantum Heisenberg XXZ ferromagnet. With this observation, we discover a remarkable classical-quantum correspondence for the macroscopic spin transport with domain-wall initial condition.

Explicitly, we consider the initial condition

$$\vec{S}(x,t=0) = (\mathrm{sech}(x/x_0), 0, \tanh(x/x_0))^{\mathrm{T}}, \tag{4.1}$$

evolving under the Landau–Lifshitz Hamiltonian (2.4) with anisotropic parameter δ. This is an analogue of the quantum domain-wall state

$|\cdots \uparrow\uparrow\downarrow\downarrow \cdots\rangle$. Instead of being defined in a lattice, the spin field is defined in $\mathbb{R}$. We use hyperbolic functions to imitate the domain-wall property, where ξ denotes the width of the domain wall.

It is worth noting that if we rescale the profile as $x \to xx_0$ and $t \to tx_0^2$, according to the equation of motion (2.1), it is equivalent to the rescaling of the anisotropy $\delta \to \delta x_0^2$. Hence, our quench protocol is equivalent both to quenching the initial profile and quenching the anisotropy parameter δ. Without losing generality, we consider the initial condition with $x_0 = 1$ and arbitrary anisotropy parameter δ.

4.1 Landau–Lifshitz model as semi-classical limit of XXZ model

In this section we show that the classical Landau–Lifshitz model is the semi-classical limit of the quantum Heisenberg XXZ model from the integrability perspective. Equivalently, one may obtain the same result by considering the low energy excitation (spin wave) above the ferromagnetic vacuum in the XXZ model in the spin coherent state formalism. After taking the continuum limit, we would arrive at the classical Landau–Lifshitz model too. This method provides us a physical intuition that the Landau–Lifshitz model can describe the low-energy (long-wavelength) spin wave excitations above the ferromagnetic state of XXZ model. We will not explain the procedure in details[1], and rather focus on the integrability side.

We start with showing how the (classical) Lax connection (2.8) and (2.9) in Chapter 2 can be retrieved from the Lax operator of the quantum model (3.4) in Chapter 3. The fundamental Lax operator $\mathbf{L}(u)$ acts on a one-site (physical) Hilbert space $\mathcal{V}_p \cong \mathbb{C}^2$ of a spin-1/2 degree of freedom and an auxiliary space $\mathcal{V}_a$ associated to the fundamental representation of the quantum group $\mathcal{U}_q(\mathfrak{sl}(2))$ (with deformation parameter $q = e^\eta$), and depends analytically on the complex (spectral) parameter μ. It reads

[1] A detailed derivation can be found in [50].

explicitly

$$\mathbf{L}(u) = \frac{1}{\sinh\eta}\begin{pmatrix}\sinh(u+\eta\mathbf{S}^{\mathrm{z}}) & \sinh\eta\mathbf{S}^{-}\\ \sinh\eta\mathbf{S}^{+} & \sinh(u-\eta\mathbf{S}^{\mathrm{z}})\end{pmatrix}, \tag{4.2}$$

in terms of auxiliary spin generators which enclose the q-deformed commutation relations [2]

$$[\mathbf{S}^{+},\mathbf{S}^{-}] = [2\mathbf{S}^{z}]_q, \quad q^{2\mathbf{S}^{z}}\mathbf{S}^{\pm} = q^{\pm 2}\mathbf{S}^{\pm}q^{2\mathbf{S}^{z}}, \tag{4.3}$$

with the standard notation $[x]_q = \frac{q^x - q^{-x}}{q-q^{-1}}$.

The fundamental row transfer matrix of the quantum XXZ spin chain is given in (3.3), and we rewrite it here,

$$\mathbf{T}(u) = \mathrm{Tr}_{\mathcal{V}_a}\,\mathbf{M}(u) = \mathrm{Tr}_{\mathcal{V}_a}\mathbf{L}_{aN}(u)\cdots\mathbf{L}_{a2}(u)\cdots\mathbf{L}_{a2}(u). \tag{4.4}$$

By virtue of the quantum Yang–Baxter relation, matrices $\mathbf{T}(u)$ mutually commute, $[\mathbf{T}(u),\mathbf{T}(u')] = 0$ for all $u,u' \in \mathbb{C}$. Therefore, commuting transfer matrices serve as the generating operator for the local (and nonlocal) conserved charges [49, 13]. An infinite tower of commuting fused transfer matrices $T_j(u)$ with $(2j+1)$-dimensional auxiliary unitary representations of $\mathcal{U}_q(\mathfrak{sl}(2))$ can be constructed in a similar manner, providing additional quasilocal conservation laws of the XXZ model. While these are of utmost importance for thermodynamic properties at finite energy density (see e.g. Refs. [51, 52, 34, 53]), they do not play any role upon taking the semi-classical limit.

We take the asymptotic scaling limit $L \to \infty$ at the level of the transfer matrix by parametrising the interaction parameter as $\eta = \epsilon\,\ell/L \to 0$ and subsequently taking $\eta \to 0$ $(q \to 1)$. We will consider either $\ell \to \infty$ in this chapter or $\ell \in \mathcal{O}(1)$ in Chapter 5. As we will see, ℓ has the physical meaning of classical circumstance. In this case we are allowed to substitute the q-deformed spin generators with the fundamental $\mathfrak{sl}(2)$ spins, $\mathbf{S}^{\alpha} \to \hat{S}^{\alpha} = \frac{1}{2}\sigma^{\alpha}$ for $\alpha \in \{\mathrm{x},\mathrm{y},\mathrm{z}\}$. The diagonal elements of the quantum Lax operator become

$$\lim_{\eta\to 0}\frac{\sinh(u\mathbb{1}+\eta\mathbf{S}^{\mathrm{z}})}{\sinh\eta} = \frac{\sinh u}{\eta}\mathbb{1} + \cosh(u)\hat{S}^{\mathrm{z}} + \mathcal{O}(\eta), \tag{4.5}$$

[2] Discussions about different Lax operators for quantum XXZ model can be found in Chapter 6.

while

$$\mathbf{L}(u) \simeq \frac{\sinh u}{\eta}\left[\mathbb{1} + \eta \begin{pmatrix} \coth(\mu)\hat{S}^{\mathrm{z}} & \operatorname{csch}(\mu)\hat{S}^{-} \\ \operatorname{csch}(u)\hat{S}^{+} & -\coth(u)\hat{S}^{\mathrm{z}} \end{pmatrix}\right]. \tag{4.6}$$

By reinstating the lattice spacing $a = \ell/L$ and using the spectral parameter

$$\mu = \frac{\epsilon}{\tanh u}, \tag{4.7}$$

the Lax matrix reads

$$\mathbf{L}(\mu) \simeq \frac{1}{a\sqrt{\mu^2+\delta}}\left[\mathbb{1} + \mathrm{i}a \begin{pmatrix} \mu\hat{S}^{\mathrm{z}} & \sqrt{\mu^2+\delta}\hat{S}^{-} \\ \sqrt{\mu^2+\delta}\hat{S}^{+} & -\mu\hat{S}^{\mathrm{z}} \end{pmatrix}\right], \tag{4.8}$$

whereas the asymptotic scaling limit of the associated monodromy matrix $\mathbf{M}(\mu)$ is given by the following path-ordered product

$$\frac{\mathbf{M}(\mu)}{(a\sqrt{\mu^2+\delta})^L} \sim \prod_{j=L}^{1}\left[\mathbb{1} + \mathrm{i}a \begin{pmatrix} \mu\hat{S}^{\mathrm{z}}_j & \sqrt{\mu^2+\delta}\,\hat{S}^{-}_j \\ \sqrt{\mu^2+\delta}\,\hat{S}^{+}_j & -\mu\,\hat{S}^{\mathrm{z}}_j \end{pmatrix}\right]. \tag{4.9}$$

In the final step we replace the quantum spins $\hat{S}^{\alpha}$ with classical spin variables via $\mathcal{S}^{\alpha}_j \equiv \mathcal{S}^{\alpha}(x = j\,a)$, and subsequently take the continuum limit. We thus arrive as the following semi-classical approximation of the quantum monodromy matrix

$$\mathbf{M}_{\mathrm{cl}}(\mu) \equiv \mathcal{P}\exp\left[\frac{\mathrm{i}}{2}\oint_0^{\ell}\frac{\mathrm{d}x}{2\pi}\mathbf{U}(\mu;x,t)\right], \tag{4.10}$$

with $\mathbf{U}(\mu;x,t)$ being the spatial component of the Lax connection introduced earlier in Eq. (2.8).

4.2 Properties of the scattering data

In Chapter 2, we obtained the scattering data for a domain wall profile,

$$\begin{aligned} a(\mu,0) &= \frac{\sqrt{\mu^2+\epsilon^2}\boldsymbol{\Gamma}^2\left(\frac{1}{2}-\frac{\mathrm{i}}{2}\mu\right)}{2\boldsymbol{\Gamma}\left(1-\frac{\mathrm{i}}{2}(\mu+\mathrm{i}\epsilon)\right)\boldsymbol{\Gamma}\left(1-\frac{\mathrm{i}}{2}(\mu-\mathrm{i}\epsilon)\right)}, \\ b(\mu,0) &= \mathrm{i}\frac{\cos(\frac{\pi}{2}\epsilon)}{\cosh(\frac{\pi}{2}\mu)}. \end{aligned} \tag{4.11}$$

When $\delta \leq 0$, i.e. $\epsilon \in \mathrm{i}\mathbb{R}$, scattering data $a(\mu)$ has no zeros in the upper half plane. This means that the domain wall profile (4.1) contains only radiation modes and no soliton.

However, when $\delta > 0$, i.e. $\epsilon \in \mathbb{R}/\{0\}$, scattering data $a(\mu)$ always has zero(s) in the upper half plane, implying the existence of the soliton(s) in the domain wall profile (4.1). Furthermore, when $\epsilon = 2j - 1$ with $j \in \mathbb{Z}$, $b(\mu) = 0$. In that scenario, the domain wall profile consists of only soliton(s)!

Using the uniformisation parameter z, in the case of $b(\mu) = 0$, we have

$$a(z) = \mathrm{i}\frac{z - \mathrm{i}|\epsilon|}{z + \mathrm{i}|\epsilon|} \prod_{m=1}^{(|\epsilon|-1)/2} \frac{z^2 + \epsilon^2 - 2\mathrm{i}z(2m-1)}{z^2 + \epsilon^2 + 2\mathrm{i}z(2m-1)}. \tag{4.12}$$

We will analyse the soliton spectrum in details in Sec. 4.5.

4.3 Easy-plane regime: hydrodynamics

The absence of zeros of $a(\mu)$ in the upper half μ plane for the easy-plane regime ($\delta < 0$) means that the spectrum comprises only a dispersive continuum of radiative modes. We find ballistic spin transport in this case, as exemplified in the first panel of Fig. 4.2. The emergence of ballistic spin transport can be explained without using the non-linear transformation of classical inverse scattering transformation. Instead, we make the hydrodynamic approximation of the equation of motion (2.1), which reveals the leading order of the spin transport.

We start with introducing two slow variables S^{z} and $v = -\mathrm{i}(\log S^{+})_x$. We use shorthand notation $(\cdots)_x := \partial_x \cdots$ here. We recast the equation of motion (2.1) into

$$S^{\mathrm{z}}_t - \left(\left[1 - (S^{\mathrm{z}})^2\right] v\right)_x = 0, \quad v_t + \left((\varepsilon^2 + v^2) S^{\mathrm{z}}\right)_x = R, \tag{4.13}$$

where the non-linear coefficient R satisfies

$$R = \left[\left(\frac{S^{\mathrm{z}}_x}{\sqrt{1 - (S^{\mathrm{z}})^2}}\right)_x \frac{1}{\sqrt{1 - (S^{\mathrm{z}})^2}}\right]_x. \tag{4.14}$$

Neglecting the non-linear coefficient R, we obtain

$$\begin{pmatrix} S^{\mathrm{z}} \\ v \end{pmatrix}_t = \begin{pmatrix} -2S^{\mathrm{z}}v & 1-(S^{\mathrm{z}})^2 \\ -\varepsilon^2 - v^2 & -2S^{\mathrm{z}}v \end{pmatrix} \begin{pmatrix} S^{\mathrm{z}} \\ v \end{pmatrix}_x . \tag{4.15}$$

This WKB-type approximation can alternatively be viewed as the simplest case of a more general Whitham theory describing modulation of multiphase solutions to nonlinear wave equations.

Next, we would like to bring the Whitham-like equation (4.15) into the Riemann diagonal form

$$\partial_t r_\pm(x,t) + V_\pm(x,t)\partial_t r_\pm(x,t) = 0 \tag{4.16}$$

through diagonalising the 2×2 matrix in (4.15). We have

$$\begin{aligned} r_\pm &= S^{\mathrm{z}}v \pm \sqrt{[1-(S^{\mathrm{z}})^2](\varepsilon^2 - v^2)}, \\ V_+ &= \frac{r_-}{2} + \frac{3r_+}{2}, \quad V_- = \frac{r_+}{2} + \frac{3r_-}{2}. \end{aligned} \tag{4.17}$$

The absence of scale in the initial profile motivates us to seek a self-similar solution depending on the ray coordinate $\xi = x/t$, which yields the hydrodynamic equation

$$[V_\pm(\xi) - \xi]\partial_\xi r_\pm(\xi) = 0. \tag{4.18}$$

In order to solve the hydrodynamic equation, we need to provide appropriate boundary conditions. In the domain-wall case, we have

$$S^{\mathrm{z}}(\xi_\pm) = \pm 1, \quad v(\xi_\pm) = v_0 = \mathrm{const}, \tag{4.19}$$

with $\xi_\pm$ being the boundaries of the ballistically expanding region connecting two vacua ($S^{\mathrm{z}}(+\infty) = +1$ and $S^{\mathrm{z}}(-\infty) = -1$). Inside the ballistic region the solution reads

$$S^{\mathrm{z}}(\xi) = \frac{\xi}{2|\epsilon|}, \quad v = |\epsilon| = v_0, \qquad \xi_\pm = \pm 2|\epsilon|, \tag{4.20}$$

which implies linear growth of magnetisation, cf. Fig. 4.2. Integrating along the x axis, we have the magnetisation profile

$$m(t) \simeq t\int_0^{2|\epsilon|} \mathrm{d}\xi\,(1 - S_{\mathrm{z}}(\xi)) = |\epsilon|t, \tag{4.21}$$

signalling the ballistic spin transport. The density of states $\rho(\mu) = \log|a(\mu)|^2$ develops a singularity at $\mu_* = |\epsilon|$, which defines a natural scale in the spectrum. The velocity of the hydrodynamic region is nothing but the velocity of the critical dispersive modes $V_* = 2\mu_* = |\xi_\pm|$.

The non-trivial solution at the Euler scale (depending only in variable $\xi = x/2$) exists only strictly in the easy-plane regime $\delta = \epsilon^2 < 0$, whereas for $\delta = \varepsilon^2 \geq 0$ the hydrodynamic solution trivializes, implying sub-ballistic transport that cannot be captured by the hydrodynamic approximation. We need to fully take into account the effect of non-linearity of the equation of motion (2.1) for isotropic and easy-axis regimes.

4.4 Isotropic regime: log-enhanced diffusion

For $\epsilon = 0$, the density of states $\rho(\mu)$ diverges logarithmically at $\mu \to 0$, since $a(0) = 0$ when $\delta = 0$. As we demonstrate, this turns out to be an artefact of the specific domain-wall profile with perfectly anti-parallel asymptotic spin fields ($S^z(\pm\infty) = \pm 1$). For this reason, we now consider a deformed profile $\vec{S} = (\cos\Phi, 0, \sin\Phi)^{\mathrm{T}}$, where $\Phi = (\gamma/\pi)\arcsin(\tanh x)$ with the 'twisting angle' $\gamma \in [0, \pi)$. We recover the anti-parallel domain wall profile (4.1) in the limit $\gamma \to \pi$. The induced correction to the scattering data for $\gamma \approx \pi$, computed with the first order perturbation theory, displaces the zero of $a(\mu)$ at the origin, $a(0) \approx \mathrm{i}(\pi - \gamma)/2$, rendering the density of states $\rho(\mu)$ finite.

At the isotropic point, there is a unique class of self-similar solutions to equations of motion (2.1) which depend on the scaling variable $\zeta = x/\sqrt{t}$, governed by an ODE [54],

$$-2\zeta\vec{S}_\zeta = \vec{S} \times \vec{S}_{\zeta\zeta}, \tag{4.22}$$

which has been studied in the context of the vortex filament dynamics [55]. For initial conditions with a jump discontinuity at the origin, Eq. (4.22) can be solved analytically. For large times, we observe that the twisted domain wall approaches the self-similar profile. The latter manifestly

yields normal spin diffusion $m(t) \sim \mathfrak{D}(\gamma)\sqrt{t}$. The diffusion constant [3] $\mathfrak{D}(\gamma)$ plays a role of the filament curvature and can be approximated as $c\sqrt{E}$, with $c = \sqrt{2}(\pi - 2\log(\sqrt{2}+1)) \approx 2$ and $E = \vec{S}_\zeta^2$ being the conserved energy [56]. Using relation $e^{-\pi E/2} = \cos(\gamma/2)$, we conclude that $\mathfrak{D}(\gamma)$ diverges as $\gamma \to \pi$, explaining the breakdown of normal diffusion for the untwisted profile (4.1). Diverging diffusion coefficient hints at superdiffusive behaviour of the spin transport.

In order to quantify it, we have implemented an efficient numerical solver of the inverse (GLM) transform explained in Sec. 2.2.2. The numerical data indicates a mild logarithmic (in time) divergence of $m(t)$ (cf. Fig. 4.1, inset plot), which nicely conforms with the type of singularity in the density of states. The twist of the boundary conditions removes the singularity and restores normal spin diffusion, as shown in Fig. 4.1.

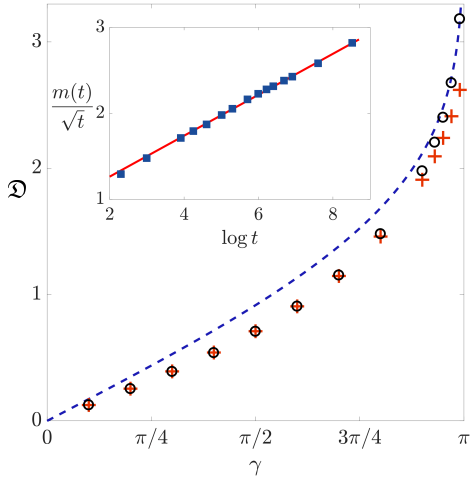

Figure 4.1: Spin diffusion constant $\mathfrak{D}(\gamma)$ as a function of the twisting angle γ, shown for the self-similarity solutions (open circles) and numerical integration up to $t = 2000$ (red crosses). The blue dashed line shows the leading term in the large-E asymptotic expansion of the self-similar solution. Inset: Numerical solution to the inverse scattering transform of the untwisted domain wall profile (4.1).

[3] This definition of the diffusions constant should not be confused with that of the Kubo linear response theory.

4.5 Easy-axis regime: stable kink

In distinction to the previous two regimes, the scattering data $a(\mu)$ acquire an additional discrete component (zeros at the upper half plane), which corresponds to the (multi)soliton modes. The simplest among them are static (anti)-kink modes with topological charge $Q = \pm 1$, which coincide with domain wall (4.1) for $x_0 = 1$ and $\delta = \epsilon = 1$. In this case, we have

$$a(z) = \mathrm{i}\frac{z - \mathrm{i}}{z + \mathrm{i}}, b(z) = 0. \tag{4.23}$$

From inverse scattering calculation, we find that the spin field is time independent, i.e.

$$\vec{S}(x,t) = \vec{S}(x,0) = (\operatorname{sech} x, 0, \tanh x)^{\mathrm{T}}. \tag{4.24}$$

We will discuss the manifestation of the static kink in the periodic case in Chapter 5.

The kink persists in the spectrum for all $\delta > 0$. Besides solitons, the spectrum involves a continuous spectrum of radiative modes, which, however, vanish for the the discrete set of 'reflectionless anisotropies' $\epsilon = (2m - 1)$, $m \in \mathbb{Z}$. The analyticity of $a(\mu)$ can be restored with the uniformization map, $\mu(z) = (z - \epsilon^2 z^{-1})/2$.

The spectrum of the domain wall (4.1) does not involve any asymptotically free solitons, implying the absence of ballistic transport. Therefore, the asymptotic scaling $m(t) \sim t^0$ is a consequence of the finite difference between the domain wall profile and the stable kink, i.e. the radiation modes. For instance, on the interval $0 < \varepsilon < 3\mathrm{i}$, the kink is the only soliton mode and the steady state of the domain wall dynamics in the limit $t \to \infty$. On the other hand, for larger values of anisotropy we obtained an infinite family of bound states which undergo periodic oscillatory motion, the existence of breathers. Such solutions have not been explicitly described previously in the literature [57, 58, 59, 60], but similar 'wobbling kinks' have been already identified in the sine–Gordon model [61, 62, 63, 64].

Let us focus on the case with $\epsilon = 3$ and $x_0 = 1$. The scattering data

can be extracted from (2.26),

$$a(z) = \mathrm{i}\frac{(z-3\mathrm{i})(z^2-2\mathrm{i}z+9)}{(z+3\mathrm{i})(z^2+2\mathrm{i}z+9)} = \mathrm{i}\frac{z-z_0}{z+z_0}\frac{z-z_+}{z-\bar{z}_+}\frac{z-z_-}{z-\bar{z}_-}, \qquad b(z)=0, \tag{4.25}$$

where $z_0 = 3\mathrm{i}$, $z_\pm = \mathrm{i} \pm 2\sqrt{2}$.

Solving the Goursat equations (2.32), (2.33) and (2.34) which become algebraic with only solitons in the spectrum, we obtain the solution describing the kink-breather bound state that can be compactly parametrised by a complex stereographic angle φ,

$$S^z = \frac{1-|\varphi|^2}{1+|\varphi|^2}, \qquad S^x + \mathrm{i}S^y = \frac{2\varphi}{1+|\varphi|^2}, \tag{4.26}$$

where

$$\varphi = \frac{e^{\eta_0} + e^{\eta_+} + 2e^{\eta_-}}{1 + 2e^{\eta_0+\eta_-} + e^{\eta_0+\eta_+}}. \tag{4.27}$$

The phases $\eta_i(x,t) = \mathrm{i}(k_i x + \omega_i t)$ and $k_0 = -3\mathrm{i}$, $\omega_0 = 0$, and $k_\pm = \pm\mathrm{i}$ and $\omega_\pm = k_\pm^2 - \varepsilon^2 = -10$ are determined from the scattering data (4.25). This wobbling kink solution is plotted in the third panel of Fig. 4.2, with oscillatory period $T = \frac{2\pi}{|\omega_\pm|} = \frac{\pi}{5}$.

4.6 Classical-quantum correspondence

The quantum integrable (lattice) counterpart to the equation of motion (2.1) is the quantum spin-1/2 XXZ model (3.11), as explained in Sec. 4.1. The time-evolution following a sharp magnetic domain and its dependence on anisotropy Δ has already been a subject of study in the past [65, 66, 36, 67, 68, 69, 70].

In the remainder of this chapter, we would like to elaborate on the perfect *qualitative* agreement in the spin dynamics of the classical and quantum anisotropic ferromagnets, in spite of rather discernible differences in the respective microscopic dynamics: the spectrum of excitations of quantum dynamics (classified in [71, 72]) consists of magnons (and bound states) carrying a quantised amount of spin, whereas classical dynamics corresponds to the semi-classical long-wavelength spectrum of large spin-coherent states [73, 74, 13, 75].

In order to facilitate the comparisons, we review the key known results. Ballistic expansion of the magnetic domain wall in the gapless regime $|\Delta| < 1$ has been first computed numerically using the hydrodynamic theory for quantum integrable models [36] and latter obtained analytically in [67]. The dynamical freezing of the magnetic domain wall in the gapped regime $|\Delta| > 1$ has been reported in [65, 68, 69]. In fact, the observed effect is once again a consequence of stable topological kink vacua, representing an inhomogeneous (infinite-volume) ground states with a finite spectral gap [76, 77, 78, 79] (which become unstable at $\Delta = 1$). At the isotropic point, the observed logarithmically enhanced diffusion law in the isotropic Landau–Lifshitz model (cf. Fig. 4.1 and the second panel of Fig. 4.2) appears to be compatible with the state-of-the-art numerical study [69]. In the meantime, the same type of correction has been found in the asymptotic behaviour of the return probability amplitude for the domain wall initial state [80] too. Our twisted domain wall profile should be understood as a classical analogue of the tilted domain wall product states employed in [70] which also exhibit normal spin diffusion.

Comparing to the results in the previous sections, and noticing the relation between classical anisotropic parameter δ and quantum counterpart Δ, it is remarkable that the spin transport in all three regimes (easy-plane, isotropic and easy-axis) behaves qualitatively the same as the quantum cases, strongly supported by the numerical results in previous works. It is thus convincing to expect such classical-quantum correspondence holds even quantitatively. We explore this direction in the easy-axis regime, where we study the stable kink after the semi-classical quantisation in Chapter 5.

Although in this chapter we concentrated on the spin transport dynamics in the far-from-equilibrium regime (with domain wall initial condition), there exists other evidence that the classical-quantum correspondence holds also in thermal equilibrium in the conventional framework of linear response theory. The thermal spin diffusion constant (at half filling) in the classical lattice Landau–Lifshitz model (the lattice version of Landau–Lifshitz model studied here) – defined via the thermal average of the time-dependent auto-correlation $C(t) = \langle J(0)J(t)\rangle/L$ of the spin current $J(t)$ – has been numerically investigated in [81], where three distinct regimes have been identified: ballistic transport with a finite Drude

weight $\mathcal{D} = \lim_{t\to\infty} C(t)$ in the easy-plane regime, normal diffusion with finite $D = \lim_{t\to\infty} \int_0^t C(t')\mathrm{d}t'$ in the easy-axis regime, and superdiffusion with a time-dependent diffusion constant $D(t) \sim t^{1/3}$ at the isotropic point. In the quantum spin-1/2 XXZ model, the picture remains qualitatively the same: in the easy-plane regime ($|\Delta| < 1$), the finite spin Drude weight has been attributed to quasi-local conservation laws [82, 53] (also see discussions in Chapter 6) and computed exactly in [40, 41] using the generalised hydrodynamics for quantum integrable models [35, 36]. In the easy-axis regime ($|\Delta| > 1$) one finds normal diffusion, theoretically explained in [42]. Finally, the divergence of the spin diffusion constant at the isotropic point (at finite temperature and half filling) has been established in [43]. Numerical simulations [68] provide a convincing evidence for super-diffusion with the Kardar-Parisi-Zhang (KPZ) dynamical exponent $\alpha = 2/3$, later theoretically justified with the aid of a dimensional analysis in [44].

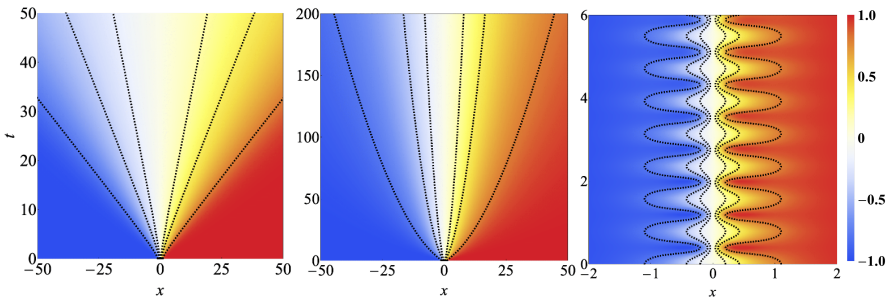

Figure 4.2: Time-dependent density profiles of S^z component in the easy-plane $\delta = -1$ (left), isotropic $\delta = 0$ (middle) and easy-axis $\delta = 9$ (right) regimes, displaying ballistic spin transport, logarithmically enhanced diffusion and absence of transport, respectively. The dashed lines show $|S^z| = \{0.2, 0.4, 0.8\}$.

4.7 Summary of results

We studied the spin transport in the anisotropic Landau–Lifshitz ferromagnet initialised in the domain wall profile, summarised in Fig. 4.2. We

calculated the exact spectrum of nonlinear normal modes analytically and expressed the time-evolved spin field as a solution of the inverse scattering transformation.

In the easy-plane regime we observe a ballistic expansion of the magnetisation profile, which, to the leading order, can be captured by a Riemannian hydrodynamic theory.

For the isotropic interaction, we rigorously established a divergent spin diffusion constant and explain the origin of the a modified diffusion law with a multiplicative logarithmic correction. The effect is shown to be a particularity of the initial state and can be regularized by a twist of the boundary conditions which restores normal diffusion. Such a 'π-anomaly' can be understood as an 'infrared catastrophe' due to a logarithmic divergence of the mode occupation function in the low-energy $\lambda \to 0$ limit.

In the easy-axis regime, the spectrum of the domain wall acquires non-trivial topologically charged (multi)soliton states which consists of breather modes superimposed on a kink. It remains an interesting open question whether wobbling kinks survive quantization, similar to the problem of quantum stability of cnoidal waves addressed in [75]. Analytic continuation into the easy-plane phase, $\varepsilon \to -\mathrm{i}\varepsilon$, can also be understood as destabilization of the kink mode into a dynamical domain wall.

Chapter 5

Semi-classical quantisation of magnetic solitons in Landau–Lifshitz model

The contents of this chapter were published in [2, 3].

In this chapter, we will take the semi-classical limit of the Bethe ansatz equations of quantum spin-1/2 XXZ model, obtaining asymptotic Bethe ansatz equations, which is equivalent to the equations that quasi-momentum of finite-gap solution in classical Landau–Lifshitz model. This construction reveals the connections between the spectral problem of classical Landau–Lifshitz model and the distribution of Bethe roots of spin-1/2 XXZ model. Moreover, the corresponding semi-classical eigenstates of the quantum model can be considered as the quantised non-linear spin waves of the classical counterpart. This leads to a quantitative description of the classical-quantum correspondence in Chapter 4. The study of semi-classical eigenstates of quantum integrable lattice models has been initiated in [73, 74], and the method is often referred to as *Asymptotic Bethe ansatz* [83]. In recent years, asymptotic Bethe ansatz has drawn lots of attention originated from the AdS/CFT integrability side [13], which has been proven to be a crucial tool to study the correlation functions in four-dimensional supersymmetric Yang-Mills gauge theories. In fact, the semi-classical limit of quantum isotropic XXX model is of particular interest [13, 75], due to its close relation to the $SU(2)$ sector of $\mathcal{N} = 4$ supersymmetric gauge theories. We extend the study of the isotropic case to

the anisotropic case, i.e. the semi-classical limit of quantum XXZ model, which can be equivalently considered to be the semi-classical quantisation of the classical anisotropic Landau–Lifshitz model.

We only consider the case with $|\Delta| > 1$ in this chapter. We will focus on the finite-gap solutions which only involves finitely many degrees of freedom. In particular, we aim to bring further understanding of the bion solution which becomes static kink described in Chapter 4 in the soliton limit. In the regime $0 < |\Delta| < 1$, the bion solution does not exist, similar to the non-existence of static kink in the domain-wall quench in the same regime.

5.1 Semi-classical limit of Bethe ansatz equations: asymptotic Bethe ansatz

We start from the Bethe ansatz equations (3.25), where we use spectral parameter $\vartheta = -\mathrm{i}u$, i.e.

$$\left[\frac{\sin(\vartheta_j + i\frac{\eta}{2})}{\sin(\vartheta_j - i\frac{\eta}{2})}\right]^L \prod_{k\neq j}^{M} \frac{\sin(\vartheta_j - \vartheta_k - i\eta)}{\sin(\vartheta_j - \vartheta_k + i\eta)} = 1, \tag{5.1}$$

The total momentum and energy of an eigenstate are obtained by summing over all the constituent magnons, yielding manifestly additive expressions of the form

$$P\big(\{\vartheta_j\}_M\big) = \sum_{j=1}^{M} p(\vartheta_j), \quad E\big(\{\vartheta_j\}_M\big) = \sum_{j=1}^{M} \frac{\sin^2 \mathrm{i}\eta}{\cos 2\vartheta_j - \cos \mathrm{i}\eta}, \tag{5.2}$$

with pseudo-momentum of each magnon defined as

$$p(\vartheta) = -\mathrm{i}\log \frac{\sin(\vartheta + \mathrm{i}\frac{\eta}{2})}{\sin(\vartheta - \mathrm{i}\frac{\eta}{2})}. \tag{5.3}$$

We introduce the Q function (polynomial) of any eigenstate $|\{\vartheta_j\}\rangle$,

$$Q(\vartheta; \{\vartheta_j\}) = \prod_{j=1}^{M} \sin\left(\vartheta - \vartheta_j\right), \tag{5.4}$$

which is proportional to the eigenvalue of the Q operator, which will be crucial in Chapter 6. Here we use the notation

$$f^{[\pm j]}(\vartheta) = f(\vartheta \pm \mathrm{i}j\eta/2) \tag{5.5}$$

for the simplicity of the derivations.

Q function is a 'trigonometric polynomial' of degree M whose zeros correspond precisely to the Bethe roots of a given eigenstate. Denoting $Q_0(\vartheta) \equiv \sin^L(\vartheta)$, and making use of compact notations for imaginary shifts, $f^{[\pm k]}(\vartheta) \equiv f(\vartheta \pm \mathrm{i}\eta/2)$, the Bethe equations can be presented in the form

$$\frac{Q_0^+(\vartheta_j)}{Q_0^-(\vartheta_j)} = \frac{Q_j^{[+2]}(\vartheta_j)}{Q_j^{[-2]}(\vartheta_j)}, \tag{5.6}$$

where $Q_j(\vartheta) \equiv \prod_{k\neq j}^{M} \sin(\vartheta - \vartheta_k)$. In an equivalent logarithmic form, we have

$$\log Q_0^+(\vartheta_j) - \log Q_0^-(\vartheta_j) = 2n_j\pi\mathrm{i} + \log Q_j^{[+2]}(\vartheta_j) - \log Q_j^{[-2]}(\vartheta_j). \tag{5.7}$$

The above form is universal and provides a useful starting point to obtain the semi-classical limits in many other quantum integrable models.

5.1.1 Derivation of asymptotic Bethe ansatz equations

In order to derive the asymptotic Bethe ansatz equations, we need to start with a small parameter that can be effectively treated as the "$\hbar$". We start with a low-energy scaling limit (with respect to the ferromagnetic vacua) by taking the number of sites $L \to \infty$ and number of magnons $M \to \infty$ while demanding that all magnons have low momentum $\sim \mathcal{O}(1/L)$. In this limit, we have only finitely many $m \sim \mathcal{O}(1)$ macroscopic bound states. This low-energy effective limit is different from the conventional thermodynamic limit, where the number of bound states $m \sim \mathcal{O}(L)$.

This low-energy eigenstates have been first investigated by Sutherland [73] and afterwards also in [74], where they are dubbed as 'quantum Bloch walls'. Their classical nature has been elucidated in [13], establishing an explicit connection with (nonlinear) spin waves governed by the continuous Landau–Lifshitz ferromagnet with isotropic interaction.

The method outlined in [13, 75] can be extended to accommodate also for the interaction anisotropy. In the presence of the interaction anisotropy η, the thermodynamic scaling limit that governs the semi-classical spectrum of low-energy eigenstates requires to additionally assume that anisotropy is weak, $\Delta \gtrsim 1$. After reinstating lattice spacing a and writing $\ell \equiv L\,a \in \mathcal{O}(1)$, we can express the anisotropy parameter $\eta \sim \mathcal{O}(1/L) \to 0$ as

$$\eta = \frac{\epsilon\,\ell}{L} + \mathcal{O}\left(\frac{1}{L^2}\right), \tag{5.8}$$

with parameter

$$\epsilon \equiv \sqrt{\delta}, \qquad \delta = \frac{2(\Delta - 1)}{a^2} \in \mathcal{O}(1), \tag{5.9}$$

kept fixed while taking the continuum thermodynamic limit, $L \to \infty$ and $a \to 0$. The same limit has been discussed in Sec. 4.1 when considering Landau–Lifshitz model as semi-classical limit of quantum XXZ model. Here parameter ℓ plays the role of a length, corresponding to the circumference of the emergent classical phase space.

Expanding the logarithm of $Q_0^{\pm}$, we obtain

$$\begin{aligned}\log Q_0^{\pm}(\vartheta_j) = &\log Q_0(\vartheta_j) \pm \frac{i\eta}{2}\frac{\mathrm{d}}{\mathrm{d}\vartheta}\log Q_0(\vartheta)|_{\vartheta=\vartheta_j} \\ &- \frac{\eta^2}{8}\frac{\mathrm{d}^2}{\mathrm{d}\vartheta^2}\log Q_0(\vartheta)|_{\vartheta=\vartheta_j} + \mathcal{O}\left(\frac{1}{L^2}\right),\end{aligned} \tag{5.10}$$

where we have assumed that $\vartheta \in \mathcal{O}(1)$. It is convenient to perform a change of variable by introducing new spectral parameter

$$\mu = \frac{\eta}{\ell}\frac{\mathrm{d}}{\mathrm{d}\vartheta}\log Q_0(\vartheta) = \frac{\epsilon}{\tan\vartheta}, \qquad \mu_j = \lim_{\vartheta\to\vartheta_j}\mu. \tag{5.11}$$

We rewrite the expansion using the new spectral parameter μ,

$$\log Q_0^{+}(\vartheta_j) - \log Q_0^{-}(\vartheta_j) = \mathrm{i}\ell\mu_j + \mathcal{O}\left(\frac{1}{L^2}\right). \tag{5.12}$$

The part involving $Q(\vartheta)$ can be treated analogously. By combining the two contributions, we finally arrive at the following compact repre-

sentation in the μ-variable

$$\mu_j = \frac{2\pi}{\ell} n_j - \frac{2}{L} \sum_{k \neq j}^{M} \frac{\mu_j \mu_k + \delta}{\mu_j - \mu_k} + \mathcal{O}\left(\frac{1}{L}\right). \tag{5.13}$$

Taking the low-energy scaling limit, the Bethe roots μ_j condense along certain one-dimensional segments (contours). In general, there are several disjoint contours $\mathcal{C} \equiv \cup_j \mathcal{C}_j$. Accordingly, the Bethe equations turn into singular integral equations of the form

$$\frac{\ell \mu}{2} = \pi n_j - \ell \fint_{\mathcal{C}} \mathrm{d}\lambda \, \mathcal{K}_\delta(\mu, \lambda) \rho(\lambda), \qquad \mu \in \mathcal{C}_j, \tag{5.14}$$

with integral kernel

$$\mathcal{K}_\delta(\mu, \lambda) \equiv \frac{\mu\lambda + \delta}{\mu - \lambda}. \tag{5.15}$$

Eqs. (5.14) are known as the *asymptotic Bethe ansatz equations* (ABE). To satisfy the reality constraint, the Bethe roots must appear in complex-conjugate pairs, implying that contours $\mathcal{C}_j$ are symmetric under reflection about the real axis. The leading correction term to Eq. (5.13) is of the order $\mathcal{O}(1/L)$, derived in Appendix B

$$\frac{1}{L} \pi \rho'(\mu) \ell^2 (\mu^2 + \delta)^2 \coth\left[\pi \ell (\mu^2 + \delta) \rho(\mu)\right]. \tag{5.16}$$

The correction to Eqs. (5.14) can be neglected only when

$$\pi \ell (\mu^2 + \delta) \rho(\mu) \neq \mathrm{i}\pi n, \qquad n \in \mathbb{Z}, \tag{5.17}$$

i.e. the density of roots near the real axis is sufficiently low. In contrast, when the density of Bethe roots is high enough, the assumptions underlying the above perturbative expansion are no longer justified and one has to solve the full quantum Bethe equations non-perturbatively. We study this non-perturbative behaviour in Sec. 5.4.2 and examine it closely on a specific class of solutions. As it turns out, the effect is responsible for emergence of certain special features in the solutions called *condensates* [13, 75].

The asymptotic Bethe ansatz equations (5.14) can be formulated as a Riemann-Hilbert problem. We define the *spectral resolvent*

$$G(\mu) = \ell \int_{\mathcal{C}} \mathrm{d}\lambda \mathcal{K}_\delta(\mu, \lambda)\rho(\lambda), \tag{5.18}$$

and define

$$\mathfrak{p}(\mu) = G(\mu) + \frac{\ell\mu}{2}. \tag{5.19}$$

At every point μ along the density contour $\mathcal{C}_j$ function $\mathfrak{p}(\mu)$ experiences a jump discontinuity that is proportional to the density (of Bethe roots) $\rho(\mu)$,

$$\mathfrak{p}(\mu + \mathrm{i}0) - \mathfrak{p}(\mu - \mathrm{i}0) = 2\mathrm{i}\pi\ell(\mu^2 + \delta)\rho(\mu), \qquad \mu \in \mathcal{C}_j, \tag{5.20}$$

with $\pm\mathrm{i}0$ denoting infinitesimal displacements to either side of the contour. Individual contour $\mathcal{C}_j$ is depicted as the jth branch cut (of square-root type) of a two-sheeted Riemann surface. The end points of $\mathcal{C}_j$ correspond to branch points. In this view, function $\mathfrak{p}(\mu)$ is a double-valued complex function which, apart from contours $\mathcal{C}_j$, is analytic everywhere on the complex μ-plane. A branch cut of square-root type implies that upon crossing it the function jumps to the other Riemann sheet and $\mathfrak{p}(\mu)$ flips its sign. In addition, $\mathfrak{p}(\mu)$ picks up an integer multiple of 2π, namely

$$\mathfrak{p}(\mu + \mathrm{i}0) + \mathfrak{p}(\mu - \mathrm{i}0) = 2\pi n_j, \qquad \mu \in \mathcal{C}_j. \tag{5.21}$$

Remarkably, $\mathfrak{p}(\mu)$ is precisely the classical quasi-momentum pertaining to the completely integrable classical anisotropic ferromagnet (2.59), which has been introduced in Chapter 2. Alternatively, quasi-momentum encodes the eigenvalues of the classical monodromy matrix obtained from a path-ordered exponential of the classical Lax connection, which has been demonstrated partially in Sec. 4.1.

5.2 An exact solution to the discrete asymptotic Bethe ansatz equations

When there is only one branch cut in the Riemann surface and the density of Bethe roots is sufficiently low, there exists an exact solution to the

discrete asymptotic Bethe ansatz equations (5.13) where the Bethe roots are zeros of a generalised Jacobi polynomial. When system size $L \to \infty$, the distribution of the Bethe roots on the Riemann surface is described exactly by the distribution of the zeros of generalised Jacobi polynomial. The isotropic case has been studied in [84] and the Bethe roots in the isotropic case are zeros of a Laguerre polynomial.

To illustrate this, we define two polynomials $\mathcal{P}(\mu)$ and $\tilde{\mathcal{P}}(\mu)$ similar to Baxter's Q function,

$$\mathcal{P}(\mu) = \prod_{j=1}^{M} (\mu - \mu_j), \tag{5.22}$$

and

$$\tilde{\mathcal{P}}(\mu) = \prod_{j=1}^{M} \left(\frac{1}{\mu} - \frac{1}{\mu_j} \right). \tag{5.23}$$

For those two polynomials, we have the following identities,

$$2 \sum_{j \neq k} \frac{1}{\mu_j - \mu_k} = \frac{\mathrm{d}^2 \mathcal{P}}{\mathrm{d}\mu^2} \Big/ \frac{\mathrm{d}\mathcal{P}}{\mathrm{d}\mu}\Big|_{\mu=\mu_j}, \tag{5.24}$$

$$2 \sum_{j \neq k} \frac{1}{1/\mu_j - 1/\mu_k} = \frac{\mathrm{d}^2 \tilde{\mathcal{P}}}{\mathrm{d}(1/\mu)^2} \Big/ \frac{\mathrm{d}\tilde{\mathcal{P}}}{\mathrm{d}(1/\mu)}\Big|_{\mu=\mu_j}. \tag{5.25}$$

Denoting $\mathcal{P}'(\mu) = \frac{\mathrm{d}}{\mathrm{d}\mu}\mathcal{P}(\mu)$, we obtain

$$\begin{aligned} \frac{\mathrm{d}\tilde{P}}{\mathrm{d}(1/\mu)} &= \frac{\mathrm{d}\mu}{\mathrm{d}(1/\mu)} \frac{\mathrm{d}}{\mathrm{d}\mu} \left(\frac{\mathcal{P}(\mu)}{(-1)^M \mu^M \prod_{j=1}^{M} \mu_j} \right) \\ &= \frac{M\mu\mathcal{P}(\mu) - \mu^2 \mathcal{P}'(\mu)}{(-1)^M \mu^M \prod_{j=1}^{M} \mu_j}, \end{aligned} \tag{5.26}$$

and

$$\frac{\mathrm{d}^2 \tilde{\mathcal{P}}}{\mathrm{d}(1/\mu)^2} = \frac{M(M-1)\mu^2 \mathcal{P}(\mu) - 2(M-1)\mu^3 \mathcal{P}'(\mu) + \mu^4 \mathcal{P}''(\mu)}{(-1)^M \mu^M \prod_{j=1}^{M} \mu_j}. \tag{5.27}$$

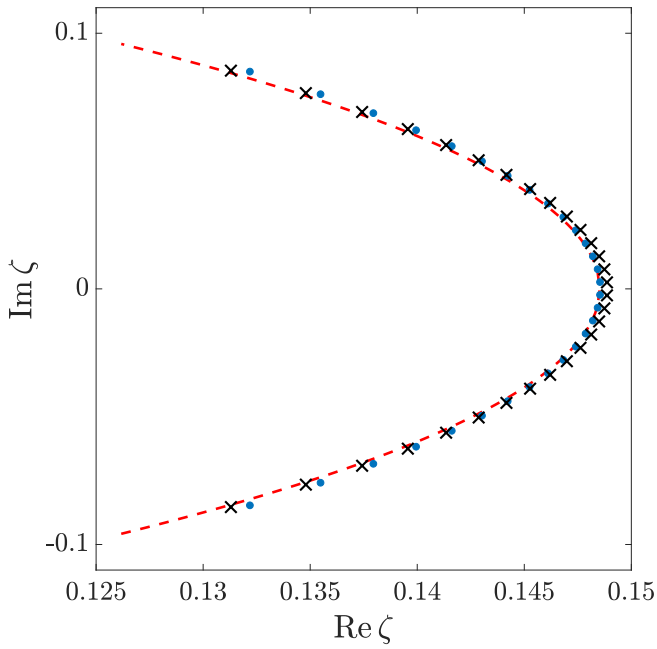

Figure 5.1: Comparison between solution to Eq. (5.33), the numerical solution to a finite-size Bethe equation and the branch cut for $L = 300$, $M = 30$, $n_1 = 1$. The figure is plotted in $\zeta = 1/\mu$ variable. The blue dots denote the numerical solution to Bethe equation (5.1). The black crosses are the solution to Eq. (5.33) and the red dashed line is the location of the branch cut in the limit $L \to \infty$.

Therefore, we can recast the discrete asymptotic Bethe ansatz equations (5.13) to an equation of polynomial $\mathcal{P}$ using (5.26) and (5.27), i.e.

$$(\mu_j^2 + \delta)\mathcal{P}''(\mu_j) + \left[(L - 2M + 2)\mu_j - \frac{2\pi n_1}{\ell} L\right] \mathcal{P}'(\mu_j) = 0 \propto \mathcal{P}(\mu_j),$$
$$\forall j = 1, \cdots M. \tag{5.28}$$

By matching the coefficient of the highest order, $\mathcal{P}(\mu)$ satisfies the

following ordinary differential equation,

$$\begin{aligned}&(\mu^2+\delta)\mathcal{P}''(\mu)+\left[(L-2M+2)\mu-\frac{2\pi n_1}{\ell}L\right]\mathcal{P}'(\mu)\\&-M(L-M+1)\mathcal{P}(\mu)=0.\end{aligned}\tag{5.29}$$

The solution to the ordinary differential equation is given by the generalised Jacobi polynomial $J_K^{(a,b)}$ which has the property

$$\begin{aligned}&(1-y^2)P''(y)+[b-a-(a+b+2)y]P'(y)\\&+K(K+a+b+1)P(y)=0,\quad P(y)=J_K^{(a,b)}(y).\end{aligned}\tag{5.30}$$

Through a simple change of variable $z=\mu/(i\sqrt{\delta})$, we have

$$\begin{aligned}&(z^2-1)\mathsf{P}''(z)+\left[(L-2M+2)z-\frac{2\pi n_1}{i\sqrt{\delta}\ell}L\right]\mathsf{P}'(z)\\&-M(L-M+1)\mathsf{P}(z)=0,\end{aligned}\tag{5.31}$$

with $\mathsf{P}(z)=\prod_{j=1}^{M}(z-z_j)$. We can identify the coefficients thereof,

$$a-b=-\frac{2\pi n_1}{i\sqrt{\delta}\ell}L,\quad a+b=L-2M,\quad K=M.\tag{5.32}$$

The (polynomial) solution to the original ordinary differential equation is given as

$$\mathcal{P}(\mu)\propto P_M^{a,b}\left(\frac{\mu}{i\sqrt{\delta}}\right).\tag{5.33}$$

The comparison of the zeros of (5.33) and the solutions to the Bethe equations (5.1) is given in Fig. 5.1.

We end up with this discussion by stressing that the zeros of generalised Jacobi polynomial are solutions to the discrete asymptotic Bethe ansatz equations, which is valid only when the density of Bethe roots is sufficiently small. In that case, we can neglect the contribution from the higher order term (5.16). When the density of Bethe roots increases, we need to take into account the "quantum correction" non-perturbatively.

5.3 Two examples of finite-gap solutions

Before studying the semi-classical quantisation of the classical finite-gap solutions, we give two explicit examples of finite-gap solutions, one-cut rational solution and bion solution, which serve as the benchmark for the semi-classical quantisation. Moreover, these two examples are of particular interest, since they are closely related to the low-energy excitations above the ferromagnetic vacuum $S(x) = 1$. The bion solution is responsible for the domain-wall frozen phenomenon in the easy-axis regime in Chapter 4, which becomes the static kink solution in the soliton limit.

5.3.1 One-cut rational solutions

The simplest solutions of the Riemann-Hilbert problem (5.21) belong to algebraic curves of genus zero (Riemann surfaces with a single branch cut). The Riemann surface is characterised by a quadratic polynomial of the form

$$\mathcal{R}_2(\mu) = (\mu - \mu_1)(\mu - \bar{\mu}_1), \tag{5.34}$$

where branch points $\mu_1, \bar{\mu}_1 \in \mathbb{C}$ are conjugate to one another in order to obey the reality condition. This leads to solutions that involve two real degrees of freedom.

In what follows, we set the classical period to $\ell = 1$. With this choice, the admissible values of the wave numbers are $k = 2\pi\, n$ with $n \in \mathbb{Z}$. As a consequence, the branch points cannot be chosen arbitrarily but get "quantised" as well.

The quasi-momentum $\mathfrak{p}(\mu)$ for one-cut solution becomes

$$\mathfrak{p}(\mu) = -\frac{\ell}{2}\left(\sqrt{\mathcal{R}_2(\mu)} - \frac{1}{2}\Big(\sqrt{\mathcal{R}_2(\mathrm{i}\epsilon)} + \sqrt{\mathcal{R}_2(-\mathrm{i}\epsilon)}\Big)\right). \tag{5.35}$$

To satisfy the "quantisation condition" and to obtain the prescribed filling fraction (2.68), we have

$$\begin{aligned} &\frac{1}{2}\left(\sqrt{\mathcal{R}_2(\mathrm{i}\epsilon)} + \sqrt{\mathcal{R}_2(-\mathrm{i}\epsilon)}\right) = 2\pi n, \\ &-\frac{1}{4}\left(\sqrt{\mathcal{R}_2(\mathrm{i}\epsilon)} - \sqrt{\mathcal{R}_2(-\mathrm{i}\epsilon)}\right) = -\frac{\mathrm{i}\epsilon}{2}(1-2\nu), \end{aligned} \tag{5.36}$$

allowing us to parametrise the branch points as

$$\mu_1 + \bar{\mu}_1 = 4\pi n(1-2\nu), \quad |\mu_1|^2 = 4\pi^2 n^2 + 4\delta\nu(1-\nu). \tag{5.37}$$

The algebraic curve can be expressed in terms of the mode number n and filling fraction ν,

$$y^2(\mu) = \mathcal{R}_2(\mu) = \mu^2 - 4\pi n(1-2\nu)\mu + 4\pi^2 n^2 + 4\delta(1-\nu), \tag{5.38}$$

as well as the quasi-momentum,

$$\begin{aligned} \mathfrak{p}_1(\mu) &= -\pi n - \frac{1}{2}\sqrt{(\mu-\mu_1)(\mu-\bar{\mu}_1)} \\ &= -\pi n - \frac{1}{2}\sqrt{\mu^2 - 4\pi n(1-2\nu)\mu + 4\pi^2 n^2 + 4\delta(1-\nu)}. \end{aligned} \tag{5.39}$$

Notice that presently (i.e. in the zero-genus case) there is no canonical $\mathcal{A}$-cycle. There is a single wave number which can be retrieved by evaluating the 'open' $\mathcal{B}$-cycle

$$k = \oint_{\mathcal{B}_1} \mathrm{d}\mathfrak{p}_1 = -\left(\mathfrak{p}_1(\infty_+) + \mathfrak{p}_1(\infty_-)\right) = 2\pi n. \tag{5.40}$$

Here $n \in \mathbb{Z}$ is the mode number of the solution.

Coefficients of the asymptotic expansion of $\mathfrak{p}_1$

$$\mu \to \infty : \qquad \mathfrak{p}_1(\mu) \sim -\frac{\mu}{2} - \frac{\mathcal{P}}{2} - \frac{\mathcal{H}}{\mu} + \mathcal{O}\left(\mu^{-2}\right), \tag{5.41}$$

provide phase-space averages of local charges evaluated on a particular one-cut solution. The initial two coefficients correspond to total momentum and energy, reading explicitly

$$\mathcal{P} = 2\pi n\nu, \qquad \mathcal{H} = \frac{1}{2}(4\pi^2 n^2 + \delta)\nu(1-\nu). \tag{5.42}$$

The knowledge of the one-cut quasi-momentum allows to express the dynamics of the spin field $\vec{S}(x,t)$ in terms of canonical separated γ-variables. However, since we deal with an algebraic curve of genus zero, there is no genuine γ-variable present. Instead, the only dynamical degree

of freedom is the transversal spin component $S^-(x,t)$. We use (2.73) to obtain the longitudinal component

$$S^{\rm z}(x,t) = \frac{\sqrt{\mathcal{R}_2(\gamma_1)}}{(\gamma_1-\gamma_2)} + \frac{\sqrt{\mathcal{R}_2(\gamma_2)}}{(\gamma_2-\gamma_1)} = 1-2\nu, \tag{5.43}$$

where we have made use of the frozen (i.e. non-dynamical) γ-variables $\gamma_1 = {\rm i}\epsilon$ and $\gamma_2 = -{\rm i}\epsilon$.

In the next step, we solve Eqs. (2.74) and (2.75) to obtain the transversal component of the spin field,

$${\rm i}\partial_x \log S^- = 2\pi n,\ {\rm i}\left(\partial_t \log S^- - \pi n(1-2\nu)\partial_x \log S^-\right) = \delta(1-2\nu). \tag{5.44}$$

By imposing normalisation constraint $|\vec{S}(x,t)| = 1$, we finally arrive at the following general form of the one-cut solution

$$S^{\rm z}(x,t) = 1-2\nu = \cos\theta_0, \quad S^{\pm}(x,t) = \sin\theta_0 \exp\left[\pm{\rm i}(kx-wt)\right], \tag{5.45}$$

with the wave number and frequency

$$k = 2\pi n, \quad w = (4\pi^2 n^2 + \delta)\cos\theta_0. \tag{5.46}$$

The momentum and energy can be alternatively computed by direct integration

$$\begin{aligned} \mathcal{P} &= \frac{1}{2{\rm i}}\int_0^1 {\rm d}x\, \frac{S^- S^+_x - S^+ S^-_x}{1+S^{\rm z}} = 2\pi n\nu, \\ \mathcal{H} &= \frac{1}{2}\int_0^1 {\rm d}x\, \left[\vec{S}_x\cdot\vec{S}_x + \delta(1-(S^{\rm z})^2)\right] = \frac{1}{2}(4\pi^2 n^2+\delta)\nu(1-\nu), \end{aligned} \tag{5.47}$$

in agreement with (5.42).

5.3.2 Classical bion solution

We now focus on the class of two-cut solutions, which have non-trivial dynamics in both $S^{\rm z}$ and $S^{\pm}$. Two-cut solutions are periodic elliptic magnetisation waves which are often referred to as 'cnoidal waves'. Two-cut solutions are associated to elliptic algebraic curves corresponding to

Riemann surfaces of genus $\mathfrak{g} = 1$, characterised by two branch cuts. In the special limit of unit elliptic modulus (soliton limit), the physical solutions become trigonometric and one retrieves the celebrated soliton solutions.

In the case of the easy-axis anisotropic Landau–Lifshitz model, there exist special types of two-cut solutions known as *bions*, i.e. two-mode bound states formed of a kink and an anti-kink. Moreover, a special degeneration of such a bion solution produces a static kink. Kinks are responsible for the observed freezing of a magnetic domain wall in Chapter 4. In Sec. 5.4.3, we shall perform the semi-classical quantisation on a bion.

The elliptic curve encoding the bion spectrum has the form

$$\mathcal{R}^2_{\text{bion}}(\mu) = \mathcal{R}^2_4(\mu) = (\mu^2 + \xi_1^2)(\mu^2 + \xi_2^2), \tag{5.48}$$

parametrised by two pairs of complex-conjugate branch points located on the imaginary axis $\text{Re}(\mu) = 0$ at $\mu_j \in \{\pm i\xi_1, \pm i\xi_2\}$, satisfying

$$\xi_1 > \epsilon > 0, \qquad 0 < \xi_2 < \epsilon. \tag{5.49}$$

It is obvious that the bion solutions can only be found in the regime $\delta > 0$ (the easy-axis regime). For the sake of simplicity, we set $\delta = \epsilon = 1$ for the rest of the section. In fact, from the classical equation of motion for the spin field $\vec{S}(x,t)$ given by (2.1), the solution at $\delta = 1$ can be mapped to another solution with $\delta' > 0$ by a simple rescaling

$$\vec{S}(x,t) \quad \mapsto \quad \vec{S}(x' = \epsilon\, x, t' = \delta\, t). \tag{5.50}$$

Now we outline the procedure of the reconstruction of the spin field from the algebraic curve. We introduce the standard full elliptic integrals, cf. Appendix C,

$$K_1 = K\left(\frac{\xi_2^2}{\xi_1^2}\right), \qquad K_2 = K\left(1 - \frac{\xi_2^2}{\xi_1^2}\right). \tag{5.51}$$

When the argument of the elliptic function is omitted, we adopt that $\mathrm{k} = \xi_2/\xi_1$.

Since the Riemann surface involves two branch cuts, we have a genuine dynamical γ-variable $\gamma_1(x,t)$. The same as before, there exist two extra

non-dynamical variables pinned to locations $\gamma_2 = \mathrm{i}$ and $\gamma_3 = -\mathrm{i}$ (recall that $\epsilon = 1$). From the Dubrovin equations (2.71) we have

$$\gamma_1(x,t) = \frac{\mathrm{i}\xi_1}{\mathrm{sn}(u)} = -\mathrm{i}\xi_2\,\mathrm{sn}(u + \mathrm{i}K_2), \qquad u = \xi_1 x + \varrho, \tag{5.52}$$

where we made use of $\mathrm{sn}(x + \mathrm{i}K_2)\mathrm{sn}(x)\mathrm{k} = 1$ (ϱ denotes the integration constant). Remarkably, it turns out that in this particular type of two-cut solutions, bions, even γ_1 is *static*.

Using the reconstruction formulae (2.73), we find

$$S^{\mathrm{z}} = \frac{\sqrt{\mathcal{R}_4(\gamma_1)} + \mathrm{i}\sqrt{\mathcal{R}_4(\mathrm{i})}\gamma_1}{\gamma_1^2 + 1}. \tag{5.53}$$

To fix the integration constant ϱ, we impose the reality condition $S^{\mathrm{z}} \in \mathbb{R}$,

$$\varrho = \mathrm{arcsn}\left(\mathrm{i}\frac{\xi_1}{\xi_2}\sqrt{\frac{1-\xi_2^2}{\xi_1^2-1}}\right), \tag{5.54}$$

which yields a time-independent profile

$$S^{\mathrm{z}}(x) = -\xi_2\frac{\mathrm{cn}(\xi_1 x)}{\mathrm{dn}(\xi_1 x)}. \tag{5.55}$$

The solution has a spatial period

$$\ell = \frac{4nK_1}{\xi_1}, \tag{5.56}$$

where $\pm n$ are the mode numbers associated with the two cuts. Variable γ_1 can be expressed as

$$\gamma_1(x) = -\xi_1\xi_2\frac{-\mathrm{i}\xi_1\sqrt{\mathcal{R}_4(\mathrm{i})}\,\mathrm{cn}(\xi_1 x)\mathrm{dn}(\xi_1 x) + \mathrm{i}(\xi_1^2 - \xi_2^2)\mathrm{sn}(\xi_1 x)}{\xi_1^2(1-\xi_2^2) + (\xi_1^2-1)\xi_2^2\,\mathrm{sn}(\xi_1 x)^2}. \tag{5.57}$$

The other independent component of the spin field, $S^-(x,t)$, can be reconstructed with the aid of formulae (2.74) and (2.75),

$$S^-(x,t) = \frac{1}{\sqrt{1+\gamma_1^2(x,t)}}\exp\left(-\mathrm{i}\int \mathrm{d}x\frac{-\mathrm{i}\sqrt{\mathcal{R}_4(\mathrm{i})}}{1+\gamma_1^2(x,t)}\right). \tag{5.58}$$

Using the properties of elliptic functions in Appendix C, we obtain

$$S^{-}(x) = C\frac{\Theta(\xi_1 x + \varrho + \mathrm{i}K_2)}{\Theta(\xi_1 x + K_1)} \exp\left(\xi_1 x \frac{\pi \mathrm{i}}{2K_1} + \xi x \frac{\Theta'(\beta)}{\Theta(\beta)}\right), \tag{5.59}$$

where function $\Theta(x)$ is defined as

$$\Theta(x) = \vartheta_3\left(\frac{\pi x}{2K_1} + \frac{\pi}{2}, -i\frac{K_2}{K_1}\right). \tag{5.60}$$

Finally, constant C is can be fixed by requiring normalisation $\vec{\mathcal{S}}^2 = 1$, yielding

$$\begin{aligned} S^{-}(x) =& \sqrt{1-\xi_2^2}\frac{\Theta(\xi_1 x + \rho + \mathrm{i}K_2)}{\Theta(\xi_1 x + K_1)} \\ & \exp\left(\xi_1 x \frac{\pi \mathrm{i}}{2K_1} + \xi x \frac{\Theta'(\beta)}{\Theta(\beta)} + \mathrm{i}\phi_0\right), \end{aligned} \tag{5.61}$$

where $\phi_0 \in \mathbb{R}$ is a phase that is determined by the initial condition. Remarkably, for the bion solutions S^{-} is time-independent as well. A representative example of a bion solution is shown in Fig. 5.2.

Static kink. In order to see the connection between the bion solution and the domain-wall frozen phenomenon [1], we consider a particular degeneration of a bion solution which produces a static kink. One of the consequences of taking soliton limit is that the classical period $\ell \to \infty$. This requires to bring both branch points of $\sqrt{\mathcal{R}_4(\mu)}$ in the upper-half plane together to meet at $\mathrm{i}\epsilon$, i.e. we send $\xi_{1,2} \to \epsilon$ (presently $\epsilon = 1$), collapsing both branch cuts to a point.

In order to perform this soliton limit, we first shift the argument of the elliptic function by quarter period K_1/ξ_1; for instance the $\S^{\mathrm{z}}$ field takes the form (cf. Eqs. (C.6))

$$S^{\mathrm{z}}(x) = -\xi_1 \frac{\mathrm{cn}(\xi_1(x + K_1/\xi_1))}{\mathrm{dn}(\xi_1(x + K_1/\xi_1))} = \xi_1 \mathrm{sn}(\xi_1 x). \tag{5.62}$$

Now taking the limits $\xi_{1,2} \to 1$ and accordingly $\mathrm{k} = \xi_2/\xi_1 \to 1$, we find

$$S^{\mathrm{z}}_{\mathrm{kink}}(x) = \tanh(x), \tag{5.63}$$

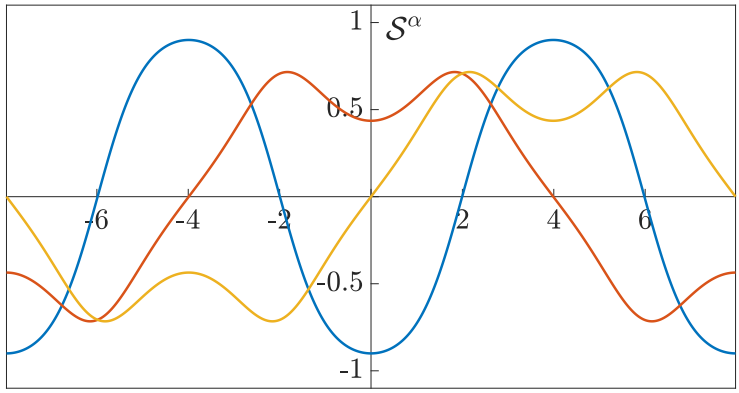

Figure 5.2: Spin-field components of a typical bion solution, depicted for anisotropy parameter $\delta = 1$ and branch points $\xi_1 \simeq 1.0583559$ and $\xi_2 = 0.9$. Components $S^{\mathrm{z}}(x)$, $S^{\mathrm{x}}(x) = \mathrm{Re}\, S^-(x)$, and $S^{\mathrm{y}}(x) = -\mathrm{Im}\, S^-(x)$ are shown by blue, yellow and red curves, respectively. The bion solution is periodic with period $\ell_2 = 4K_1/\xi_1 \simeq 15.956517$.

which is precisely a *static kink*. The transversal components can be easily deduced from the equation of motion (2.1), yielding

$$S^-_{\mathrm{kink}}(x) = \mathrm{sech}(x)\, e^{\mathrm{i}\phi_0}, \tag{5.64}$$

where $\phi_0 \in \mathbb{R}$ is a phase determined by the initial condition. The static kink solution is the same as the frozen domain-wall configuration without breathers in Chapter 4.

5.4 Semi-classical quantisation

In the following, we carry out the semi-classical quantisation on finite-gap solutions, which paves the way to quantitative studies of quantum correlation functions in the semi-classical limit. In this respect, the associated spectral curves, which encode complete information about the conserved quantities, will be of vital importance.

Before proceeding, we would like to make a remark on the choice of branch cuts of the classical spectral curve. First, recall that moduli

of algebraic curves are completely fixed by locations of the square-root branch points, i.e. roots of polynomial $\mathcal{R}_{2\mathfrak{g}+2}(\mu)$, which have to appear in complex-conjugate pairs due to reality condition. Local conserved charges are expressible as functions of symmetric polynomials of branch points, namely coefficients r_j of $\mathcal{R}_{2\mathfrak{g}+2}(\mu)$. While branch points $\{\mu_j\}$ themselves are directly linked physical quantities, the branch cuts (of square-root type) obtained by pairwise connecting the branch points are not physical but merely a matter of convention in the classical regime. There is plenty of freedom in assigning branch cuts to a given set of branch points. For instance, the prevalent choice in the finite-gap literature [11] is to place the cuts along straight vertical lines connecting every complex conjugate pair of branch points, which are in turn encircled by the canonical basis $\mathcal{A}$-cycles. Such a choice is, purely from the standpoint of classical finite-gap solutions, perfectly adequate. On the other hand, if classical solutions are instead considered as emergent macroscopic bound states of magnons of the corresponding quantum integrable lattice model, it is natural to cut the surface along one-dimensional disjoint segments associated to forbidden zones of the classical transfer function [13], corresponding to contours on which magnons (Bethe roots) condense.

This prescription for the branch cuts is physically distinguished. As demonstrated in this section, such physical cuts not only differ from the conventional straight cuts in general, but also undergo the phenomenon of condensate formation. Computing the Bethe root densities along the physical contours is thus the essential step to perform the semi-classical quantisation.

5.4.1 Physical contours

We describe a general procedure to determine the physical contours that magnons condense onto. The algorithm we employ here has been proposed and implemented in Ref. [75]. We also facilitate a direct comparison with exact low-momentum quantum eigenstates at finite L in the weakly-anisotropic regime. For our convenience, we carry out this computation

in the ζ-plane [1] by applying the following transformation [2]

$$\mu \mapsto \zeta(\mu): \qquad \zeta = \frac{1}{\mu} = \frac{\tan\vartheta}{\epsilon}. \tag{5.65}$$

First, we introduce the *complex* density function

$$\rho(\zeta) = \frac{\mathfrak{p}(\zeta+\mathrm{i}0) - \mathfrak{p}(\zeta-\mathrm{i}0)}{2\mathrm{i}\pi\ell(1+\delta\zeta^2)} = \pm\frac{\mathfrak{p}(\zeta\pm\mathrm{i}0) - \pi n_j}{\mathrm{i}\pi\ell(1+\delta\zeta^2)}, \qquad \zeta\in\mathcal{C}_j, \tag{5.66}$$

where $n_j \in \mathbb{Z}$ is the mode number associated to cut $\mathcal{C}_j$. By virtue of the second equality in (5.66), the density function $\rho(\zeta)$ can be defined on the entire Riemann surface. As a consequence of $\mathfrak{p}(\zeta=\zeta_\star)=\pi n_j$ at the square root branch points $\zeta_\star \in \{\zeta_j, \bar{\zeta}_j\}$, the density always vanishes at the branch points, $\rho(\zeta_\star)=0$. In a small neighbourhood around it, one finds $\rho(\zeta=\zeta_\star+\varepsilon)=\mathcal{O}(\sqrt{\varepsilon})$ [75]. Away from the branch points $\rho(\zeta)$ in general takes complex values.

Now we would like to determine the physical contours $\mathcal{C}_j$. The latter can be singled out by the following condition: starting from the branch point ζ_j, the integrated density differential $\rho(\zeta)\mathrm{d}\zeta$ must always remain real,

$$\int_{\zeta_j}^{\zeta} \mathrm{d}\zeta'\rho(\zeta') \in \mathbb{R} \qquad \text{for} \qquad \zeta\in\mathcal{C}_j. \tag{5.67}$$

This prescription has a transparent physical interpretation: physically $\rho(\zeta)\mathrm{d}\zeta$ corresponds to the number of magnon excitations (Bethe roots) within an infinitesimal interval in ζ-plane, which is a positive definite quantity by definition.

This condition alone is however not sufficient yet. It turns out that there are three distinct contours emanating out of each branch point compatible with the above positivity requirement [75]. Among those three contours, one of them carries an infinite filling fraction and can be thus immediately ruled out as unphysical. Out of the remaining two contours, only one can be physical. The remaining condition is that the total filling fraction does not exceed the threshold value of maximal total filling

[1] Our variable ζ is analogous to variable x used in Refs. [13, 85, 75] in the case of the isotropic Heisenberg model.

[2] Upon this transformation, the orientation of integration contours gets reversed.

$\nu_{\max} = 1/2$, that is

$$\int_{\mathcal{C}} \mathrm{d}\zeta' \rho(\zeta') \leq \nu_{\max}, \qquad \mathcal{C} = \bigcup_j \mathcal{C}_j. \tag{5.68}$$

Consider now a certain reference finite-gap solution. To quantise it at the semi-classical level, every density contour (physical cut) has to be dissolved into a large (but finite) number of individual magnons. This requires us to reinstate the length L of the underlying spin chain, thus rendering the total magnetisation carried by individual coherent states to come in integer quanta of $M_j \sim \mathcal{O}(L)$.

The precise requirements are that (i) $M_j/L \approx \nu_j$ and (ii) that the Bethe roots are distributed approximately with density $\rho_j(\zeta)$ along $\mathcal{C}_j$. It is crucial to make a distinction with the exact quantisation which takes quantum fluctuations fully into account to all orders in the effective Planck constant. This means that the semi-classical solutions produced with the outlined procedure can be at best an approximation of finite-volume exact quantum-mechanical eigenstates at long wavelengths, while a full non-perturbative (i.e. exact) quantisation would require obtaining the exact solutions to the Bethe ansatz equations (5.1).

Single contour at low density. To benchmark the above procedure, we start with illustrating how one-cut solutions in Sec. 5.3.1 emerge as semi-classical eigenstates in the anisotropic easy-axis quantum spin-1/2 XXZ model.

We first suppose that the filling fraction of a physical cut is sufficiently *low*, ensuring that the finite-size effects (cf. Eqs. (5.16) and (B.16)) can be safely neglected at large system sizes. We then find that the Bethe roots patterns which solve the asymptotic Bethe equations (5.14) distribute along certain arcs in the complex rapidity plane, as exemplified in Fig. 5.3. To be concrete, we put anisotropy to $\delta = 1$ and set the filling fraction to $\nu = 0.1$ and the mode number to $n = 1$. Using the above prescription, we next compute the density contour satisfying Eqs. (5.67) and (5.68), as shown in Fig. 5.3. Taking the $L \to \infty$ limit and rescaling the rapidity variable, the semi-classical eigenstate will eventually be described by a dense arrangement of Bethe roots distributing along the contour specified by the conditions (5.67) and (5.68).

By increasing the filling fraction ν, we observe that 'quantum fluctuations', which are contained in higher order terms in the ABE (5.16), progressive amplify. As announced earlier, this eventually leads to a critical phenomenon of condensate formation. This feature will be closely examined in the following section.

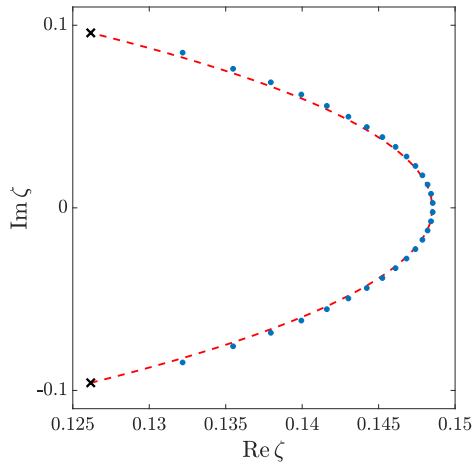

Figure 5.3: Direct comparison between the physical density contour of a classical one-cut solution (red dashed line, corresponding to anisotropy $\delta = 1$, filling fraction $\nu = 0.1$ and mode number $n = 1$) determined by imposing the positivity condition (5.67), and the corresponding solution to Bethe ansatz equations (5.1) with $M = 30$ Bethe roots, system size $L = 300$ and anisotropy $\eta = \sqrt{\delta}/L = 1/300$ (blue dots). The Bethe roots are given by $\zeta_j = \tan(\vartheta_j)/\sqrt{\delta}$.

5.4.2 Formation of condensates

Condensates refer to segments of a uniform density as a part of a physical contour. The phenomenon has first been studied in Refs. [86, 13] where the term has been coined. Condensates appear as part of the physical contours whenever the maximal density along one of the physical contours exceeds a particular critical value which is signalled by a divergence of the finite-size correction given by Eq. (5.16) (see also Eq. (B.16)).

We first examine the phenomenon on the simplest case of the one-cut solution, using the ζ-plane parametrisation. Starting at some sufficiently low filling fraction ν, we observe that as we gradually increase the filling fraction, the value of $\rho(\zeta)(1+\delta\zeta^2)$ on the real axis approaches the critical value i.

This value is reached at the critical filling fraction $\nu_{\rm crit}$, precisely when quantum fluctuation of order $\mathcal{O}(1/L)$ become divergent, cf. (B.16). For larger fillings $\nu > \nu_{\rm crit}$, the density contour develops a vertically straight segment of unit uniform density. Such a condensate appears first on the real axis (right after crossing $\nu_{\rm cric}$) and expands outwards when further increasing ν.

From the viewpoint of the underlying quantum model, the spacing between constituent Bethe roots is always equal to $i\eta$. One can consider condensates as giant regular Bethe strings. In the complex spectral plane associated to finite-gap solutions, the end points of a condensate correspond to branch cuts of *logarithmic* type. [3]

Despite the appearance of an additional condensate above $\nu > \nu_{\rm crit}$, it is still possible to obtain the physical contour solely from the knowledge of a finite-gap solution by taking into account conditions (5.67) and (5.68).

The emergence of condensates is intimately related to the notion of 'fluctuation points', which plays a pivotal role in classical modulation stability theory [87]. Fluctuation points can be perceived as small fluctuations of a reference finite-gap solution, corresponding to tiny cuts associated with infinitesimal filling fraction. While increasing their filling fractions, they become nonlinear finite-gap mode.

Consider a reference finite-gap solution with m cuts, and let $\{n_1, n_2 \cdots n_m\}$ be the occupied mode numbers for each cut respectively. To excite a mode with an unoccupied n, call it n_*, the quasi-momentum $\mathfrak{p}(\zeta)$ has to satisfy the periodic boundary condition,

$$\mathfrak{p}(\zeta_{m,n_*}) = n_*\pi, \tag{5.69}$$

[3] Logarithmic branch cuts get likewise produced in a well-known soliton degeneration process, corresponding to merging two nearby standard square-root branch cuts by coalescing their branch points in a pairwise manner. In that case, finite-gap quasi-momentum is no longer meromorphic. Condensates are different in this respect, as their quasi-momentum differential remains meromorphic all the way through.

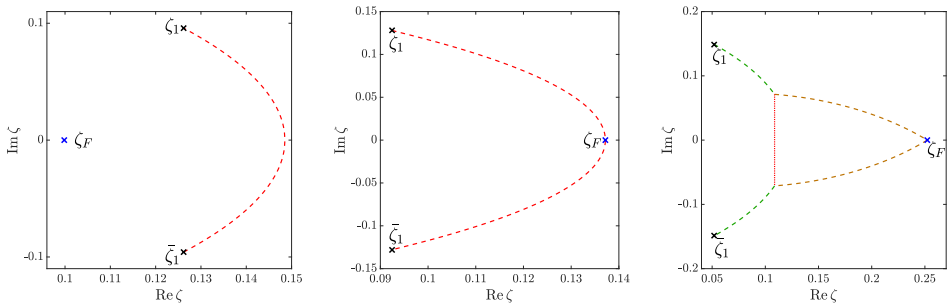

Figure 5.4: Branch points (ζ_1 and $\bar{\zeta}_1$) and fluctuation points (ζ_F) for the one-cut solution with anisotropy parameter $\delta = 1$ and various filling fractions $\nu = \{0.1, 0.206354963, 1/3\}$, increasing from left to right. Panel (b) corresponds to the critical filling fraction $\nu_c \simeq 0.206354963$, when the fluctuation point ζ_F collide with the physical cut.

where we use ζ_{m,n_*} to label distinct fluctuation points. Note that these can either be real, or may occur in complex-conjugate pairs due to the square-root branch cut nature of the quasi-momentum.

Fluctuation points are treated as "almost degenerate" branch cuts, so small that they do not affect the form of the quasi-momentum $\mathfrak{p}(\zeta)$. This raises an interesting question whether classically any given finite-gap solution is modulationally stable under such fluctuations, see for instance discussions in Ref. [87]. In this respect, we observe that the stability condition coincides with the condition for the formation of condensates in the semi-classical quantisation of finite-gap solutions.

We first take a look at the basic case with a single cut. We find the physical contours made out of Bethe roots consist of three pieces: two parts of to the contours which connect to the square-root branch points are joined by a uniform condensate attached to 'the middle', with two additional bent contours emanating from the intersection points that connect to the nearby fluctuation point(s). We give an explicit demonstration of this scenario in Sec. 5.4.2. Presence of multiple excited cuts makes the situation even more involved as cuts experience among themselves an effectively attractive interaction. This situation is described in

Sec. 5.4.2.

Let us also mention that a reminiscent phenomenon is known to appear in the context of matrix models [88] (which are described by a similar type of Riemann-Hilbert problems) and also elsewhere, e.g. in the large-N Yang–Mills theory [89, 90, 91] and random tiling models [92, 93]. They are commonly called as the Douglas–Kazakov phase transition [91], a variant of a third-order phase transition.

Analogous condensates also appear in the semi-classical regime of the Lieb-Liniger model with attractive interaction [94, 95] where a quantum phase transition can be detected through the calculation of correlation functions in the ground state [95]. We emphasise however that in our case there is no real phase transition going on in the sense that branch points and the quasi-momentum $\mathfrak{p}(\zeta)$ itself do not undergo any discontinuous change, in distinction with the case of Douglas–Kazakov transition where the free energy becomes non-smooth after formation of a "condensate" [93].

One-cut case with condensate

In the case of a single cut, we have

$$\int_{\mathcal{C}_1} \mathrm{d}\zeta \rho(\zeta) = \nu_1 \in \mathcal{O}(1), \tag{5.70}$$

with an upper-bounded filling fraction $\nu_1 < 1/2$. Locations of fluctuation points, denote below by $\zeta_{1,k}$, can be obtained from the density

$$\rho_k(\zeta) = \pm \frac{\mathfrak{p}(\zeta) - \pi k}{2\pi i(1+\delta\zeta^2)}, \qquad \mathfrak{p}(\zeta_{1,k}) = k\pi, \tag{5.71}$$

Mode number $n = 1$. The condensate phenomenon can be best illustrated on the basic example of a one-cut solution with mode number $n = 1$. Below the density threshold we find a single smooth arc-shaped contour, as exemplified in panel (a) in Fig. 5.4. The closest fluctuation point sits at a finite distance away from the cut (somewhere to the left of it), whereas the density at the real axis satisfies

$$\rho(\zeta_*)(1+\delta\zeta_*^2) < \mathrm{i}. \tag{5.72}$$

Increasing the filling fraction leads to an increase in the density on the real axis. During the process, the nearby fluctuation point approaches the physical contour until at the critical filling it eventually collides with it at ζ_*, i.e.

$$\rho(\zeta_*)(1+\delta\zeta_*^2) = \mathrm{i}. \tag{5.73}$$

This event is depicted in panel (b) in Fig. 5.4. [4]

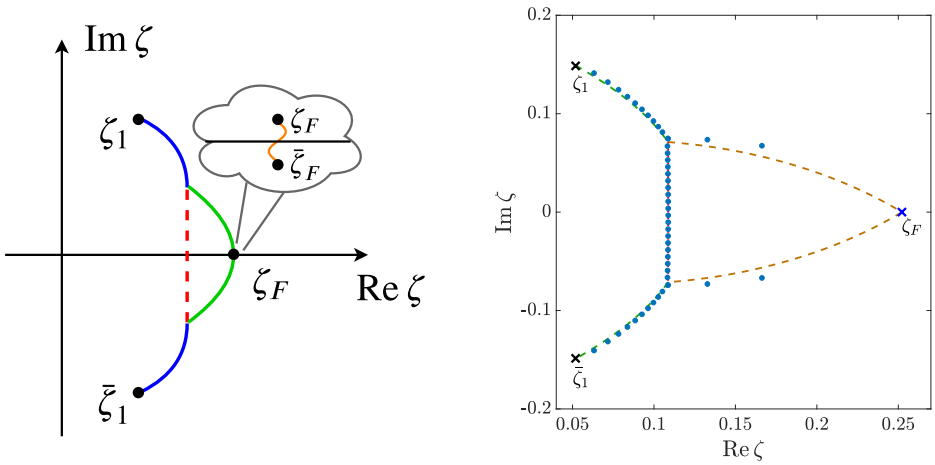

(a) (b)

Figure 5.5: (a) Fluctuation point ζ_F, lying on the real axis, can be viewed as an infinitesimal (collapsed) branch cut – a deactivated mode. (b) Comparison between the classical contour (dashed line) with anisotropic parameter $\delta = 1$, filling fraction $\nu = 0.3$, and mode number $n = 1$ (computed based on reality condition (5.67)) with a condensate (red dashed line) and an additional contour originating from ζ_F (brown dashed line) and the corresponding solution to the Bethe equations (cf. Eq. (5.1)) with $M = 48$, $L = 144$ and $\eta = \frac{\sqrt{\delta}}{L} = \frac{1}{144}$ (blue dots). Notice that the Bethe roots plotted are reparametrised as $\frac{\tan\vartheta}{\sqrt{\delta}}$.

Increasing the filling fraction even further, the fluctuation points after collision 'tunnel through' the branch cut. This results in a straight

[4] Comparing to the isotropic case in [75], $\nu_c \simeq 0.2092896452$, the condensate appears with a slightly smaller filling fraction.

condensate positioned in the vertical direction. The nearest fluctuation point on the real axis appears to the right of the physical cut, as pictured in panel (c) in Fig. 5.4. One can nonetheless recover the same quasi-momentum $\mathfrak{p}(\zeta)$ by considering an additional pair of contours which emanate out of the fluctuation point(s), satisfying $\rho_2(\zeta)\mathrm{d}\zeta \in \mathbb{R}$ with density defined through Eq. (5.71) (depicted by brown dashed lines in panel (c) in Fig. 5.4). Due to the existence of an extra condensate, the original contour cannot accommodate for all the Bethe roots, and the "excess" Bethe roots lie along those additional contours. We would like to emphasise again that the quasi-momentum $\mathfrak{p}(\zeta)$ remains intact.

There is a suggestive explanation behind the above picture if one considers a one-cut solution as a limiting (degenerate) case of a more general two-cut solution with one of its cuts 'shrinks' to a fluctuation point. This is demonstrated in Fig. 5.5 in panel (a), where the blue solid lines represent parts of the original physical connecting to the pair branch points $(\zeta_1, \bar{\zeta}_1)$, while the red dashed line depicts the Bethe-root condensate of uniform density. The extra green solid line belongs to one of the "unphysical contours"[5] associated with the infinitesimal branch cut $(\zeta_F, \bar{\zeta}_F)$. Combining all the ingredients, we are able to determine the densities of Bethe roots along these three contours. This amounts to account for the leading-order quantum corrections to ABE (5.14) in a non-perturbative fashion.

An indirect confirmation of the physical interpretation of the condensate and additional contours is achieved by calculating leading order of Gaudin norm of the semi-classical eigenstate associated with condensate [2]. The functional approach of calculating Gaudin norms of semi-classical states [96] depends on the choice of physical contours and the correct results are obtained using the contours with condensate in [2].

Mode number $n \geq 2$. One may encounter even more exotic situations with larger mode number. While $\mathfrak{p}(\zeta_*) = (n+1)\pi$ has only one real solution for $n = 1$, higher mode numbers $n \geq 2$ permit for complex-conjugate pairs of fluctuation points [75]. In this scenario, the same

[5] We call it "unphysical" because the green contour alone does not yield the correct value for the filling fraction for the infinitesimal cut. Yet the combination of all three parts here has clear physical meaning.

condition $\rho_{n+1}(\zeta)\mathrm{d}\zeta \in \mathbb{R}$ yields an additional contour with a condensate appearing between the intersection points. Such contours can be understood at the classical level as arising from a three-cut solution with one large physical cut and two almost degenerate tiny cuts located at the complex-conjugated fluctuation points ζ_F and $\bar{\zeta}_F$ with infinitesimal filling fractions.

For instance, in Fig. 5.6 we give an illustration of that for the isotropic Heisenberg XXX model with mode number $n = 2$. Unfortunately, for the anisotropic ferromagnet the employed numerical method for producing analogous solutions no longer works for $n \geq 2$ [2]. Given that the distributions of Bethe roots do not change much upon introducing a tiny deformation parameter $\eta \sim \mathcal{O}\left(\frac{1}{L}\right)$, we expect the phenomenon to remain the same in the presence of weak interaction anisotropy.

Multiple cuts

When multiple branch cuts get involved, the situation becomes more complicated. In that case, the condensates can appear not only out of fluctuation points but also via the effectively attractive interaction between the physical cuts. For simplicity we focus on the two-cut case, since a general scenario with more cuts can be described based on the phenomenology of the two-cut case. In Ref. [75], the authors made an exhaustive survey on the two-cut case at isotropic point ($\delta = 0$). The anisotropic case with $\eta = \frac{\epsilon}{L} > 0$ can be analysed in a similar fashion. There are several discernible features we wish to highlight.

First, when two physical cuts are far apart from one another, each branch cut can produce a condensate from colliding with their nearby fluctuation points, in analogy with the one-cut case discussed in Sec. 5.4.2. However, when the physical cuts approach each other, their mutual attraction increases until they eventually merge with one another. This phenomenon results in two joined contours glued via a condensate at the cusps.

An example of the above phenomenon involves two branch cuts with consecutive mode numbers, namely $n_2 = n_1 + 1$. The moment the two physical contours intersect, say at points ζ_{int} and $\bar{\zeta}_{\text{int}}$, the combined den-

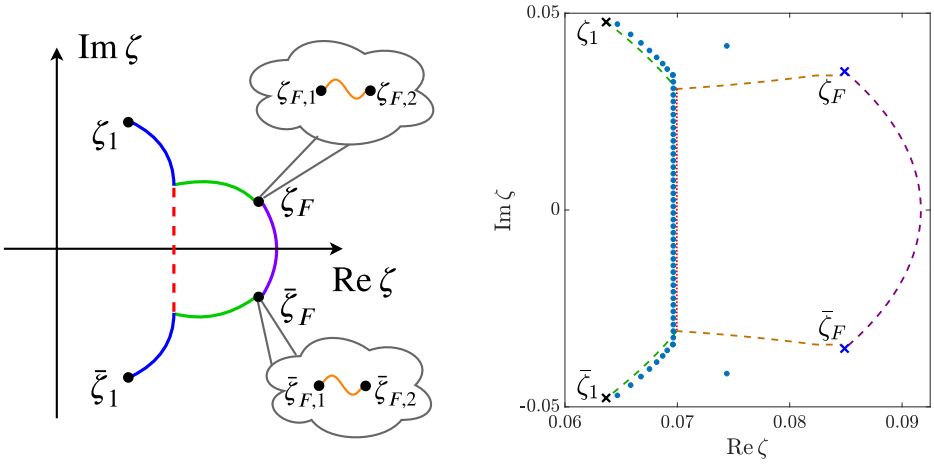

Figure 5.6: (Left) Complex fluctuation points ζ_F and $\bar{\zeta}_F$. They can be seen as collapsed cuts of a three-cut solution with $\zeta_{F,1} \to \zeta_{F,2} \to \zeta_F$ and $\bar{\zeta}_{F,1} \to \bar{\zeta}_{F,2} \to \bar{\zeta}_F$. (Right) Comparison between the classical density contour (dashed line), including with the condensate (red dashed line) and the additional contours emanating from fluctuation points ζ_F and $\bar{\zeta}_F$ (brown and purple dashed lines), obtained from reality condition (5.67) for the case of isotropic interaction ($\delta = 0$), with filling fraction $\nu = 0.1$ and mode number $n = 2$, to the corresponding solution to Bethe equations (5.1) with $M = 60$, $L = 600$ and $\eta = 0$. The Bethe roots ζ_j (blue dots) are rescaled by the system size L and plotted in the inverse spectral plane, i.e. $\zeta_j = 1/(L\lambda_j)$, where λ_j solve the isotropic Bethe equations, $\left(\frac{\lambda_j+\mathrm{i}/2}{\lambda_j-\mathrm{i}/2}\right)^L = \prod_{k\neq j}^{M} \frac{\lambda_j-\lambda_k+\mathrm{i}}{\lambda_j-\lambda_k-\mathrm{i}}$.

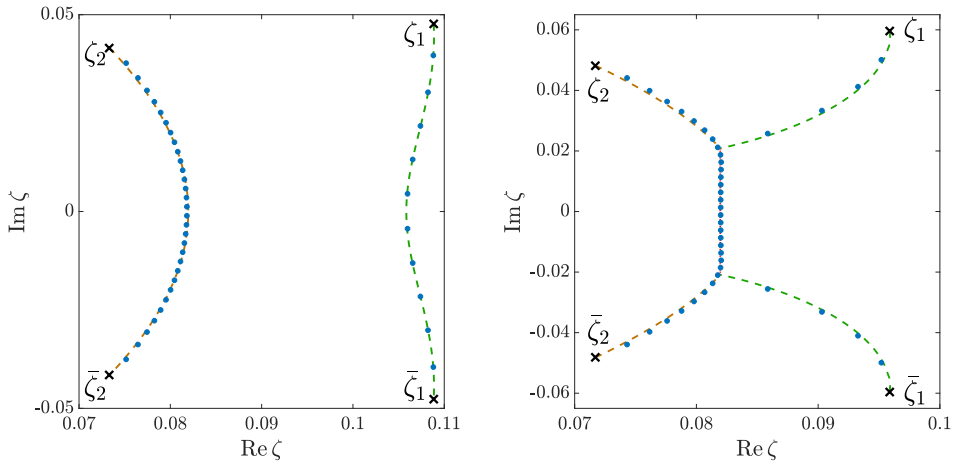

(a) (b)

Figure 5.7: (Left) Comparison between the density contour (dashed line) of a classical two-cut solution (shown for the isotropic case ($\delta = 0$), with partial filling fractions $\nu_1 = 0.02$, $\nu_2 = 0.06$ and mode numbers $n_1 = 1$, $n_2 = 2$), obtained from reality condition (5.67), and the corresponding numerical solution to Bethe equations (5.1) with $M_1 = 10$, $M_2 = 30$, $L = 500$ and $\eta = 0$ (blue dots). (Right) Comparison between the classical contour (dashed line) (shown for the isotropic case ($\delta = 0$), with partial filling fractions $\nu_1 = 0.025$, $\nu_2 = 0.075$ and mode numbers $n_1 = 1$, $n_2 = 2$), obtained from reality condition (5.67), to the corresponding numerical solution to Bethe equations (5.1) with $M1 = 10$, $M_2 = 30$, $L = 400$ and $\eta = 0$ (blue dots). The Bethe roots plotted are $\zeta_j = 1/(L\lambda_j)$, same as in Fig. 5.6.

sity satisfies

$$\begin{aligned}\left[\rho_{n_1}(\zeta_{\text{int}}) + \rho_{n_1+1}(\zeta_{\text{int}})\right]\left(1+\delta\zeta_{\text{int}}^2\right) = \\ \left[\rho_{n_1}(\bar{\zeta}_{\text{int}}) + \rho_{n_1+1}(\bar{\zeta}_{\text{int}})\right]\left(1+\delta\bar{\zeta}_{\text{int}}^2\right) = \text{i},\end{aligned} \tag{5.74}$$

which yields the appearance of a condensate. Indeed, adding a condensate between the two intersection points does not alter the quasi-momentum and hence the filling fraction remains the same. We have confirmed this to be the case by numerically solving the Bethe ansatz equations for moderately large system sizes, as demonstrated in Fig. 5.7 (again for the isotropic case).

In particular, at low filling fractions for both cuts their mutual attraction becomes apparent (cf. the second cut connecting $(\zeta_1, \bar{\zeta}_1)$ in panel (a) in Fig. 5.7). The four branch points in panel (a) of Fig. 5.7 are $\zeta_1 = 0.10884679 + 0.047665716\text{i}$ and $\zeta_2 = 0.07330641 + 0.04152184\text{i}$ (with filling fractions $\nu_1 = 0.02$, $\nu_2 = 0.06$, $\ell = 1$ and mode numbers $n_1 = 1$, $n_2 = 2$). At a certain critical value of the filling fractions the two cuts merge together. The intersection point becomes a logarithmic branch point of a condensate, as exemplified in panel (b) of Fig. 5.7. The four branch points in panel (b) in Fig. 5.7 are $\zeta_1 = 0.09587725 + 0.05961115\text{i}$ and $\zeta_2 = 0.07169871 + 0.04814544\text{i}$ with filling fractions $\nu_1 = 0.025$, $\nu_2 = 0.075$, $\ell = 1$ and mode numbers $n_1 = 1$, $n_2 = 2$. For the anisotropic interaction we encountered the same numerical difficulties as previously for the one-cut solution with $n \geq 2$ [2]. However, we do not expect any qualitative difference in the anisotropic case compared to the isotropic model.

5.4.3 Special case: bion

The easy-axis regime (i.e. for $\delta > 0$) permits for a distinguished subclass of two-cut solutions that do not take place in the other two (that is isotropic and easy-plane) regimes, bion solutions, as described and parametrised in Sec. 5.3.2. One part of the motivation for investigating this case is to elucidate the microscopic origin and stability of kinks in Landau–Lifshitz model, which we expect to have a pivotal importance for understanding the freezing property of a domain-wall profile in Chapter 4. This has been investigated recently in Refs. [1, 97] as well.

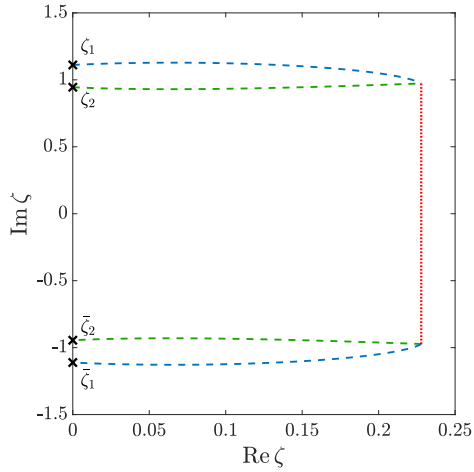

Figure 5.8: Quantised bion configuration with the proposed density contours (physical cuts). The two nonlinear modes with $\delta = 1$, parametrised by pairs of branch points $(\zeta_1, \bar{\zeta}_1)$ and $(\zeta_2, \bar{\zeta}_2)$ on imaginary ζ-axis, have associated mode numbers $n_1 = 1$ and $n_2 = -1$. The branch points have been found numerically and are located at $\zeta_1 = (1/0.9)\mathrm{i}$ and $\zeta_2 = (1/1.058355921)\mathrm{i}$. The red dashed line represents the "double condensate". The corresponding classical solution is plotted in Fig. 5.2.

In order to quantise the classical bion solution, we use the same reality conditions as previously in the one-cut case. Notice however that bion solutions belong to maximally saturated states with the total filling $\nu = \frac{1}{2}$. Condensates appear to be a common feature at half filling. When describing the bion solution, we fix the mode numbers of the two cuts to ± 1, such that $\Delta n = 2$. Recall that in a general situation with two cuts being far apart, each cut can form a condensate on its own. The bion case is quite different because the two branch cuts reside close to each other and share a condensate in common therefore.

In fact, in the isotropic ferromagnet studied in Refs. [75, 86], the two-cut solution with mode numbers set to ± 1 is able to form a "double condensate". Motivated by this observation, we conjecture that the same phenomenon takes place in the case of bions; a "double condensate" emerges when a pair of branch cuts with mode numbers ± 1 intersect with

one another, thereby producing a logarithmic cut with of 'doubled' uniform density 2i. Analogous objects which are twice as dense as ordinary Bethe strings have been previously found numerically in Ref. [86] in the study of solutions to the isotropic Bethe equations.

Semi-classically we quantise the bion solution using the conjectured contours with a double condensate, depicted in Fig. 5.8 by the red dashed line satisfying

$$\rho(\zeta)(1+\delta\zeta^2) = 2\mathrm{i}. \tag{5.75}$$

We have been able to explicitly match the classical values of the filling fraction, momentum and energy: the two partial filling fractions add up exactly to one half, i.e. $\nu = \nu_1 + \nu_2 = \frac{1}{2}$, whereas total momentum $P = 0 \,(\mathrm{mod}\, 2\pi)$ and total energy $E = 3.96045$ (obtained by numerically integrating along the proposed contours) match those of a classical bion configuration, with $P = 0$ and $E = 3.960358(6)$. These results strongly indicate that we have indeed correctly identified the physical contours associated to a quantised bion.

As discussed earlier in Sec. 5.3.2, stable kink arises as the soliton limit of a bion solution in which the two branch points ζ_1, ζ_2 on the imaginary axis coalesce at i/ϵ. By inspecting this degeneration process at the level of semi-classical eigenstates, we find a uniform condensate with a double density of Bethe roots running along the imaginary axis between $-\mathrm{i}/\epsilon$ and i/ϵ. Kinks and anti-kinks are not compatible with periodic boundary conditions. In an infinitely extended quantum chain however, the kink and antikink eigenstates exist and represent the extra degenerate ground states (with broken translational symmetry) of the XXZ ferromagnet in the easy-axis regime [76, 77]. Kink eigenstates have been derived in [78, 79] using a curious correspondence between the quantum XXZ model and the problem of a melting crystal corner. This derivation however does not require any use of the Bethe quantisation condition (Bethe ansatz equations) and consequently cannot reveal the internal magnon structure of the kink. It would be valuable to devise a method to extract the corresponding numerical solution to the Bethe equations for large system sizes. The task of solving the anisotropic Bethe equations (5.1) in the vicinity of half filling remains quite challenging at this moment. Perhaps one could get some hints by first scanning through the complete list of exact eigenstates for relatively small system sizes (typically of order $L \sim$

10, using e.g. the techniques proposed in [98, 99]) and look for traces of quantised bions in the setting of finite system sizes. So far, our conclusions regarding the kink solutions remain conjectural.

5.5 Summary of results

In this chapter we have studied the finite-gap solutions of classical Landau–Lifshitz model and their semi-classical quantisation in depth. More specifically, we investigated the phenomenology of finding the Bethe root densities of one-cut solutions and forming of condensate due to the non-perturbative quantum corrections. The one-cut solutions, representing the spin precession as the low-energy excitations above the ferromagnetic vacuum, are well understood now. A more interesting setup, i.e. bion solutions in the easy-axis regime, is discussed too, but the results remain conjectural so far.

Using the semi-classical quantisation described here, we can also employ the functional approach to study quantum quantities such as Slavnov overlaps between semi-classical eigenstates [96, 100, 101, 102, 103]. This opens a possibility of studying the semi-classical limit of quench action, and are summarised in [2]. As it turns out, the classical-quantum correspondence between the semi-classical eigenstates and the classical finite-gap solutions can be extended to correlation functions too, which is studied in [2].

Chapter 6

Q operator and spectrum of XXZ model at root of unity

> Algebra is the offer made by the devil to the mathematician.
>
> Michael Atiyah

The contents of this chapter were published in [4].

After focusing on the quantum spin-1/2 XXZ model at weak anisotropy and its semi-classical limit, Landau–Lifshitz model, we move on to the quantum regime. We start with constructing Baxter's Q operator for quantum spin-1/2 XXZ model with arbitrary anisotropy, which is related to the Lax operator with auxiliary space being infinite-dimensional complex spin representation. Despite the difficulty of dealing with infinite-dimensional auxiliary space, the problem simplifies to a finite-dimensional auxiliary space when the anisotropy parameter is at root of unity. Quantum XXZ model at root of unity has further impact on the spectrum, resulting in the descendant-tower structures of eigenstates. In this case, the conventional algebraic Bethe ansatz introduced in Chapter 3 cannot be applied to construct all the eigenstates. We present a set of conjectures on the creation/annihilation operators for solutions associated with the *Fabricius–McCoy* exact strings. Further effects on the thermodynamic

limit of the quantum XXZ model at root of unity are discussed using the theory developed for deciphering the spectrum.

6.1 Some examples of special solutions

Before we start to construct the Q operator for XXZ model, we first show the phenomenology of Bethe roots at infinity and Fabricius–McCoy exact strings, which are of great use when considering the descendant tower structure for XXZ model at root of unity.

6.1.1 Bethe roots at infinity

When $\Delta = \pm 1$ the spectrum exhibits degeneracies due to $\mathfrak{sl}_2$-invariance of the model. Although there are additional degeneracies in the spectrum of $\mathbf{H}$ due to parity invariance, the latter are lifted when taking into account the momentum, or any other parity-odd charges generated by the transfer matrix. The lowering operator $\sum_j \sigma_j^-$ of $\mathfrak{sl}_2$ can be thought of as adding a magnon with vanishing quasimomentum; indeed, it can be shown that a Bethe-ansatz vector has highest weight iff $p_m \neq 0 \bmod 2\pi$ [20]. The isotropic limit of (3.28) (by rescaling $u_m \to \eta\, u_m$ and taking the limit $\eta \to 0$) shows that $p_m = 0$ corresponds to $u_m = \pm\infty$. Therefore, for the XXX model, Bethe roots at infinity lead to descendant states of the global $\mathfrak{sl}_2$ symmetry.

Now let us consider the cases with the anisotropy parameter $\Delta \neq \pm 1$. $\sum_j \sigma_j^\pm$ are no longer generators of global symmetries, so one might expect that there is no more Bethe roots at infinity. However, numerical solutions of the Bethe equations (e.g. via the recipe from Appendix E.0.1) show that infinite Bethe roots are in fact present for the XXZ model.

To understand when Bethe roots at infinity would occur, we turn to the Bethe equations (3.25). Write $n_{\pm\infty}$ for the number of Bethe roots at $\pm\infty$, so that of course $n_{+\infty} + n_{-\infty} \leq M$. Note that $p_m \to \mp \mathrm{i}\eta$ for $u_m \to \pm\infty$, while $S(u_m, u_n) \to e^{\mp 2\eta}$ as long as u_n is finite or goes to $\mp\infty$. Let us assume that the roots at $\pm\infty$ do not scatter ($S = 1$) amongst each other. Then the Bethe equation for the infinite root $u_m = \pm\infty$

becomes [104, 105, 106]

$$\exp\big[\pm\big(N-2\,(M-n_{\pm\infty})\big)\eta\big]=\exp(-\mathrm{i}\phi). \tag{6.1}$$

Let us examine the possible values of $n_{\pm\infty}\in\mathbb{N}$ in each regime of the XXZ spin chain.

For $\eta\in\mathbb{R}$, i.e. in the gapped regime ($|\Delta|>1$), and twist $\phi\in\mathbb{R}$ the only solutions are

$$\phi=0,\qquad n_{+\infty}=n_{-\infty}=\frac{2M-N}{2}. \tag{6.2}$$

This implies that physical solutions with Bethe roots at infinity only exist when $M>N/2$ (also known as 'beyond the equator') and N is even, and that the infinite Bethe roots appear in pairs.

Next consider the gapless regime ($|\Delta|<1$). When $\eta\in\mathrm{i}\,(\mathbb{R}\setminus\pi\,\mathbb{Q})$, so *not* at root of unity, there are more possibilities to allow for Bethe roots at infinity, as long as the twist ϕ is tuned to an (even or odd, depending on the parity of N) integer multiple of $\mathrm{i}\,\eta$:

$$n_{\pm\infty}=\frac{2M-N\mp\mathrm{i}\phi/\eta}{2}. \tag{6.3}$$

In particular, the number of roots at $+\infty$ and $-\infty$ do not coincide if $\phi\neq 0$. Finally, at root of unity $\eta=\mathrm{i}\pi\,\ell_1/\ell_2$ the condition becomes

$$n_{\pm\infty}=\frac{2M-N\mp\mathrm{i}\phi/\eta+2\pi\mathrm{i}\,k_{\pm}/\eta}{2},\qquad k_{\pm}\in\mathbb{Z}. \tag{6.4}$$

In this case there is an additional condition that we will discuss momentarily, see (6.6).

The meaning of $n_{\pm\infty}\neq 0$ for the XXZ model can be understood from the algebraic Bethe ansatz (cf. Chapter 3). Bethe roots at infinity correspond to applications of the lowering operators of the global $U_q(\mathfrak{sl}_2)$ algebra (see Appendix D.1). Namely, when N is even and ϕ vanishes, each eigenstate beyond the equator (say at $M'>N/2$) is obtained from a Bethe eigenvector at $M=N-M'<N/2$ by $M'-N/2=N/2-M$ applications of the parity-invariant product $\mathbf{S}^-\,\bar{\mathbf{S}}^-$. Up to an overall factor

the result is the spin-reverse of the Bethe vector we started with. We find that

$$|\{v_{m'}\}_{m'=1}^{M'}\rangle \propto \left(\mathbf{S}^- \bar{\mathbf{S}}^-\right)^{N/2-M} |\{u_m\}_{m=1}^{M}\rangle \propto \prod_{k=1}^{N}\sigma_k^x \; |\{u_m\}_{m=1}^{M}\rangle\,. \quad (6.5)$$

If N is odd the XXZ spin chain is still invariant under a global spin flip, reversing $\uparrow \leftrightarrow \downarrow$ everywhere, but there are no infinite roots and we have not been able to find a simple relation between the Bethe roots $\{v_{m'}\}_{m'=1}^{M'}$ and $\{u_m\}_{m=1}^{M}$ on the two sides of the equator.

At root of unity we have to be more careful, because $\mathbf{S}^-$ and $\bar{\mathbf{S}}^-$ are nilpotent. Here an additional requirement is needed to ensure that (6.5) is nonzero:

$$0 \le n_{+\infty} \le \ell_2 - 1, \qquad 0 \le n_{-\infty} \le \ell_2 - 1. \quad (6.6)$$

In particular, in the periodic case ($\phi = 0$) there is at most one nonzero solution to (6.4) in the range (6.6), leaving only three possible scenarios:

$$n_{+\infty} = n_{-\infty}; \qquad n_{+\infty} > n_{-\infty} = 0; \qquad n_{-\infty} > n_{+\infty} = 0. \quad (6.7)$$

The method that we develop in the following sections will help to elucidate the structure present in the spectrum in the presence of Bethe roots at infinity. The conclusion (6.7) will be useful in Section 6.7.1 when we discuss applications to the spectrum of the XXZ model.

6.1.2 Fabricius–McCoy strings

At root of unity $\eta = \mathrm{i}\pi\ell_1/\ell_2$, the spectrum of the XXZ spin chain possesses many degeneracies than the spectrum not at root of unity [107]. Fabricius and McCoy realised [105, 108] that this is related to solutions to the Bethe equations (3.25) that contain exact ℓ_2-strings. An earlier work of Baxter [109] has shown similar solutions in the 8-vertex model (XYZ model). A *Fabricius–McCoy (FM) string* consists of ℓ_2 Bethe roots that are equally spaced (in the imaginary direction) around a string centre $\alpha^{\mathrm{FM}} \in \mathbb{C}$:

$$u_m = \alpha^{\mathrm{FM}} + \frac{2\,m - 1 - \ell_2}{2\,\ell_2}\,\mathrm{i}\pi, \qquad 1 \le m \le \ell_2. \quad (6.8)$$

This describes a bound state, which as a whole does not scatter with other Bethe roots:

$$\prod_{m=1}^{\ell_2} S(u_m, u_{m'}) = 1, \qquad \ell_2 < m' \leq M. \tag{6.9}$$

A FM string is not only 'transparent' in scattering, but carries vanishing energy. In fact, it does not carry any local charge generated by transfer matrix $\mathbf{T}_{1/2}(u)$, except that it may carry momentum π as we explain Section 6.7. It actually carries a specific type of quasilocal charges called the *Z charges* [110, 52, 111]. The physical implications of this will be discussed in Section 6.9.2.

When any FM string is present among the Bethe roots for a given eigenstate, it is impossible to determine the location of the string centre α_j^{FM} by solving Bethe ansatz equations (3.25) or the (functional) TQ relation using method in Appendix E.0.1. In this thesis we present a method to determine α_j^{FM}. We begin with a concrete example.

Example. Consider a homogeneous spin chain with $N = 6$, $\phi = 0$ and $\Delta = 1/2 = \cos(\pi/3)$, i.e. $\ell_1 = 1$ and $\ell_2 = 3$. At $M = 3$ there are two degenerate states with the same eigenvalues of $\mathbf{T}_s(u)$, $2s \in \mathbb{Z}_{>0}$. These eigenvalues moreover coincide with those of $|\uparrow\uparrow\uparrow\uparrow\uparrow\uparrow\rangle$ and $|\downarrow\downarrow\downarrow\downarrow\downarrow\downarrow\rangle$ up to a π phase. Using the techniques from Section 6.5 we find that the two degenerate states have FM strings whose centres we can determine exactly:

$$\begin{aligned} u_m &= \alpha_1^{\text{FM}} + (m-2)\frac{\mathrm{i}\pi}{3}, \\ v_m &= \alpha_2^{\text{FM}} + (m-2)\frac{\mathrm{i}\pi}{3}, \\ \alpha_{1,2}^{\text{FM}} &= \pm\frac{\log(10+3\sqrt{11})}{6} + \frac{\mathrm{i}\pi}{6}, \quad 1 \leq m \leq 3, \end{aligned} \tag{6.10}$$

where the Bethe roots are found analytically using the truncated two-parameter transfer matrix that we will introduce in Section 6.5.

The degeneracies imply additional symmetry acquired by the XXZ model at root of unity. Namely, in this case a there is a representation of the loop algebra $\widehat{\mathfrak{sl}_2}$ [107]. Although the ℓ_2th powers of $\mathbf{S}^{\pm}$ and $\bar{\mathbf{S}}^{\pm}$

vanish one can regularise these operators to get generators of the loop algebra. This yields lowering operators that produce the eigenvectors corresponding to the FM string (6.10): the eigenspace is spanned by any two of the four vectors

$$\begin{aligned} &\lim_{\eta\to \mathrm{i}\pi/3} \frac{(\mathbf{S}^-)^3}{[3]_q!}\,|{\uparrow\uparrow\uparrow\uparrow\uparrow\uparrow}\rangle\,, && |\{u_1,u_2,u_3\}\rangle\,, \\ &\lim_{\eta\to \mathrm{i}\pi/3} \frac{(\bar{\mathbf{S}}^-)^3}{[3]_q!}\,|{\uparrow\uparrow\uparrow\uparrow\uparrow\uparrow}\rangle\,, && |\{v_1,v_2,v_3\}\rangle\,. \end{aligned} \tag{6.11}$$

The Bethe vectors are nontrivial linear combinations of the two 'loop descendants' on the left in (6.11). We would like to remark that the loop descendants are not eigenvectors of the two-parameter transfer matrix $\tilde{\mathbb{T}}(x,y)$ that we will introduce in Section 6.5.2.

6.2 Two-parameter transfer matrix

In this section, we generalise the Lax operator with two-dimensional spin-1/2 auxiliary space to Lax operator with auxiliary space being other representation of quantum algebra $\mathcal{U}_q(\mathfrak{sl}_2)$.

We start with the Lax operator associated to a single spin-1/2 site. Consider an auxiliary space V_a, which is an irreducible representation of $U_q(\mathfrak{sl}_2)$. Generators $\mathbf{S}_a^{\pm}$ along with $\mathbf{K}_a = q^{\mathbf{S}_a^z}$ satisfies the following commutation relations,

$$\mathbf{K}_a\,\mathbf{S}_a^{\pm}\,\mathbf{K}_a^{-1} = q^{\pm 1}\,\mathbf{S}_a^{\pm}, \quad \left[\mathbf{S}_a^{+},\mathbf{S}_a^{-}\right] = \frac{\mathbf{K}_a^2-\mathbf{K}_a^{-2}}{q-q^{-1}}. \tag{6.12}$$

Although the local Hilbert space of the spin-1/2 model is always two-dimensional, we consider various representations V_a for the auxiliary space. The representations of $\mathcal{U}_q(\mathfrak{sl}_2)$ used in this thesis are summarised in Ap-

pendix D.2. The Lax operator on $V_a \otimes \mathbb{C}^2$ is

$$\begin{aligned}\mathbf{L}_{aj}(u) &= \sinh(u)\,\frac{\mathbf{K}_a + \mathbf{K}_a^{-1}}{2} + \cosh(u)\,\frac{\mathbf{K}_a - \mathbf{K}_a^{-1}}{2}\,\sigma_j^z \\ &\quad + \sinh(\eta)\big(\mathbf{S}_a^+\,\sigma_j^- + \mathbf{S}_a^-\,\sigma_j^+\big) \\ &= \frac{1}{2}\begin{pmatrix} e^u\,\mathbf{K}_a - e^{-u}\,\mathbf{K}_a^{-1} & 2\sinh(\eta)\,\mathbf{S}_a^- \\ 2\sinh(\eta)\,\mathbf{S}_a^+ & e^u\,\mathbf{K}_a^{-1} - e^{-u}\,\mathbf{K}_a \end{pmatrix}_j \\ &= \begin{pmatrix} \sinh\big(u + \eta\,\mathbf{S}_a^z\big) & \sinh(\eta)\,\mathbf{S}_a^- \\ \sinh(\eta)\,\mathbf{S}_a^+ & \sinh\big(u - \eta\,\mathbf{S}_a^z\big) \end{pmatrix}_j,\end{aligned} \tag{6.13}$$

where the matrix acts on the spin-$\frac{1}{2}$ representation at site j and the entries are operators acting on the auxiliary space a. Importantly, the Lax operator $\mathbf{L}_{aj}(u)$ obeys the RLL relations

$$\mathbf{R}_{ab}(u-v)\,\mathbf{L}_{aj}(u)\,\mathbf{L}_{bj}(v) = \mathbf{L}_{bj}(v)\,\mathbf{L}_{aj}(u)\,\mathbf{R}_{ab}(u-v) \tag{6.14}$$

on $V_a \otimes V_b \otimes \mathbb{C}^2$, where $V_b \cong V_a$ is a second copy of the auxiliary space. We parametrise the entries of the R matrix as $\mathbf{R}_{ab}(u) = \mathbf{L}_{ab}(u+\eta/2)$, keeping the current form of RLL relation (6.14). In case the auxiliary space is the spin-1/2 representation the R-matrix becomes (3.4) introduced in Chapter 3.

Now consider N spin-1/2 sites, each with its own (local) Lax operator $\mathbf{L}_{aj}(u)$. The monodromy matrix on $V_a \otimes (\mathbb{C}^2)^{\otimes N}$ is defined as[1]

$$\mathbf{M}_a(u,\phi) = \mathbf{L}_{aN}(u)\cdots\mathbf{L}_{a2}(u)\,\mathbf{L}_{a1}(u)\,\mathbf{E}_a(\phi), \tag{6.15}$$

where twist ϕ is introduced through the twist operator $\mathbf{E}_a(\phi)$. We will only consider diagonal twists, so that the R-matrix commutes with $\mathbf{E}_a(\phi)\,\mathbf{E}_b(\phi)$. When V_a is the spin-$\frac{1}{2}$ irrep we have $\mathbf{E}_a(\phi) = \mathrm{diag}(e^{\mathrm{i}\phi}, 1)$; see Appendix F for the other representations that we will use. It is easy to show that the monodromy matrix obeys the RLL relations (6.14) as well using the "train argument".

From the monodromy matrix whose auxiliary space is in spin-1/2 representation we can construct the Hamiltonian (3.11) as demonstrated in Chapter 3. The transfer matrix $\mathbf{T}$ is the trace of monodromy matrix $\mathbf{M}_a$ over the auxiliary space

$$\mathbf{T}(u,\phi) = \mathrm{tr}_a\,\mathbf{M}_a(u,\phi). \tag{6.16}$$

[1] We omit the inhomogeneities here for simplicity.

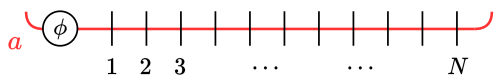

Figure 6.1: Graphical representation of the transfer matrix with N sites. The red line represents the auxiliary space and the black lines represent the spin-1/2 spaces. The twist operator is labelled by ϕ.

The RLL relations imply that there is a one-parameter family of commuting operators,

$$[\mathbf{T}(u,\phi),\mathbf{T}(v,\phi)]=0 \qquad \text{for all} \quad u,v\in\mathbb{C}. \tag{6.17}$$

As a consequence any expansion in u generates a hierarchy of commuting operators that do not depend on u. In particular, important conserved charges are obtained by taking logarithmic derivatives with respect to the spectral parameter u at $u=\eta/2$:

$$\mathbf{I}^{(j)}=-\mathrm{i}\frac{\mathrm{d}^{j-1}}{\mathrm{d}u^{j-1}}\log\mathbf{T}(u,\phi)\Big|_{u=\eta/2}, \tag{6.18}$$

because of their "locality". Those conserved charges can be expressed in local density terms when auxiliary space a is in spin-1/2 representation. More generally, when $V_a\cong\mathbb{C}^{2s+1}$ is the spin-s irrep of $U_q(\mathfrak{sl}_2)$ with $s\geq 1$ the resulting conserved charges are quasilocal [110, 52, 111].

The spectrum of the transfer matrix with $V_a\cong\mathbb{C}^2$ can be characterised via the algebraic Bethe ansatz, which is briefly introduced in Chapter 3. In the presence of a diagonal twist, the operators on the diagonal in (3.13) give rise to the (twisted) transfer matrix,

$$s=1/2: \qquad \mathbf{T}(u,\phi)=e^{\mathrm{i}\phi}\mathbf{A}(u)+\mathbf{D}(u). \tag{6.19}$$

The eigenstates of transfer matrix can be constructed through the off-diagonal terms of (3.13)

$$|\{v_m\}_{m=1}^M\rangle=\prod_{m=1}^M\mathbf{B}(v_m)\;|\Omega\rangle \tag{6.20}$$

with eigenvalue

$$T(u,\{v_m\}_{m=1}^M,\phi) = e^{\mathrm{i}\phi}\,\sinh^N(u+\eta/2)\prod_{m=1}^M\frac{\sinh(v_m-u+\eta)}{\sinh(v_m-u)} + \sinh^N(u-\eta/2)\prod_{m=1}^M\frac{\sinh(u-v_m+\eta)}{\sinh(u-v_m)} \tag{6.21}$$

provided the parameters $\{v_m\}$ satisfy the Bethe ansatz equations (3.25).

Remark. When the spectrum of transfer matrices of a system at root of unity contains eigenstates associated with FM strings, the construction (6.20) is *not* enough to obtain all the eigenstates [105, 108, 106]. However, it is still possible to label the eigenstates as $|\{u_j\}_{j=1}^M\rangle$ where $\{u_j\}_{j=1}^M$ are interpreted as the zeros of the eigenvalue of the Q operator constructed in Section 6.5.2. We will use this definition to label all the eigenstates of Q operator. In the absence of FM strings they can be explicitly constructed via the algebraic Bethe ansatz (6.20); for the case with FM strings see our conjectures in Section 6.8.

6.2.1 Transfer matrices

Different transfer matrices are obtained by using different representations in the auxiliary space. For example, we have already constructed the ('fundamental') $s = 1/2$ transfer matrix of the six-vertex model in (3.3) in Chapter 3. We denote the transfer matrices with different representation by decorating each $\mathbf{T}$ with a subscript that reminds us of the choice of representation in the auxiliary space V_a that was traced over. For example, from now on we denote the fundamental transfer matrix (3.3) by $\mathbf{T}_{1/2}$.

We will work with the following choices, see Appendix D.2 for the details:

- The unitary spin-s representation with $s \in \frac{1}{2}\mathbb{Z}_{\geq 0}$. Here $V_s \cong \mathbb{C}^{2s+1}$. We denote the monodromy and transfer matrices by $\mathbf{M}_s$ and $\mathbf{T}_s$. This generalises the case $s = 1/2$ considered so far, and leads to the quasilocal charges mentioned above.

- The highest-weight spin-s representation with 'complex spin' $s \in \mathbb{C}$. We denote its transfer matrix by $\mathbf{T}_s^{\mathrm{hw}}$.

  - For generic q (not at root of unity) this representation is infinite dimensional. One has to take care that the trace in (6.16) makes sense in this case.

  - If $s \in \frac{1}{2}\mathbb{Z}_{\geq 0}$ it can be truncated to a $(2s+1)$-dimensional (sub)representation. The result coincides with the unitary spin-s representation up to a gauge transformation (conjugation). In particular, having taken the trace over the auxiliary space, the truncated transfer matrix is equal to $\mathbf{T}_s$. See Section 6.4.1.

  - At root of unity both the lowering and raising operators of the complex-spin highest-weight representation become nilpotent, allowing for another truncation to a ℓ_2-dimensional subspace for any $s \in \mathbb{C}$. We will denote this truncated transfer matrix by $\tilde{\mathbf{T}}_s$.

There is an important difference between the two truncated transfer matrices. Since ℓ_2 varies as $\eta = \mathrm{i}\pi\frac{\ell_1}{\ell_2}$ runs through $\mathrm{i}\pi\,\mathbb{Q}$, the spectra of the truncated transfer matrices $\tilde{\mathbf{T}}_s$, with ℓ_2-dimensional auxiliary space, are *not* continuous when varying η. Instead, the transfer matrices $\mathbf{T}_s$ for $s \in \frac{1}{2}\mathbb{Z}$ have spectra that vary smoothly with respect to η.

The RLL relations (6.14) guarantee that each of the above transfer matrices commute among themselves, like in (6.17), as well as with each other (for different s, s'). As a result, they share the eigenvectors produced by the algebraic Bethe ansatz (6.20).

The *transfer matrix fusion relations* are a system of equations that show how the higher-spin transfer matrices $\mathbf{T}_s$ can be constructed from $\mathbf{T}_{1/2}$. These relations are typically obtained by fusion, i.e. taking the tensor product of several spin-$\frac{1}{2}$ representations and projecting onto the spin-s submodule [112, 113]. We instead obtain the transfer matrix fusion relations via decomposing the auxiliary space representation, cf. Section 6.4.3.

6.2.2 Q operators

There have been numerous endeavours to understand the relations between the different transfer matrices and how they can be used to characterise all eigenstates of the XXZ model. The most famous of these was found by Baxter in the 70s [114, 115, 109], where he constructed the Q operator that satisfies the *matrix TQ relation* (with respect to $\mathbf{T}_{1/2}$) for the eight-vertex model, which is closely related to the quantum spin-1/2 XYZ model. A similar construction can be performed for the six-vertex model and the XXZ model [19]. The eigenvalues of the Q operator are called *Q functions* which have been already mentioned in Chapter 5, and their zeros are precisely Bethe roots, i.e. solutions to the Bethe equations (3.25). The corresponding eigenvectors are constructed via ABA in (6.20). Baxter constructed the Q operator by solving the matrix TQ relation directly. For the purpose of numerically obtaining Bethe roots it is much easier to solve the *functional* TQ relation, i.e. the relation between the eigenvalues of $\mathbf{T}_{1/2}$ and the Q operator. Functional TQ relation can be solved as coupled linear equations so long as we know the eigenvalues of transfer matrix $\mathbf{T}_{1/2}$ for certain eigenvector, instead of coupled nonlinear equations in Bethe equations (3.25). At root of unity, however, the functional TQ relation is not enough to determine the full spectrum due to the existence of exact FM strings.

We will construct the Q operator explicitly and prove the matrix TQ relation and the transfer matrix fusion relation. We use a new approach that is based on the factorisation and decomposition of transfer matrix $\mathbf{T}_s^{\mathrm{hw}}$ associated to an auxilary space that is an infinite-dimensional complex-spin representation [116]. This construction works for any anisotropy parameter $\Delta \in \mathbb{R}$. In the case of root of unity, we further prove the truncated fusion relations for the transfer matrices $\tilde{\mathbf{T}}_s$ using the same method.

These truncated fusion relations allow us to prove a conjecture made in Refs. [117, 118, 119]. This enables us to construct the Q operator explicit at root of unity using a finite-dimensional monodromy matrix, and elucidate the exponentially many degeneracies, which are closely related to the FM string but cannot be resolved via the functional TQ relation.

6.3 Factorisation of $\mathbf{T}_s^{\mathrm{hw}}$

We start with showing that the spin $s \in \mathbb{C}$ highest-weight transfer matrix gives rise to a two-parameter transfer matrix that can be factorised. In this section we consider the cases with arbitrary q (thus $\Delta \in \mathbb{R}$). We will specialise to root of unity later.

6.3.1 Factorisation of Lax operator

Before we start to prove the factorisation of the transfer matrix $\mathbf{T}_s^{\mathrm{hw}}$ we need to study the factorisation of the Lax operator with the auxiliary space V_a being an infinite-dimensional complex spin-s representation. Although for $\mathbf{T}_s^{\mathrm{hw}}$ we are interested in the 'half-infinite' highest-weight (Verma) module (D.9), we start with infinite-dimensional auxiliary space that does not have a highest-weight vector.

We need to truncate the auxiliary space for such a monodromy matrix in order to take the trace. Let V_a be the infinite-dimensional Hilbert space with orthonormal basis $|n\rangle_a$, $n \in \mathbb{Z}$. It decomposes as a direct sum $V_a = V_a^+ \oplus V_a^-$, where V_a^+ is spanned by $|n\rangle_a$ with $n \geq 0$, which is the space that we are after, while V_a^- is the span of $|n\rangle_a$ with $n < 0$. For this auxiliary space we implicitly assume that the trace in (6.16) is only over V_a^+.

We denote $|n\rangle\langle n'|_a \coloneqq |n\rangle_a \, {}_a\langle n'|$ as the matrix basis. Consider the following operators:

$$\mathbf{W}_a = \sum_{n=-\infty}^{\infty} q^n \, |n\rangle\langle n|_a, \quad \mathbf{X}_a = \sum_{n=-\infty}^{\infty} |n+1\rangle\langle n|_a. \tag{6.22}$$

If we think of V_a as the sequence space ℓ^2 by identifying $|n\rangle_a$ with the sequence δ_n with entries $(\delta_n)_i = \delta_{ni}$ then $\mathbf{X}_a$ is the right shift. The two operators (6.22) form a Weyl pair, $\mathbf{W}_a \mathbf{X}_a = q \, \mathbf{X}_a \mathbf{W}_a$. We also use the adjoint $\mathbf{X}_a^\dagger = \sum_n |n\rangle\langle n+1|_a$. On V_a it is the inverse of $\mathbf{X}_a$. In particular $\mathbf{X}_a^\dagger$ commutes with $\mathbf{X}_a$ on V_a.

The half-infinite space V_a^+ is preserved by both of (6.22), but not by

$\mathbf{X}_a^\dagger$. Instead of $\mathbf{X}_a^\dagger$, we use the following operator in V_a^+,

$$\mathbf{Y}_a = \sum_{n=0}^{\infty} |n\rangle\langle n+1|_a. \tag{6.23}$$

Hence, on V_a^+ we have $\mathbf{Y}_a \mathbf{X}_a = \mathbb{1}$ while $\mathbf{X}_a \mathbf{Y}_a = \sum_{n>0} |n\rangle\langle n|_a \neq \mathbb{1}$. Together, (6.22) and (6.23) can be used to give a highest-weight representation of $U_q(\mathfrak{sl}_2)$ on V_a^+ with spin $s \in \mathbb{C}$:

$$\begin{aligned}
\mathbf{K}_a &= q^{-s}\,\mathbf{W}_a = \sum_{n=0}^{\infty} q^{n-s}\,|n\rangle\langle n|_a, \\
\mathbf{S}_a^+ &= \frac{q^{2s+1}\,\mathbf{W}_a^{-1} - q^{-2s-1}\,\mathbf{W}_a}{q-q^{-1}}\,\mathbf{X}_a = \sum_{n=0}^{\infty} [2s-n]_q\,|n+1\rangle\langle n|_a, \\
\mathbf{S}_a^- &= \mathbf{Y}_a\,\frac{\mathbf{W}_a - \mathbf{W}_a^{-1}}{q-q^{-1}} = \sum_{n=0}^{\infty} [n+1]_q\,|n\rangle\langle n+1|_a.
\end{aligned} \tag{6.24}$$

See also Appendix D.2.

Now we turn to the Lax operator $\mathbf{L}_{aj}(u,s)$ associated to a site j. We introduce two 'spectral parameters' x and y as simple combinations of u and s,

$$x := u + \frac{2s+1}{2}\eta, \qquad y := u - \frac{2s+1}{2}\eta. \tag{6.25}$$

They are convenient when deriving the transfer matrix fusion relations. Starting with the auxiliary space V_a the Lax operator can be decomposed into a product of operators separating the dependence on these spectral parameters (see also appendix B of Ref. [120]):

$$\mathbf{L}_{aj}(u,s) = \frac{1}{2}\begin{pmatrix} \mathbf{X}_a^\dagger & 0 \\ 0 & 1 \end{pmatrix}_j \mathbf{u}_j(x) \begin{pmatrix} \mathbf{W}_a & 0 \\ 0 & \mathbf{W}_a^{-1} \end{pmatrix}_j \mathbf{v}_j(y)^{\mathrm{T}} \begin{pmatrix} \mathbf{X}_a & 0 \\ 0 & 1 \end{pmatrix}_j, \tag{6.26}$$

where the two by two matrices $\mathbf{u}(x)$ and $\mathbf{v}(y)$ are defined as

$$\mathbf{u}(x) = \begin{pmatrix} 1 & -1 \\ -e^{-x+\eta/2} & e^{x-\eta/2} \end{pmatrix}, \qquad \mathbf{v}(y) = \begin{pmatrix} e^{y-\eta/2} & e^{-y+\eta/2} \\ 1 & 1 \end{pmatrix}. \tag{6.27}$$

The factorisation (6.26) coincides with the one introduced in [121]. To understand (6.26) we compute the product on the right-hand side. The

result is

$$\mathbf{L}_{aj}(x,y) = \frac{1}{2}\begin{pmatrix} e^{y+\eta/2}\,\mathbf{W}_a - e^{-y-\eta/2}\,\mathbf{W}_a^{-1} & \mathbf{X}_a^\dagger\,(\mathbf{W}_a - \mathbf{W}_a^{-1}) \\ (e^{x-y}\,\mathbf{W}_a^{-1} - e^{-x+y}\,\mathbf{W}_a)\,\mathbf{X}_a & e^{x-\eta/2}\,\mathbf{W}_a^{-1} - e^{-x+\eta/2}\,\mathbf{W}_a \end{pmatrix}_j, \tag{6.28}$$

where we simplified the top-left entry using $\mathbf{W}_a\,\mathbf{X}_a = q\,\mathbf{X}_a\mathbf{W}_a$ and $\mathbf{X}_a^\dagger\,\mathbf{X}_a = 1$. Importantly, the four matrix elements preserve the subspace V_a^+. This is obvious for all but the top-right entry, for which the point is that $\mathbf{X}_a^\dagger\,(\mathbf{W}_a - \mathbf{W}_a^{-1})\,|n\rangle_a = (q^n - q^{-n})\,|n-1\rangle_a$ has vanishing prefactor when $n = 0$. Thus the effect of the restriction is to replace $\mathbf{X}_a^\dagger$ by $\mathbf{Y}_a$. In view of (6.24) and $q = e^\eta$ we recognise the entries of (6.28) as

$$\begin{aligned} &e^{u}\,\mathbf{K}_a = e^{y+\eta/2}\,\mathbf{W}_a, \qquad e^{-u}\,\mathbf{K}_a = e^{-x+\eta/2}\,\mathbf{W}_a, \\ \text{on } V_a^+: \quad &2\sinh(\eta)\,\mathbf{S}_a^+ = (e^{x-y}\,\mathbf{W}_a^{-1} - e^{-x+y}\,\mathbf{W}_a)\,\mathbf{X}_a, \\ &2\sinh(\eta)\,\mathbf{S}_a^- = \mathbf{Y}_a\,(\mathbf{W}_a - \mathbf{W}_a^{-1}). \end{aligned} \tag{6.29}$$

This shows that the right-hand side of (6.26) is the same as that in (6.13). The point of this discussion is to show that (6.26) can be used instead of (6.13) when computing the transfer matrix provided that we restrict the trace to V_a^+.

6.3.2 Intertwiners

For convenience, we denote the product on the right-hand side of (6.26) by $\mathbf{L}_{aj}(\mathbf{u}_x, \mathbf{v}_y)$. Exchanging $\mathbf{u}_x$ and $\mathbf{v}_y$ we obtain

$$\begin{aligned} &\mathbf{L}_{aj}(\mathbf{v}_y, \mathbf{u}_x) \\ &= \frac{1}{2}\begin{pmatrix} e^{y+\eta/2}\,\mathbf{W}_a - e^{-y-\eta/2}\,\mathbf{W}_a^{-1} & \mathbf{X}_a^\dagger\,(e^{x-y}\,\mathbf{W}_a^{-1} - e^{-x+y}\,\mathbf{W}_a) \\ (\mathbf{W}_a - \mathbf{W}_a^{-1})\,\mathbf{X}_a & e^{x-\eta/2}\,\mathbf{W}_a^{-1} - e^{-x+\eta/2}\,\mathbf{W}_a \end{pmatrix}_j \\ &= \mathbf{L}_{aj}(\mathbf{u}_x, \mathbf{v}_y)^{\mathrm{T}}. \end{aligned} \tag{6.30}$$

In the second line the transpose is both in the auxiliary space and in the physical space; note that (on the auxiliary space) $\mathbf{X}_a^{\mathrm{T}} = \mathbf{X}_a^\dagger$ while the diagonal operator $\mathbf{W}_a^{\mathrm{T}} = \mathbf{W}_a$ is symmetric.

This time the matrix elements clearly preserve V_a^-, which allows us to consider their action on the quotient $V/V_a^- \cong V_a^+$ i.e. we treat all basis $|n\rangle_a$ with $n < 0$ as zero. When acting on V_a^+, (6.30) is equivalent to

substitute $\mathbf{Y}_a$ for $\mathbf{X}_a^\dagger$. Therefore we construct the monodromy matrix as in (6.15). We take the trace over V_a^+ as in (6.16) to obtain the transfer matrix.

It is straightforward to intertwine $\mathbf{L}_{aj}(\mathbf{u}_x, \mathbf{v}_y)$ with $\mathbf{L}_{aj}(\mathbf{v}_y, \mathbf{u}_x)$ when both are viewed as acting on V_a^+:

$$\mathbf{F}_a(x,y)\,\mathbf{L}_{aj}(\mathbf{u}_x,\mathbf{v}_y) = \mathbf{L}_{aj}(\mathbf{v}_y,\mathbf{u}_x)\,\mathbf{F}_a(x,y), \tag{6.31}$$

where the solution for the intertwiner is

$$\begin{aligned} \mathbf{F}_a(x,y) &= \mathbf{F}_a(x-y) = \sum_{n=0}^{\infty} \begin{bmatrix} (x-y-\eta)/\eta \\ n \end{bmatrix}_q^{-1} |n\rangle\langle n|_a, \\ \begin{bmatrix} (x-y-\eta)/\eta \\ n \end{bmatrix}_q &= \begin{bmatrix} 2s \\ n \end{bmatrix}_q = \prod_{k=1}^{n} \frac{\sinh[(2s+1-k)\eta]}{\sinh(k\eta)}. \end{aligned} \tag{6.32}$$

Note that $\mathbf{F}_a(x,y)$ only depends on $x-y = (2s+1)\eta$, and not on the original spectral parameter u. It is well defined for generic values of this quantity, namely for $x-y \notin \eta\,\mathbb{Z} \oplus 2\pi\mathrm{i}\,\mathbb{Z}$. It is clear that the intertwining relation holds for the entries on the diagonal. For the remaining two entries (which are related by transposition) the relation follows from

$$\begin{bmatrix} 2s \\ n+1 \end{bmatrix}_q [n+1]_q = \begin{bmatrix} 2s \\ n \end{bmatrix}_q [2s-n]_q.$$

Now we introduce a copy $V_b \cong V_a$ with its own spectral parameter u' and spin $s' \in \mathbb{C}$, or equivalently x', y' as in (6.25). Consider the product $\mathbf{L}_{aj}(\mathbf{u}_x, \mathbf{v}_y)\,\mathbf{L}_{bj}(\mathbf{v}_{y'}, \mathbf{u}_{x'})$. We can construct an intertwiner $\mathbf{G}_{ab}(y,y')$ that interchanges $\mathbf{v}_y$ and $\mathbf{v}_{y'}$ in this product:

$$\begin{aligned} &\mathbf{G}_{ab}(y,y')\,\mathbf{L}_{aj}(\mathbf{u}_x,\mathbf{v}_y)\,\mathbf{L}_{bj}(\mathbf{v}_{y'},\mathbf{u}_{x'}) \\ &\qquad = \mathbf{L}_{aj}(\mathbf{u}_x,\mathbf{v}_{y'})\,\mathbf{L}_{bj}(\mathbf{v}_y,\mathbf{u}_{x'})\,\mathbf{G}_{ab}(y,y'). \end{aligned} \tag{6.33}$$

To solve this we first consider the big space $V_a \otimes V_b$ and write the Lax operators as products like in (6.26). We look for $\mathbf{G}_{ab}(y,y') = g_{y,y'}(\mathbf{X}_a\,\mathbf{X}_b^\dagger)$ in the form of a power series $g_{y,y'}$ in $\mathbf{Z}_{ab} \coloneqq \mathbf{X}_a\,\mathbf{X}_b^\dagger$. This commutes with $\mathbf{X}_a^\dagger$ on the left and with $\mathbf{X}_b$ on the right. Further using $\mathbf{Z}_{ab}\,\mathbf{W}_a^{\pm 1} =$

$q^{\mp 1}\,\mathbf{W}_a^{\pm 1}\,\mathbf{Z}_{ab}$ and $\mathbf{W}_b^{\pm 1}\,\mathbf{Z}_{ab} = q^{\mp 1}\,\mathbf{Z}_{ab}\,\mathbf{W}_b^{\pm 1}$ (6.33) reduces to

$$\begin{aligned}&\begin{pmatrix} g_{y,y'}(q^{-1}\,\mathbf{Z}_{ab}) & 0 \\ 0 & g_{y,y'}(q\,\mathbf{Z}_{ab}) \end{pmatrix}_j \mathbf{v}_j(y)^{\mathrm{T}} \begin{pmatrix} \mathbf{Z}_{ab} & 0 \\ 0 & 1 \end{pmatrix}_j \mathbf{v}_j(y') \\ &= \mathbf{v}_j(y')^{\mathrm{T}} \begin{pmatrix} \mathbf{Z}_{ab} & 0 \\ 0 & 1 \end{pmatrix}_j \mathbf{v}_j(y) \begin{pmatrix} g_{y,y'}(q^{-1}\,\mathbf{Z}_{ab}) & 0 \\ 0 & g_{y,y'}(q\,\mathbf{Z}_{ab}) \end{pmatrix}_j .\end{aligned} \tag{6.34}$$

Using (6.27) this reduces to the functional equation

$$g_{y,y'}(qz)\,(1 + z\,e^{-y+y'}) = g_{y,y'}(q^{-1}z)\,(1 + z\,e^{y-y'}), \tag{6.35}$$

which is solved by

$$\begin{aligned} g_{y,y'}(z) &= \sum_{n=0}^{\infty} \begin{bmatrix} (y-y')/\eta \\ n \end{bmatrix}_q z^n, \\ \begin{bmatrix} (y-y')/\eta \\ n \end{bmatrix}_q &= \prod_{k=1}^{n} \frac{\sinh[y-y'-(k-1)\eta]}{\sinh(k\eta)}. \end{aligned} \tag{6.36}$$

Since $\mathbf{X}_a\,\mathbf{X}_b^\dagger$ preserves the subspace $V_a^+ \otimes V_b^-$ the intertwiner does so too. Restricting to V_a^+ and passing to the quotient $V_b/V_b^- \cong V_b^+$, we replace $\mathbf{X}_b^\dagger$ by $\mathbf{Y}_b$. Then the relation (6.33) is obeyed on $V_a^+ \otimes V_b^+$ with

$$\mathbf{G}_{ab}(y,y') = \sum_{n=0}^{\infty} \begin{bmatrix} (y-y')/\eta \\ n \end{bmatrix}_q (\mathbf{X}_a\,\mathbf{Y}_b)^n. \tag{6.37}$$

Similarly, we define an intertwiner $\mathbf{H}_{ab}(x,x')$ which interchanges $\mathbf{u}_x$ and $\mathbf{u}_{x'}$:

$$\begin{aligned}&\mathbf{H}_{ab}(x,x')\,\mathbf{L}_{aj}(\mathbf{v}_y,\mathbf{u}_x)\,\mathbf{L}_{bj}(\mathbf{u}_{x'},\mathbf{v}_{y'}) \\ &\qquad = \mathbf{L}_{aj}(\mathbf{v}_y,\mathbf{u}_{x'})\,\mathbf{L}_{bj}(\mathbf{u}_x,\mathbf{v}_{y'})\,\mathbf{H}_{ab}(x,x').\end{aligned} \tag{6.38}$$

This time the roles of V_a and V_b are reversed and we seek a power series in $\mathbf{X}_a^\dagger\,\mathbf{X}_b$. Proceeding as before, now taking the quotient $V_a/V_a^- \cong V_a^+$ and restricting V_b to V_b^+, we find

$$\mathbf{H}_{ab}(x,x') = \sum_{n=0}^{\infty} \begin{bmatrix} (x-x')/\eta \\ n \end{bmatrix}_q (\mathbf{Y}_a\,\mathbf{X}_b)^n. \tag{6.39}$$

6.3.3 Two-parameter transfer matrix

As discussed above, we reparametrise the transfer matrix with infinite-dimensional complex spin-s auxiliary space as a *two*-parameter transfer matrix:

$$\mathbb{T}(x, y, \phi) \coloneqq \mathbf{T}_s^{\mathrm{hw}}(u, \phi). \tag{6.40}$$

There are two spectral parameters, x, y or equivalently u, s, related by (6.25). The twist ϕ can be considered as a parameter of the transfer matrix that does not change. Due to the existence of the intertwiners this two-parameter transfer matrix satisfies

$$\begin{aligned} \mathbb{T}(x, y, \phi)\, \mathbb{T}(x', y', \phi) &= \mathbb{T}(x', y, \phi)\, \mathbb{T}(x, y', \phi) \\ &= \mathbb{T}(x, y', \phi)\, \mathbb{T}(x', y, \phi), \end{aligned} \tag{6.41}$$

and in particular forms a family of commuting operators,

$$\mathbb{T}(x, y, \phi)\, \mathbb{T}(x', y', \phi) = \mathbb{T}(x', y', \phi)\, \mathbb{T}(x, y, \phi). \tag{6.42}$$

The proofs of (6.41) are routine, using a variation of the argument that establishes (6.17). We demonstrate the first equality in (6.41), and the rest can be obtained in similar manner. We start with site j, for which the preceding implies

$$\begin{aligned} &\mathbf{F}_a(x', y)^{-1}\, \mathbf{H}_{ab}(x, x')\, \mathbf{F}_a(x, y)\, \mathbf{L}_{aj}(\mathbf{u}_x, \mathbf{v}_y)\, \mathbf{L}_{bj}(\mathbf{u}_{x'}, \mathbf{v}_{y'}) \\ &= \mathbf{L}_{aj}(\mathbf{u}_{x'}, \mathbf{v}_y)\, \mathbf{L}_{bj}(\mathbf{u}_x, \mathbf{v}_{y'})\, \mathbf{F}_a(x', y)^{-1}\, \mathbf{H}_{ab}(x, x')\, \mathbf{F}_a(x, y). \end{aligned} \tag{6.43}$$

By the 'train argument' this readily extends to the two-parameter monodromy matrix:

$$\begin{aligned} &\mathbf{F}_a(x', y)^{-1}\, \mathbf{H}_{ab}(x, x')\, \mathbf{F}_a(x, y)\, \mathbb{M}_a(x, y)\, \mathbb{M}_b(x', y') \\ &= \mathbb{M}_a(x', y)\, \mathbb{M}_b(x, y')\, \mathbf{F}_a(x', y)^{-1}\, \mathbf{H}_{ab}(x, x')\, \mathbf{F}_a(x, y). \end{aligned} \tag{6.44}$$

We assume that $\mathbf{H}_{ab}(x, x')$ is invertible; this is true so long as $x - x' \notin -\eta\, \mathbb{Z}_{\geq 0} \oplus 2\pi \mathrm{i}\, \mathbb{Z}$.

Then we multiply from the left by $\mathbf{F}_a(x, y)^{-1}\, \mathbf{H}_{ab}(x, x')^{-1}\, \mathbf{F}_a(x', y)$ and take the trace over $V_a^+ \otimes V_b^+$. By the cyclicity of the trace the conjugation by $\mathbf{F}_a(x', y)\, \mathbf{H}_{ab}(x, x')^{-1}\, \mathbf{F}_a(x, y)^{-1}$ drops out on the right-hand side, and we arrive at the desired equality.

More precisely, $\mathbf{F}_a$ is well defined for $s \notin \frac{1}{2}\mathbb{Z}_{\geq 0} \oplus 2\pi\mathrm{i}\,\mathbb{Z}$, and we furthermore need $x - x' \notin -\eta\,\mathbb{Z}_{\geq 0} \oplus 2\pi\mathrm{i}\,\mathbb{Z}$ to ensure that $\mathbf{H}_{ab}$ is invertible. Thus the preceding argument establishes the first equality in (6.41) only for almost all values of x, y. However, the Lax operator, and therefore the two-parameter transfer matrix, are continuous in these two spectral parameters. Thus the conclusion holds in full generality by continuity. (The situation is analogous in the standard proof of commutativity of ordinary transfer matrices from the RLL relations; there the R matrix is only invertible for almost all values of the spectral parameter.)

The exchange of y and y' is shown analogously. Let us note that, together, the intertwiners give rise to an R matrix

$$\begin{aligned}\mathbf{R}_{ab}(x,y;x',y') \coloneqq \mathbf{P}_{ab}\,\mathbf{F}_b(x,y)^{-1}\,\mathbf{G}_{ab}(y,y')\,\mathbf{F}_b(x,y')\\ \times \mathbf{F}_a(x',y)^{-1}\,\mathbf{H}_{ab}(x,x')\,\mathbf{F}_a(x,y),\end{aligned} \tag{6.45}$$

where $\mathbf{P}_{ab}$ is the permutation operator between the auxiliary spaces V_a^+ and V_b^+. Using the properties of the intertwiners one can show that this is the R matrix for which the Lax operator (6.26) satisfies the RLL relation,

$$\begin{aligned}\mathbf{R}_{ab}(x,y;x',y')\,\mathbf{L}_{aj}(\mathbf{u}_x,\mathbf{v}_y)\,\mathbf{L}_{bj}(\mathbf{u}_{x'},\mathbf{v}_{y'}) =\\ \mathbf{L}_{bj}(\mathbf{u}_{x'},\mathbf{v}_{y'})\,\mathbf{L}_{aj}(\mathbf{u}_x,\mathbf{v}_y)\,\mathbf{R}_{ab}(x,y;x',y').\end{aligned} \tag{6.46}$$

A direct proof of the commutativity (6.42) is done using the train argument.

6.3.4 Factorisation of two-parameter transfer matrix

The property (6.41) implies that the two-parameter transfer matrix $\mathbb{T}(x,y,\phi)$ can be factorised into two parts that only depend on the spectral parameter x or y, respectively. Namely,

$$\mathbb{T}(x,y,\phi) = \mathbf{Q}_{y_0}(x,\phi)\,\mathbf{P}_{x_0,y_0}(y,\phi), \tag{6.47}$$

where

$$\begin{aligned}\mathbf{Q}_{y_0}(x,\phi) &\coloneqq \mathbb{T}(x,y_0,\phi),\\ \mathbf{P}_{x_0,y_0}(y,\phi) &\coloneqq \mathbb{T}(x_0,y,\phi)\,\mathbb{T}(x_0,y_0,\phi)^{-1},\end{aligned} \tag{6.48}$$

provided that $\mathbb{T}(x_0, y_0, \phi)$ is invertible, which is the case for generic values of x_0 and y_0. It further allows us to change the value of y_0 at will: note that

$$\mathbf{Q}_{y_1}(x, \phi) = \mathbf{Q}_{y_0}(x, \phi)\, \mathbb{T}(x_0, y_1, \phi)\, \mathbb{T}(x_0, y_0, \phi)^{-1}. \tag{6.49}$$

Therefore we omit the dependence on y_0. A similar argument applies to $\mathbf{P}_{x_0,y_0}(y, \phi)$, whose dependence on x_0, y_0 will from now on be omitted.

According to (6.41) the operators (6.48) commute with themselves (at different values of the spectral parameter) and with each other:

$$\begin{aligned} [\mathbf{Q}(x, \phi), \mathbf{Q}(x', \phi)] &= 0, \quad x, x' \in \mathbb{C}, \\ [\mathbf{Q}(x, \phi), \mathbf{P}(y, \phi)] &= 0, \quad x, y \in \mathbb{C}, \\ [\mathbf{P}(y, \phi), \mathbf{P}(y', \phi)] &= 0, \quad y, y' \in \mathbb{C}. \end{aligned} \tag{6.50}$$

6.4 Matrix TQ relation and transfer matrix fusion relation

We will show in the following that $\mathbf{Q}$ from (6.48) is precisely Baxter's Q operator, satisfying the matrix TQ relation with twist ϕ, see (6.60). Moreover, $\mathbf{P}$ obeys a very similar matrix 'TP relation', see (6.61).

In particular, in the periodic case ($\phi = 0$) $\mathbf{Q}, \mathbf{P}$ are two linearly independent solutions of the matrix TQ relation. We will furthermore derive the transfer matrix fusion relations as well as an interpolation formula that expresses the half-integer spin transfer matrix in terms of Q operators. We would like to remark that in this section q is arbitrary, i.e. the construction works for both gapped and gapless regime of XXZ model.

6.4.1 Decomposition of highest-weight transfer matrix

In order to demonstrate that the Q operator in (6.48) is indeed the same as Baxter's Q operator, satisfying matrix TQ relation, we need to decompose the two-parameter transfer matrix $\mathbb{T}(x, y, \phi)$, when specialising the complex spin to $2s \in \mathbb{Z}_{\geq 0}$. Recall from Section 6.3.1 that the auxiliary space is spanned by $|n\rangle$ for $n \geq 0$; this is what we denoted by V_a^+ in

Section 6.3.1. When $2s \in \mathbb{Z}_{\geq 0}$ we can decompose the infinite-dimensional auxiliary space as $V_{a'}^{+} \oplus V_{a''}$, where $V_{a'}^{+}$ is the span of all $|n\rangle$ with $n > 2s$, while the finite-dimensional piece $V_{a''}$ is spanned by $|2s\rangle, \cdots, |1\rangle, |0\rangle$. The latter is certainly preserved by the diagonal operator $\mathbf{K}_a$ as well as by $\mathbf{S}_a^{-}$, whose block-triangular form is shown in Fig. 6.2. Since $2s \in \mathbb{Z}_{\geq 0}$ the operator $\mathbf{S}_a^{+}$ preserves $V_{a''}$ too. Indeed, as $[2s-n]_q = 0$ for $n = 2s$ the coefficient of $|2s+1\rangle\langle 2s|_a$ in $\mathbf{S}_a^{+}$ vanishes: this entry is marked in red in Fig. 6.2. That is, all of $\mathbf{K}_a, \mathbf{S}_a^{\pm}$ are of block lower triangular form. The $(2s+1) \times (2s+1)$ blocks that act on $V_{a''}$ differ from the unitary spin-s representation by a simple gauge transformation.

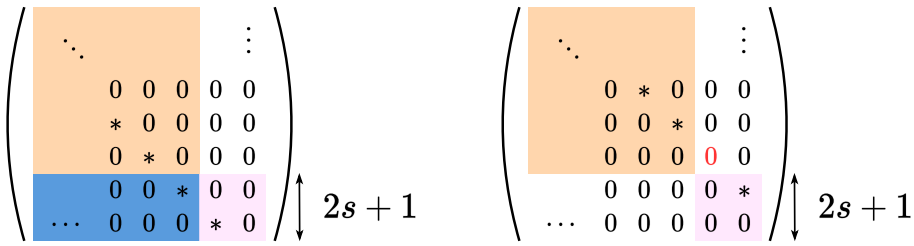

Figure 6.2: The decomposition of $\mathbf{S}_s^{-}$ (left) and $\mathbf{S}_s^{+}$ (right) in the infinite-dimensional highest-weight auxiliary space $V_{a'}^{+} \oplus V_{a''}$ for $s \in \frac{1}{2}\mathbb{Z}_{\geq 0}$. The $*$ represent non-zero entries. The square orange (pink) block acts on $V_{a'}^{+}$ (resp. $V_{a''}$), while the rectangular blue block maps $V_{a'}^{+}$ to $V_{a''}$. Note that we order the basis decreasingly, $\cdots, |1\rangle, |0\rangle$, cf. Appendix D.2.

Since the Lax operator is built from $\mathbf{K}_a, \mathbf{S}_a^{\pm}$, see (6.13), for $2s \in \mathbb{Z}_{\geq 0}$ it assumes a block lower triangular form with respect to the decomposition $V_{a'}^{+} \oplus V_{a''}$ too. Let us indicate its block structure, paralleling that in Fig. 6.2, by

$$\mathbf{L}_{aj} = \begin{pmatrix} \mathbf{L}_{a'j} & 0 \\ \mathbf{L}_{a''j} & \mathbf{L}_{a''j} \end{pmatrix}_a , \tag{6.51}$$

in auxiliary space a. Here we can think of $\mathbf{L}_{a'j}$ as a square infinite matrix acting on $V_{a'}^{+}$, $\mathbf{L}_{a''j}$ as a square matrix on $V_{a''}$, and (for want of a better notation) $\mathbf{L}_{a''j}$ as a rectangular matrix sending $V_{a'}^{+}$ to $V_{a''}$; all with entries that are operators acting at site j. Note that the blocks on the diagonal

only 'interact' amongst themselves:

$$\mathbf{L}_{aj}\,\mathbf{L}_{ak} = \begin{pmatrix} \mathbf{L}_{a'j}\,\mathbf{L}_{a'k} & 0 \\ \mathbf{L}_{a'''j}\,\mathbf{L}_{a'k} + \mathbf{L}_{a''j}\,\mathbf{L}_{a'''k} & \mathbf{L}_{a''j}\,\mathbf{L}_{a''k} \end{pmatrix}. \tag{6.52}$$

Hence the monodromy matrix inherits the block triangular form

$$\mathbf{M}_a = \begin{pmatrix} \mathbf{M}_{a'} & 0 \\ \mathbf{M}_{a'''} & \mathbf{M}_{a''} \end{pmatrix}. \tag{6.53}$$

By taking the trace we obtain the transfer matrix

$$\mathbf{T}_s^{\mathrm{hw}} = \mathrm{tr}_a\,\mathbf{M}_a = \mathrm{tr}_{a'}\,\mathbf{M}_{a'} + \mathrm{tr}_{a''}\,\mathbf{M}_{a''}. \tag{6.54}$$

Since the unitary spin-s representation differs from that on $V_{a''}$ only by a gauge transformation, $\mathrm{tr}_{a''}\,\mathbf{M}_{a''}$ is nothing but the transfer matrix $\mathbf{T}_s$ for spin $s \in \frac{1}{2}\mathbb{Z}_{\geq 0}$. As $V_{a'}^+ \cong V_a^+$ moreover $\mathrm{tr}_{a'}\,\mathbf{M}_{a'}$ is another complex-spin highest-weight transfer matrix! Accounting for the twist and the correct value of the new complex spin we arrive at the decomposition

$$\mathbf{T}_s^{\mathrm{hw}}(u,\phi) = e^{\mathrm{i}(2s+1)\phi}\,\mathbf{T}_{-s-1}^{\mathrm{hw}}(u,\phi) + \mathbf{T}_s(u,\phi). \tag{6.55}$$

6.4.2 Generalised Wronskian and matrix TQ relation

From (6.25) and (6.40), we rewrite (6.47) as

$$\mathbf{T}_s^{\mathrm{hw}}(u,\phi) = \mathbf{Q}\Big(u + \frac{2s+1}{2}\eta, \phi\Big)\,\mathbf{P}\Big(u - \frac{2s+1}{2}\eta, \phi\Big). \tag{6.56}$$

In these terms the decomposition (6.55) becomes

$$\begin{aligned} \mathbf{T}_s(u,\phi) = {} & \mathbf{Q}\Big(u + \frac{2s+1}{2}\eta, \phi\Big)\,\mathbf{P}\Big(u - \frac{2s+1}{2}\eta, \phi\Big) \\ & - e^{(2s+1)\mathrm{i}\phi}\,\mathbf{Q}\Big(u - \frac{2s+1}{2}\eta, \phi\Big)\,\mathbf{P}\Big(u + \frac{2s+1}{2}\eta, \phi\Big). \end{aligned} \tag{6.57}$$

This is the *generalised Wronskian relation*.

For $s = 0$ the operator $\mathbf{T}_0(u, \phi)$ is a scalar, which is independent of the twist according to our choice of the latter. We use $T_0(u) = \sinh^N(u)$ instead. We obtain the Wronskian relation

$$\begin{aligned} T_0(u) = \mathbf{Q}\Big(u + \frac{\eta}{2}, \phi\Big)\, \mathbf{P}\Big(u - \frac{\eta}{2}, \phi\Big) \\ - e^{\mathrm{i}\phi}\, \mathbf{Q}\Big(u - \frac{\eta}{2}, \phi\Big)\mathbf{P}\Big(u + \frac{\eta}{2}, \phi\Big). \end{aligned} \tag{6.58}$$

Note that $T_0(u)$ is independent of the twist ϕ while $\mathbf{Q}$ and $\mathbf{P}$ in the right-hand side do depend on ϕ.

When $s = 1/2$ we obtain a relation for the fundamental (six-vertex) transfer matrix:

$$\mathbf{T}_{1/2}(u, \phi) = \mathbf{Q}(u+\eta, \phi)\, \mathbf{P}(u-\eta, \phi) - e^{2\mathrm{i}\phi}\, \mathbf{Q}(u-\eta, \phi)\, \mathbf{P}(u+\eta, \phi). \tag{6.59}$$

Multiplying both sides by $\mathbf{Q}(u, \phi)$ and using Wronskian relation (6.58) to eliminate $\mathbf{P}$, we find

$$\begin{aligned} \mathbf{T}_{1/2}(u, \phi)\, \mathbf{Q}(u, \phi) = & T_0(u - \eta/2)\, \mathbf{Q}(u + \eta, \phi) \\ & + e^{\mathrm{i}\phi}\, T_0(u + \eta/2)\, \mathbf{Q}(u - \eta, \phi). \end{aligned} \tag{6.60}$$

We have recovered Baxter's matrix TQ relation [19]!

If we instead multiply by $\mathbf{P}(u, \phi)$ and use (6.58) to eliminate the Q operator we analogously obtain a matrix 'TP relation'

$$\begin{aligned} \mathbf{T}_{1/2}(u, \phi)\, \mathbf{P}(u, \phi) = & e^{\mathrm{i}\phi}\, T_0(u - \eta/2)\, \mathbf{P}(u + \eta, \phi) \\ & + T_0(u + \eta/2)\, \mathbf{P}(u - \eta, \phi), \end{aligned} \tag{6.61}$$

Note the different positions at which the twist $e^{\mathrm{i}\phi}$ appears in (6.60) and (6.61). More precisely, the TP relation for the rescaled operator $e^{\mathrm{i}\phi u/\eta}\, \mathbf{P}(u, \phi)$ becomes the TQ relation with the opposite twist $-\phi$. In the periodic case, $\phi = 0$, the Q and P operators are two linearly independent solutions to the matrix TQ relation (6.60). They are linearly independent because their Wronskian, the right-hand side of (6.58), is nonzero ($T_0 \neq 0$).

6.4.3 Transfer matrix fusion relations

The decomposition of the two-parameter transfer matrix $\mathbb{T}(x, y, \phi)$ further allows us to derive the transfer matrix fusion relations [122, 123, 112, 113].

Based on the derivation for the Wronskian relation, a simple derivation is given as follows. We multiply both sides of (6.57) from the left by $\mathbf{T}_{1/2}(u \pm \frac{2s+1}{2}\eta, \phi)$ and apply (6.60)–(6.61). Collecting terms with the same T_0 and using (6.57) for each side, we obtain

$$\begin{aligned}\mathbf{T}_{1/2}\Big(u \pm \frac{2s+1}{2}\eta, \phi\Big)\mathbf{T}_s(u, \phi) = T_0\big(u \pm s\,\eta\big)\,\mathbf{T}_{s+1/2}\Big(u \pm \frac{\eta}{2}, \phi\Big) \\ + e^{\mathrm{i}\phi}\,T_0\big(u \pm (s+1)\eta\big)\,\mathbf{T}_{s-1/2}\Big(u \mp \frac{\eta}{2}, \phi\Big).\end{aligned} \tag{6.62}$$

These two equations are exactly the transfer matrix fusion relations. Taken together for all half-integer values of the spin s the functional form of these relations, i.e. the analogous relations for the eigenvalues T_s, comprises a system of difference relations called a *T-system*. Together with a reformulation known as the *Y-system* it is of vital significance for physical applications like the thermodynamic Bethe ansatz. See Ref. [124] for a thorough review and further references.

6.4.4 Interpolation formula

When $2s \in \mathbb{Z}_{\geq 0}$ the transfer matrix $\mathbf{T}_s$ can be expressed in terms of $\mathbf{Q}$. We rewrite (6.57) as

$$\begin{aligned}&\frac{\mathbf{T}_s(u)}{\mathbf{Q}\big(u + \frac{2s+1}{2}\eta\big)\mathbf{Q}\big(u - \frac{2s+1}{2}\eta\big)} \\ &= \frac{\mathbf{P}\big(u - \frac{2s+1}{2}\eta\big)}{\mathbf{Q}\big(u - \frac{2s+1}{2}\eta\big)} - e^{(2s+1)\mathrm{i}\phi}\frac{\mathbf{P}\big(u + \frac{2s+1}{2}\eta\big)}{\mathbf{Q}\big(u + \frac{2s+1}{2}\eta\big)}.\end{aligned} \tag{6.63}$$

The meaning of the fractions for multiplication with the inverse is unambiguous since the operators involved all commute. For the case of $s = 0$, we rewrite (6.58) as

$$\frac{T_0(u)}{\mathbf{Q}(u + \eta/2)\,\mathbf{Q}(u - \eta/2)} = \frac{\mathbf{P}(u - \eta/2)}{\mathbf{Q}(u - \eta/2)} - e^{\mathrm{i}\phi}\,\frac{\mathbf{P}(u + \eta/2)}{\mathbf{Q}(u + \eta/2)}. \tag{6.64}$$

We translate the arguments of (6.64) by $k\eta$, multiply by $e^{\mathrm{i}k\phi}$ and sum over k from 0 to $2s \in \mathbb{Z}$. The telescoping sum on the right-hand side yields the right-hand side of (6.63). We obtain the interpolation formula [112, 113]

$$\begin{aligned}\mathbf{T}_s(u) &= \mathbf{Q}\Big(u + \frac{2s+1}{2}\eta\Big)\,\mathbf{Q}\Big(u - \frac{2s+1}{2}\eta\Big) \\ &\times \sum_{k=0}^{2s} e^{\mathrm{i}k\phi}\,\frac{T_0\big(u + (k-s)\,\eta\big)}{\mathbf{Q}\big(u + (k-s+1/2)\eta\big)\,\mathbf{Q}\big(u + (k-s-1/2)\eta\big)}.\end{aligned} \tag{6.65}$$

6.4.5 Structure of the eigenvalues of Q and P

Now we focus on the properties of the Q and P operators, and their eigenvalues, on their respective spectral parameters. It is convenient to use multiplicative spectral parameters $r := e^x$ and $t := e^y$. For the Lax operator, we have

$$\mathbf{L}_{aj}(x,y) = \begin{pmatrix} \mathbf{L}_a^{11}(x,y) & \mathbf{L}_a^{12}(x,y) \\ \mathbf{L}_a^{21}(x,y) & \mathbf{L}_a^{22}(x,y) \end{pmatrix}_j. \tag{6.66}$$

We start with the dependence on t. We call that a Laurent polynomial $f(t)$ is a 'trigonometric polynomial of degree n' if $t^n f(t)$ is a polynomial in t^2 of degree n. From (6.28) we see that $\mathbf{L}_a^{11}, \mathbf{L}_a^{21}$ are trigonometric polynomials of degree one in t while $\mathbf{L}_a^{12}, \mathbf{L}_a^{22}$ are independent of t. It follows that on a vector with $S^z = N/2 - M$ the two-parameter monodromy matrix $\mathbf{M}_a(x, y, \phi)$ acts by a matrix whose entries are trigonometric polynomials of degree $N - M$ in t. Thus the same holds for the two-parameter transfer matrix $\mathbb{T}(x, y, \phi)$.

For the other spectral parameter r, we see that $\mathbf{L}_a^{11}, \mathbf{L}_a^{12}$ are both degree zero while $\mathbf{L}_a^{21}, \mathbf{L}_a^{22}$ are trigonometric polynomials in r of degree one. This implies that when acting to the *left* on (the dual of) the M-particle subspace, $\mathbf{M}_a(x, y)$ has entries that are trigonometric polynomials in r of degree M. This carries over to $\mathbb{T}(x, y, \phi)$. Since the latter preserves the value of M, this remains true when acting to the *right*. Eventually, the operator $\mathbb{T}(x, y, \phi)$ acts on the M-particle subspace, with $S^z = N/2 - M$ fixed, by a matrix with entries that are trigonometric polynomials of degree M in r and degree $N - M$ in t. Therefore, $\mathbf{Q}(x, \phi)$ acts by a matrix

consisting of trigonometric polynomials in r of degree M, and $\mathbf{P}(y,\phi)$ likewise by a matrix of trigonometric polynomials in t of degree $N-M$. These properties are inherited by the eigenvalues, since the eigenvectors are independent of r,t.

Using the commutativity of all transfer matrices, the eigenvalues of the Q and P operators are constructed by the algebraic Bethe ansatz with the exception of the FM strings, cf. Sec. 6.8. For any on-shell Bethe state, i.e. (6.20) subject to the Bethe equations (3.25), we have

$$\mathbf{Q}(u,\phi)\ |\{u_m\}_{m=1}^M\rangle = Q(u,\{u_m\}_{m=1}^M,\phi)\ |\{u_m\}_{m=1}^M\rangle\,. \tag{6.67}$$

The TQ relation determines the eigenvalues Q in the same way. The eigenvalues Q are trigonometric polynomials of degree M in $t := e^u$ with zeros denoted by t_m,

$$Q(u,\phi) = \mathrm{cst} \times \prod_{m=1}^{M} \left(t_m^{-1}\, t - t_m\, t^{-1}\right). \tag{6.68}$$

According to the matrix TQ relation (6.60), the eigenvalues obey the functional TQ relation

$$\begin{aligned} T_{1/2}(u,\phi)\, Q(u,\phi) =& T_0(u-\eta/2)\, Q(u+\eta,\phi) \\ &+ e^{\mathrm{i}\phi}\, T_0(u+\eta/2)\, Q(u-\eta,\phi). \end{aligned} \tag{6.69}$$

Taking the limit $u \to u_m = \log t_m$, the left-hand side of (6.69) vanishes. We recover the Bethe ansatz equations (3.25). It means that the zeros of the eigenvalues of the Q operator are precisely the Bethe roots [19].

This observation can be used to find Bethe roots numerically. Once knowing the eigenvalues of transfer matrix $\mathbf{T}_{1/2}$, the functional TQ relation is a set of coupled linear equations of the coefficients of $Q \propto t^{-M}(\sum_{j=0}^{M} c_j t^j)$. In the meantime, the Bethe equations (3.25) are coupled non-linear equations which are much harder to solve. In the presence of any Bethe root at infinity, which does occur for XXZ, the form of the eigenvalues has to be modified a little. Indeed,

$$\begin{aligned} &u_m \to +\infty: \qquad t_m \to \infty, \qquad t_m^{-1}\, t - t_m\, t^{-1} \to t^{-1}, \\ &u_m \to -\infty: \qquad t_m \to 0, \qquad\ \ t_m^{-1}\, t - t_m\, t^{-1} \to t. \end{aligned} \tag{6.70}$$

Therefore, Bethe roots at infinity show up in the eigenvalues of the Q operator: if we rearrange the u_j so that the infinite roots are last then

$$Q(u,\phi) = \mathrm{cst} \times t^{n_{-\infty}-n_{+\infty}} \times \prod_{m=1}^{M-n_{-\infty}-n_{+\infty}} \left(t_m^{-1}\, t - t_m\, t^{-1}\right). \tag{6.71}$$

One can similarly show that the eigenvalues of the P operator $\mathbf{P}$ are of the form (6.71) but with M replaced by $N-M$. The functional version of the TP relations (6.61) gives rise to Bethe-type equations for the $N-M$ zeros of the eigenvalues $P(v,\phi)$ for an M-particle eigenvector:

$$\left(\frac{\sinh(v_n+\eta/2)}{\sinh(v_n-\eta/2)}\right)^N \prod_{n'(\neq n)}^{N-M} \frac{\sinh(v_n-v_{n'}-\eta)}{\sinh(v_n-v_{n'}+\eta)} = e^{\mathrm{i}\phi}. \tag{6.72}$$

These are precisely the Bethe equations for a Bethe state $|\{v_n\}_{n=1}^{N-M}\rangle$ of the XXZ model with opposite twist $-\phi$. Note that (6.20) only uses the pseudovacuum $|\uparrow\cdots\uparrow\rangle$ and the B operator $\mathbf{B}(u)$, which is independent of the twist ϕ, cf. (3.13). Therefore, the off-shell Bethe state $|\{v_m\}_{m=1}^{N-M}\rangle$ does not depend on the twist either; the latter only enters on shell, i.e. upon imposing the Bethe equations. When we impose (6.72) the Bethe vector $|\{v_n\}_{n=1}^{N-M}\rangle$ is not an eigenstate of $\mathbf{T}_s(u,\phi)$, but rather of $\mathbf{T}_s(u,-\phi)$. In particular, in the periodic case ($\phi=0$) it can be interpreted as a Bethe vector beyond the equator (if $M<N/2$, so that $N-M>N/2$). A detailed calculation is presented in Appendix E.0.3.

6.5 Truncated transfer matrix at root of unity

Now we concentrate on the cases with anisotropy parameter q at root of unity,

$$q = \exp\eta, \quad \eta = \mathrm{i}\pi\frac{\ell_1}{\ell_2}, \tag{6.73}$$

where ℓ_1 and ℓ_2 are coprimes. In this scenario the infinite-dimensional auxiliary space V_a^+ has a finite-dimensional subspace $\tilde{V}_a$, whose size only depends on the parameter ℓ_2, preserved by $U_q(\mathfrak{sl}_2)$. Truncating to $\tilde{V}_a$

allows for another decomposition of the two-parameter transfer matrix that leads to a proof of a conjecture of an interpolation formula specialised for root of unity cases [117, 118, 119] and to truncated fusion relations.

The truncation enables us to construct the Q operators explicitly, using finite-dimensional matrices at all intermediate steps. In practice we can construct the Q operator for all eigenvectors of a spin-1/2 spin chain with $N \leq 16$ at root of unity and thus obtain the full spectrum of the XXZ spin chain with arbitrary twist ϕ, revealing the conditions for the appearance of exponential degeneracies that have been observed before [106]. This has significant consequences for the thermodynamic limit, too.

6.5.1 Truncation and intertwiners at root of unity

At root of unity $\eta = \mathrm{i}\pi\frac{\ell_1}{\ell_2}$ the matrix elements of the Lax operator (6.28) in the auxiliary space acquire the periodicity:

$$ {}_a\langle k+\ell_2|\ \mathbf{L}_{aj}\ |m+\ell_2\rangle_a = \varepsilon \times {}_a\langle k|\ \mathbf{L}_{aj}\ |m\rangle_a\,, \tag{6.74}$$

where we recall that $\varepsilon = q^{\ell_2} = e^{\mathrm{i}\pi\ell_1}$. The periodicity implies that only a finite part of the Lax operator is really relevant, allowing us to truncate the auxiliary space to a finite-dimensional subspace.

We decompose the infinite-dimensional highest-weight $U_q(\mathfrak{sl}_2)$-module V_a^+ as $V_{a'}^+ \oplus \tilde{V}_{a''}$, where $V_{a'}^+$ is the span of $|n\rangle_a$ with $n \geq \ell_2$ and $\tilde{V}_{a''}$ be the span of $|n\rangle_a$ for $0 \leq n \leq \ell_2 - 1$. At root of unity we have $[\ell_2]_q = 0$ so one of the entries of $\mathbf{S}_a^-$ vanishes as illustrated in Fig. 6.3. This time all generators of $U_q(\mathfrak{sl}_2)$ preserve the infinite-dimensional subspace $V_{a'}^+$. We are interested in the finite-dimensional subspace $\tilde{V}_{a''}$. Like in Section 6.3.2 we can get there by taking the quotient $\tilde{V}_{a''} \cong V_a^+/V_{a'}^+$. In this way we get a finite-dimensional representation of $U_q(\mathfrak{sl}_2)$ on $\tilde{V}_{a''}$, see also Appendix D.2. More concretely, all of $\mathbf{K}_a$, $\mathbf{S}_a^\pm$ are block upper triangular with respect to the decomposition $V_a^+ = V_{a'}^+ \oplus \tilde{V}_{a''}$, see again Fig. 6.3. This property is inherited by the Lax operator

$$\mathbf{L}_{aj} = \begin{pmatrix} \mathbf{L}_{a'j} & \mathbf{L}_{a''j} \\ 0 & \tilde{\mathbf{L}}_{a''j} \end{pmatrix}, \tag{6.75}$$

where $\mathbf{L}_{a'j}$ can be viewed as an infinite square matrix on $V_{a'}^+$, $\mathbf{L}_{a''j}$ as an $\ell_2 \times \infty$ rectangular matrix mapping $\tilde{V}_{a''}$ to $V_{a'}^+$, and $\tilde{\mathbf{L}}_{a''j}$ as an $\ell_2 \times \ell_2$

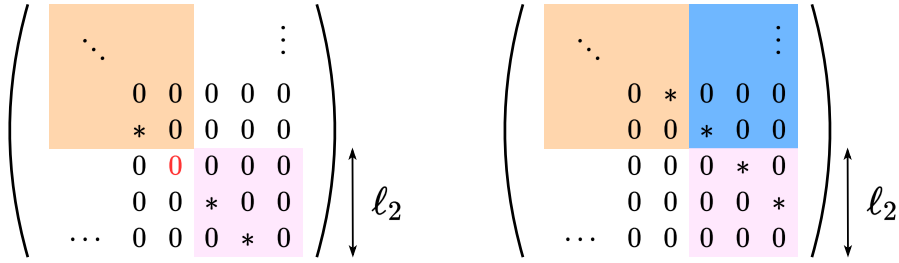

Figure 6.3: The decomposition of $\mathbf{S}_a^-$ (left) and $\mathbf{S}_a^+$ (right) at root of unity with $\ell_2 = 3$, where $*$ represents non-zero elements of the matrices. As in Fig. 6.2 the bottom-right entry corresponds to $|0\rangle\langle 0|$.

matrix on $\tilde{V}_{a''}$. The entries of each of these are 2×2 matrices acting at site j. The truncation to the ℓ_2-dimensional space $\tilde{V}_{a''}$ amounts to treating all $|n\rangle_a$ with $n \geq \ell_2$ as zero.

In the following, we only focus on the ℓ_2-dimensional auxiliary space $\tilde{V}_a$, dropping the double prime. We denote the Lax operator $\tilde{\mathbf{L}}_s(u)$ defined in (6.13) with ℓ_2-dimensional auxiliary space $\tilde{V}_a$, which also satisfies RLL relations.

6.5.2 Truncated Wronskian and TQ relations

Repeating the arguments from Section 6.4.1 for an arbitrary complex spin $s \in \mathbb{C}$ we have the decomposition of the highest-weight transfer matrix at root of unity

$$\mathbf{T}_s^{\mathrm{hw}}(u,\phi) = e^{\mathrm{i}\ell_2\phi}\,\mathbf{T}_{s-\ell_2}^{\mathrm{hw}}(u,\phi) + \tilde{\mathbf{T}}_s(u,\phi), \tag{6.76}$$

where up to the twist factor, $\mathbf{T}_{s-\ell_2}^{\mathrm{hw}}(u,\phi)$ coincides with the matrix $\mathbf{T}_s^{\mathrm{hw}}(u,\phi)$ restricted to the basis $|m+\ell_2\rangle$ with $m \geq 0$. With (6.74), we simplify the decomposition (6.76) into

$$\tilde{\mathbf{T}}_s(u,\phi) = \left(1 - \varepsilon^N e^{\mathrm{i}\ell_2\phi}\right)\mathbf{T}_s^{\mathrm{hw}}(u,\phi). \tag{6.77}$$

This implies the similar decomposition of the transfer matrix $\tilde{\mathbf{T}}_s(u,\phi)$, i.e.

$$\tilde{\mathbf{T}}_s(u,\phi) = \tilde{\mathbf{Q}}\left(u + \frac{2s+1}{2}\eta, \phi\right)\tilde{\mathbf{P}}\left(u - \frac{2s+1}{2}\eta, \phi\right). \tag{6.78}$$

We define the two-parameter transfer matrix as

$$\tilde{\mathbb{T}}(x, y, \phi) := \tilde{\mathbf{T}}_s(u, \phi), \tag{6.79}$$

such that

$$\tilde{\mathbb{T}}(x, y, \phi) = \tilde{\mathbf{Q}}_{y_0}(x, \phi)\, \tilde{\mathbf{P}}_{x_0, y_0}(y, \phi), \tag{6.80}$$

where the truncated Q and P operators are defined as

$$\tilde{\mathbf{Q}}_{y_0}(x, \phi) := \tilde{\mathbb{T}}(x, y_0, \phi),\ \tilde{\mathbf{P}}_{x_0, y_0}(y, \phi) := \tilde{\mathbb{T}}(x_0, y, \phi)\, \tilde{\mathbb{T}}(x_0, y_0, \phi)^{-1}. \tag{6.81}$$

The truncated Q and P operators share the same eigenvalues up to a constant as Q and P operators in (6.56). Therefore, the eigenvalues share the same zeros, cf. (6.67). We find all the eigenvalues of Q operator and their zeros (Bethe roots) by dealing with only finite-dimensional monodromy matrices at root of unity!

When $2s \in \mathbb{Z}_{\geq 0}$, the decompositions (6.55) and (6.77) yield a decomposition of $\mathbf{T}_s$ in terms of $\tilde{\mathbf{T}}_s$:

$$\begin{aligned} &\left(1 - \varepsilon^N e^{\mathrm{i}\ell_2\phi}\right) \mathbf{T}_s(u, \phi) \\ &= \left(1 - \varepsilon^N e^{\mathrm{i}\ell_2\phi}\right) \left(\mathbf{T}_s^{\mathrm{hw}}(u, \phi) - e^{\mathrm{i}(2s+1)\phi}\, \mathbf{T}_{-s-1}^{\mathrm{hw}}(u, \phi)\right) \\ &= \tilde{\mathbf{T}}_s(u, \phi) - e^{\mathrm{i}(2s+1)\phi}\, \tilde{\mathbf{T}}_{-s-1}(u, \phi). \end{aligned} \tag{6.82}$$

From (6.78) we obtain the *truncated Wronksian relation*

$$\begin{aligned} \left(1 - \varepsilon^N e^{\mathrm{i}\ell_2\phi}\right) \mathbf{T}_s(u, \phi) &= \tilde{\mathbf{Q}}\left(u + \frac{2s+1}{2}\eta, \phi\right) \tilde{\mathbf{P}}\left(u - \frac{2s+1}{2}\eta, \phi\right) \\ - e^{\mathrm{i}(2s+1)\phi}\, \tilde{\mathbf{Q}}\left(u - \frac{2s+1}{2}\eta, \phi\right) &\tilde{\mathbf{P}}\left(u + \frac{2s+1}{2}\eta, \phi\right). \end{aligned} \tag{6.83}$$

When $1 - \varepsilon^N e^{\mathrm{i}\ell_2\phi} = 0$, i.e. for *commensurate twist*

$$\begin{aligned} \varepsilon^N = +1: &\quad \phi = \frac{(2n-2)\pi}{\ell_2}, \\ \varepsilon^N = -1: &\quad \phi = \frac{(2n-1)\pi}{\ell_2}, \end{aligned} \qquad 1 \leq n \leq \ell_2, \tag{6.84}$$

the left-hand side of (6.83) vanishes. Comparing (6.84) to the conditions (6.4) for the existence of Bethe roots at infinity we see that when

(6.84) is satisfied there exist certain numbers M of down spins for which (6.4) is satisfied too.

Proceeding exactly as before we obtain TQ and TP relations that look the same as (6.60)–(6.61), now involving truncated matrices

$$\begin{aligned}\mathbf{T}_{1/2}(u,\phi)\,\tilde{\mathbf{Q}}(u,\phi) =& T_0(u-\eta/2)\,\tilde{\mathbf{Q}}(u+\eta,\phi)\\ &+ e^{\mathrm{i}\phi}\,T_0(u+\eta/2)\,\tilde{\mathbf{Q}}(u-\eta,\phi),\end{aligned} \tag{6.85}$$

and

$$\begin{aligned}\mathbf{T}_{1/2}(u,\phi)\,\tilde{\mathbf{P}}(u,\phi) =& e^{\mathrm{i}\phi}\,T_0(u-\eta/2)\,\tilde{\mathbf{P}}(u+\eta,\phi)\\ &+ T_0(u+\eta/2)\,\tilde{\mathbf{P}}(u-\eta,\phi).\end{aligned} \tag{6.86}$$

6.5.3 Truncated fusion relations

Proceeding as in Section 6.4.3, but using (6.78) instead of (6.57), we readily obtain fusion-like relations for $\tilde{\mathbf{T}}_s$:

$$\begin{aligned}\mathbf{T}_{1/2}\Big(u\pm\frac{2s+1}{2}\eta,\phi\Big)\tilde{\mathbf{T}}_s(u,\phi) = T_0(u\pm s\eta)\,\tilde{\mathbf{T}}_{s+1/2}\Big(u\pm\frac{\eta}{2},\phi\Big)\\ + e^{\mathrm{i}\phi}\,T_0\big(u\pm(s+1)\eta\big)\,\tilde{\mathbf{T}}_{s-1/2}\Big(u\mp\frac{\eta}{2},\phi\Big).\end{aligned} \tag{6.87}$$

In analogy to the cases of general q, we dub these relations the *truncated fusion relations*. However, we stress that in the present case the internal auxiliary spaces have the same dimensions ℓ_2 for all truncated transfer matrices in (6.87), unlike for the fusion relations (6.62).

6.5.4 Interpolation formula: proof of a conjecture

In Refs. [117, 118, 119], e.g. Eq. (S22) in the supplementary material of Ref. [119], it has been conjectured that the complex spin transfer matrix eigenvalues can be expressed in terms of $\tilde{\mathbf{Q}}$, similarly for the situation of half-integral spin representations from Section 6.4.4. In our notation, after introducing the dependence on the twist, the formula reads

$$\begin{aligned}\tilde{\mathbf{T}}_s(u) = \tilde{\mathbf{Q}}\Big(u+\frac{2s+1}{2}\eta\Big)\,\tilde{\mathbf{Q}}\Big(u-\frac{2s+1}{2}\eta\Big)\\ \times\sum_{k=0}^{\ell_2-1} e^{\mathrm{i}k\phi}\frac{T_0\big(u+(k-s)\,\eta\big)}{\tilde{\mathbf{Q}}\big(u+(k-s-\frac{1}{2})\eta\big)\,\tilde{\mathbf{Q}}\big(u+(k-s+\frac{1}{2})\eta\big)}.\end{aligned} \tag{6.88}$$

We prove this using arguments like those leading to (6.65). We start with rewriting (6.78) as

$$\frac{\tilde{\mathbf{T}}_s(u)}{\tilde{\mathbf{Q}}\big(u+(s+1/2)\eta\big)\,\tilde{\mathbf{Q}}\big(u-(s+1/2)\eta\big)}=\frac{\tilde{\mathbf{P}}\big(u-(s+1/2)\eta\big)}{\tilde{\mathbf{Q}}\big(u-(s+1/2)\eta\big)}. \tag{6.89}$$

Setting $s=0$, we have

$$\begin{aligned}&\big(1-\varepsilon^N e^{\mathrm{i}\ell_2\phi}\big)\,\frac{T_0(u)}{\tilde{\mathbf{Q}}(u+\eta/2)\,\tilde{\mathbf{Q}}(u-\eta/2)}\\&=\frac{\tilde{\mathbf{P}}(u-\eta/2)}{\tilde{\mathbf{Q}}(u-\eta/2)}-e^{\mathrm{i}\phi}\,\frac{\tilde{\mathbf{P}}(u+\eta/2)}{\tilde{\mathbf{Q}}(u+\eta/2)}.\end{aligned} \tag{6.90}$$

Translating u by $(k-s)\eta$, multiplying both sides by $e^{\mathrm{i}k\phi}$ and summing over k from 0 to ℓ_2-1, we obtain

$$\begin{aligned}&\big(1-\varepsilon^N e^{\mathrm{i}\ell_2\phi}\big)\\&\times\sum_{k=0}^{\ell_2-1}e^{\mathrm{i}k\phi}\,\frac{T_0\big(u+(k-s)\,\eta\big)}{\tilde{\mathbf{Q}}\big(u+(k-s+1/2)\eta\big)\,\tilde{\mathbf{Q}}\big(u+(k-s-1/2)\eta\big)}\\&=\frac{\tilde{\mathbf{P}}\big(u-(s+1/2)\eta\big)}{\tilde{\mathbf{Q}}\big(u-(s+1/2)\eta\big)}-e^{\mathrm{i}\ell_2\phi}\,\frac{\tilde{\mathbf{P}}\big(u+(\ell_2-s-1/2)\eta\big)}{\tilde{\mathbf{Q}}\big(u+(\ell_2-s-1/2)\eta\big)}.\end{aligned} \tag{6.91}$$

Using (6.77), the second ratio in the second line simplifies to ε^N times the first ratio in that line. As long as the twist is *not* commensurate, i.e. does not obey (6.84), we can cancel $1-\varepsilon^N e^{\mathrm{i}\ell_2\phi}$ on both sides of the equation. In fact, since the two sides of (6.91) are continuous in the twist, the result holds for any twist. So we have

$$\begin{aligned}&\sum_{k=0}^{\ell_2-1}e^{\mathrm{i}k\phi}\,\frac{T_0\big(u+(k-s)\,\eta\big)}{\tilde{\mathbf{Q}}\big(u+(k-s+1/2)\eta\big)\,\tilde{\mathbf{Q}}\big(u+(k-s-1/2)\eta\big)}\\&=\frac{\tilde{\mathbf{P}}\big(u-(s+1/2)\eta\big)}{\tilde{\mathbf{Q}}\big(u-(s+1/2)\eta\big)}.\end{aligned} \tag{6.92}$$

Multiplying both sides by $\tilde{\mathbf{Q}}\left(u+\frac{2s+1}{2}\eta\right)$, and using (6.78) we arrive at (6.88).

6.5.5 Structure of eigenvalues of $\tilde{\mathbf{Q}}$ and $\tilde{\mathbf{P}}$

Similar to the discussion in Section 6.4.5 the eigenvalues of the truncated Q operator,

$$\tilde{\mathbf{Q}}(u,\phi)\ |\{v_m\}_{m=1}^M\rangle = \tilde{Q}(u,\{v_m\}_{m=1}^M,\phi)\ |\{v_m\}_{m=1}^M\rangle\,, \tag{6.93}$$

can be expressed as

$$\tilde{Q}(u,\{v_m\}_{m=1}^M,\phi) = \mathrm{cst}\times\prod_{m=1}^M \left(t_m^{-1}\,t - t_m\,t^{-1}\right), \tag{6.94}$$

with $v_m = \log t_m$ obeying the Bethe ansatz equations (3.25) due to the truncated TQ relations (6.85). In particular, the eigenvalues $Q(u,\phi)$ and $\tilde{Q}(u,\phi)$ of a given eigenvector share the same zeros.

Since we are at root of unity, the eigenvalues of the truncated Q operator on the M-particle sector are quasiperiodic too:

$$\tilde{Q}(u\pm\ell_2\eta,\phi) = \varepsilon^M\,\tilde{Q}(u,\phi). \tag{6.95}$$

Similarly it follows that

$$\tilde{\mathbf{Q}}(u\pm\ell_2\eta,\phi) = \varepsilon^{N/2-\mathbf{S}^z}\,\tilde{\mathbf{Q}}(u,\phi). \tag{6.96}$$

Likewise, we can show that the eigenvalues of the truncated P operator are of the form (6.71) but with M replaced by $N-M$, and

$$\tilde{\mathbf{P}}(u\pm\ell_2\eta,\phi) = \varepsilon^{N/2+\mathbf{S}^z}\,\tilde{\mathbf{P}}(u,\phi). \tag{6.97}$$

6.6 Applications to XXZ at root of unity: general results

Now we apply the general formalism developed in previous sections to the spectrum of the XXZ model at root of unity. The results derived in this section and other features of the spectrum at root of unity are illustrated by numerous examples in Section 6.7.

6.6.1 Preliminaries

Recall that the Q operator and all transfer matrices commute with each other. The eigenvectors of Q operator are *states* denoted as $|\{u_m\}_{m=1}^M\rangle$, which are labelled by the zeros of their Q functions. We assume that the Bethe ansatz is complete, so that any state is of the form $|\{u_m\}_{m=1}^M\rangle$.

For the XXZ model at root of unity there are states $|\{u_m\}_{m=1}^M\rangle$ for which certain special roots can be added to get another state without affecting the values of $\{u_m\}_{m=1}^M$ or eigenvalues. We will call states that are minimal in this sense 'primitive'; it is analogous to a highest-weight condition except that we do not use representation theory to characterise it. We call a state $|\{u_m\}_{m=1}^M\rangle$ *primitive* if no nontrivial subset of $\{u_m\}_{m=1}^M$ corresponds to a physical state whose eigenvalue for $\mathbf{T}_s$ differs at most by a sign. (For the reason why we allow for a sign see Section 6.6.2.)

Primitive states contain no FM strings. We denote the numbers of Bethe roots at $\pm\infty$ as $n_{\pm\infty}$. Typically, namely for twist $\phi \notin \{0,\pi\}$, a primitive state has no roots at infinity either.[2] In the (anti)periodic case $\phi \in \{0,\pi\}$ a primitive state may have $n_{\pm\infty} \neq 0$ as long as $n_{\mp\infty} = 0$, cf. Section 6.7.1.

We remark that it is possible for two primitive eigenstates to be degenerate, namely when N is odd and the two states are related by the spin flip operator $\prod_j \sigma_j^x$. We discuss this case in Section 6.6.4.

Any state that is not primitive is a *descendant* of certain primitive state: it satisfies

$$\begin{aligned}&\mathbf{Q}(u,\phi)\ |\{v_{m'}\}_{m'=1}^{M'}\rangle \\ &\propto \prod_{m=1}^{M}\sinh(u-u_m)\prod_{n=M+1}^{M'}\sinh(u-w_n)\ |\{v_{m'}\}_{m'=1}^{M'}\rangle\,,\end{aligned} \tag{6.98}$$

where $|\{u_m\}_{m=1}^M\rangle$ is primitive and the additional Bethe roots $\{w_n\}_{n=M+1}^{M'}$ consist of FM strings and pairs of roots located at $\pm\infty$. Away from the isotropic points descendant states only exist when condition (6.84) is satisfied.

[2] States with $n_{\pm\infty} \neq 0$ but $n_{\mp\infty} = 0$ do occur at twist $\phi \notin \{0,\pi\}$. In Section 6.7.2 we show that they have the same $\mathbf{T}_s$-eigenvalues as certain primitive states at twist $-\phi$ that have the same finite Bethe roots, and of which they should be considered descendants.

Remark. Unlike the descendant states in the isotropic XXX model, those descendant states considered here do contribute to the Thermodynamic Bethe Ansatz calculations, cf. Sec. 6.9.2. One should notice the difference here.

Finally, for $\phi \notin \{0, \pi\}$ away from the (anti)periodic points, a primitive state and its descendants might be eigenstates for Hamiltonians with opposite twist, ϕ and $-\phi$, see Appendix E.0.3. The sign of the twist in $\mathbf{T}_s(u, \pm\phi)$ is fixed accordingly. We further illustrate this in Section 6.7.2.

6.6.2 Impact of FM strings on transfer-matrix eigenvalues

With this terminology let us show that a descendant state $|\{v_{m'}\}_{m'=1}^{M'}\rangle$ of a primitive state $|\{u_m\}_{m=1}^{M}\rangle$ has $\mathbf{T}_s(u, \pm\phi)$-eigenvalues that differ by at most a sign. This means that the momentum of the primitive state and its descendant may differ by π while all other (quasi-)local charges generated by $\mathbf{T}_s(u, \pm\phi)$ are identical.

The eigenvalues of $\mathbf{T}_{1/2}$ and the Q operator for the primitive state $|\{u_m\}_{m=1}^{M}\rangle$ are

$$\begin{aligned} \mathbf{T}_{1/2}(u, \phi)\ |\{u_m\}_{m=1}^{M}\rangle &= T_{1/2}(u)\ |\{u_m\}_{m=1}^{M}\rangle\,, \\ \mathbf{Q}(u, \phi)\ |\{u_m\}_{m=1}^{M}\rangle &= Q(u)\ |\{u_m\}_{m=1}^{M}\rangle\,. \end{aligned} \tag{6.99}$$

For simplicity we assume that $|\{u_m\}_{m=1}^{M}\rangle$ does not contain any Bethe roots at $\pm\infty$. By Section 6.4.5 the eigenvalue of the Q operator is a trigonometric polynomial of degree M,

$$Q(u) \propto \prod_{m=1}^{M} (t_m^{-1}\, t - t_m\, t^{-1}), \quad t = e^u, \tag{6.100}$$

and satisfies the functional TQ relation

$$T_{1/2}(u)\, Q(u) = T_0(u - \eta/2)\, Q(u + \eta) + e^{\mathrm{i}\phi}\, T_0(u + \eta/2)\, Q(u - \eta). \tag{6.101}$$

A descendant $|\{v_{m'}\}_{m'=1}^{M'}\rangle$ of the primitive state $|\{u_m\}_{m=1}^{M}\rangle$ is also an eigenvector of the Q operator,

$$\mathbf{Q}(u, \pm\phi)\ |\{v_{m'}\}_{m'=1}^{M'}\rangle = Q'(u)\ |\{v_{m'}\}_{m'=1}^{M'}\rangle\,, \tag{6.102}$$

where for $\phi \notin \{0, \pi\}$ the sign of the twist $\pm\phi$ has to be chosen to match that of the Hamiltonian, see Section 6.7.2. From the definition (6.8) of an FM string we note that the eigenvalue of the Q operator on the descendant state is

$$Q'(u) \propto Q(t)\, t^{n_{-\infty}-n_{+\infty}} \prod_{m=1}^{n_{\rm FM}} \left(t^{\ell_2} - e^{2\ell_2 \alpha_m^{\rm FM}}\, t^{-\ell_2}\right), \quad t = e^u, \tag{6.103}$$

where $n_{\pm\infty}$ and $n_{\rm FM}$ are the numbers of roots at $\pm\infty$ and FM strings, respectively, of the descendant state. Observe that $Q'(u)$ satisfies the TQ relation

$$\begin{aligned} \varepsilon^{n_{\rm FM}}\, T_{1/2}(u)\, Q'(u) =& T_0(u-\eta/2)\, Q'(u+\eta) \\ &+ e^{{\rm i}\phi}\, T_0(u+\eta/2)\, Q'(u-\eta), \end{aligned} \tag{6.104}$$

where we recall that $\varepsilon = q^{\ell_2} \in \{\pm 1\}$. Hence, the eigenvalue of $\mathbf{T}_{1/2}$ for the descendant state $|\{v_{m'}\}_{m'=1}^{M'}\rangle$ is

$$\mathbf{T}_{1/2}(u, \pm\phi)\ |\{v_{m'}\}_{m'=1}^{M'}\rangle = \varepsilon^{n_{\rm FM}}\, T_{1/2}(u)\ |\{v_{m'}\}_{m'=1}^{M'}\rangle\,. \tag{6.105}$$

Since the $\mathbf{T}_{1/2}$-eigenvalue of the descendant state differs by at most a sign from that of the primitive state, the descendant has the same local charges generated by $\mathbf{T}_{1/2}$ as the primitive state, except that its momentum might differ by π. More generally, from the transfer matrix fusion relations (6.62) we obtain

$$\begin{aligned} \mathbf{T}_s(u, \phi)\ |\{u_m\}_{m=1}^{M}\rangle &= T_s(u)\ |\{u_m\}_{m=1}^{M}\rangle\,, \\ \mathbf{T}_s(u, \pm\phi)\ |\{v_{m'}\}_{m'=1}^{M'}\rangle &= \varepsilon^{2s\, n_{\rm FM}}\, T_s(u)\ |\{v_{m'}\}_{m'=1}^{M'}\rangle\,. \end{aligned} \tag{6.106}$$

We will give several explicit examples of the descendant states associated with primitive states, and the descendant towers that they form, in Secs. 6.7.1 and 6.7.2.

6.6.3 FM strings at commensurate twist

In Section 6.5.2 we saw that, at root of unity, when the twist ϕ is commensurate as in (6.84) the truncated Wronskian relations (6.83) trivialise in the sense that the eigenvalues of $\tilde{\mathbf{Q}}$ and $\tilde{\mathbf{P}}$ are proportional to each

other. This can only be achieved when the eigenvalues of $\tilde{\mathbf{P}}$ are related to those of $\tilde{\mathbf{Q}}$ through adding or subtracting Bethe roots at infinity or FM strings, cf. (6.83): eigenstates with FM strings must occur when the twist is commensurate. Conversely, if FM strings are present among the zeros of the eigenvalues of $\tilde{\mathbf{Q}}$ or $\tilde{\mathbf{P}}$ the truncated Wronskian relations (6.83) vanish, since for $s = 0$ the left-hand side of (6.83) does not contain zeros of FM strings while the right-hand side does. This means that descendants containing FM strings can only exist when the twist ϕ is commensurate. In conclusion, FM strings can only, and necessarily do, occur at commensurate twist.

From (6.77), whenever $\tilde{\mathbf{T}}_s(u,\phi)$ has nonzero eigenvalues it follows that the eigenvalues $\mathbf{T}_s^{\mathrm{hw}}(u,\phi)$ must have poles if $(1-\varepsilon^N e^{\mathrm{i}\ell_2\phi}) = 0$ to compensate the vanishing prefactor. This corroborates Refs. [125, 126] in which it was shown that terms proportional to $\log t$ can arise when solving the functional TQ relations, yielding eigenvalues that are *quasi-polynomials* in t [126]. As it turns out, the appearance of these quasi-polynomials is also closely related to the FM strings and their string centres, cf. (6.84). A detailed discussion of this is postponed to future work.

When (6.84) is satisfied, a quantisation condition for the centres of FM strings based on (6.92) was obtained in Refs. [117, 118, 127]. Let us review their arguments. For an eigenstate $|\{u_m\}_{m=1}^M\rangle$ we have

$$\begin{aligned}\tilde{\mathbf{Q}}(u,\phi)\ |\{u_m\}_{m=1}^M\rangle &= Q(u)\ |\{u_m\}_{m=1}^M\rangle\,,\\ \tilde{\mathbf{P}}(u,\phi)\ |\{u_m\}_{m=1}^M\rangle &= P(u)\ |\{u_m\}_{m=1}^M\rangle\,,\end{aligned} \tag{6.107}$$

where the eigenvalues are trigonometric polynomials in $t = e^u$. Let us decompose the Q function in to a 'regular' part $Q_{\mathrm{r}}(u)$, consisting of n_{r} factors whose zeros are Bethe roots that are neither FM strings nor infinite, a 'singular' part $Q_{\mathrm{s}}(u)$, consisting of n_{FM} FM strings, along with factors accounting for Bethe roots at infinity as in (6.71):

$$\begin{aligned}&Q(u) = Q_{\mathrm{r}}(u)\,Q_{\mathrm{s}}(u)\,t^{n_{-\infty}-n_{+\infty}}, \quad t = e^u,\\ &Q_{\mathrm{r}}(u) \propto \prod_{m=1}^{n_{\mathrm{r}}}\left(t_m^{-1}\,t - t_m\,t^{-1}\right), \quad Q_{\mathrm{s}}(u) \propto \prod_{m=1}^{n_{\mathrm{FM}}}\left(t_m^{-\ell_2}\,t^{\ell_2} - t_m^{\ell_2}\,t^{-\ell_2}\right),\end{aligned} \tag{6.108}$$

where the number of down spins $M = n_{\mathrm{r}} + \ell_2\,n_{\mathrm{FM}} + n_{+\infty} + n_{-\infty}$. Because the Wronskian (6.83) vanishes, the eigenvalue $P(u)$ has the same regular

zeros as $Q(u)$:

$$P(u) = Q_{\mathrm{r}}(u)\, P_{\mathrm{s}}(u)\, t^{\bar{n}_{-\infty}-\bar{n}_{+\infty}}, \quad P_{\mathrm{s}}(u) \propto \prod_{m=1}^{\bar{n}_{\mathrm{FM}}} \big(\bar{t}_m^{-\ell_2}\, t^{\ell_2} - \bar{t}_m^{\ell_2}\, t^{-\ell_2}\big), \tag{6.109}$$

where $\bar{n}_{\pm\infty}$ and $\bar{n}_{\mathrm{FM}}$ are the number of Bethe roots at $\pm\infty$ and FM strings, respectively, present among the zeros of the P operator. The total number of zeros of $Q(u)$ and $P(u)$ is equal to the system size N:

$$N = 2\, n_{\mathrm{r}} + \ell_2\, n_{\mathrm{FM}} + \ell_2\, \bar{n}_{\mathrm{FM}} + n_{+\infty} + n_{-\infty} + \bar{n}_{+\infty} + \bar{n}_{-\infty}. \tag{6.110}$$

Consider the functional form of the interpolation formula (6.92),

$$P(u) = Q(u) \sum_{k=0}^{\ell_2-1} e^{\mathrm{i}k\phi} \frac{T_0\big(u + (k+1/2)\,\eta\big)}{Q(u + k\,\eta)\, Q\big(u + (k+1)\,\eta\big)}. \tag{6.111}$$

Using (6.108)–(6.109) and the fact that $Q_{\mathrm{s}}(u+\eta) = \varepsilon^{n_{\mathrm{FM}}}\, Q_{\mathrm{s}}(u)$ this can be rewritten as

$$\begin{aligned} &\varepsilon^{n_{\mathrm{FM}}}\, Q_{\mathrm{s}}(u)\, P_{\mathrm{s}}(u)\, t^{n_{-\infty}-n_{+\infty}+\bar{n}_{-\infty}-\bar{n}_{+\infty}} \\ &\quad = \sum_{k=0}^{\ell_2-1} e^{\mathrm{i}k\phi} \frac{T_0\big(u + (k+1/2)\,\eta\big)}{Q_{\mathrm{r}}(u + k\,\eta)\, Q_{\mathrm{r}}\big(u + (k+1)\,\eta\big)\, e^{\mathrm{i}(2k+1)(n_{-\infty}-n_{+\infty})\eta}}. \end{aligned} \tag{6.112}$$

This is a 'quantisation condition' for the string centres of FM strings. Indeed, (6.112) implies that for any two states belonging to the same descendant tower, i.e. sharing the same regular part of their Q functions, the combination $Q_{\mathrm{s}}(u)\, P_{\mathrm{s}}(u)$ contains the same zeros. In other words, the string centres of FM strings for any state belonging to a descendant tower are determined solely by the regular part of the Q functions. Moreover, string centres of FM strings are *free* within a descendant tower in the sense that adding or removing FM strings whose string centres are given by the zeros of $Q_{\mathrm{s}}(u)\, P_{\mathrm{s}}(u)$ results in other eigenstates within the same descendant tower. We can add FM strings from the zeros of $Q_{\mathrm{s}}(u)\, P_{\mathrm{s}}(u)$ to the primitive state in order to generate the descendant states. We present explicit examples of the resulting tower structures in Secs. 6.7.1 and 6.7.2.

6.6.4 Primitive degenerate eigenstates

When the system size N is odd and condition (6.84) for a commensurate twist is satisfied, it is possible to have two primitive eigenstates with degenerate eigenvalues of $\mathbf{T}_s$ [128]. Namely, the two eigenstates are related by reversing all spins,

$$|\{v_{m'}\}_{m'=1}^{N-M}\rangle = \prod_{j=1}^{N} \sigma_j^x \; |\{u_m\}_{m=1}^{M}\rangle\,, \tag{6.113}$$

and, most importantly, their Bethe roots $\{v_{m'}\}_{m'=1}^{N-M}$ and $\{u_m\}_{m=1}^{M}$ are completely different: both are primitive states. This is only possible when the parities of M and $N-M$ differ, i.e. the system size N is odd.

When this happens, the eigenvalues of $\tilde{\mathbf{T}}_s$ are zero for both states,

$$\tilde{\mathbf{T}}_s(u,\phi)\; |\{u_m\}_{m=1}^{M}\rangle = \tilde{\mathbf{T}}_s(u,-\phi)\; |\{v_{m'}\}_{m'=1}^{N-M}\rangle = 0. \tag{6.114}$$

In this case, the matrix $\tilde{\mathbb{T}}(x,y,\phi) = \tilde{\mathbf{T}}_s(u,\phi)$ can not be inverted for any $x, y \in \mathbb{C}$. Despite this, the decomposition (6.89) still applies, where rather than via (6.81) the P operator is defined through the TQ relation for the state beyond the equator with opposite twist. However, it is no longer possible determine the eigenvalues of the Q operator $\tilde{\mathbf{Q}}$ for the degenerate primitive states. This is not a problem since, as both states are primitive, we can use the numerical recipe in Appendix E.0.1 to find the zeros of the Q functions (Bethe roots) for both states by solving the functional TQ relation numerically.

Curiosity at supersymmetric point. In general the number of degenerate primitive eigenstates at root of unity and commensurate twist increases as the (odd) system size N grows. The exception to this rule is the special point $\eta = \frac{2\pi}{3}$, $\phi = 0$ (or $\eta = \frac{\pi}{3}$, $\phi = \pi$, cf. Appendix E.0.2), for which there are only two degenerate primitive eigenstates for any odd N. (There are no degenerate primitive eigenstate when N is even.) These values of η correspond to the supersymmetric point $\Delta = -\frac{1}{2}$. For commensurate twist $\phi = 0$ and odd system size N, the antiferromagnetic ground states are always doubly degenerate, and have been well studied. We call them *Razumov–Stroganov (RS) states*, from the conjecture made

in Ref. [129] and later proven in Ref. [130]. RS states are closely related to lattice supersymmetry [131, 132]. (Note that in our convention for the Hamiltonian the RS states are the *highest* excited states in the spectrum.)

Interestingly, RS states are the only two primitive degenerate states at $\Delta = -1/2$ and $\phi = 0$, for any odd N. Let us denote them by $|\mathrm{RS}_1\rangle$, in the sector with $M = (N-1)/2$ down spins, and $|\mathrm{RS}_2\rangle = \prod_{j=1}^{N} \sigma_j^x \ |\mathrm{RS}_1\rangle$, with $M = (N+1)/2$. Their eigenvalues for $\mathbf{T}_{1/2}$ are

$$\begin{aligned} \mathbf{T}_{1/2}(u,0) \ |\mathrm{RS}_1\rangle &= \sinh^N(u) \ |\mathrm{RS}_1\rangle \,, \\ \mathbf{T}_{1/2}(u,0) \ |\mathrm{RS}_2\rangle &= \sinh^N(u) \ |\mathrm{RS}_2\rangle \,. \end{aligned} \tag{6.115}$$

The Bethe roots can be obtained using numerical method in Appendix E.0.1. For instance, for $N = 5$ we have

$$\begin{aligned} |\mathrm{RS}_1\rangle &= |\{u_m\}_{m=1}^{2}\rangle \,, \\ u_1 &= \frac{\log(11-\sqrt{21}) - \log 10}{2} + \frac{\mathrm{i}\pi}{2}, \\ u_2 &= \frac{\log(11+\sqrt{21}) - \log 10}{2} + \frac{\mathrm{i}\pi}{2}, \end{aligned} \tag{6.116}$$

and

$$\begin{aligned} |\mathrm{RS}_2\rangle &= |\{v_{m'}\}_{m'=1}^{3}\rangle \,, \\ v_1 &= \frac{\mathrm{i}\pi}{2}, \quad v_2 = \frac{\log(2-\sqrt{3})}{2} + \frac{\mathrm{i}\pi}{2}, \\ v_3 &= \frac{\log(2+\sqrt{3})}{2} + \frac{\mathrm{i}\pi}{2}. \end{aligned} \tag{6.117}$$

Naturally one might wonder what the structure of the truncated two-parameter transfer matrix $\tilde{\mathbb{T}}(x,y,\phi)$ is at $\Delta = 1/2$, and how it relates to the RS states. We postpone this question to future work.

6.6.5 Q functions for fully polarised states

Since all transfer matrices and the Hamiltonian commute with the total magnetisation $\mathbf{S}^z$, the two fully polarised states $|\uparrow\uparrow\cdots\uparrow\rangle$ and $|\downarrow\downarrow\cdots\downarrow\rangle$ are eigenstates of all transfer matrices, and therefore of the Q and P operators. Let us study this in more detail.

For the pseudovacuum $|\uparrow\uparrow\cdots\uparrow\rangle$ on top of which magnon excitations are built it is easy to see that for any system size N and twist ϕ,

$$\tilde{\mathbf{Q}}(u,\phi)\ |\uparrow\uparrow\cdots\uparrow\rangle = Q_{\Uparrow}(u,\phi)\ |\uparrow\uparrow\cdots\uparrow\rangle\,, \quad Q_{\Uparrow}(u,\phi) = \text{cst}, \tag{6.118}$$

with Q function that does not depend on u or ϕ.

From the definition of the two-parameter transfer matrix (6.16), we have

$$\tilde{\mathbf{Q}}(u,\phi)\ |\downarrow\downarrow\cdots\downarrow\rangle = Q_{\Downarrow}(u,\phi)\ |\downarrow\downarrow\cdots\downarrow\rangle\,, \tag{6.119}$$

where the Q function is

$$\begin{aligned} Q_{\Downarrow}(u,\phi) &= \langle\downarrow\downarrow\cdots\downarrow|\ \tilde{\mathbb{T}}(u,0,\phi)\ |\downarrow\downarrow\cdots\downarrow\rangle \\ &= \mathrm{tr}_a\Big[\big(e^{u-\eta/2}\,\tilde{\mathbf{W}}_a^{-1} - e^{-u+\eta/2}\,\tilde{\mathbf{W}}_a\big)^N\,\tilde{\mathbf{E}}(\phi)\Big] \\ &= \sum_{k=0}^{\ell_2-1}\big(q^{-k-1/2}\,t - q^{k+1/2}\,t^{-1}\big)^N e^{\mathrm{i}k\phi}, \quad t = e^u \end{aligned} \tag{6.120}$$

which is consistent with (6.112). (Beware that one needs to compare $Q_{\Downarrow}(u,\phi)$ with $P_{\Uparrow}(u,-\phi)$.)

From the final expression in (6.120) we see that

$$\begin{aligned} Q_{\Downarrow}(u+\eta,\phi) = e^{\mathrm{i}\phi}\Bigg[&\sum_{k=0}^{\ell_2-2}\big(q^{-k-1/2}\,t - q^{k+1/2}\,t^{-1}\big)^N e^{\mathrm{i}k\phi} \\ &+ \big(q^{-\ell_2+1/2}\,t - q^{\ell_2-1/2}\,t^{-1}\big)^N e^{\mathrm{i}(\ell_2-1)\phi}\big(\varepsilon^N\,e^{-\mathrm{i}\ell_2\phi}\big)\Bigg], \end{aligned} \tag{6.121}$$

and since $\varepsilon = q^{\ell_2} = \pm 1$, we conclude that if $1 - \varepsilon^N e^{\mathrm{i}\ell_2\phi} = 0$ then

$$Q_{\Downarrow}(u+\eta,\phi) = e^{\mathrm{i}\phi}\,Q_{\Downarrow}(u,\phi). \tag{6.122}$$

This is precisely the commensurate-twist condition (6.84) for the appearance of FM strings. When $\phi = 0$ and the condition (6.84) is satisfied $Q_{\Downarrow}(u,\phi)$ is a trigonometric polynomial in $z = t^{\xi\ell_2} = e^{\xi\ell_2 u}$ with $\xi = 1$ ($\xi = 2$) if ℓ_1 is even (odd). In that case the Bethe roots, i.e. the zeros of (6.120), consist of only FM strings and pairs $+\infty, -\infty$.

6.7 Applications to XXZ at root of unity: examples

The physical Hilbert space $(\mathbb{C}^2)^{\otimes N}$ consists of all joint eigenstates of the transfer matrices. Assuming the completeness of the Bethe ansatz these states can be distinguished by their Bethe roots. Degeneracies are known to occur in terms of the eigenvalues of the transfer matrices $\mathbf{T}_s$ when the condition (6.84) for commensurate twist is satisfied [105, 108, 106]. At first sight, this might resemble the degeneracies due to the $SU(2)$, or $\mathfrak{sl}_2 = (\mathfrak{su}_2)_{\mathbb{C}}$, symmetry at the isotropic point. Yet such degeneracies are not expected away from the isotropic point. In this section we will show with several concrete examples how to construct the descendant towers (Hasse diagrams) that link all different eigenstates with the same eigenvalues (possibly up to a sign for $\mathbf{T}_{n/2}$, $n \in \mathbb{Z}_{>0}$, cf. Section 6.6.2), for the transfer matrices. Moreover, we illustrate in Section 6.7.1 that these degeneracies grow exponentially. These degeneracies have significant consequences in the thermodynamic limit, which are discussed in Section 6.9.2.

We use the following method. In order to study the spectrum of XXZ spin chain at root of unity we need to know the Bethe roots associated to the eigenstates of the model, which is equivalent to knowing the Q functions, i.e. the eigenvalues of the Q operator, for these eigenstates. Making use of the decomposition of the truncated two-parameter transfer matrix $\tilde{\mathbf{Q}}(x,\phi) = \tilde{\mathbb{T}}(x,0,\phi)$, we construct the Q operator for the XXZ spin chain at root of unity explicitly for system size $N \leq 16$. This is possible owing to the truncation of the auxiliary space at root of unity. All the explicit examples in Secs. 6.7.1 and 6.7.2 are obtained through this procedure. In many instances, analytic expressions can be obtained using symbolic algebra software.

6.7.1 Descendant towers in periodic case

Let us first consider cases with twist $\phi = 0$, i.e. periodic boundary conditions, and illustrate how descendant states can be found from a primitive state together with FM strings or pairs $+\infty, -\infty$. The result is a *descendant tower*, consisting of all eigenstates with degenerate (possibly up to a sign for $s = 1/2$) eigenvalues of $\mathbf{T}_s$ for all $2s \in \mathbb{Z}_{>0}$. At $\phi = 0$ every

eigenstate $|\{u_m\}_{m=1}^{M}\rangle$ ($M < \frac{N}{2}$) has at least one eigenstate with the same eigenvalue for $\mathbf{T}_s$, namely the spin-flipped state *beyond the equator*,

$$|\{v_{m'}\}_{m'=1}^{N-M}\rangle \propto \prod_{j=1}^{N}\sigma_j^x \ |\{u_m\}_{m=1}^{M}\rangle\,. \tag{6.123}$$

We refer to $|\{u_m\}_{m=1}^{M}\rangle$ and $|\{v_{m'}\}_{m'=1}^{N-M}\rangle$ as states on the opposite side of the equator with respect to each other. These two states are closely related when (6.84) is satisfied, forming the top and bottom of a descendant tower that includes various intermediate states.

In this section we focus on the case with system size $N = 12$, anisotropy $\Delta = \frac{1}{2}$ ($\eta = \frac{\mathrm{i}\pi}{3}$), and twist $\phi = 0$. Similar constructions of descendant towers apply to the antiperiodic case $\phi = \pi$, which we shall not discuss separately.

Descendant towers of FM strings and their 'free-fermion' nature

We start with an example of a descendant tower that is generated by adding FM strings to a primitive state. Consider the simplest primitive state: the pseudovacuum state $|\{\varnothing\}\rangle = |\uparrow\uparrow\cdots\uparrow\rangle$, with no magnons ($M_0 = 0$ spins down). The corresponding state beyond the equator, $\prod_{j=1}^{12}\sigma_j^x \ |\{\varnothing\}\rangle = |\downarrow\downarrow\cdots\downarrow\rangle$ has Q function given by (6.120):

$$Q(t) \propto t^{12} + 220\,t^6 + 924 + 220\,t^{-6} + t^{-12}. \tag{6.124}$$

The zeros of this Q function[3] are of the form

$$\alpha_1^{\mathrm{FM}} = \alpha_1 + \mathrm{i}\frac{\pi}{6}, \quad \alpha_2^{\mathrm{FM}} = \alpha_2 + \mathrm{i}\frac{\pi}{6}, \quad \alpha_3^{\mathrm{FM}} = \alpha_3 + \mathrm{i}\frac{\pi}{6}, \quad \alpha_4^{\mathrm{FM}} = \alpha_4 + \mathrm{i}\frac{\pi}{6} \tag{6.125}$$

with numerical values of the real parts of the Bethe roots given by

$$\begin{aligned} &\alpha_1 = -0.89566465, \quad \alpha_2 = -0.23210918, \\ &\alpha_3 = 0.23210918, \quad \alpha_4 = 0.89566465. \end{aligned} \tag{6.126}$$

Thus the state corresponding to $|\{\varnothing\}\rangle$ beyond the equator is itself a Bethe vector:

$$\prod_{j=1}^{12}\sigma_j^x \ |\{\varnothing\}\rangle = |\{v_{m'}\}_{m'=1}^{12}\rangle =: |\{\alpha_1^{\mathrm{FM}}, \alpha_2^{\mathrm{FM}}, \alpha_3^{\mathrm{FM}}, \alpha_4^{\mathrm{FM}}\}\rangle\,. \tag{6.127}$$

[3] Recall that each pair $\pm t$ of zeros of Q corresponds to one Bethe root: $u + \mathrm{i}\pi \equiv u$.

Recall that each $\{\alpha_j^{\rm FM}\}$ stands for the FM string with $\ell_2 = 3$ Bethe roots sharing the centre $\alpha_j^{\rm FM}$.

For any root of unity, (6.112) implies that FM strings behave like *free fermions* within a descendant tower. For a primitive state $|\{u_m\}_{m=1}^M\rangle$, if the state $|\{u_m\}_{m=1}^M \cup \{\alpha_1^{\rm FM}, \alpha_2^{\rm FM}\}\rangle$ belongs to the descendant tower, then so does $|\{u_m\}_{m=1}^M \cup \{\alpha_n^{\rm FM}\}\rangle$ for $n \in \{1, 2\}$. That is, FM strings are 'transparent': they do not scatter with (feel or influence the values of) other roots.

This observation yields the following descendant tower. Given a primitive state, we first construct the corresponding eigenstate beyond the equator and find its Bethe roots as above. The descendant tower is obtained from the primitive state through adding FM strings one by one, with magnetisation M jumping by ℓ_2 each time, until we reach the eigenstate beyond the equator at the bottom. For example, the descendant tower obtained in this way from the pseudovacuum that we considered above is illustrated in Fig. 6.4. This structure is easily verified by explicitly constructing the Q operator, and one sees that the eigenvalues of the transfer matrices $\mathbf{T}_s$ are degenerate (up to a sign) for all descendant states.

In particular, we observe that the number of descendant states within the magnetisation sector with number of down spins fixed to $M = M_0 + n\,\ell_2$ is equal to $\binom{n_{\rm FM}}{n}$, i.e. grows binomially with respect to the number $n_{\rm FM}$ of FM strings for the state beyond the equator. By adding up all descendant states at the occurring values of M we find that the total number within the descendant tower is

$$n_{\rm total} = \sum_{n=0}^{n_{\rm FM}} \binom{n_{\rm FM}}{n} = 2^{n_{\rm FM}}, \tag{6.128}$$

in agreement with the $\widehat{\mathfrak{sl}_2}$ prediction [117]. The descendant tower is exponentially large in the number $n_{\rm FM}$ of FM strings present in the state beyond the equator corresponding to the primitive state.

Descendant towers with pairs of roots at infinity

Next we turn to an example of a descendant tower that is generated by adding FM strings as well as pairs $+\infty, -\infty$ to the Bethe roots of a

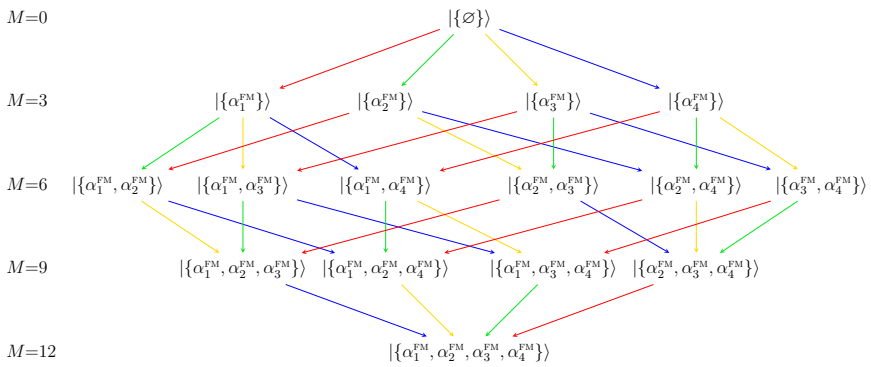

Figure 6.4: Illustration of a descendant tower from the pseudovacuum for $N = 12$, $\Delta = 1/2$, $\phi = 0$. Arrows of different colours correspond to the addition of different FM strings.

primitive state. Recall that Bethe roots at infinity correspond to applications of the lowering operators of $U_q(\mathfrak{sl}_2)$ (see Appendix D.1). At root of unity ℓ_2 applications of either of $\mathbf{S}^{\pm}$ or $\bar{\mathbf{S}}^{\pm}$ already gives zero, so the total numbers of Bethe roots at $+\infty$ and $-\infty$ must be smaller than ℓ_2, i.e. $n_{\pm\infty} < \ell_2$. Pairs of Bethe roots at $+\infty, -\infty$ play a similar role as FM strings.

We continue with the example $N = 12$, $\Delta = \frac{1}{2}$ ($\eta = \frac{\mathrm{i}\pi}{3}$), $\phi = 0$. Let us now start from a primitive state with one down spin ($M_0 = 1$), $|\{u_1\}\rangle$. We pick the solution to Bethe ansatz equations (3.25) given by $u_1 = \frac{1}{2}\log\frac{\sqrt{3}+1}{\sqrt{3}-1}$. We consider the corresponding state beyond the equator, $|\{v_{m'}\}_{m'=1}^{11}\rangle \propto \prod_{j=1}^{N}\sigma_j^x\ |\{u_1\}\rangle$. We obtain its eigenvalue for the Q operator by solving (6.112), yielding the Q function

$$\begin{aligned} Q(t) &\propto \prod_{m'=1}^{11}\left(t - e^{2v_{m'}}\,t^{-1}\right) \\ &= \left(t - \frac{\sqrt{3}+1}{\sqrt{3}-1}\,t^{-1}\right) \\ &\quad \times \left(t^6 - \frac{59}{74}(-8+3\sqrt{3}) + \frac{91-48\sqrt{3}}{37}\,t^{-6}\right). \end{aligned} \tag{6.129}$$

The zeros of this Q function are u_1, two FM strings, along with (cf. Section 6.4.5) two pairs of roots $+\infty, -\infty$:

$$\begin{aligned} &v_1 = u_1, \\ &v_{3(n-1)+k+1} = \alpha_n^{\text{FM}} + \frac{\mathrm{i}(k-2)\pi}{3}, \\ &1 \le n \le n_{\text{FM}} = 2\,, \quad 1 \le k \le \ell_2 = 3\,, \\ &v_8 = v_{10} = +\infty, \quad v_9 = v_{11} = -\infty. \end{aligned} \tag{6.130}$$

Here the FM strings are centred at

$$\alpha_1^{\text{FM}} = \alpha_1 + \mathrm{i}\frac{\pi}{6}, \quad \alpha_2^{\text{FM}} = \alpha_2 + \mathrm{i}\frac{\pi}{6}, \tag{6.131}$$

with real parts that have numerical values

$$\alpha_1 = -0.38464681, \quad \alpha_2 = 0.12649136, \tag{6.132}$$

satisfying the quantisation condition (6.112). Note that $n_{\pm\infty} = 2 < \ell_2 = 3$.

Unlike for FM strings, Bethe roots at infinity cannot added one by one: $\{u_1, \pm\infty\}$ does not satisfy the Bethe equations, as it violates the condition (6.1). On the other hand, using (D.7) we can easily check that

$$\begin{aligned} |\{u_1, 2\times\pm\infty\}\rangle &\coloneqq |\{u_1, +\infty, -\infty, +\infty, -\infty\}\rangle \\ &\propto (\mathbf{S}^-)^2\,(\bar{\mathbf{S}}^-)^2\;|\{u_1\}\rangle \end{aligned} \tag{6.133}$$

is an eigenstate with the same eigenvalues for $\mathbf{T}_s$ as $|\{u_1\}\rangle$.

Hence, pair(s) of Bethe roots $+\infty, -\infty$ can be viewed as a 'bound state'. These roots always appear together in order to satisfy condition (6.4). Like FM strings, pair(s) of Bethe roots $+\infty, -\infty$ do not scatter with other magnons. Therefore, when the corresponding descendant state beyond the equator contains one pair of infinite Bethe roots as in our example, the total number of states in the descendant tower is

$$n_{\text{total}} = \sum_{m=0}^{n_{\text{FM}}+1} \binom{n_{\text{FM}}+1}{m} = 2^{n_{\text{FM}}+1}, \tag{6.134}$$

as illustrated in Fig. 6.5.

Almost all (primitive) states at $M = 1$ give rise to a descendant tower of this form, only differing in the locations of the FM string centres. There are two exceptions which we study next.

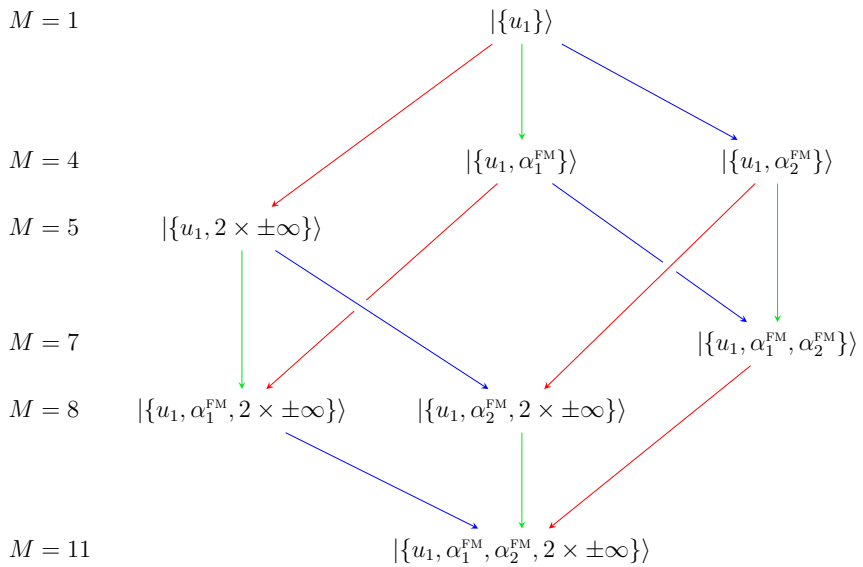

Figure 6.5: The descendant tower of $|\{u_1\}\rangle$ with finite u_1 for $N = 12$, $\Delta = 1/2$, $\phi = 0$.

Mirroring descendant towers

There is one more interesting feature present in the spectrum for $N = 12$, $\Delta = \frac{1}{2}$ ($\eta = \frac{\mathrm{i}\pi}{3}$), $\phi = 0$. When $M = 1$, there are two eigenstates, namely $|\{+\infty\}\rangle$ and $|\{-\infty\}\rangle$, which have an infinite Bethe root. These are primitive: their $\mathbf{T}_s$-eigenvalues are different from those of the pseudovacuum. We concentrate on $|\{+\infty\}\rangle$ in this section, while the situation for $|\{-\infty\}\rangle$ is analogous.

In general, in the (anti)periodic case $\phi \in \{0, \pi\}$, the existence of an eigenstate of the form $|\{u_m\}_{m=1}^M \cup \{n \times +\infty\}\rangle$ for some $n > 0$ implies the existence of another eigenstate $|\{u_m\}_{m=1}^M \cup \{(\ell_2 - n) \times -\infty\}\rangle$ with the same eigenvalues of $\mathbf{T}_s$ (up to a sign), whose Bethe roots can be found from the Bethe equations (3.25). (Likewise, the presence of a state $|\{u_m\}_{m=1}^M \cup \{n \times -\infty\}\rangle$ implies that of $|\{u_m\}_{m=1}^M \cup \{(\ell_2 - n) \times +\infty\}\rangle$.)

One can verify that the state beyond the equator corresponding to $|\{+\infty\}\rangle$ does *not* belong to the same descendant tower as $|\{+\infty\}\rangle$, unlike for the examples presented in the previous sections. The eigenvalue for the Q operator on the corresponding state beyond the equator,

$|\{v_{m'}\}_{m'=1}^{11}\}\rangle \propto \prod_{j=1}^{12}\sigma_j^x\ |\{+\infty\}\rangle$, is obtained through (6.112), yielding

$$Q(t) \propto \prod_{m'=1}^{11}\left(t - e^{2v_{m'}}\,t^{-1}\right) = t^{11} + \frac{165}{4}\,t^5 + 66\,t^{-1} + \frac{11}{2}\,t^{-7}. \tag{6.135}$$

Its zeros contain three FM strings and two Bethe roots at $-\infty$,

$$\begin{aligned} &v_1 = v_2 = -\infty, \\ &v_{3(n-1)+k+2} = \alpha_n^{\mathrm{FM}} + \frac{\mathrm{i}(k-2)\pi}{3}, \\ &1 \le n \le n_{\mathrm{FM}} = 3, \quad 1 \le k \le \ell_2 = 3, \end{aligned} \tag{6.136}$$

where the FM strings have centres

$$\begin{aligned} &\alpha_n^{\mathrm{FM}} = \alpha_n + \mathrm{i}\frac{\pi}{6}, \quad \alpha_1 = -0.404723313, \\ &\alpha_2 = 0.075767627, \quad \alpha_3 = 0.613080368, \end{aligned} \tag{6.137}$$

which satisfy the quantisation condition (6.112).

The resulting descendant-tower structure is as follows. The primitive state $|\{+\infty\}\rangle$ gives rise to descendants via the addition of the above FM strings. This yields a descendant tower that accounts for half of the states with the same eigenvalues (possibly up to a sign) of the transfer matrices $\mathbf{T}_s$. The other half of the states form a 'mirroring tower', obtained from the first tower by spin reversal. At the top of the mirroring tower we find the primitive eigenstate $|\{2\times-\infty\}\rangle$, whose eigenvalues for $\mathbf{T}_s$ are the same as those of $|\{+\infty\}\rangle$ except for a sign for $s = 1/2$. Spin reversal relates states on opposite sides of the equator as

$$\begin{aligned} \prod_{j=1}^{12}\sigma_j^x\ |\{u_m\}_{m=1}^{M}\rangle &\propto |\{v_{m'}\}_{m'=1}^{12-M}\rangle \\ &= |\{+\infty, 2\times-\infty, \alpha_1^{\mathrm{FM}}, \alpha_2^{\mathrm{FM}}, \alpha_3^{\mathrm{FM}}\} \setminus \{u_m\}_{m=1}^{M}\rangle\,. \end{aligned} \tag{6.138}$$

See Fig. 6.6 for an illustration.

6.7.2 Descendant towers for nonzero commensurate twist

Now we turn to cases with commensurate twist $\phi \notin \{0, \pi\}$. It is useful to consider two commensurate twists $\pm\phi$ simultaneously. Similar to the

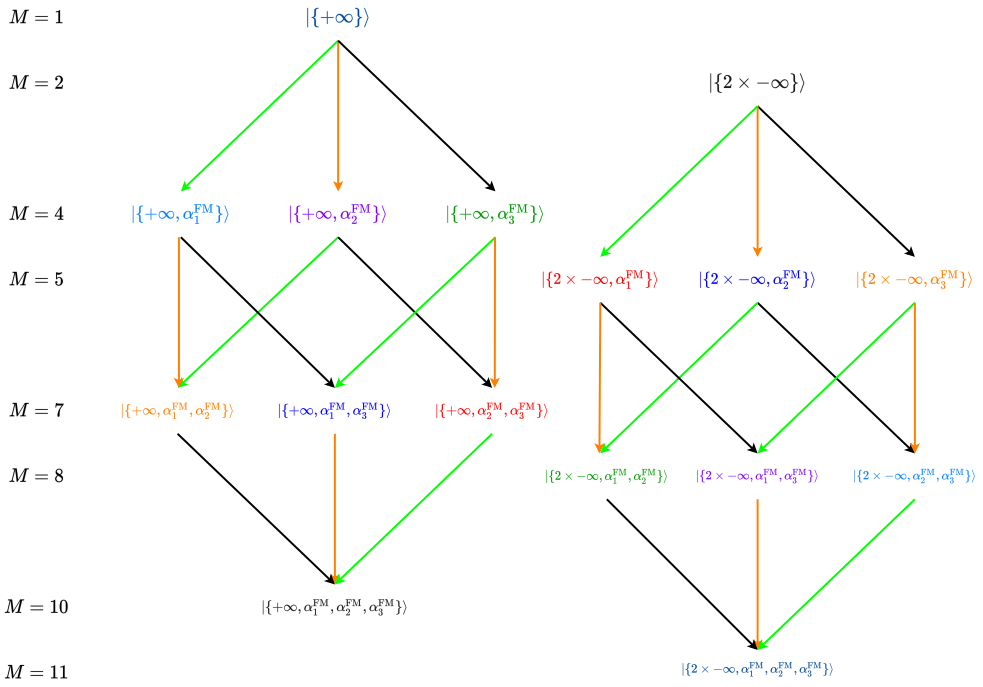

Figure 6.6: Illustration of descendant towers from degenerate primitive states at $M_0 = 1, 2$ with Bethe roots at infinity for $N = 12$, $\Delta = 1/2$, $\phi = 0$. Global spin reversal acts by reflection through the middle of the figure: the states with the same colour are pairs corresponding to each other beyond the equator.

mirror-pair of descendant towers in Section 6.7.1 we need to consider two copies of descendant towers. This time, however, the two copies include states at twist ϕ as well as states at *opposite* twist $-\phi$. In Appendix E.0.3, we show that the transfer matrices $\mathbf{T}_s(u,\phi)$ with twist ϕ are related to those with opposite twist by flipping all spins,

$$\prod_{j=1}^{N}\sigma_j^x\ \mathbf{T}_s(u,\phi)\prod_{j=1}^{N}\sigma_j^x = e^{2si\phi}\,\mathbf{T}_s(u,-\phi). \tag{6.139}$$

Thus $\prod_{j=1}^{N}\sigma_j^x\ |\{u_m\}_{m=1}^{M}\rangle$ is an eigenstate of (the Hamiltonian, and more generally) the transfer matrices $\mathbf{T}_s(u,-\phi)$ whenever $|\{u_m\}_{m=1}^{M}\rangle$ is so for

$\mathbf{T}_s(u,\phi)$, cf. (E.17). (Observe that $\phi = 0, \pi$ are the only two values for which $\phi = -\phi \bmod 2\pi$.)

We study the example $N = 6$, $\Delta = \frac{1}{2}$ (so $\eta = \mathrm{i}\pi/3$) and commensurate twist $\phi = \pm\frac{2\pi}{3}$. We wish to understand the descendant tower for primitive states with $M_0 = 1$ down spin. Consider $|\{u_1\}\rangle$ with $u_1 = \operatorname{arctan}\frac{\tan(\pi/18)}{\sqrt{3}}$, which is an eigenvector for the Hamiltonian with twist $\phi = \frac{2\pi}{3}$. Its quasi-momentum is

$$\widetilde{p} = \mathrm{i}\log\frac{\sinh(u_1 - \eta/2)}{\sinh(u_1 + \eta/2)} = \frac{6\pi - \phi}{6} = \frac{8\pi}{9}. \tag{6.140}$$

Next consider the primitive state $|\{u_2\}\rangle'$ with $u_2 = -\operatorname{arctan}\frac{\tan(\pi/18)}{\sqrt{3}}$, where we add a prime to the state to indicate that it is an eigenstate for the Hamiltonian with twist $\phi' = -\frac{2\pi}{3}$. This second state has opposite quasimomentum

$$\widetilde{p}' = \mathrm{i}\log\frac{\sinh(u_2 - \eta/2)}{\sinh(u_2 + \eta/2)} = \frac{-6\pi - \phi'}{6} = -\frac{8\pi}{9} = \frac{10\pi}{9} \bmod 2\pi. \tag{6.141}$$

These two primitive states have the same eigenvalues for the energy

$$\begin{aligned} H(\phi)\ |\{u_1\}\rangle\ &= E\ \ |\{u_1\}\rangle\,, \\ H(-\phi)\ |\{u_2\}\rangle' &= E'\ |\{u_2\}\rangle'\,, \end{aligned} \qquad E = E' = -\cos\frac{\pi}{9} - \frac{1}{2}. \tag{6.142}$$

We would like to remark that these two states are *not* degenerate for the transfer matrices. For example, the fundamental transfer matrix $\mathbf{T}_{1/2}$ acts by

$$\begin{aligned} \mathbf{T}_{1/2}(u,\phi)\ |\{u_1\}\rangle = \frac{e^{\mathrm{i}\phi/2}}{64}\big(&a_1\,t^6 + a_2\,t^4 + a_3\,t^2 + a_4 \\ &+ a_5\,t^{-2} + a_6\,t^{-4} + a_7\,t^{-6}\big)\ |\{u_1\}\rangle\,, \end{aligned} \tag{6.143}$$

in terms of $t = e^u$ as usual, while

$$\begin{aligned} \mathbf{T}_{1/2}(u,\phi')\ |\{u_2\}\rangle' = \frac{e^{\mathrm{i}\phi'/2}}{64}\big(&a_7\,t^6 + a_6\,t^4 + a_5\,t^2 + a_4 \\ &+ a_3\,t^{-2} + a_2\,t^{-4} + a_1\,t^{-6}\big)\ |\{u_2\}\rangle' \end{aligned} \tag{6.144}$$

has the opposite order of the coefficients. The coefficients read

$$\begin{aligned} a_1 &= -2, \quad a_2 = a_5 = 9 - 6\sin\frac{\pi}{18} - 6\cos\frac{\pi}{9}, \\ a_3 &= -6\left(1 - 3\cos\frac{\pi}{9} + \cos\frac{2\pi}{9} - 4\sin\frac{\pi}{18}\right), \\ a_4 &= -1 + 18\cos\frac{2\pi}{9} - 18\sin\frac{\pi}{18}, \\ a_6 &= -6\left(1 + \cos\frac{2\pi}{9} - \sin\frac{\pi}{18}\right), \quad a_7 = 1. \end{aligned} \tag{6.145}$$

To construct the descendant towers we turn to the corresponding states beyond the equator. For $|\{u_1\}\rangle$ this is $\prod_{j=1}^{6}\sigma_j^x\ |\{u_1\}\rangle \propto |\{u_1, -\infty, \alpha_1^{\text{FM}}\rangle'$, whose eigenvalue for the Q operator $\tilde{\mathbf{Q}}(t,\phi')$ is

$$\begin{aligned} Q'(t) &\propto t\left(t - e^{2u_1}t^{-1}\right)\left(t^3 - e^{6\alpha_1^{\text{FM}}}t^{-3}\right) \\ &\approx t^5 - 1.2266816\,t^3 + 3.4456224\,t^{-1} - 4.2266816\,t^{-3}. \end{aligned} \tag{6.146}$$

The state beyond the equator corresponding to $|\{u_2\}\rangle'$ is $|\{u_2, +\infty, \alpha_2^{\text{FM}}\rangle$, with eigenvalue for the Q operator $\tilde{\mathbf{Q}}(t,\phi)$ given by

$$\begin{aligned} Q(t) &\propto t^{-1}\left(t - e^{2u_2}t^{-1}\right)\left(t^3 - e^{6\alpha_2^{\text{FM}}}t^{-3}\right) \\ &\approx t^3 - 0.8152075\,t + 0.2902233\,t^{-3} - 0.2365922\,t^{-5}. \end{aligned} \tag{6.147}$$

Here the numerical values of the two FM string centres are

$$\alpha_1^{\text{FM}} = 0.20618409 + \frac{\mathrm{i}\pi}{6}, \quad \alpha_2^{\text{FM}} = -0.20618409 + \frac{\mathrm{i}\pi}{6}. \tag{6.148}$$

The descendant towers can again be constructed using the 'free fermion'-like property as in Section 6.7.1. The resulting tower structure is depicted in Fig. 6.7, where in general states come in pairs that have the same (possibly up to a sign, as always) eigenvalues for all transfer matrices $e^{\mp \mathrm{i}s\phi}\,\mathbf{T}_s(u, \pm\phi)$, where the sign in $\pm\phi$ is determined by the Hamiltonian for which the state is an eigenvector.

A key difference with the (anti)periodic case is that, in order to construct the descendant tower by considering the state beyond the equator corresponding to the primitive state, we need to consider the systems with twists ϕ and $\phi' = -\phi$ simultaneously. The states *within* either tower

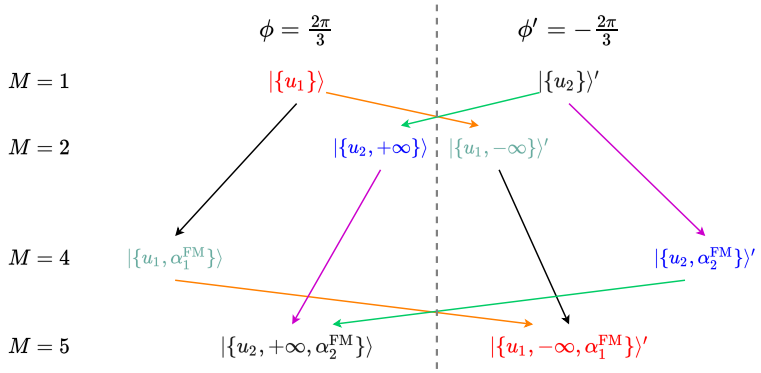

Figure 6.7: Illustration of descendant towers from the primitive states $|\{u_1\}\rangle$ and $|\{u_2\}\rangle'$ for $N = 6$, $\Delta = 1/2$ and commensurate twist $\phi = \frac{2\pi}{3}$ and $\phi' = -\phi$. Like in Fig. 6.6 states of the same colour correspond to each other via global spin reversal.

in Fig. 6.7, e.g. $|\{u_1\}\rangle$ and $|\{u_1, -\infty\}\rangle'$, have degenerate (possibly up to a sign) eigenvalues for all $e^{\mp is\phi}\,\mathbf{T}_s(u, \pm\phi)$, with sign of the twist determined by the states. On the other hand, *between* the two different towers, the eigenstates are only degenerate for the energy. For the two primitive states, the degeneracy of eigenvalues does *not* extend to the higher order charges generated by the transfer matrices. This is the second important difference with the (anti)periodic case from Section 6.7.1, where all eigenstates in Fig. 6.6 have degenerate (up to a possible sign) eigenvalues for $\mathbf{T}_s$. We remark that the descendant-tower structure for twists $\pm\phi \notin \{0, \pi\}$ can get more complicated for roots of unity with $\ell_2 > 3$.

6.7.3 Full spectrum at root of unity: an example

Although we have not been able to construct an algorithmic description of the structure of the spectrum for given values of the spin-chain parameters N, Δ, ϕ, our numerical investigations of numerous examples suggest that the full spectrum can be described in terms of the descendant towers that we have described in this section. Let us demonstrate this for a system with $N = 10$, $\Delta = \frac{1}{2}$ ($\eta = \frac{i\pi}{3}$) and $\phi = 0$. The resulting description of the full spectrum is given in Table 6.1.

We stress that, due to the vanishing Wronskian relation (6.83) and the 'free fermion'-like behaviour of FM strings, each primitive state is at the top of a descendant tower, with descendants that are obtained by adding FM strings or pairs of Bethe roots $+\infty, -\infty$. By (6.7) the states come in three categories, classified by the number of Bethe roots located at infinity:

i) $n_{+\infty} = n_{-\infty}$ ($= 0$ for primitive states),

ii) $n_{+\infty} > n_{-\infty} = 0$,

iii) $n_{-\infty} > n_{+\infty} = 0$.

More precisely, the conditions (6.4) and (6.6) allow for $n_{\pm\infty} = (M + 1) \bmod 3$. Since of course $n_{+\infty} + n_{-\infty} \leq M$ infinite roots can first occur at $M = 3$ ($n_{\pm\infty} = 1$), then at $M = 4$ ($n_{\pm\infty} = 2$), not at $M = 5$ ($n_{\pm\infty} = 0$), after which the pattern repeats.

We begin with $|\uparrow\cdots\uparrow\rangle = |\{\varnothing\}\rangle$. From the zeros of the Q function (6.120), we find that the corresponding state beyond the equator is $|\downarrow\cdots\downarrow\rangle \propto |\{\alpha_1^{\mathrm{FM}}, \alpha_2^{\mathrm{FM}}, 2 \times \pm\infty\}\rangle$, with FM strings of length $\ell_2 = 3$. We can use the result in Section 6.7.1. Note that (6.4) and (6.6) require that all four infinite roots must be added at the same time. The primitive state at $M = 0$ thus gives rise to a descendant tower with two descendants at $M = 3$ and at $M = 7$, and one descendant at each of $M = 4, 6, 10$.

All ten states $|\{u_1\}\rangle$ at $M = 1$ are primitive. Their Bethe roots are finite in accord with (6.4) and (6.6). The corresponding states beyond the equator have room for two FM strings and one pair of infinite roots ($n_{+\infty} = n_{-\infty} = 1$, allowed at $M = 9$). The descendant tower is similar to Fig. 6.5, except that there is just a single pair of infinite roots. All intermediate descendants can be easily obtained. The pair of infinite roots at $M = 3, 6, 9$ is allowed by (6.4) and (6.6). Each $M = 1$ vector thus sits at the top of a descendant tower containing one descendant at each of $M = 3, 7$ and two descendants at $M = 4, 6$.

The 45 states at $M = 2$ are also primitive, and have finite Bethe roots. The corresponding states beyond the equator allow for two FM strings. By the free-fermion property each descendant tower contains four states.

Now we consider the cases with $M = 3$, where there are $120 - 12 = 108$ primitive states. In this scenario, infinite Bethe roots ($n_{\pm\infty} = 1$) may occur within primitive states. Due to parity invariance there must be equally

many states in the classes (ii) and (iii). Suppose that $n_{+\infty} = 1$, $n_{-\infty} = 0$ (the opposite case is treated analogously). There are two finite Bethe roots left to be determined. Their Bethe equations effectively acquire a twist due to the presence of the infinite root, cf. the discussion preceding (6.1). We solve these Bethe ansatz equations, and remove solutions of these two roots that contain infinite root(s). The corresponding states beyond the equator need four more Bethe roots. For the primitive states with $n_{+\infty} = n_{-\infty} = 0$ these extra roots come from $n_{+\infty} = n_{-\infty} = 2$, while for the primitive states with $n_{\pm\infty} = 1$ and $n_{\mp\infty} = 0$ these descendants have $n_{\pm\infty} = 2$, $n_{\mp\infty} = 0$ plus one FM string.

We proceed in similar manner for the $210 - 12 = 198$ primitive states at $M = 4$. The corresponding states beyond the equator need two more Bethe roots, which come from adding a pair $+\infty, -\infty$ for the primitive states in class (i). For class (ii) they are of the form $|\{u_1, u_2, +\infty, +\infty\}\rangle$, but the corresponding states beyond the equator are only allowed to have one infinite root. In this case one of the infinite roots is removed to make place for an FM string: the descendants are $|\{u_1, u_2, \alpha^{\text{FM}}, +\infty\}\rangle$.

The $252 - 90 = 162$ primitive states left at the equator must fall in class (i).

The resulting spectrum is summarised in Table 6.1, where '$\times k$' counts the different FM string configurations (choices of α_n^{FM}) for the descendant states at a given magnetisation.

6.8 Conjectures for FM creation and annihilation operators

We use semi-cyclic representation of $\mathcal{U}_q(\mathfrak{sl}_2)$ as the auxiliary space of the transfer matrix in order to construct degenerate states with different magnetisation. Our construction is a continuation of the ideas in [133, 127]. We present conjectures for explicit constructions of the FM string creation and annihilation operators that commute with the XXZ transfer matrix while changing the magnetisation in steps of ℓ_2.

M	total #	# prim. $n_{\pm\infty} = 0$	# prim. $n_{+\infty} > 0$	# prim. $n_{-\infty} > 0$	# desc. $n_{+\infty} = n_{-\infty}$	# desc. $n_{+\infty} > 0$	# desc. $n_{-\infty} > 0$
0	1	1	0	0	0	0	0
1	10	10	0	0	0	0	0
2	45	45	0	0	0	0	0
3	120	40	34	34	$1\times2+10$	0	0
4	210	121	34	34	$1+10\times2$	0	0
5	252	162	0	0	45×2	0	0
6	210	0	0	0	$1+10\times2+121$	34	34
7	120	0	0	0	$1\times2+10+40$	34	34
8	45	0	0	0	45	0	0
9	10	0	0	0	10	0	0
10	1	0	0	0	1	0	0

Table 6.1: The full spectrum for $N = 10$, $\Delta = \frac{1}{2}$ ($\eta = \frac{\mathrm{i}\pi}{3}$) and $\phi = 0$, organised in terms of primitive and descendant states with $n_{+\infty} = n_{-\infty}$, $n_{+\infty} > n_{-\infty} = 0$, $n_{-\infty} > n_{+\infty} = 0$.

6.8.1 Case $q^{\ell_2} = +1$

We start with roots of unity satisfying $\varepsilon = q^{\ell_2} = +1$. We start with modifying the matrix entry $\mathbf{S}^{+}_{a} = \mathbf{L}^{21}_{a}/\sinh\eta$ to

$$\mathbf{S}^{+,\mathrm{sc}}_{a} = \mathbf{S}^{+}_{a} + \beta\,|0\rangle\langle\ell_2 - 1|_a, \tag{6.149}$$

while keeping the other three matrix elements in (6.28) unchanged. In this way we obtain a Lax operator $\mathbf{L}^{\mathrm{sc}}_{aj}$, and the usual construction (6.15)–(6.16) gives the transfer matrix

$$\mathbf{T}^{\mathrm{sc}}_{s}(u,\phi,\beta) = \mathrm{tr}_a\big[\mathbf{L}^{\mathrm{sc}}_{aN}(u,\beta)\cdots\mathbf{L}^{\mathrm{sc}}_{a1}(u,\beta)\,\mathbf{E}_a(\phi)\big] \tag{6.150}$$

depending on $s \in \mathbb{C}$ and $\beta \in \mathbb{C}$. Here the twist $\mathbf{E}_a(\phi)$ acts on V^{sc}_a in the same way as before, i.e. (F.1). The matrix elements of (6.150) change the magnetisation $(N-2M)/2$ by $-n\,\ell_2$ and are proportional to β^n for positive $n \in \mathbb{Z}_{>0}$. For example, in a chain of length $N = \ell_2$, the expansion of the transfer matrix contains a term $\mathrm{tr}_a[(\mathbf{S}^{+,\mathrm{sc}}_a)^N]\,\prod_{j=1}^{N}\sigma^-_j$ that changes the magnetisation by $-\ell_2$, creating ℓ_2 magnon excitations.

The matrices $\mathbf{T}^{\mathrm{sc}}_{s}(u,\phi)$ do *not* commute with each other at different values of u, but *do* commute with $\mathbf{T}_{1/2}(u,\phi)$ when the twist is commen-

surate. To see this, note that the construction of the semi-cyclic Lax operator guarantees that the following version of the RLL relation (6.14) with (six-vertex) R-matrix (3.4) holds true for any β:

$$\mathbf{R}_{jk}(u-v)\,\mathbf{L}^{\mathrm{sc}}_{aj}(u,\beta)\,\mathbf{L}^{\mathrm{sc}}_{ak}(v,\beta) = \mathbf{L}^{\mathrm{sc}}_{ak}(v,\beta)\,\mathbf{L}^{\mathrm{sc}}_{aj}(u,\beta)\,\mathbf{R}_{jk}(u-v). \quad (6.151)$$

This is an identity of operators on $V_j \otimes V_k \otimes V^{\mathrm{sc}}_a$. The symmetry property $\mathbf{R}_{jk} = \mathbf{R}_{kj}$ of (3.4) allows us to view the R-matrix as a Lax matrix $\mathbf{L}_{bj}$, whereas $\mathbf{L}^{\mathrm{sc}}_{ak}$ takes the role of an R-matrix $\mathbf{R}^{\mathrm{sc}}_{ab}$. Reversing the two sides of (6.151) and changing $v \mapsto u - v$ we arrive at an equivalent RLL relation on $V^{\mathrm{sc}}_a \otimes V_b \otimes V_j$:

$$\mathbf{R}^{\mathrm{sc}}_{ab}(u-v,\beta)\,\mathbf{L}^{\mathrm{sc}}_{aj}(u,\beta)\,\mathbf{L}_{bj}(v) = \mathbf{L}_{bj}(v)\,\mathbf{L}^{\mathrm{sc}}_{aj}(u,\beta)\,\mathbf{R}^{\mathrm{sc}}_{ab}(u-v,\beta). \quad (6.152)$$

Here a corresponds to the semi-cyclic auxiliary space, b to a spin-1/2 auxiliary space, and k to a spin-1/2 physical space. The train argument implies that the twisted semi-cyclic transfer matrix (6.150) commutes with the twisted fundamental transfer matrix (6.15)–(6.16), *provided* $\mathbf{R}^{\mathrm{sc}}_{ab}$ commutes with the tensor product of the twists matrices. This requires the twist to be commensurate, $e^{\mathrm{i}\ell_2\phi} = 1$, cf. (6.84).

Using transfer matrix fusion (6.150), $\mathbf{T}^{\mathrm{sc}}_s$ also commutes with $\mathbf{T}_{s'}(u,\phi)$ for any $2\,s' \in \mathbb{Z}_{>0}$:

$$[\mathbf{T}^{\mathrm{sc}}_s(u,\phi,\beta), \mathbf{T}_{s'}(v,\phi)] = 0, \quad s \in \mathbb{C}, \quad \beta \in \mathbb{C}, \quad 2s' \in \mathbb{Z}_{>0}. \quad (6.153)$$

Since the twisted semi-cyclic transfer matrix $\mathbf{T}^{\mathrm{sc}}_s(u,\phi,\beta)$ changes the magnetisation of an eigenstate of the Q operator in steps of ℓ_2, it mixes states that are degenerate for $\mathbf{T}_{s'}(u,\phi)$ within each descendant tower.

We use $\mathbf{T}^{\mathrm{sc}}_s(u,\phi,\beta)$ to construct eigenstates of the Q operator itself. Because the part of $\mathbf{T}^{\mathrm{sc}}_s(u,\phi,\beta)$ of first order in β changes the magnetisation of eigenstates of the Q operator by $-\ell_2$, we make the following conjectures.

Conjecture 1. When $\varepsilon = q^{\ell_2} = +1$ the linearisation in β of (6.150) at $s = (\ell_2 - 1)/2$,

$$\mathbf{B}^{\mathrm{FM}}(u) \coloneqq \partial_\beta\, \mathbf{T}^{\mathrm{sc}}_s(u,\phi,\beta)\big|_{\beta=0,\, 2s=\ell_2-1}, \quad (6.154)$$

is the creation operator for the FM string $\{\alpha^{\mathrm{FM}}\} = \{u, u + \frac{\mathrm{i}\pi}{\ell_2}, \cdots, u + \mathrm{i}\pi\frac{\ell_2-1}{\ell_2}\}$. The spectral parameter can be taken to be any Bethe root from the FM string, e.g. u as in (6.154).

Note that at $\beta = 0$ the semi-cyclic Lax operator becomes the Lax operator whose auxiliary space is the ℓ_2-dimensional highest-weight representation. By (6.150) the operator (6.154) can thus be expressed more explicitly as

$$\begin{aligned}\mathbf{B}^{\mathrm{FM}}(u) = \sum_{j=1}^{N} \mathrm{tr}_a \big[\mathbf{L}_{aN}(u) \cdots \mathbf{L}_{a,j+1}(u)\, \mathbf{e}_a^{0,\ell_2-1} \sigma_j^- \\ \mathbf{L}_{a,j-1}(u) \cdots \mathbf{L}_{a1}(u)\, \mathbf{E}_a(\phi) \big],\end{aligned} \tag{6.155}$$

where we write $\mathbf{e}_a^{n,n'} = |n\rangle\langle n'|_a$ acting on V_a.

The construction of the FM-string creation operator (6.154) is similar to that of the generating function of the quasilocal Y charges proposed in Ref. [133], except that the transfer matrices are evaluated at different values of s. Therefore $\mathbf{B}^{\mathrm{FM}}(u)$, like those Y charges, commutes with $\mathbf{T}_s(u)$ with $2s \in \mathbb{Z}_{>0}$ but not with $\tilde{\mathbf{T}}_{s'}(u)$ when $2s' \in \mathbb{C} \setminus \mathbb{Z}_{>0}$.

Example. We verify our conjecture in many examples. To illustrate this consider $N = 6$, $\Delta = -\frac{1}{2}$ ($\eta = \frac{2\mathrm{i}\pi}{3}$) and $\phi = 0$. The descendant tower of the pseudovacuum $|\{\varnothing\}\rangle = |\uparrow\uparrow\uparrow\uparrow\uparrow\uparrow\rangle$ contains three descendants:

$$|\{\alpha_1^{\mathrm{FM}}\}\rangle\,, \quad |\{\alpha_2^{\mathrm{FM}}\}\rangle\,, \quad |\{\alpha_1^{\mathrm{FM}}, \alpha_2^{\mathrm{FM}}\}\rangle = |\downarrow\downarrow\downarrow\downarrow\downarrow\downarrow\rangle, \tag{6.156}$$

with FM strings centred at

$$\alpha_1^{\mathrm{FM}} = -\frac{\log(10+3\sqrt{11})}{6}, \quad \alpha_2^{\mathrm{FM}} = +\frac{\log(10+3\sqrt{11})}{6}. \tag{6.157}$$

We verify that (6.154) does indeed create these FM strings:

$$|\{\alpha_n^{\mathrm{FM}}\}\rangle \propto \mathbf{B}^{\mathrm{FM}}(\alpha_n^{\mathrm{FM}})\, |\{\varnothing\}\rangle\,, \quad n = 1, 2, \tag{6.158}$$

and the consistency condition

$$|\{\alpha_1^{\mathrm{FM}}, \alpha_2^{\mathrm{FM}}\}\rangle \propto \mathbf{B}^{\mathrm{FM}}(\alpha_1^{\mathrm{FM}})\, |\{\alpha_2^{\mathrm{FM}}\}\rangle = \mathbf{B}^{\mathrm{FM}}(\alpha_2^{\mathrm{FM}})\, |\{\alpha_1^{\mathrm{FM}}\}\rangle \tag{6.159}$$

holds, even though the $\mathbf{B}^{\mathrm{FM}}$ do not commute with each other in general. More generally, whenever two FM strings with centres $\alpha_n^{\mathrm{FM}}, \alpha_{n'}^{\mathrm{FM}}$ occur among the descendants of some primitive state $|\{u_m\}_m\rangle$ we find that

$$\begin{aligned}\mathbf{B}^{\mathrm{FM}}(\alpha_n^{\mathrm{FM}})\, |\{u_m\}_m \cup \{\alpha_{n'}^{\mathrm{FM}}\}\rangle &= \mathbf{B}^{\mathrm{FM}}(\alpha_{n'}^{\mathrm{FM}})\, |\{u_m\}_m \cup \{\alpha_n^{\mathrm{FM}}\}\rangle \\ &\propto |\{u_m\}_m \cup \{\alpha_n^{\mathrm{FM}}, \alpha_{n'}^{\mathrm{FM}}\}\rangle\,.\end{aligned} \tag{6.160}$$

The creation operator (6.154) can be used to construct the whole descendant tower described in Section 6.7.1.

The annihilation operator can be obtained in the same fashion. We denote the parameter of the cyclic representation by γ. If we repeat the same construction with the transposed Lax matrix $\mathbf{L}_{aj}(\mathbf{v}_y, \mathbf{u}_x)$ from (6.30), this time replacing the entry $\hat{\mathbf{S}}_a^- := \mathbf{L}_a^{12}(\mathbf{v}_y, \mathbf{u}_x)/\sinh\eta$ by

$$\hat{\mathbf{S}}_a^{-,\mathrm{sc}} = \hat{\mathbf{S}}_a^- + \gamma\,|\ell_2 - 1\rangle\langle 0|_a, \tag{6.161}$$

we obtain a semi-cyclic transfer matrix

$$\hat{\mathbf{T}}_s^{\mathrm{sc}}(u,\phi,\gamma) = \mathrm{tr}_a\big[\hat{\mathbf{L}}_{aN}^{\mathrm{sc}}(u,\gamma)\cdots\hat{\mathbf{L}}_{a1}^{\mathrm{sc}}(u,\gamma)\,\mathbf{E}_a(\phi)\big] \tag{6.162}$$

that changes the magnetisation by positive multiples of ℓ_2. Similarly, we have

Conjecture 2. When $\varepsilon = q^{\ell_2} = +1$ the linearisation in γ at $s = (\ell_2 - 1)/2$,

$$\begin{aligned}\mathbf{C}^{\mathrm{FM}}(u) &:= \partial_\gamma\,\hat{\mathbf{T}}_s^{\mathrm{sc}}(u,\phi,\gamma)\big|_{\gamma=0,\,2s=\ell_2-1}\\ &= \sum_{j=1}^{N}\mathrm{tr}_a\big[\mathbf{L}_{aN}(u)\cdots\mathbf{L}_{a,j+1}(u)\;\mathbf{e}_a^{\ell_2-1,0}\sigma_j^+\\ &\qquad\qquad \mathbf{L}_{a,j-1}(u)\cdots\mathbf{L}_{a1}(u)\,\mathbf{E}_a(\phi)\big],\end{aligned} \tag{6.163}$$

annihilates the FM string with Bethe roots $\{u, u+\frac{\mathrm{i}\pi}{\ell_2},\cdots,u+\mathrm{i}\pi\frac{\ell_1-1}{\ell_2}\}$.

We checked the constructions in many examples, e.g. the one above. We find that the consistency condition

$$\begin{aligned}&\mathbf{C}^{\mathrm{FM}}(\alpha_n^{\mathrm{FM}})\,\mathbf{B}^{\mathrm{FM}}(\alpha_{n'})\;|\{u_m\}_m\cup\{\alpha_n^{\mathrm{FM}}\}\rangle = |\{u_m\}_m\cup\{\alpha_{n'}^{\mathrm{FM}}\}\rangle\\ &= \mathbf{B}^{\mathrm{FM}}(\alpha_{n'})\,\mathbf{C}^{\mathrm{FM}}(\alpha_n^{\mathrm{FM}})\;|\{u_m\}_m\cup\{\alpha_n^{\mathrm{FM}}\}\rangle\end{aligned} \tag{6.164}$$

holds so long as $|\{u_m\}_m\cup\{\alpha_n^{\mathrm{FM}}\}\rangle$ and $|\{u_m\}_m\cup\{\alpha_{n'}^{\mathrm{FM}}\}\rangle$ are eigenstates of the Q operator, even though we do not know the commutation relations between $\mathbf{B}^{\mathrm{FM}}(u)$ and $\mathbf{C}^{\mathrm{FM}}(v)$ in general. We postpone these relations to future work.

6.8.2 Case $q^{\ell_2} = -1$

When $\varepsilon = q^{\ell_2} = -1$ the RLL relation (6.152) has to be modified and it becomes

$$\begin{aligned}&\mathbf{R}^{\mathrm{sc}}_{ab}(u-v,\beta)\,\mathbf{L}^{\mathrm{sc}}_{aj}(u,-\beta)\,\mathbf{L}_{bj}(v)\\&=\mathbf{L}_{bj}(v)\,\mathbf{L}^{\mathrm{sc}}_{aj}(u,\beta)\,\mathbf{R}^{\mathrm{sc}}_{aj}(u-v,-\beta).\end{aligned}\tag{6.165}$$

This RLL relation can be shown by direct calculation on $V_b \otimes V_j$. The resulting monodromy matrix is 'staggered', with alternating sign of β, similar to the inhomogeneities added to the Lax operator. For general $\varepsilon = q^{\ell_2} = \pm 1$ the semi-cyclic monodromy matrix can thus be defined as

$$\begin{aligned}\mathbf{M}^{\mathrm{sc}}_{a}(u,s,\phi,\beta) :=&\mathbf{L}^{\mathrm{sc}}_{aN}(u,s,\varepsilon^N\beta)\cdots\mathbf{L}^{\mathrm{sc}}_{aj}(u,s,\varepsilon^j\beta)\\&\cdots\mathbf{L}^{\mathrm{sc}}_{a1}(u,s,\varepsilon\beta)\,\mathbf{E}_a(\phi).\end{aligned}\tag{6.166}$$

When $\varepsilon = +1$ all βs have the same sign, reproducing the result in (6.152), while for $\varepsilon = -1$ the sign alternates. Taking the trace we obtain the general expression for the semi-cyclic transfer matrix

$$\begin{aligned}\mathbf{T}^{\mathrm{sc}}_{s}(u,\phi,\beta) = \mathrm{tr}_a\big[&\mathbf{L}^{\mathrm{sc}}_{aN}(u,s,\varepsilon^N\beta)\cdots\mathbf{L}^{\mathrm{sc}}_{aj}(u,s,\varepsilon^j\beta)\\&\cdots\mathbf{L}^{\mathrm{sc}}_{a1}(u,s,\varepsilon\beta)\,\mathbf{E}_a(\phi)\big].\end{aligned}\tag{6.167}$$

For $\varepsilon = +1$ this reduces to (6.167); in particular, the use of the same notation as in (6.167) should not cause any confusion.

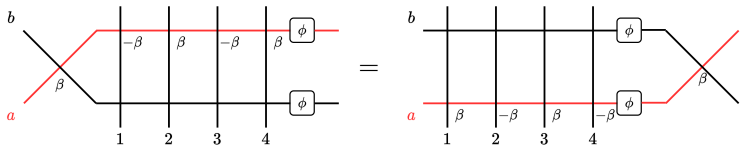

Figure 6.8: Graphical proof of Eq. (6.169) for an even number N of sites.

Recall that for $\varepsilon = -1$ the commensurate twist ϕ depends on the system size N through the condition $e^{\mathrm{i}\ell_2\phi} = (-1)^N$ from (6.84). Therefore on $V^{\mathrm{sc}}_a \otimes V_b$ we have

$$\mathbf{E}_a(\phi)\,\mathbf{E}_b(\phi)\,\mathbf{R}^{\mathrm{sc}}_{ab}(u,\beta) = \mathbf{R}^{\mathrm{sc}}_{ab}\big(u,(-1)^N\beta\big)\,\mathbf{E}_a(\phi)\,\mathbf{E}_b(\phi).\tag{6.168}$$

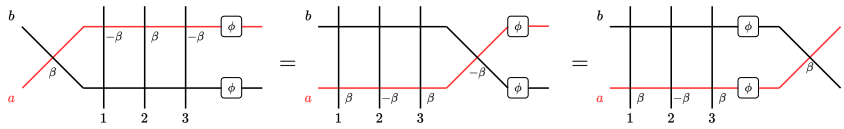

Figure 6.9: Graphical proof of Eq. (6.169) for an odd number N of sites.

Combining (6.165) and (6.168) the train argument, illustrated in Figs. 6.8 and 6.9, yields

$$\begin{aligned}&\mathbf{R}^{\mathrm{sc}}_{ab}(u-v,\beta)\,\mathbf{M}^{\mathrm{sc}}_{a}(u,s,\beta,\phi)\,\mathbf{M}_{b}(v,\phi)\\&=\mathbf{M}_{b}(v,\phi)\,\mathbf{M}^{\mathrm{sc}}_{a}(u,s,-\beta,\phi)\,\mathbf{R}^{\mathrm{sc}}_{ab}(u-v,\beta).\end{aligned}\tag{6.169}$$

Multiplying by $\mathbf{R}^{\mathrm{sc}}_{ab}(u-v,\beta)^{-1}=\mathbf{R}^{\mathrm{sc}}_{ab}(v-u+\eta,-\beta)/\sinh^2(u-v+\eta)$, provided it exists, and taking the trace over the ℓ_2-dimensional auxiliary space we see that the semi-cyclic transfer matrix (6.167) commutes with the fundamental transfer matrix in the sense that

$$\mathbf{T}^{\mathrm{sc}}_{s}(u,\beta,\phi)\,\mathbf{T}_{1/2}(v,\phi)=\mathbf{T}_{1/2}(v,\phi)\,\mathbf{T}^{\mathrm{sc}}_{s}(u,-\beta,\phi),\quad u,v,s\in\mathbb{C}.\tag{6.170}$$

With the aid of the fusion relation we obtain the commutation relations

$$\begin{aligned}&\mathbf{T}^{\mathrm{sc}}_{s}(u,\beta,\phi)\,\mathbf{T}_{s'}(v,\phi)=\mathbf{T}_{s'}(v,\phi)\,\mathbf{T}^{\mathrm{sc}}_{s}\big(u,(-1)^{2s'}\beta,\phi\big),\\&u,v,s\in\mathbb{C},\quad 2s'\in\mathbb{Z}_{>0}.\end{aligned}\tag{6.171}$$

In particular, the semi-cyclic transfer matrix commutes with $\mathbf{T}_{s'}$ for integer s'.

Therefore, we have

Conjecture 3. For any $\varepsilon=q^{\ell_2}=\pm1$ the linearisation in β of (6.167) at $s=(\ell_2-1)/2$,

$$\begin{aligned}\mathbf{B}^{\mathrm{FM}}(u)&\coloneqq\partial_\beta\mathbf{T}^{\mathrm{sc}}_{s}(u,\phi,\beta)\big|_{\beta=0,\,2s=\ell_2-1}\\&=\sum_{j=1}^{N}\varepsilon^j\mathrm{tr}_a\big[\mathbf{L}_{aN}(u)\cdots\mathbf{L}_{a,j+1}(u)\;\mathbf{e}_a^{0,\ell_2-1}\sigma_j^-\\&\qquad\mathbf{L}_{a,j-1}(u)\cdots\mathbf{L}_{a1}(u)\,\mathbf{E}_a(\phi)\big],\end{aligned}\tag{6.172}$$

creates an FM string with Bethe roots $\{u',u'+\frac{\mathrm{i}\pi}{\ell_2},\cdots,u'+\mathrm{i}\pi\frac{\ell_2-1}{\ell_2}\}$. The spectral parameter in (6.172) is related to the FM string by $u=u'$ if $\varepsilon=+1$ and $u=u'-\frac{\mathrm{i}\pi}{2\ell_2}$ when $\varepsilon=-1$.

This conjecture has been successfully tested on all examples in Section 6.7, as well as for various cases when ℓ_2 is even.

We demonstrate another property with $\varepsilon = -1$. Taking the derivative of (6.171) with respect to the parameter β we obtain the (anti)commutation relations

$$\begin{aligned} \big\{\mathbf{B}^{\text{FM}}(u), \mathbf{T}_{s'}(v)\big\} &= 0, \quad 2s'+1 \in \mathbf{Z}_{>0}, \\ \big[\mathbf{B}^{\text{FM}}(u), \mathbf{T}_{s'}(v)\big] &= 0, \quad s' \in \mathbf{Z}_{>0}. \end{aligned} \tag{6.173}$$

The *anti*commutation of $\mathbf{B}^{\text{FM}}(u)$ with $\mathbf{T}_{1/2}(v)$ for $\varepsilon = -1$ might seem surprising at the first sight, but it can be elucidated as follows. When $\varepsilon = -1$, each FM string adds π momentum to the state without affecting the energy or other higher order charges. This means that $\mathbf{B}^{\text{FM}}(u)$ anticommutes with the translation operator, and commutes with all higher conserved charges, which are logarithmic derivatives of $\mathbf{T}_{1/2}$. This yields the anticommutation.

The annihilation operator for FM strings can be defined like in (6.163). We generalise the semi-cyclic transfer matrix (6.162) to arbitrary $\varepsilon \in \{+1, -1\}$ by modifying into $\varepsilon^j \gamma$ like in (6.167). We propose

Conjecture 4. When $\varepsilon = q^{\ell_2} = \pm 1$ the operator

$$\begin{aligned} \mathbf{C}^{\text{FM}}(u) &:= \partial_\gamma \, \hat{\mathbf{T}}^{\text{sc}}_s(u, \phi, \gamma)\big|_{\gamma=0,\, 2s=\ell_2-1} \\ &= \sum_{j=1}^{N} \varepsilon^j \operatorname{tr}_a \big[\mathbf{L}_{aN}(u) \cdots \mathbf{L}_{a,j+1}(u)\, \mathbf{e}_a^{\ell_2-1,0} \sigma_j^+ \\ &\qquad \mathbf{L}_{a,j-1} \cdots \mathbf{L}_{a1}(u)\, \mathbf{E}_a(\phi)\big] \end{aligned} \tag{6.174}$$

annihilates an FM string with Bethe roots $\{u', u' + \frac{\mathrm{i}\pi}{\ell_2}, \cdots, u' + \mathrm{i}\pi\frac{\ell_2-1}{\ell_2}\}$. The spectral parameter is again related to the FM string by $u = u'$ if $\varepsilon = 1$ and $u = u' - \frac{\mathrm{i}\pi}{2\ell_2}$ for $\varepsilon = -1$.

6.9 Thermodynamic limit

6.9.1 FM strings and Z charges

In Section 6.6.2 we have seen that all states within a descendant tower have the same eigenvalues (up to a possible minus sign) for $\mathbf{T}_s$. This

may lead one to wonder if those states can be distinguished at all using charges that are (quasi)local in the thermodynamic limit. The answer to this question is positive: the (exponentially many) degeneracies can be lifted by taking into account the quasilocal *Z charges* [110, 52, 111, 53] that can be constructed at root of unity as logarithmic derivatives of the truncated transfer matrix $\tilde{\mathbf{T}}_s$ from Section 6.5. The quasilocality of the Z charges in the thermodynamic limit was demonstrated in Refs. [110, 52, 111, 53]. The Z charges were used to study out-of-equilibrium phenomena such as quantum quenches in Ref. [119]. Here we focus on their role in distinguishing states that are degenerate for $\mathbf{T}_s$.

In Section 6.5 we already studied the key ingredient for the construction of the Z charges, viz. the truncated two-parameter transfer matrix $\tilde{\mathbb{T}}(x, y, \phi) = \tilde{\mathbf{T}}_s(u, \phi)$ at root of unity. Similar to Ref. [119] we define the generating function of the Z charges as

$$\begin{aligned}\mathbf{Z}(u,\phi) &\coloneqq \frac{1}{2\eta}\,\partial_s \log \tilde{\mathbf{T}}_s(u,\phi)\big|_{s=(\ell_2-1)/2} \\ &= \frac{1}{2\eta}\,\tilde{\mathbf{T}}^{-1}_{(\ell_2-1)/2}(u,\phi)\,\partial_s \tilde{\mathbf{T}}_s(u,\phi)\big|_{2s=\ell_2-1}.\end{aligned} \tag{6.175}$$

Like in (6.18) the quasilocal Z charges are the coefficients of the expansion around $u = \frac{\eta}{2}$,

$$\mathbf{Z}^{(j)} \coloneqq -\mathrm{i}\,\frac{\mathrm{d}^{j-1}}{\mathrm{d}u^{j-1}}\,\mathbf{Z}(u,\phi)\Big|_{u=\eta/2}. \tag{6.176}$$

The Z charges are able to distinguish each member of the descendant tower. Let us illustrate this for the example $N = 6$, $\Delta = \frac{1}{2}$ ($\eta = \frac{\mathrm{i}\pi}{3}$) and $\phi = 0$ from Section 6.1.2. Consider the descendant tower formed by

$$|\{\varnothing\}\rangle = |\uparrow\uparrow\uparrow\uparrow\uparrow\uparrow\rangle\,, \quad |\{\alpha_1^{\mathrm{FM}}\}\rangle\,, \quad |\{\alpha_2^{\mathrm{FM}}\}\rangle\,, \quad |\{\alpha_1^{\mathrm{FM}}, \alpha_2^{\mathrm{FM}}\}\rangle \propto |\downarrow\downarrow\downarrow\downarrow\downarrow\downarrow\rangle\,, \tag{6.177}$$

where the string centres for the two FM strings are

$$\alpha_1^{\mathrm{FM}} = -\frac{\log(10+3\sqrt{11})}{6} + \frac{\mathrm{i}\pi}{6}, \quad \alpha_2^{\mathrm{FM}} = \frac{\log(10+3\sqrt{11})}{6} + \frac{\mathrm{i}\pi}{6}. \tag{6.178}$$

The generating function (6.175) acts on the descendant tower as

$$\begin{aligned}
\mathbf{Z}(u,0)\,|\{\varnothing\}\rangle &= \frac{18\cosh(6u)}{10-\cosh(6u)}\,|\{\varnothing\}\rangle,\\
\mathbf{Z}(u,0)\,|\{\alpha_1^{\mathrm{FM}}\}\rangle &= \frac{9\sqrt{11}}{10-\cosh(6u)}\,|\{\alpha_1^{\mathrm{FM}}\}\rangle,\\
\mathbf{Z}(u,0)\,|\{\alpha_2^{\mathrm{FM}}\}\rangle &= -\frac{9\sqrt{11}}{10-\cosh(6u)}\,|\{\alpha_2^{\mathrm{FM}}\}\rangle,\\
\mathbf{Z}(u,0)\,|\{\alpha_1^{\mathrm{FM}},\alpha_2^{\mathrm{FM}}\}\rangle &= -\frac{18\cosh(6u)}{10-\cosh(6u)}\,|\{\alpha_1^{\mathrm{FM}},\alpha_2^{\mathrm{FM}}\}\rangle.
\end{aligned} \tag{6.179}$$

The eigenvalues of $\mathbf{Z}(u)$ are different for each eigenstate.

Now consider the thermodynamic limit $N\to\infty$. There is a subtlety in the presence of FM strings. For instance, when $\phi=0$ and $\eta=\mathrm{i}\pi\ell_1/\ell_2$ with ℓ_1 odd, (6.84) implies that for odd N there are no FM strings in the spectrum, while for even N there are (exponentially many) states associated with FM strings. The spectrum of systems at finite size is therefore sensitive to the parity of N, and it is not a priori clear whether the thermodynamic limit is well defined. However, numerics suggests that at odd N there are states in the spectrum that differ by terms that vanish as $N\to\infty$ to give rise to the same asymptotic degeneracies as obtained when taking the limit via even N. Thus the result in the thermodynamic limit should be independent of the way in which the limit $N\to\infty$ is taken.

The role of the Z charges in separating the degeneracies in the presence of FM strings has important implications for the thermodynamic limit. In practice, Z charges have to be taken into account when constructing the generalised Gibbs ensemble (GGE) for the non-equilibrium steady state after a quantum quench with XXZ model at root of unity[119].

6.9.2 TBA, string-charge duality, and a conjecture for string centres of FM strings

One of the cornerstones in the study of the thermodynamic properties of quantum integrable models is the thermodynamic Bethe ansatz (TBA) [71, 72, 134], which has been used extensively to study out-of-equilibrium

problems such as transport, quantum quenches and generalised hydrodynamics.

In order to solve the TBA equations for the XXZ spin chain at root of unity one relies on the *string hypothesis* [72], which stipulates the types of bound states that the model permits. This is a powerful tool that has produced numerous results for thermodynamic properties of the XXZ model. In the following we will use the notation of Ref. [135].

As shown in [135], the root densities of the Bethe strings (bound states) are in one-to-one correspondence with the generating functions of (quasi)local charges (6.18) of the model. This *string-charge duality* is very convenient for the study of expectation values of (quasi)local charges, especially for quantum quenches [34]. For example, we can obtain the root densities for the non-equilibrium steady states using string-charge duality [135, 136]. However, at root of unity there seems to be an ambiguity when determining the root density of the 'last two string types' in the list of Takahashi [72, 134]. This ambiguity was elucidated in [119] by relating the root densities of the last two string types to the generating function of Z charges (6.175). Together with the generating functions $\partial_u \log \mathbf{T}_s(u)$ one can obtain the long-time steady state with microcanonical GGE described by root densities of allowed Bethe strings for a quantum quench with any initial state [136].

The existence of FM strings at root of unity is closely related to the truncated two-parameter transfer matrix $\tilde{\mathbb{T}}(x, y, \phi)$ and the Z charges that it generates. The string-charge duality implies that the eigenvalues of the generating function of the Z charges have a functional relation to the root densities of the last two string types [135, 119]. This suggests that at root of unity the last two string types might be directly linked to the FM strings. In fact, two Bethe strings, one of each of the last two string types, that have coinciding real parts of their string centres [4] together form an FM string. For example, consider $\Delta = \frac{1}{2}$ ($\eta = \frac{\mathrm{i}\pi}{3}$), for which the string hypothesis says that the last two string types are $(2, +)$ and $(1, -)$. Call a bound state with n magnons whose Bethe roots have the same real part an 'n-string'. Then '$(2, +)$' denotes a 2-string with even parity (centred at the real axis, i.e. a complex conjugate pair), and '$(1, -)$' a 1-string

[4] Of course we need to take into account the 'Brillouin zone': $u_m + \mathrm{i}\pi \equiv u_m$, cf. Footnote 3 on p. 118.

with odd parity (centred at $\operatorname{Im} u_m = \mathrm{i}\pi/2$). For $\eta = \frac{\mathrm{i}\pi}{3}$ the imaginary parts of the 2-string with even parity are $\pm\frac{\mathrm{i}\pi}{6}$ while the imaginary part of the 1-string with odd parity is $\mathrm{i}\frac{\pi}{2}$. On the other hand, according to the examples in Section 6.7, FM strings for $\eta = \mathrm{i}\pi/3$ can be expressed as

$$u_1 = \xi - \frac{\mathrm{i}\pi}{6}, \quad u_2 = \xi + \frac{\mathrm{i}\pi}{6}, \quad u_3 = \xi + \frac{\mathrm{i}\pi}{2}, \quad \xi \in \mathbb{R}. \tag{6.180}$$

But this can be viewed as strings of types $(2,+)$ and $(1,-)$ with the same real part of the string centre.

We expect that for any system size with commensurate twist FM strings can be decomposed in terms of the last two string types of the string hypothesis in this way, even at finite system size. Indeed, for any principal root of unity $\eta = \mathrm{i}\frac{\pi}{\ell_2}$ with $\ell_1 = 1$ the last two string types are $(\ell_2 - 1, +)$ and $(1,-)$. We have checked FM strings for all $\ell_2 \leq 6$ and found that they can all be viewed of strings of the last two string types with equal real parts of the string centres. In addition we have verified it for various examples with non-principal root of unity, including $\eta = \frac{2\mathrm{i}\pi}{3}$, for which the last two string types are $(2,+)$ and $(1,+)$, and $\eta = \frac{2\mathrm{i}\pi}{5}$, where they are $(3,+)$ and $(2,+)$.

Combining with numerical evidence in [4], we have

Conjecture 5. For any finite system size N and root of unity $\eta = \mathrm{i}\pi\frac{\ell_1}{\ell_2}$ with commensurate twist, any Fabricius–McCoy string

$$\alpha_k = \alpha^{\mathrm{FM}} + \frac{\mathrm{i}\pi}{\ell_2}\left(\frac{\ell_2+1}{2} - k\right), \quad 1 \leq k \leq \ell_2, \tag{6.181}$$

has string centre imaginary part

$$\operatorname{Im}\alpha^{\mathrm{FM}} = \begin{cases} \mathrm{i}\frac{\pi}{2\ell_2} & \text{if } \ell_1 \text{ is odd,} \\ 0 & \text{if } \ell_1 \text{ is even,} \end{cases} \tag{6.182}$$

This conjecture has been confirmed for all examples in Section 6.7. If this conjecture is correct then the generating function of the Z charge (6.175) is *dual* to the root density of FM strings in the sense of the string-charge duality.

Meanwhile, we remark that the descendant states that we define in this thesis (at root of unity) contain FM strings and they do contribute

in TBA. Their root densities of last two types of strings in the thermodynamic limit are fixed with Z charges. They are completely different from the $\mathfrak{sl}_2$ descendant states in XXX model, which do not contribute to TBA directly, after fixing the total spin of the state.

6.9.3 FM strings and spin Drude weight

One of the most important physical consequences of the quasilocal Z charges is the non-vanishing high-temperature spin Drude weight of the XXZ model at root of unity, due to the non-commutativity between the spin flip operator $\prod_j \sigma_j^x$ and the Z charges [110, 52, 111]. It can be considered as a manifestation of the exponentially many degeneracies in the thermodynamic limit.

In [4] it is shown that perturbing the anisotropy parameter η away from root of unity can change the structure of the Bethe roots dramatically. Meanwhile, the spin Drude weight [110] also changes significantly under such perturbations. This hints at a connection between the existence of FM strings at root of unity and the fractal structure of the spin Drude weight.

Another example is the domain-wall quench, i.e. the time evolution of an initial state $|\uparrow\cdots\uparrow\uparrow\downarrow\downarrow\cdots\downarrow\rangle$, for the XXZ model at root of unity. Here ballistic spin transport (non-vanishing spin Drude weight) can be treated analytically using generalised hydrodynamics [67]. The right half of the system, i.e. the fully polarised state $|\downarrow\downarrow\cdots\downarrow\rangle$, has Q function given in Section 6.6.5 for finite size. In the thermodynamic limit, according to the TBA, this fully polarised state consists of a filled 'Fermi sea' with Bethe roots of the last two string types [134, 67], cf. Section 6.9.2, combining into FM strings. For the domain-wall quench the ballistic spin transport from the right half of the system is solely carried out by the quasilocal Z charges [67]. Notice that, even though the FM strings do not directly contribute to the dynamics, the 'FM strings' of the right half of the system are not true excitations from the perspective of the whole system. Thus they *do* contribute to the dynamics, as combinations of Bethe strings of the last two string types, resulting in the domain-wall melting phenomenon.

6.10 Summary of results

In this chapter, we have studied the full spectrum of the transfer matrices associated to the quantum spin-1/2 XXZ model, focussing on root of unity with arbitrary twist. First, we constructed the Baxter's Q operator from the factorisation of a two-parameter transfer matrix (6.47). The eigenvalues of the Q operator, i.e. Q functions, are polynomials whose zeroes encode the physical solutions of the Bethe equations (3.25). As a by-product, we rederived the matrix TQ relation (6.60) and transfer-matrix fusion relations (6.62) from a decomposition of the two-parameter transfer matrix, providing a simplification of the conventional approach. At root of unity we derived truncated transfer-matrix fusion and Wronskian relations from the two-parameter transfer matrix with auxiliary space truncated to a finite-dimensional space. We also proved an interpolation-type formula previously conjectured in Refs. [117, 118, 119].

Using the method developed for XXZ model at root of unity, we analysed the full spectrum at root of unity, obtaining analytic results on the properties of primitive states and their descendant towers. We elucidated the exponentially many degeneracies in the spectrum at root of unity in terms of states with FM strings, and provided numerous examples of different descendant tower structures. We found new semicyclic transfer matrices that satisfy unconventional RLL relations (6.169), from which we conjectured an explicit expression for the creation and annihilation operators of FM strings (Section 6.8).

Eventually, we compared our results with recent works on the thermodynamic limit (Section 6.9). We explained the relation between the truncated two-parameter transfer matrices and the quasilocal Z charges, which are directly related to out-of-equilibrium phenomena such as quantum quenches and spin transport at root of unity.

The spectra at different roots of unity are similar to each other, where at the free fermion point ($\Delta = 0$, $\eta = \mathrm{i}\pi/2$) it is known to possess Onsager algebra symmetry. This leads to the results in Chapter 7.

Chapter 7

Hidden Onsager algebra symmetries in XXZ model

The contents of this chapter were published in [5].

The Onsager algebra was used for the first time to solve two-dimensional Ising model with zero magnetic field by Lars Onsager in his seminal paper in 1944 [137], which is considered to be the herald of exactly solvable models in statistical mechanics.

Later the Onsager algebra has been used to study two-dimensional chiral Potts model, a generalisation of Ising model and its quantum counterpart, the $\mathbb{Z}_N$-symmetric spin chain [138, 139, 140, 141, 142]. Those models studied via the Onsager algebra are integrable and possess Kramers–Wannier duality [143]. Later, Dolan and Grady used the self-duality of these models to construct infinitely many conserved charges without using integrability [144], and the equivalence to the Onsager algebra has been discovered by Perk [145]. This approach has led to a deeper understanding of the algebraic structure of the Onsager algebra and its relation to self-duality and integrability [146, 147, 148, 149]. A thorough and comprehensive summary of the mathematical structures of the Onsager algebra is provided in [150]. Recently, the Onsager algebra has been used to study the spectra of quantum lattice models [127], the out-of-equilibrium dynamics of quantum states [151], and the construction of quantum many-body scars [152], eigenstates of non-integrable models that fall out of the paradigm of Eigenstate Thermalisation Hypothesis.

Following the results of Chapter 6, the spectra of quantum XXZ model at root of unity are of particular interest, and the models coincide with the ones in [127] despite being investigated with different techniques. In particular, XX model with Hamltonian in the form of (7.21) possesses the Onsager algebra symmetry [127], cf. Sec. 7.2.1. Moreover, from Chapter 6 we observe that the underlying quantum group structure at root of unity results in huge degeneracies (of transfer matrices $\mathbf{T}_s(u)$ as well as the Hamiltonian) in the spectrum of quantum many-body systems. In the meantime, we can identify similar degeneracies of spectrum for eigenstates of free fermionic Hamiltonian. For instance, taking the limit $\Delta \to 0$ for XXZ Hamiltonian (3.11), we obtain the XX model, which can be mapped into a free fermionic model with aid of Jordan-Wigner transformation. In that case, $q = \exp(\mathrm{i}\pi/2)$, i.e. at root of unity. We can construct the Onsager algebra symmetry for XX model explicitly, cf. Sec. 7.2.1, which motivates us to consider the possibility of the existence of similar Onsager algebra symmetries for XXZ model at arbitrary roots of unity [5]. The difficulty of finding the hidden Onsager algebra symmetries at other roots of unity is that the Onsager generators in XX model are expressed in terms of local operators, while the generators at other roots of unity are not if they were to exist, which are discussed in Sec. 7.3. We make use of the analogue between XX model and XXZ models at other roots of unity, and formulate a series of conjectures on the existence of the hidden Onsager algebra symmetries in XXZ model at arbitrary root of unity.

7.1 Onsager algebra in a nutshell

We use the notations in Onsager's original paper [137] to define the Onsager algebra. Consider the following infinite-dimensional Lie algebra with basis

$$\{\mathbf{A}_m, \mathbf{G}_n | m, n \in \mathbb{Z}\}. \tag{7.1}$$

The *canonical* generators are defined with the following properties,

$$\begin{aligned} &[\mathbf{A}_m, \mathbf{A}_n] = 4\mathbf{G}_{m-n}, \\ &[\mathbf{G}_m, \mathbf{A}_n] = 2\left(\mathbf{A}_{n+m} - \mathbf{A}_{n-m}\right), \quad [\mathbf{G}_m, \mathbf{G}_n] = 0. \end{aligned} \tag{7.2}$$

From the definition, we have

$$\mathbf{G}_{-m} = -\mathbf{G}_m, \quad \forall m \in \mathbb{Z}. \tag{7.3}$$

As shown and proven by Perk [145] and Davies [146], the Onsager algebra is equivalent to the *Dolan–Grady (DG) relation*, which imposes requirement only on two generators $\mathbf{A}_0$ and $\mathbf{A}_1$, i.e.

$$\Big[\mathbf{A}_0, \Big[\mathbf{A}_0, \big[\mathbf{A}_0, \mathbf{A}_1\big]\Big]\Big] = 16\big[\mathbf{A}_0, \mathbf{A}_1\big], \quad \Big[\mathbf{A}_1, \Big[\mathbf{A}_1, \big[\mathbf{A}_1, \mathbf{A}_0\big]\Big]\Big] = 16\big[\mathbf{A}_1, \mathbf{A}_0\big]. \tag{7.4}$$

We mainly use the DG relation in this chapter as the defining property for the Onsager algebra. Namely, once finding two operators that satisfy DG relation in certain physical systems, we can construct a family of operators fulfilling the canonical definition (7.2), which can be considered as a specific representation of the Onsager algebra. For example, one-dimensional transverse field Ising model can be expressed in the Onsager generators, cf. Sec.7.1.1.

Let us assume that

$$\mathbf{A}_0 = \sum_{j=1}^{N} \sigma_j^{\mathrm{z}}. \tag{7.5}$$

In this scenario, we rewrite the operators in three parts, i.e.

$$\mathbf{A}_m = \mathbf{A}_m^0 + \mathbf{A}_m^+ + \mathbf{A}_m^-, \tag{7.6}$$

where $\mathbf{A}_m^0$ commute with total magnetisation $\mathbf{A}_0^0 = \sum_{j=1}^{N} \sigma_j^z$, and $\mathbf{A}_m^\pm$ satisfy

$$\big[\mathbf{A}_0^0, \mathbf{A}_m^\pm\big] = \pm 4\mathbf{A}_m^\pm. \tag{7.7}$$

From relation (7.2), we obtain the following relations,

$$\mathbf{A}_{-m}^0 = \mathbf{A}_m^0, \quad \mathbf{A}_{-m}^\pm = -\mathbf{A}_m^\pm, \tag{7.8}$$

$$[\mathbf{A}_m^r, \mathbf{A}_n^r] = 0, \ r \in \{0, +, -\}; \quad \big[\mathbf{A}_m^-, \mathbf{A}_n^+\big] = \mathbf{A}_{n+m}^0 - \mathbf{A}_{n-m}^0, \tag{7.9}$$

$$\big[\mathbf{A}_m^-, \mathbf{A}_n^0\big] = 2\left(\mathbf{A}_{n+m}^- - \mathbf{A}_{n-m}^-\right), \quad \big[\mathbf{A}_m^+, \mathbf{A}_n^0\big] = 2\left(\mathbf{A}_{n-m}^+ - \mathbf{A}_{n+m}^+\right). \tag{7.10}$$

Using these recursive relations, we can generate all higher order generators from knowing just the $\mathbf{A}_1$.

Self-duality DG relation (7.4) also implies the Kramers–Wannier self-duality [143], which has been used to obtain the value of the phase transition point of models possessing the Onsager algebra. Suppose that the operators $\mathbf{A}_0$ and $\mathbf{A}_1$ can be expressed in terms of local terms, i.e.

$$\mathbf{A}_0 = \sum_{j=1}^{N} \mathbf{a}_{0,j}, \quad \mathbf{A}_1 = \sum_{j=1}^{N} \mathbf{a}_{1,j}. \tag{7.11}$$

Kramers–Wannier self-duality implies that the mapping $\mathbf{a}_{0,j} \to \mathbf{a}_{1,j}$ (and conversely $\mathbf{a}_{1,j} \to \mathbf{a}_{0,j}$) leaves the algebraic structure intact, which is obvious from DG relation (7.4). Let us consider a Hamiltonian $\mathbf{H}$ that can be expressed in terms of $\mathbf{A}_0$ and $\mathbf{A}_1$,

$$\mathbf{H} = \mathbf{A}_0 + \lambda \mathbf{A}_1, \quad \lambda \in \mathbb{R}, \tag{7.12}$$

such as 1-dimensional transverse field Ising model and chiral Potts model, cf. Sec. 7.1.1. Using Kramers–Wannier self-duality, one could detect a phase transition at $\lambda = 1$ without solving the entire system [143].

7.1.1 Example: transverse field Ising model

We give an explicit example of one-dimensional transverse field Ising model, which can be solved via the Onsager algebra approach. A quantum phase transition is present due to the Kramers–Wannier self-duality.

The Hamiltonian of one-dimensional transverse field Ising model in terms of Pauli matrices are

$$\mathbf{H}_{\text{Ising}} = \sum_{j=1}^{N} \left(\sigma_j^x \sigma_{j+1}^x + \lambda \sigma_j^z \right). \tag{7.13}$$

For the sake of convenience, we consider periodic boundary condition and even number of sites $N \bmod 2 = 0$. The Hamiltonian can be mapped into a free fermionic one with aid of Jordan–Wigner transformation [1]. We instead use the Onsager algebra to solve the model, aiming at obtaining extensively many conserved charges.

[1] There is a subtlety with the boundary condition (Neveu–Schwarz or Ramond) after the Jordan–Wigner transformation. We will not use it in this thesis though.

First of all, we identify the Onsager generators, i.e.

$$\mathbf{A}_0 = \sum_{j=1}^{N} \sigma_j^z, \quad \mathbf{A}_1 = \sum_{j=1}^{N} \sigma_j^x \sigma_{j+1}^x, \tag{7.14}$$

satisfying DG relation (7.4). Therefore, the Hamiltonian in terms of the Onsager generators reads

$$\mathbf{H}_{\text{Ising}} = \mathbf{A}_0 + \lambda \mathbf{A}_1. \tag{7.15}$$

From the Onsager algebra (7.2), we obtain extensively many conserved charges that commute with the transverse field Ising Hamiltonian,

$$\mathcal{Q}_j = (\mathbf{A}_j + \mathbf{A}_{-j}) + \lambda(\mathbf{A}_{1+j} + \mathbf{A}_{1-j}), \quad j \in \mathbb{Z}. \tag{7.16}$$

It is easy to observe that $\mathcal{Q}_0 = 2\mathbf{H}_{\text{Ising}}$. Using the definition (7.2), we show that these conserved charges are in involution, i.e.

$$[\mathbf{Q}_j, \mathbf{Q}_k] = 0, \quad j, k \in \mathbb{Z}. \tag{7.17}$$

These conserved charges are expressed in terms of fermionic bilinears, which are linear combinations of conserved charges found in the solutions of the model in terms of free fermions.

A quantum phase transition happens at $\lambda = 1$ due to the Kramers–Wannier self-duality, as demonstrated in the previous section.

Transverse field Ising model does not possess the property of being $U(1)$-invariant, i.e.

$$[\mathbf{H}_{\text{Ising}}, \mathbf{A}_j] \neq 0, \quad j \in \mathbb{Z}, \tag{7.18}$$

when $\lambda \neq 0$. We will focus on the other example, spin-1/2 XX model, which is a $U(1)$-invariant Hamiltonian, mainly in the scope of the thesis.

7.2 $U(1)$-invariant Hamiltonian

In the remaining part of the chapter, we concentrate on a specific type of Hamiltonians that commutes with both $\mathbf{A}_0$ and $\mathbf{A}_1$, i.e.

$$[\mathbf{H}, \mathbf{A}_0] = [\mathbf{H}, \mathbf{A}_1] = 0. \tag{7.19}$$

These models are referred as $U(1)$-invariant [127], because both operators $\mathbf{A}_0$ and $\mathbf{A}_1$ are considered as $U(1)$ charges. However, $\mathbf{A}_0$ and $\mathbf{A}_1$ do not commute with each other, cf. (7.2).

From (7.2), it is easy to observe that $\mathbf{H}$ commutes with all generators in the Onsager algebra,

$$[\mathbf{H}, \mathbf{A}_m^r] = 0, \quad r \in \{0, +, -\}, \, m \in \mathbb{Z}. \tag{7.20}$$

Two examples of $U(1)$-invariant Hamiltonians are spin-1/2 XX model and spin-1 ZF model with anisotropy parameter $\eta = \frac{\mathrm{i}\pi}{3}$ or $\frac{2\mathrm{i}\pi}{3}$. These examples belong to the $U(1)$-invariant clock models defined in [127] and they are quantum integrable lattice models at root of unity. Now we examine the case of XX model in details.

7.2.1 Example: XX model

We illustrate the relation between the Onsager generators and semi-cyclic transfer matrix $\mathbf{T}_s^{\mathrm{sc}}(u, \beta, \phi)$ using the example of spin-1/2 XX model. Twist ϕ considered here is always commensurate, satisfying (6.84). When system size N is even, $\phi \in \{0, \pi\}$, and $\phi \in \{\pi/2, 3\pi/2\}$ with system size N being odd.

The XX Hamiltonian is written as

$$\mathbf{H}_{\mathrm{XX}} = \sum_{j=1}^{N} \frac{1}{2}\big(\sigma_j^+ \, \sigma_{j+1}^- + \sigma_j^- \, \sigma_{j+1}^+\big), \tag{7.21}$$

where the Onsager generators are

$$\mathbf{Q}_0^0 = \frac{1}{2}\sum_{j=1}^{N} \sigma_j^z, \quad \mathbf{Q}_0^{\pm} = 0, \quad \mathbf{Q}_0 = \mathbf{Q}_0^0 + \mathbf{Q}_0^+ + \mathbf{Q}_0^-, \tag{7.22}$$

$$\begin{aligned} &\mathbf{Q}_1^0 = \frac{\mathrm{i}}{2}\sum_{j=1}^{N} \left(\sigma_j^+\sigma_{j+1}^- - \sigma_j^-\sigma_{j+1}^+\right), \quad \mathbf{Q}_1^+ = -\frac{\mathrm{i}}{2}\sum_{j=1}^{N}(-1)^j\sigma_j^+\sigma_{j+1}^+, \\ &\mathbf{Q}_1^- = \frac{\mathrm{i}}{2}\sum_{j=1}^{N}(-1)^j\sigma_j^-\sigma_{j+1}^-, \quad \mathbf{Q}_1 = \mathbf{Q}_1^0 + \mathbf{Q}_1^+ + \mathbf{Q}_1^-. \end{aligned} \tag{7.23}$$

They satisfy DG relation (7.4) such that

$$\begin{aligned}\Big[\mathbf{Q}_0,\Big[\mathbf{Q}_0,\big[\mathbf{Q}_0,\mathbf{Q}_1\big]\Big]\Big]&=\ell_2^2\big[\mathbf{Q}_0,\mathbf{Q}_1\big],\\ \Big[\mathbf{Q}_1,\Big[\mathbf{Q}_1,\big[\mathbf{Q}_1,\mathbf{Q}_0\big]\Big]\Big]&=\ell_2^2\big[\mathbf{Q}_1,\mathbf{Q}_0\big],\end{aligned}\tag{7.24}$$

with $\ell_2=2$. It is easy to check that $\mathbf{H}_{\mathrm{XX}}$ is $U(1)$ invariant, i.e. commuting with all Onsager generators,

$$[\mathbf{H}_{\mathrm{XX}},\mathbf{Q}_m^r]=0,\quad r\in\{0,+,-\},\quad m\in\mathbb{Z}.\tag{7.25}$$

Rescaling the generators $\mathbf{Q}_m$, we obtain the canonical generators $\mathbf{A}_m$ in (7.2),

$$\mathbf{Q}_m^r=\frac{4}{\ell_2}\mathbf{A}_m^r,\quad m\in\mathbb{Z},\quad r\in\{0,+,-\}.\tag{7.26}$$

The Onsager generators in terms of local spin operators are given in Appendix G.

Since XX model is equivalent to XXZ model at root of unity $q=\exp(\mathrm{i}\pi/2)$, we can define generating functions for (quasi-)local Z and Y charges that are mentioned in Chapter 6,

$$\mathbf{Z}(u,\phi)=\frac{1}{2\eta}\,\partial_s\log\mathbf{T}_s^{\mathrm{sc}}(u,\beta,\phi)|_{s=(\ell_2-1)/2,\beta=0}\,,\tag{7.27}$$

and

$$\mathbf{Y}(u,\phi)=\frac{1}{2\sinh\eta}\,\partial_\beta\log\mathbf{T}_s^{\mathrm{sc}}(u,\beta,\phi)|_{s=(\ell_2-1)/2,\beta=0}\,,\tag{7.28}$$

where the prefactors are chosen for convenience when comparing to the Onsager generators. The definition of the generating function of Z charges coincides with (6.175). Note that we define the generating functions for Z and Y charges for arbitrary root of unity $q=\exp(\mathrm{i}\pi\ell_1/\ell_2)$.

We expand the generating functions at $u=u_0$ to obtain the (quasi-)local Z and Y charges, i.e.

$$\mathbf{Z}(u,\phi)=\sum_{n=0}^{\infty}(u-u_0)^n\,\mathbf{Z}_n,\quad \mathbf{Y}(u,\phi)=\sum_{n=0}^{\infty}(u-u_0)^n\,\mathbf{Y}_n,\tag{7.29}$$

where

$$\varepsilon = -1 \Rightarrow u_0 = \frac{\eta}{2}; \quad \varepsilon = +1 \Rightarrow u_0 = \frac{\eta - \mathrm{i}\pi}{2}. \tag{7.30}$$

The choice for the different values of u_0 with respect to different ε values is explained in Appendix H.

What is truly striking here is that the Onsager generators $\mathbf{Q}_0^r$ can be identified with the Z and Y charges $\mathbf{Z}_0$ and $\mathbf{Y}_0$, i.e.

$$\mathbf{Q}_1^0 = \mathbf{Z}_0, \quad \mathbf{Q}_1^- = \mathbf{Y}_0, \quad \mathbf{Q}_1^+ = \mathbf{Y}_0^\dagger. \tag{7.31}$$

Moreover, all operators $\mathbf{Q}_n^r$, $\mathbf{Z}_n$ and $\mathbf{Y}_n$ can be written in terms of bilinear fermion operators, reflecting the free fermion nature of XX model. One of the consequences is that there exists a closure condition for the Onsager generators in XX model, namely

$$\mathbf{Q}_{n+2N}^r = \mathbf{Q}_n^r, \quad \forall n \in \mathbb{Z}. \tag{7.32}$$

The discussion of the physical meaning of the closure condition is postponed to Sec. 7.3.1. One notices that there are infinitely many $\mathbf{Q}_n^r$, $\mathbf{Z}_n$ and $\mathbf{Y}_n$. In fact, there are the relations between all of them. All operators can be obtained recursively, and the first few read

$$\begin{aligned}
&\mathbf{Z}_1 = \frac{1}{1!}\left(\mathbf{Q}_2^0 - \mathbf{Q}_0^0\right), \quad \mathbf{Z}_2 = \frac{1}{2!}\left(2\mathbf{Q}_3^0 - \mathbf{Q}_1^0\right), \quad \mathbf{Z}_3 = \frac{1}{3!}\left(6\mathbf{Q}_4^0 - 8\mathbf{Q}_2^0 + 2\mathbf{Q}_0^0\right), \\
&\mathbf{Y}_1 = \frac{1}{1!}\left(\mathbf{Q}_2^- - \mathbf{Q}_0^-\right), \quad \mathbf{Y}_2 = \frac{1}{2!}\left(2\mathbf{Q}_3^- - \mathbf{Q}_1^-\right), \quad \mathbf{Y}_3 = \frac{1}{3!}\left(6\mathbf{Q}_4^- - 8\mathbf{Q}_2^- + 2\mathbf{Q}_0^-\right),
\end{aligned} \tag{7.33}$$

revealing a deep connection between the Onsager generators $\mathbf{Q}_n^r$ and charges $\mathbf{Z}_n$, $\mathbf{Y}_n$. Relations between higher order terms can be obtained similarly.

7.3 Conjectures on hidden Onsager algebra symmetries in spin-1/2 XXZ models at root of unity

Motivated by the exact correspondence between the Onsager generators $\mathbf{Q}_0^r$ and Z and Y charges in the XX case ($\eta = \mathrm{i}\pi/2$), cf. (7.31) and

(7.33), it is natural to generalise similar relations for the spin-1/2 XXZ model at arbitrary root of unity ($q = \exp(\mathrm{i}\pi\ell_1/\ell_2)$), despite the fact that the generators are no longer expressible in local densities but quasilocal ones [52, 111, 53, 133]. Another motivation to the following conjectures is that the structure of descendant towers and exact (Fabricius–McCoy) strings are of no difference between XX model and XXZ model at other root of unity. After numerically verifying the relations, we are able to compose the following conjectures for the existence of hidden Onsager algebra symmetry in spin-1/2 XXZ spin chain at arbitrary root of unity:

Conjecture I:
There exists a hidden Onsager algebra symmetry in spin-1/2 XXZ spin chain at root of unity with commensurate twist (6.84). Spin-1/2 XXZ models at root of unity with commensurate twist (6.84) are $U(1)$ invariant, i.e.

$$[\mathbf{H}(\phi), \mathbf{Q}^r_m] = 0, \quad r \in \{0, +, -\}, \quad m \in \mathbb{Z}. \tag{7.34}$$

The generators of the hidden Onsager algebra are

$$\mathbf{Q}^0_0 = \frac{1}{2}\sum_{j=1}^{N} \sigma^z, \quad \mathbf{Q}^{\pm}_0 = 0, \tag{7.35}$$

$$\begin{aligned}
\mathbf{Q}^0_1 = \mathbf{Z}_0 &= \frac{1}{2\eta}\partial_s \log \mathbf{T}^{\mathrm{sc}}_s(u,\beta,\phi)\Big|_{s=(\ell_2-1)/2,u=u_0,\beta=0}, \\
\mathbf{Q}^-_1 = \mathbf{Y}_0 &= \frac{1}{2\sinh\eta}\partial_\beta \log \mathbf{T}^{\mathrm{sc}}_s(u,\beta,\phi)\Big|_{s=(\ell_2-1)/2,u=u_0,\beta=0} = \big(\mathbf{Q}^+_1\big)^\dagger,
\end{aligned} \tag{7.36}$$

which satisfy DG relation

$$\begin{aligned}
\Big[\mathbf{Q}_0, \big[\mathbf{Q}_0, [\mathbf{Q}_0, \mathbf{Q}_1]\big]\Big] &= \ell_2^2 [\mathbf{Q}_0, \mathbf{Q}_1], \\
\Big[\mathbf{Q}_1, \big[\mathbf{Q}_1, [\mathbf{Q}_1, \mathbf{Q}_0]\big]\Big] &= \ell_2^2 [\mathbf{Q}_1, \mathbf{Q}_0],
\end{aligned} \tag{7.37}$$

with any $\ell_2 \in \mathbb{Z}_{>0}$. Notice that the definition of semi-cyclic transfer matrix $\mathbf{T}^{\mathrm{sc}}_s(u,\beta,\phi)$ depends on the root of unity through $\varepsilon = \pm 1$.

Similar to (7.33), the higher order Onsager generators are conjectured to be related to the higher order Z and Y charges.

Conjecture II:
In general, higher order Z and Y charges are functions of higher order Onsager generators such that

$$\begin{aligned}\mathbf{Z}_n &= \frac{1}{n!}\left(\frac{\ell_2}{2}\right)^n \sum_{j=0}^{\lfloor (n+1)/2 \rfloor} c_j^n \mathbf{Q}^0_{(n+1)-2j},\\ \mathbf{Y}_n &= \frac{1}{n!}\left(\frac{\ell_2}{2}\right)^n \sum_{j=0}^{\lfloor (n+1)/2 \rfloor} c_j^n \mathbf{Q}^-_{(n+1)-2j}, \quad n \in \mathbb{Z},\end{aligned} \tag{7.38}$$

where $c_j^n \in \mathbb{N}$. The first three terms $\mathbf{Z}_n$ and $\mathbf{Y}_n$, $n \in \{1,2,3\}$ can be expressed as

$$\begin{aligned}&\mathbf{Z}_1 = \frac{1}{1!}\frac{\ell_2}{2}\left(\mathbf{Q}^0_2 - \mathbf{Q}^0_0\right), \quad \mathbf{Z}_2 = \frac{1}{2!}\left(\frac{\ell_2}{2}\right)^2\left(2\mathbf{Q}^0_3 - \mathbf{Q}^0_1\right),\\ &\mathbf{Z}_3 = \frac{1}{3!}\left(\frac{\ell_2}{2}\right)^3\left(6\mathbf{Q}^0_4 - 8\mathbf{Q}^0_2 + 2\mathbf{Q}^0_0\right),\\ &\mathbf{Y}_1 = \frac{1}{1!}\frac{\ell_2}{2}\left(\mathbf{Q}^-_2 - \mathbf{Q}^-_0\right), \quad \mathbf{Y}_2 = \frac{1}{2!}\left(\frac{\ell_2}{2}\right)^2\left(2\mathbf{Q}^-_3 - \mathbf{Q}^-_1\right),\\ &\mathbf{Y}_3 = \frac{1}{3!}\left(\frac{\ell_2}{2}\right)^3\left(6\mathbf{Q}^-_4 - 8\mathbf{Q}^-_2 + 2\mathbf{Q}^-_0\right).\end{aligned} \tag{7.39}$$

Conjecture I (7.36) and part of Conjecture II (7.39) are proven for the case of XX model ($\ell_2 = 2$), already shown in Sec. 7.2.1. (7.38) of Conjecture II can be considered as a generalisation of (7.39). Conjectures I and II, cf. (7.36) and (7.39) have been verified numerically for cases whose roots of unity satisfy $\ell_2 = 3, 4, 5$ and all permitted values of ℓ_1 with system size N up to 12. The numerical evidence is convincing that Conjectures I and II are true for arbitrary root of unity value of the anisotropy and system size.

7.3.1 Closure condition: free v.s. interacting

In this section, we assume that the conjectures above are true. We can answer the question about the physical difference between XX model and XXZ model at root of unity other than $\exp(\mathrm{i}\pi/2)$. On the one hand, they all possess the Onsager algebra symmetries, which are identical on the level of algebraic structure, cf. (7.2); on the other hand, XX model permits a free fermionic description with Jordan–Wigner transformation, while XXZ models at other roots of unity do not, because of their intrinsically interacting nature [153].

The Onsager generators $\mathbf{Q}_m$ of different models under consideration are regarded as different representations of the Onsager algebra. Even though the algebraic structure of those generators is identical, they still might possess different properties. For XX model, all the Onsager generators are bilinear in fermionic operators after Jordan–Wigner transformation [127]. Hence, only the representation associated with $\eta = \mathrm{i}\pi/2$ has the free fermionic behaviour, guaranteed by the closure condition (7.32) [127, 151]. For other roots of unity $q = \exp\left(\mathrm{i}\pi\frac{\ell_1}{\ell_2}\right) \neq \exp(\mathrm{i}\pi/2)$, the closure condition is no longer satisfied, since these models are interacting. This observation implies that we cannot apply all the nice properties and methods used for XX model to XXZ models at other roots of unity.

7.4 Summary of results

This chapter can be considered as a continuation of Chapter 6, where we use the Z and Y charges generated by the semi-cyclic transfer matrices to construct and conjecture the existence of the hidden Onsager algebra symmetries in quantum XXZ model at arbitrary root of unity. This method can be generalised to the higher spin version of XXZ model via transfer matrix fusion relation, demonstrated in [5]. One of the most notable examples is the spin-1 Zamolodchikov–Fateev model. The physical consequences of the existence of infinitely many non-Abelian conserved charges, especially in thermodynamic limit, remain to be elucidated.

Chapter 8

Discussion and outlook

> All in all, it was just another brick in the wall.
>
> Pink Floyd

In this thesis we studied classical and quantum integrable models in great length, most focusing on the aspects that are closely related to the out-of-equilibrium properties of those models. The models under consideration are classical Landau–Lifshitz field theory and quantum spin-1/2 XXZ model. They are closely related to each other, namely classical Landau–Lifshitz field theory is the semi-classical (long-wavelength) limit of the quantum XXZ model close to the isotropic point. These two models are archetypical for classical integrability and quantum integrability, respectively.

In Chapter 2, we introduced the notion of classical integrability in two parallel approaches, i.e. classical inverse scattering method and finite-gap integration method. Classical inverse scattering method describes the classical integrable model on an infinite line, and we demonstrate the method using the example of a domain-wall profile in Landau–Lifshitz model that is the centre of attention in Chapter 4. Finite-gap integration method uses language of algebraic geometry to study the classical integrable model with periodic boundary condition. This setting is of vital importance when considering the semi-classical limit of quantum in-

tegrable models, which are typically with periodic boundary condition. The techniques developed in Chapter 2 are directly used in Chapter 5.

In Chapter 3, we briefly introduced the formalism of algebraic Bethe ansatz for quantum spin-1/2 XXZ model, motivated from the 2-dimensional statistical mechanical counterpart, 6-vertex model. We constructed the transfer matrix using Lax formalism and illustrated the Yang-Baxter relation that plays a pivotal rôle in quantum integrability. The algebraic Bethe ansatz is used in Chapter 6 when studying the eigenstates of quantum XXZ model.

After the two introductory chapters, we proceed with the main results of the thesis. To begin with, we studied the domain-wall quench problem in classical Landau–Lifshitz model in Chapter (4). We discovered three different regimes of spin transport with respect to the anisotropic parameter δ. When $\delta < 0$, i.e. easy-plane regime, we found ballistic transport of spin, explained with hydrodynamic approximation. When $\delta = 0$, i.e. isotropic regime, we found out that the spin transport is superdiffusive, which we further conjectured to be logarithmic-enhanced diffusion. When $\delta > 0$, i.e. easy-axis regime, the domain-wall profile is frozen. The reason is that the spectrum contains soliton part. Therefore, the asymptotic spin transport is absent. The soliton content consists of a static kink and possible breathers on top of the kink. What is truly remarkable is that all three regimes qualitatively behave the same as the three regimes of spin transport in the quantum domain-wall quench. This is summarised as the classical-quantum correspondence of spin transport, reported in [1].

Next, we took on the task of deeper understanding on the classical-quantum correspondence. We studied the semi-classical quantisation of the finite-gap solutions of classical Landau–Lifshitz model, which become the semi-classical eigenstates of the quantum XXZ model with weak anisotropy, in Chapter 5. We mainly focused on two types of finite-gap solutions, one-cut ration solution and two-cut bion solution. The first one describes the spin wave (precession) near the ferromagnetic state and the latter becomes the static kink in the soliton limit. Using the semi-classical quantisation procedure, we were able to obtain the distribution of Bethe roots for semi-classical eigenstates of the quantum XXZ model. Further calculations on the quantum quantities such as the Slavnov overlap can be obtained using functional method based on the semi-classical

quantisation. They are presented in [2, 3], which lead us closer to a full quantitative understanding of the classical-quantum correspondence alluded by the study of domain-wall quench.

After the investigation of semi-classical quantisation, we switched the topic to the quantum regime. Our next goal is to construct the Baxter's Q operator and study the full spectrum of quantum XXZ model at root of unity, which does not have a classical counterpart, in Chapter 6. We first used the factorisation of two-parameter transfer matrix to construct the Q operator for arbitrary anisotropy parameter Δ. A further truncation of the auxiliary space happens at root of unity $q = \exp(\mathrm{i}\pi\ell_1/\ell_2)$, and it allows us to construct the Q operator for XXZ model at root of unity with a finite-dimensional auxiliary space. We used this property to study the spectrum of XXZ model at root of unity, and we discovered the descendant tower structure that explains the exponential degeneracies of the spectrum. We substantiated the existence of descendant tower structure with numerous examples. Moreover, the degeneracies have significant consequences in thermodynamics of the model. We related the degeneracies and the existence of FM strings to quasi-local Z charges as well as the non-vanishing spin Drude weight in XXZ model at root of unity. A full exposition can be found in [4]

Ultimately, we continued with the XXZ model at root of unity. We extended the observation that XX model (XXZ model with $\Delta = 0$) possesses Onsager algebra symmetry and consequently conjectured the hidden Onsager algebra symmetries in XXZ models at other roots of unity. The Onsager algebra symmetry guarantees two sets of non-Abelian conserved charges, both infinitely many in the thermodynamic limit. These conjectures together with the higher spin generalisation are given in [5].

Even though we have presented plenty of results in classical and quantum integrable models aiming at applications to out-of-equilibrium physics, there are still many open questions to be investigated in the future.

Extended from Chapter [2], it is of great interest to formulate the out-of-equilibrium dynamics of semi-classical states of quantum integrable lattice model in the manner of Quench Action. Using the property of the semi-classical states, we hope to obtain a functional-integral formalism of Quench Action, which exploits exact knowledge of thermodynamic

overlap coefficients. This is possible with the functional approaches in [100, 101, 2]. Similarly, there is a conjecture on the classical-quantum correspondence of correlation functions for semi-classical states [2]. Making use of the quantum separation of variable approach [154, 155, 156], we hope to prove such correspondence which can help us access information of quantum correlation functions for semi-classical states. Such correlation functions are typically difficult to obtain and they are important in probing non-equilibrium dynamics.

In the quantum regime, there are several interesting open problems too. One of the most notable problems is the thermalisation in the presence of non-Abelian charges, for example from Onsager algebra symmetry. The Onsager generators can be easily constructed as the dynamical symmetry of the Hamiltonian, and they result in persistent oscillatory behaviour in the auto-correlation functions, exemplified in [157, 158]. This out-of-equilibrium phenomenon manifests to models that are not integrable, such as quantum many-body scars [152]. This also leads to the maximal number of conserved charges needed to the Generalised Gibbs Ensemble after a quantum quench, when the model possesses non-Abelian charges. Even though we conjectured about the hidden Onsager algebra symmetry in XXZ model at root of unity, a rigorous proof is still absent. Such a proof will help us understand the deep connection between the underlying quantum group structure and the hidden Onsager symmetry. Meanwhile, a generalisation of such constructions is not available for models built with higher-rank quantum algebra. We hope to comprehend the mathematical and physical properties of such models more.

To conclude, many open problems in the field of classical and quantum integrability out of equilibrium are available at present. The field is rapidly developing and both physical and mathematical breakthroughs are needed that provide us better understanding of the out-of-equilibrium physics using integrability as a tool.

Appendix A
Riemann-Hilbert problem in ζ-plane

In order to study the formation of condensates, the Riemann–Hilbert problem is most conveniently written in terms of spectral parameter $\zeta = 1/\mu$, namely

$$\mathfrak{p}(\zeta + \mathrm{i}0) + \mathfrak{p}(\zeta - \mathrm{i}0) = 2\pi n_j, \quad \zeta \in \mathcal{C}_j, \tag{A.1}$$

where $\mathcal{C}_j$ denotes the j-th branch cut in ζ plane, whereas quasi-momentum $\mathfrak{p}(\zeta)$ is defined as

$$\mathfrak{p}(\zeta) = G(\zeta) - \frac{\ell}{2\zeta} = \ell \int \mathrm{d}\xi \tilde{\mathcal{K}}_\delta(\zeta, \xi)\rho(\xi) - \frac{\ell}{2\zeta}, \tag{A.2}$$

with integration kernel

$$\tilde{\mathcal{K}}_\delta(\zeta, \xi) = \frac{1 + \delta\xi\zeta}{\zeta - \xi}. \tag{A.3}$$

The density (of the Bethe roots) is accordingly given by

$$\rho(\zeta) = \frac{\mathfrak{p}(\zeta + \mathrm{i}0) - \mathfrak{p}(\zeta - \mathrm{i}0)}{2\mathrm{i}\pi\ell(1 + \delta\zeta^2)}, \quad \zeta \in \mathcal{C}_j. \tag{A.4}$$

Note that the orientation of integration along $\mathcal{C}_j$ is now in the opposite direction as previously, i.e. it goes from the branch point with negative imaginary part to the one with positive imaginary part.

Appendix B

Finite size corrections to Riemann-Hilbert problem

Here we outline how to take the semi-classical limit of the logarithm of $Q_j^{[\pm 2]}$. The first step is to split the term into the anomalous part and normal part [85, 159], i.e.

$$\begin{aligned}\log Q_j^{[\pm 2]}(\vartheta_j) &= \sum_{k\neq j}^{M} \log\sin(\vartheta_j - \vartheta_k \pm \mathrm{i}\eta) \\ &= \sum_{0<|k-j|\leq K} \log\sin(\vartheta_j - \vartheta_k \pm \mathrm{i}\eta) + \sum_{|k-j|>K} \log\sin(\vartheta_j - \vartheta_k \pm i\eta),\end{aligned} \tag{B.1}$$

where parameter K is a cut-off with the following properties,

$$\vartheta_j - \vartheta_k \sim \begin{cases} \mathcal{O}\left(1/L\right), & |k-j| \leq K \\ \mathcal{O}\left(1\right), & |k-j| > K \end{cases}. \tag{B.2}$$

We denote the anomalous part as

$$\log Q_j^a(\vartheta_j \pm \mathrm{i}\eta) = \sum_{0<|k-j|\leq K} \log\sin(\vartheta_j - \vartheta_k \pm \mathrm{i}\eta), \tag{B.3}$$

while the normal part is

$$\log Q_j^n(\vartheta_j \pm \mathrm{i}\eta) = \sum_{|k-j|>K} \log\sin(\vartheta_j - \vartheta_k \pm \mathrm{i}\eta). \tag{B.4}$$

For the normal part, we can perform the same expansion as in Eq. (5.10), namely

$$\begin{aligned}\log Q_j^n(\vartheta_j \pm \mathrm{i}\eta) = \log Q_j^n(\vartheta_j) \pm \mathrm{i}\eta \frac{d}{d\vartheta} \log Q_j^n(\vartheta)|_{\vartheta=\vartheta_j} \\ -\frac{\eta^2}{2}\frac{d^2}{d\vartheta^2} \log Q_j^n(\vartheta)|_{\vartheta=\vartheta_j} + \mathcal{O}\left(\frac{1}{L^2}\right),\end{aligned} \tag{B.5}$$

and

$$\begin{aligned}\mathrm{i}\eta \frac{d}{d\vartheta} \log Q_j^n(\vartheta)|_{\vartheta=\vartheta_j} &= \frac{\epsilon\ell}{L} \sum_{|k-j|>K} \frac{1}{\tan(\vartheta_j - \vartheta_k)} \\ &= \frac{\ell}{L} \sum_{|k-j|>K} \frac{\mu_j\mu_k + \delta}{\mu_j - \mu_k}.\end{aligned} \tag{B.6}$$

Combining the two parts, we obtain

$$\log Q_j^n(\vartheta_j + \mathrm{i}\eta) - \log Q_j^n(\vartheta_j - \mathrm{i}\eta) = \frac{2\ell}{L} \sum_{|k-j|>K} \frac{\mu_j\mu_k + \delta}{\mu_j - \mu_k} + \mathcal{O}\left(\frac{1}{L^2}\right). \tag{B.7}$$

Meanwhile, for the anomalous part, denoting $m = k - j$, we have

$$\begin{aligned}&\log Q_j^n(\vartheta_j + \mathrm{i}\eta) - \log Q_j^n(\vartheta_j - \mathrm{i}\eta) \\ &= \sum_{0<|m|<K} \log \frac{\sin(\vartheta_j - \vartheta_{j+m} + \mathrm{i}\eta)}{\sin(\vartheta_j - \vartheta_{j+m} + \mathrm{i}\eta)} \\ &= \sum_{0<|m|<K} \log \frac{L(\mu_j - \mu_{j+m}) + \mathrm{i}\ell(\mu_j^2 + \delta)}{L(\mu_j - \mu_{j+m}) - \mathrm{i}\ell(\mu_j^2 + \delta)}.\end{aligned} \tag{B.8}$$

We can develop an expansion

$$L\mu_{j+m} \sim c_1 L + c_2 m + \frac{1}{2}\frac{c_3 m^2}{L} + \mathcal{O}\left(\frac{1}{L^2}\right), \quad |m| \le K, \tag{B.9}$$

where all the "constants" can be expressed in terms of density $\rho(\mu)$, i.e.

$$c_1 = \mu_j, \quad c_2 = \frac{1}{\rho(\mu_j)}, \quad c_3 = -\frac{\rho'(\mu_j)}{\rho(\mu_j)^3}, \tag{B.10}$$

and

$$\rho(\mu) = \frac{1}{L}\sum_{j=1}^{M}\delta(\mu-\mu_j), \quad \rho(\mu) \simeq \frac{\mathrm{d}j}{\mathrm{d}\mu}. \tag{B.11}$$

By combining the m-th and $(-m)$-th terms in the sum, we can express the leading order of the sum as

$$\begin{aligned}\sum_{m=1}^{K}\frac{1}{\mathrm{i}}\Bigg(&\log\frac{L(\mu_j-\mu_{j-m})+\mathrm{i}\ell(\mu_j^2+\delta)}{L(\mu_j-\mu_{j-m})-\mathrm{i}\ell(\mu_j^2+\delta)}\\ &+\log\frac{L(\mu_j-\mu_{j+m})+\mathrm{i}\ell(\mu_j^2+\delta)}{L(\mu_j-\mu_{j+m})-\mathrm{i}\ell(\mu_j^2+\delta)}\Bigg),\end{aligned} \tag{B.12}$$

using

$$\begin{aligned}&\frac{1}{\mathrm{i}}\Bigg(\log\frac{L(\mu_j-\mu_{j-m})+\mathrm{i}\ell(\mu_j^2+\delta)}{L(\mu_j-\mu_{j-m})-\mathrm{i}\ell(\mu_j^2+\delta)}\\ &+\log\frac{L(\mu_j-\mu_{j+m})+\mathrm{i}\ell(\mu_j^2+\delta)}{L(\mu_j-\mu_{j+m})-\mathrm{i}\ell(\mu_j^2+\delta)}\Bigg)\\ &=\frac{1}{\mathrm{i}}\log\frac{b^2m^2-[\mathrm{i}\ell(\mu_j^2+\delta)-\frac{c_3m^2}{2L}]^2}{c_2^2m^2-[\mathrm{i}\ell(\mu_j^2+\delta)+\frac{c_3m^2}{2L}]^2}\\ &=\frac{2c_3\ell(\mu_j^2+\delta)}{c_2^2L}\left(1-\frac{1}{\frac{c_2^2}{\ell^2(\mu_j^2+\delta)^2}+1}\right)+\mathcal{O}\left(\frac{1}{L^2}\right).\end{aligned} \tag{B.13}$$

The first part can be combined with the sum for $|m|>K$, since

$$\frac{2\ell(\mu_j\mu_{j-m}+\delta)}{L(\mu_j-\mu_{j-m})}+\frac{2\ell(\mu_j\mu_{j+m}+\delta)}{L(\mu_j-\mu_{j+m})}\simeq\frac{2c_3(\mu_j^2+\delta)}{c_2^2L}. \tag{B.14}$$

Taking the limit $K\to\infty$ (beware that $K/L\to 0$), for the second part we have

$$\begin{aligned}&-\sum_{m=1}^{\infty}\frac{2c_3\ell(\mu_j^2+\delta)}{c_2^2L\left[\frac{c_2^2}{\ell^2(\mu_j^2+\delta)^2}+1\right]}\\ &=\frac{c_3\ell(\mu_j^2+\delta)}{c_2^2L}\left[1-\frac{\pi\ell(\mu_j^2+\delta)}{c_2}\coth\left(\frac{\pi\ell(\mu_j^2+\delta)}{c_3}\right)\right].\end{aligned} \tag{B.15}$$

Substituting back in the values in Eq. (B.10), we will obtain the finite-size correction in Eq. (5.16).

In addition, the finite-size correction in terms of ζ variable takes the form

$$\frac{\pi\rho'(\zeta)\ell^2(1+\delta\zeta^2)^2}{L}\coth\left[\pi\ell(1+\delta\zeta^2)\rho(\zeta)\right]+\mathcal{O}\left(\frac{1}{L^2}\right). \tag{B.16}$$

Appendix C
Useful formulae for elliptic functions

We collect several useful functions and formulae used in the derivations for the classical bion solutions in Chapter 5.

We define the elliptic integral of the first kind as

$$K(\mathrm{k}^2) = \int_0^1 \frac{\mathrm{d}x}{\sqrt{(1-x^2)(1-\mathrm{k}^2x^2)}}. \tag{C.1}$$

The Jacobi elliptic function $\mathrm{sn}(x, \mathrm{k}^2)$ is defined as the inverse of the elliptic integral of the first kind,

$$\mathrm{w} = \mathrm{sn}(x, \mathrm{k}^2), \quad x = \int_0^{\mathrm{w}} \frac{\mathrm{d}z}{\sqrt{(1-z^2)(1-\mathrm{k}^2z^2)}}, \tag{C.2}$$

and, without ambiguity, we can put $\mathrm{sn}(x, \mathrm{k}^2) =: \mathrm{sn}(x)$. Other types of Jacobi elliptic functions can be defined in a similar way,

$$\mathrm{w} = \mathrm{cn}(x, \mathrm{k}^2), \quad x = \int_{\mathrm{w}}^1 \frac{\mathrm{d}z}{\sqrt{(1-z^2)(1-\mathrm{k}^2+\mathrm{k}^2z^2)}}, \tag{C.3}$$

and

$$\mathrm{w} = \mathrm{dn}(x, \mathrm{k}^2), \quad x = \int_{\mathrm{w}}^1 \frac{\mathrm{d}z}{\sqrt{(1-z^2)(z^2+\mathrm{k}^2-1)}}, \tag{C.4}$$

such that

$$\mathrm{sn}^2x + \mathrm{cn}^2x = 1, \quad \mathrm{k}^2\mathrm{sn}^2x + \mathrm{dn}^2x = 1. \tag{C.5}$$

When shifting the argument by one quarter of the period of $K(\mathrm{k}^2)$, we have

$$\begin{aligned} \mathrm{cn}\left(x + K(\mathrm{k}^2)\right) &= -\sqrt{1-\mathrm{k}^2}\frac{\mathrm{sn}(x)}{\mathrm{dn}(x)}, \\ \mathrm{cn}\left(x + K(\mathrm{k}^2)\right) &= \sqrt{1-\mathrm{k}^2}\frac{1}{\mathrm{dn}(x)}. \end{aligned} \tag{C.6}$$

We also use theta functions to express the spin field $\vec{S}(x,t)$. The most important one is

$$\vartheta_3(z,\tau) = \sum_{n=-\infty}^{+\infty} e^{\mathrm{i}\pi\tau n^2 + 2\mathrm{i}zn}. \tag{C.7}$$

For a more detailed exposition and other properties of elliptic functions we refer to Refs. [160, 161].

Appendix D

Quantum $\mathfrak{sl}_2$

The quantum group $U_q(\mathfrak{sl}_2)$ is the unital associative algebra with generators $\mathbf{S}^+, \mathbf{S}^-$ and $\mathbf{K}$ satisfying the commutation relations

$$\mathbf{K}\,\mathbf{S}^{\pm}\,\mathbf{K}^{-1} = q^{\pm 1}\,\mathbf{S}^{\pm}, \qquad \left[\mathbf{S}^+, \mathbf{S}^-\right] = \frac{\mathbf{K}^2 - \mathbf{K}^{-2}}{q - q^{-1}}. \tag{D.1}$$

We take the coproduct to be $\mathbf{S}^{\pm} \mapsto \mathbf{S}^{\pm} \otimes \mathbf{K}^{-1} + \mathbf{K} \otimes \mathbf{S}^{\pm}$ and $\mathbf{K} \mapsto \mathbf{K} \otimes \mathbf{K}$. There is a counit and antipode, see e.g. Eqs. (1.2)–(1.4) in Ref. [162] and Ref. [163].

In this appendix we summarise the representations of $U_q(\mathfrak{sl}_2)$ used in this thesis. It is easy to verify that the commutation relations (D.1) hold and that $\mathbf{K} = \exp(\eta\,\mathbf{S}^z)$. The spin of an irrep is defined by the eigenvalue $[s]_q\,[s+1]_q$ of the quantum Casimir operator

$$\frac{1}{2}\big(\mathbf{S}^+\,\mathbf{S}^- + \mathbf{S}^-\,\mathbf{S}^+\big) + \frac{[2]_q}{2}\left(\frac{\mathbf{K} - \mathbf{K}^{-1}}{q - q^{-1}}\right)^2, \tag{D.2}$$

which generates the centre of $U_q(\mathfrak{sl}_2)$.

D.1 Global representation

The physical Hilbert space $(\mathbb{C}^2)^{\otimes N}$ of the spin chain has two different 'global' representations. When $N = 1$ the representation is given by

$\mathbf{S}^{\pm} = \sigma^{\pm}$ and $\mathbf{K} = q^{\sigma^z/2}$. For $N > 2$ repeated application of the coproduct gives the (reducible) representation

$$\begin{aligned} \mathbf{S}^{\pm} &= \sum_{j=1}^{N} q^{\sigma_1^z/2} \otimes \cdots \otimes q^{\sigma_{j-1}^z/2} \otimes \sigma_j^{\pm} \otimes q^{-\sigma_{j+1}^z/2} \otimes \cdots \otimes q^{-\sigma_N^z/2}, \\ \mathbf{K} &= q^{\mathbf{S}^z} = q^{\sigma_1^z/2} \otimes q^{\sigma_2^z/2} \otimes \cdots \otimes q^{\sigma_N^z/2}, \end{aligned} \tag{D.3}$$

satisfying commutation relation (D.1). By reversing the factors (taking the opposite coproduct) we obtain another (reducible) representation:

$$\begin{aligned} \bar{\mathbf{S}}^{\pm} &= \sum_{j=1}^{N} q^{-\sigma_1^z/2} \otimes \cdots \otimes q^{-\sigma_{j-1}^z/2} \otimes \sigma_j^{\pm} \otimes q^{\sigma_{j+1}^z/2} \otimes \cdots \otimes q^{\sigma_N^z/2}, \\ \bar{\mathbf{K}} &= q^{\bar{\mathbf{S}}^z} = q^{\sigma_1^z/2} \otimes q^{\sigma_2^z/2} \otimes \cdots \otimes q^{\sigma_N^z/2} = \mathbf{K}. \end{aligned} \tag{D.4}$$

All of these operators can be obtained from the entries (3.13) of the monodromy matrix in the limits $u \to \pm\infty$. The $\mathbf{B}$ operator from the ABA (3.13) is closely related to the above spin-lowering generators. To see this we write the Lax operator (3.4) with spin-$\frac{1}{2}$ auxiliary space in the form

$$\begin{aligned} \mathbf{L}_{aj}(u) &= \begin{pmatrix} \mathbf{a}_j(u) & \mathbf{b}_j(u) \\ \mathbf{c}_j(u) & \mathbf{d}_j(u) \end{pmatrix}_a, \\ \mathbf{b}_j(u) &= \sinh(\eta)\, \sigma_j^-, \quad \mathbf{c}_j(u) = \sinh(\eta)\, \sigma_j^+. \end{aligned} \tag{D.5}$$

In the limits $u \to \pm\infty$ the diagonal entries become

$$\mathbf{a}_j(u) \sim \pm \frac{e^{\pm u}}{2}\, q^{\sigma_j^z/2}, \qquad \mathbf{d}_j(u) \sim \pm \frac{e^{\pm u}}{2}\, q^{-\sigma_j^z/2}, \qquad u \to \pm\infty. \tag{D.6}$$

Therefore, using the definition of monodromy matrix (3.13), we have

$$\begin{aligned} \lim_{u\to-\infty} (-2\, e^{u})^{N-1}\, \mathbf{B}(u) &= \sinh(\eta)\, \mathbf{S}^-, \\ \lim_{u\to+\infty} (2\, e^{-u})^{N-1}\, \mathbf{B}(u) &= \sinh(\eta)\, \bar{\mathbf{S}}^-. \end{aligned} \tag{D.7}$$

Similarly we can recover the spin-raising operators from $\mathbf{C}$, and $\mathbf{K}, \mathbf{K}^{-1}$ from either of $\mathbf{A}, \mathbf{D}$.

D.2 Auxiliary representations

We also use various choices for the auxiliary space, which is a representation of $U_q(\mathfrak{sl}_2)$. We summarise the key ingredient here.

First, we use the finite-dimensional unitary spin-s representation of $U_q(\mathfrak{sl}_2)$. Denote the orthonormal basis of $\mathbb{C}^{2s+1}$ by $|n\rangle$ for $n = 0, 1, \cdots, 2s$. Then the generators are given by

$$\begin{aligned}
\mathbf{S}^+ &= \sum_{n=0}^{2s-1} \sqrt{[2s-n]_q[n+1]_q}\ |n+1\rangle\langle n|, \\
\mathbf{S}^- &= \sum_{n=0}^{2s-1} \sqrt{[2s-n]_q[n+1]_q}\ |n\rangle\langle n+1|, \\
\mathbf{K} &= \sum_{n=0}^{2s} q^{-s+n}\,|n\rangle\langle n|, \qquad \mathbf{S}^z = \sum_{n=0}^{2s}(-s+n)\,|n\rangle\langle n|,
\end{aligned} \tag{D.8}$$

with $2s \in \mathbb{Z}_{\geq 0}$. When $s = 1/2$ this recovers the case $N = 1$ of (D.3) with $|1\rangle = |\uparrow\rangle$ and $|0\rangle = |\downarrow\rangle$.

We also use the complex spin-s highest weight representation of $U_q(\mathfrak{sl}_2)$. It is defined on an infinite-dimensional Hilbert space with orthonormal basis $\langle n|$ indexed by $n \in \mathbb{Z}_{\geq 0}$. The generators are given by

$$\begin{aligned}
\mathbf{S}^+ &= \sum_{n=0}^{\infty} [2s-n]_q\,|n+1\rangle\langle n|, \\
\mathbf{S}^- &= \sum_{n=0}^{\infty} [n+1]_q\,|n\rangle\langle n+1|, \\
\mathbf{K} &= \sum_{n=0}^{\infty} q^{-s+n}\,|n\rangle\langle n|, \qquad \mathbf{S}^z = \sum_{n=0}^{\infty}(-s+n)\,|n\rangle\langle n|,
\end{aligned} \tag{D.9}$$

with $s \in \mathbb{C}$. This is related to the transfer matrices $\mathbf{T}_s^{\mathrm{hw}}$ (6.40). When $2s \in \mathbb{Z}_{\geq 0}$, the infinite-dimensional highest-weight representation contains a finite-dimensional submodule, because the entry of $\mathbf{S}^+$ for $n = 2s$ vanishes (cf. Fig. 6.2). The subspace labelled by $0 \leq n \leq 2s$ is preserved by all of (D.9). Thus we can truncate to a representation of dimension

$2s+1$ with generators

$$\begin{aligned}
\mathbf{S}^+ &= \sum_{n=0}^{2s-1} [2s-n]_q \, |n+1\rangle\langle n|, \\
\mathbf{S}^- &= \sum_{n=0}^{2s-1} [n+1]_q \, |n\rangle\langle n+1|, \\
\mathbf{K} &= \sum_{n=0}^{2s} q^{-s+n} \, |n\rangle\langle n|, \qquad \mathbf{S}^z = \sum_{n=0}^{2s} (-s+n) \, |n\rangle\langle n|,
\end{aligned} \tag{D.10}$$

with $2s \in \mathbb{Z}_{\geq 0}$. This representation is equivalent to (D.8) by a gauge transformation.

When $\eta = \mathrm{i}\pi\ell_1/\ell_2$ (q at root of unity), there exists another truncation yielding an ℓ_2-dimensional representation, shown in Fig. 6.3. This representation is referred to as *nilpotent* representation, because $(\mathbf{S}^{\pm})^{\ell_2} = 0$ in this case. The generators act on the subspace with basis $|n\rangle$ for $0 \leq n \leq \ell_2 - 1$ by

$$\begin{aligned}
\mathbf{S}^+ &= \sum_{n=0}^{\ell_2-2} [2s-n]_q \, |n+1\rangle\langle n|, \\
\mathbf{S}^- &= \sum_{n=0}^{\ell_2-2} [n+1]_q \, |n\rangle\langle n+1|, \\
\mathbf{K} &= \sum_{n=0}^{\ell_2-1} q^{-s+n} \, |n\rangle\langle n|, \qquad \mathbf{S}^z = \sum_{n=0}^{\ell_2-1} (-s+n) \, |n\rangle\langle n|,
\end{aligned} \tag{D.11}$$

with $s \in \mathbb{C}$.

There is one more truncated ℓ_2-dimensional representation that we will use at root of unity: the *semi-cyclic* representation. It is similar to the truncated highest-weight representation (D.11) with an additional

entry in $\mathbf{S}^+$:

$$\begin{aligned}
\mathbf{S}^+ &= \beta\,|0\rangle\langle \ell_2 - 1| + \sum_{n=0}^{\ell_2-2} [2s-n]_q\,|n+1\rangle\langle n|,\\
\mathbf{S}^- &= \sum_{n=0}^{\ell_2-2} [n+1]_q\,|n\rangle\langle n+1|,\\
\mathbf{K} &= \sum_{n=0}^{\ell_2-1} q^{-s+n}\,|n\rangle\langle n|, \qquad \mathbf{S}^z = \sum_{n=0}^{\ell_2-1} (-s+n)\,|n\rangle\langle n|,
\end{aligned} \tag{D.12}$$

with $s \in \mathbb{C}$, $\beta \in \mathbb{C}$. We can also construct another semi-cyclic representation as the truncated highest-weight representation an additional entry in $\mathbf{S}^-$ analogously.

Appendix E

Some properties of eigenstates of XXZ model

E.0.1 Numerical recipe for finding Bethe roots

Here we review a numerical recipe to solve the functional TQ relation [106]. The idea is that rather than by solving the coupled nonlinear Bethe ansatz equations (3.25), one obtain the Bethe roots by solving a few sets of linear equations instead. Once we know the form of the eigenvalues of the (fundamental) transfer matrix, we can solve Q function from functional TQ relations which are linear equations. Zeros of Q functions are the Bethe roots that we desire. The recipe goes as follows:

1. Construct the transfer matrix $\mathbf{T}_{1/2}(u)$ at generic $u \in \mathbb{C}$, and numerically diagonalise it. One obtains 2^N eigenstates that span the physical Hilbert space. The eigenvectors are independent of the spectral parameter, so these will be eigenvectors for $\mathbf{T}_{1/2}(u)$ for any u, since they commute with each other.

2. The eigenvalues of $\mathbf{T}_{1/2}(u)$ depend on u. Pick one of the eigenvectors. Its eigenvalue is found by acting with $\mathbf{T}_{1/2}(u)$. This may again be done numerically by writing the eigenvalue as a Laurent polynomial in $t = e^u$ of order N,

$$T_{1/2}(t) = \sum_{m=0}^{N} c_m^T t^{N-2m} = \mathrm{cst}_T \prod_{n=1}^{N} (\tau_n^{-1}\, t - \tau_n\, t^{-1}) \tag{E.1}$$

with zeros τ_n that can be fixed by acting with $\mathbf{T}_{1/2}(u_n)$ for N distinct values $u_n \in \mathbb{C}$.

3. The corresponding Bethe roots are the zeros of the Q operator, found by solving the functional TQ relation (6.69), i.e.

$$T_{1/2}(u,\phi)\,Q(u,\phi) = T_0(u-\eta/2)\,Q(u+\eta,\phi) + e^{\mathrm{i}\phi}\,T_0(u+\eta/2)\,Q(u-\eta,\phi). \tag{E.2}$$

Here $T_0(u) = \sinh^N(u)$ and the eigenvalues are of the form

$$Q(t) = \mathrm{cst}_Q \prod_{m=1}^{M} (t_m^{-1}\,t - t_m\,t^{-1}), \tag{E.3}$$

where M is the number of down spins of the eigenvector under consideration. The zeros t_m can once more be found numerically by taking $t = e^u$ equal to the zeroes τ_n of $T_{1/2}$ and solving the linear problem.

The zeroes give the Bethe roots $u_m = \log t_m$. One needs to be careful to interpret the result correctly in the presence of Bethe roots at infinity: $u_m = \pm\infty$ corresponds to $t_m \in \{0,\infty\}$ so the corresponding factor in (E.3) collapses to $t^{\pm 1}$, yielding (6.71):

$$Q(t) = \mathrm{cst}_Q \times t^{n_{-\infty}-n_{+\infty}} \prod_{n=1}^{M-n_{+\infty}-n_{-\infty}} (t_n^{-1}\,t - t_n\,t^{-1}). \tag{E.4}$$

The numerical recipe works very well for the XXZ model away from root of unity, as well as for the XXX model ($\Delta = \pm 1$). However, one cannot find all the Bethe roots for the XXZ spin chain at root of unity, due to the existence of degenerate eigenstates of the transfer matrix $\mathbf{T}_{1/2}$ with the same magnetisation. At root of unity, we need to use the construction of Q operator in Chapter 6 instead.

E.0.2 Relation between Bethe roots for anisotropies Δ and $-\Delta$

In the gapless regime ($-1 < \Delta < 1$) there is a simple relation between Bethe roots of all the physical solutions at anisotropy Δ and those at

anisotropy $-\Delta$, even though the corresponding eigenstates are different since the **B**-operators in the algebraic Bethe ansatz differ. We will denote the parameters of the second spin chain by primes: $\Delta' = -\Delta$ and

$$\eta = \operatorname{arccosh}(\Delta) \in \mathrm{i}\,\mathbb{R}, \qquad \eta' = \operatorname{arccosh}(\Delta') = \mathrm{i}\,\pi - \eta. \tag{E.5}$$

Consider any solution to Bethe equation (3.25) with η, system size N and twist ϕ: assume that the Bethe roots $\{u_m\}_{m=1}^M$ obey

$$\left(\frac{\sinh(u_m + \eta/2)}{\sinh(u_m - \eta/2)}\right)^N \prod_{n(\neq m)}^{M} \frac{\sinh(u_m - u_n - \eta)}{\sinh(u_m - u_n + \eta)} = e^{-\mathrm{i}\phi}. \tag{E.6}$$

Then define $\{u'_m\}_{m=1}^M$ by

$$u'_m = -u_m - \frac{\mathrm{i}\pi}{2}, \qquad 1 \le m \le M. \tag{E.7}$$

In terms of these parameters (E.6) reads

$$\left(\frac{\sinh(-u'_m + \mathrm{i}\pi/2 + \eta/2)}{\sinh(-u'_m + \mathrm{i}\pi/2 - \eta/2)}\right)^N \prod_{n(\neq m)}^{M} \frac{\sinh(-u'_m + u'_n - \eta)}{\sinh(-u'_m + u'_n + \eta)} = e^{-\mathrm{i}\phi} \tag{E.8}$$

This precisely of the form (E.6) with $\eta' = \mathrm{i}\pi - \eta$ and twist ϕ' chosen such that $e^{-\mathrm{i}\phi'} = (-1)^N e^{-\mathrm{i}\phi}$. This shows that for each solution $\{u_m\}_{m=1}^M$ at anisotropy Δ there is a corresponding solution $\{u'_m\}_{m=1}^M$ at $\Delta' = -\Delta$ provided the twist is modified to

$$\phi' = \begin{cases} \phi & N \text{ even}, \\ \phi + \pi & N \text{ odd}. \end{cases} \tag{E.9}$$

The two eigenstates are related by the unitary gauge transformation

$$\mathbf{U} = \exp\left(\mathrm{i}\pi \sum_{j=1}^{N} \frac{j}{2}\,\sigma_j^z\right) = e^{\mathrm{i}\pi\, L(L+1)/4} \prod_{j=1}^{\lceil N/2 \rceil} \sigma_{2j-1}^z. \tag{E.10}$$

It is easy to check that this transformation changes the sign of Δ in the Hamiltonian (3.11):

$$\mathbf{U}\,\mathbf{H}(\Delta, \phi)\,\mathbf{U}^{-1} = -\mathbf{H}(-\Delta, \phi'). \tag{E.11}$$

Moreover, the eigenstates are related by

$$|\{u'_m\}\rangle \propto \mathbf{U}\,|\{u_m\}\rangle\,. \tag{E.12}$$

E.0.3 Relation between eigenstates with opposite twist

Recall from Section 6.4.5 that an M-particle Bethe state $|\{u_m\}_{m=1}^M\rangle$ for the XXZ model obeys

$$\begin{aligned} \mathbf{Q}(u,\phi)\ |\{u_m\}_{m=1}^M\rangle &= Q(u)\ |\{u_m\}_{m=1}^M\rangle\,, \\ \mathbf{P}(u,\phi)\ |\{u_m\}_{m=1}^M\rangle &= P(u)\ |\{u_m\}_{m=1}^M\rangle \end{aligned} \tag{E.13}$$

with eigenvalue $Q(u)$ and $P(u)$ of the form

$$\begin{aligned} Q(u) &= \mathrm{cst}_Q \times \prod_{m=1}^{M} \left(t_m^{-1}\, t - t_m\, t^{-1}\right), & t_m &= e^{u_m}, \\ & & t &= e^{u}. \\ P(u) &= \mathrm{cst}_P \times \prod_{n=1}^{N-M} \left(\xi_n^{-1}\, t - \xi_n\, t^{-1}\right), & \xi_n &= e^{v_n}, \end{aligned} \tag{E.14}$$

The zeros $u_m = \log t_m$ of $Q(u)$ are the Bethe roots. We show that the v_n can be interpreted as the Bethe roots of the spin-flipped counterpart of $|\{u_m\}_{M=1}^M\rangle$ 'beyond the equator' with opposite twist.

Under global spin inversion the transfer matrices $\mathbf{T}_s(u)$ with $2s \in \mathbb{Z}_{\geq 0}$ become

$$\prod_{j=1}^{N}\sigma_j^x\ \mathbf{T}_s(u,\phi) \prod_{j=1}^{N}\sigma_j^x = e^{2si\phi}\, \mathbf{T}_s(u,-\phi). \tag{E.15}$$

For the unitary spin-s representation (D.8) the Lax operator (6.13) is invariant under total spin reversal, which acts by conjugation by σ_j^x in the physical space and by the antidiagonal matrix $\mathbf{U} \coloneqq \sum_{n=0}^{2s} |2s-n\rangle\langle n|$ in the auxiliary space. Spin reversal in the physical space is thus equivalent to spin reversal in the auxiliary space. This property is inherited by the monodromy matrix. In the (anti)periodic case ($\phi \in \{0,\pi\}$) it follows that spin flip in the physical space does not affect the transfer matrix. In the twisted case ($\phi \notin \{0,\pi\}$) we only have to change the sign of the twist (F.1), $\mathbf{U}\,\mathbf{E}(\phi)\,\mathbf{U}^{-1} = e^{2si\phi}\,\mathbf{E}(-\phi)$. Therefore, (E.15) is proven.

Now consider the TQ equation (6.60) with ϕ inverted to $-\phi$. By conjugating both sides with the global spin-flip operator $\prod_{j=1}^N \sigma_j^x$, using (E.15) and multiplying both sides by $e^{i\phi}$ we see that $\bar{\mathbf{Q}}(u,\phi) \coloneqq \prod_{j=1}^N \sigma_j^x\ \mathbf{Q}(u,-\phi) \prod_{j=1}^N \sigma_j^x$ precisely obeys the TP equation (6.61). Moreover, comparing the eigenvalues in (E.14) shows that the eigenvalues of

$\bar{\mathbf{Q}}(u,\phi)$ on M-particle Bethe vectors are trigonometric polynomials of degree $N-M$, just as for the P operator. It follows that the eigenvalues of $\bar{\mathbf{Q}}(u,\phi)$ are proportional to those of the P operator; in particular they have the same zeros:

$$\bar{Q}(u,\phi) \propto P(u,\phi) \propto \prod_{n=1}^{N-M} \left(\xi_n^{-1}\, t - \xi_n\, t^{-1}\right). \tag{E.16}$$

Since $\bar{\mathbf{Q}}(u,\phi)$ and $\mathbf{Q}(u,-\phi)$ have the same characteristic polynomial this shows that the M-particle eigenvalues of the P operator are the same as the $(N-M)$-particle eigenvalues of $\mathbf{Q}(u,-\phi)$. But we know that the latter can be interpreted as the Bethe roots. Therefore the zeros of the P operator can be interpreted as the Bethe roots of the spin-reversed Bethe vector beyond the equator with opposite twist.

Finally notice that the Bethe vectors (3.22) are constructed using the B-operator, which is independent of the twist, see (3.13). This implies that the result of reversing all spins on an off-shell Bethe vector (for the Hamiltonian with original twist ϕ) is

$$\prod_{l=1}^{N} \sigma_l^x \; |\{u_m\}_{m=1}^{M}\rangle = |\{v_n\}_{n=1}^{N-M}\rangle\,, \tag{E.17}$$

where the Bethe roots v_n beyond the equator are related to the zeros of eigenvalues of the P operator on $|\{u_m\}_{m=1}^{M}\rangle$.

Appendix F

Quasiperiodicity: twist operator

We define the twist operator $\mathbf{E}_a(\phi)$ for the auxiliary space. Each of the $U_q(\mathfrak{sl}_2)$ representations on the auxiliary space from Appendix D.2 is expressed in terms of an orthonormal basis $\{|d-1\rangle, \cdots, |1\rangle, |0\rangle\}$ with d the dimension of the representation. Here $d = 2\,s+1$ for the unitary spin-s representation with $s \in \frac{1}{2}\,\mathbb{Z}$, $d = \infty$ for the highest-weight representation with $s \in \mathbb{C}$, and $d = \ell_2$ for the truncation at root of unity. We consider diagonal twist operator $\mathbf{E}_a(\phi)$ given by

$$\mathbf{E}_a(\phi) = \sum_{n=0}^{d-1} e^{\mathrm{i}\phi n}\, |n\rangle\langle n|_a. \tag{F.1}$$

In view of our ordering of the basis this yields the twist from (3.13) for $s = 1/2$ ($d = 2$).

In particular, the complex spin-s representation yields monodromy matrix $\mathbf{M}_s^{\mathrm{hw}}$

$$\begin{aligned} \mathbf{M}_s^{\mathrm{hw}}(u,\phi) &= \mathbf{L}_{sN}(u)\cdots\mathbf{L}_{s2}(u)\,\mathbf{L}_{s1}(u)\,\mathbf{E}_s^{\mathrm{hw}}(\phi), \\ \mathbf{E}_s^{\mathrm{hw}}(\phi) &= \sum_{n=0}^{\infty} e^{\mathrm{i}\phi n}\, |n\rangle\langle n|_s, \end{aligned} \tag{F.2}$$

resulting in the transfer matrix $\mathbf{T}_s^{\mathrm{hw}}(u,\phi) = \mathrm{tr}_s\, \mathbf{M}_s^{\mathrm{hw}}(u,\phi)$. When $|q| \leq 1$ the diagonal matrix elements of $\mathbf{M}_s^{\mathrm{hw}}$ can be bounded by $A_N\,|q^N\,e^{\mathrm{i}\phi}|^n$ for some constant A_N, and so the trace is convergent if $|e^{\mathrm{i}\phi}| < |q|^N$. At this

point we do not know if $\mathbf{T}_s^{\mathrm{hw}}$ can be analytically continued outside this disc of convergence.

The truncation at root of unity $\eta = \mathrm{i}\pi\ell_1/\ell_2$ likewise has

$$\begin{aligned} \tilde{\mathbf{M}}_s(u,\phi) &= \mathbf{L}_{sN}(u)\,\cdots\mathbf{L}_{s2}(u)\,\mathbf{L}_{s1}(u)\,\tilde{\mathbf{E}}_s(\phi), \\ \tilde{\mathbf{E}}_s(\phi) &= \sum_{n=0}^{\ell_2-1} e^{\mathrm{i}\phi n}\,|n\rangle\langle n|_s, \end{aligned} \tag{F.3}$$

and transfer matrix $\tilde{\mathbf{T}}_s(u,\phi) = \mathrm{tr}_s\,\tilde{\mathbf{M}}_s(u,\phi)$. In this case the trace is well defined for any value of the twist ϕ.

Appendix G

Onsager generators in XX case

In the case of XX model, we obtain analytically all the Onsager generators when the twist is commensurate, cf. (6.84) by calculating the recursion relation analytically. The results are as follows.

$$\begin{aligned}\mathbf{Q}_m^0 = \frac{\mathrm{i}}{2}\sum_{j=1}^{N}(-\mathrm{i})^{m-1}\sigma_j^+\sigma_{j+1}^z\cdots\sigma_{j+m-1}^z\sigma_{j+m}^- \\ -\mathrm{i}^{m-1}\sigma_j^-\sigma_{j+1}^z\cdots\sigma_{j+m-1}^z\sigma_{j+m}^+,\end{aligned} \tag{G.1}$$

$$\mathbf{Q}_m^- = \frac{\mathrm{i}}{2}\sum_{j=1}^{N}(-\mathrm{i})^{m-1}(-1)^j\sigma_j^-\sigma_{j+1}^z\cdots\sigma_{j+m-1}^z\sigma_{j+m}^- = \left(\mathbf{Q}_m^+\right)^\dagger, \tag{G.2}$$

where $\sigma_{N+k}^\pm = e^{\pm\mathrm{i}\phi/2}\sigma_k^\pm$ with $1 \le k < N$. All generators are bilinear in fermionic operators after Jordan–Wigner transformation [127].

Appendix H

Choice of u_0 in (7.30)

In (7.30) we expand the generating functions $\mathbf{Z}(u,\phi)$ and $\mathbf{Y}(u,\phi)$ at different spectral parameter values for cases with $\varepsilon = \pm 1$. We would like to provide some details in this appendix. As usual, the twist ϕ satisfies commensurate condition (6.84).

To begin with, we notice that when $\varepsilon = +1$,

$$\mathbf{T}^{\mathrm{sc}}_{(\ell_2-1)/2}\left(\frac{\eta}{2},0,\phi\right) \tag{H.1}$$

is not invertible (i.e. not full-ranked), while it is invertible when $\varepsilon = -1$. Meanwhile, transfer matrices with $\varepsilon = +1$ are related to transfer matrices with $\varepsilon = -1$. We can see that from the existence of a unitary gauge transformation $\mathbf{U}$ [20, 4]

$$\mathbf{U} = \exp\left(\mathrm{i}\pi \sum_{j=1}^{N} \frac{j}{2}\sigma_j^z\right), \tag{H.2}$$

such that

$$\mathbf{U}\mathbf{H}(\Delta,\phi)\mathbf{U}^\dagger = -\mathbf{H}(-\Delta,\phi'). \tag{H.3}$$

The twists are related as

$$\phi' = \begin{cases} \phi & N \text{ even}, \\ \phi+\pi & N \text{ odd}. \end{cases} \tag{H.4}$$

We consider 2 transfer matrices, one with η ($\varepsilon = \exp(\ell_2\eta) = -1$) and the other one with $\eta' = \mathrm{i}\pi - \eta$ ($\varepsilon' = \exp(\ell_2\eta') = +1$). This implies that ℓ_2 is odd. When $s = \frac{\ell_2-1}{2}$ and $\beta = 0$, we have

$$\mathbf{U}\mathbf{T}_s^{\mathrm{sc}}(u, 0, \phi, \eta)\mathbf{U}^\dagger = \mathbf{T}_s^{\mathrm{sc}}(-u, 0, \phi, \eta'). \tag{H.5}$$

The above equation is satisfied only when $s \in \mathbb{Z}_{>0}$. This implies that $\frac{\ell_2-1}{2} \in \mathbb{Z}_{>0}$, i.e. ℓ_2 is odd. Moreover, if ϕ with parameter η in (H.4) satisfies commensurate condition (6.84), ϕ' with parameter η' in (H.4) also satisfies commensurate condition (6.84).

Therefore, if we were to define

$$\mathbf{Q}_1^0(\eta, \phi) = \mathbf{Z}_0 = \frac{1}{2\eta}\,\partial_s \log \mathbf{T}_s^{\mathrm{sc}}(u, \beta, \phi, \eta)|_{s=(\ell_2-1)/2,\beta=0,u=\eta/2}\,, \tag{H.6}$$

it is natural to define

$$\begin{aligned}\mathbf{Q}_1^0(\eta', \phi') &= \mathbf{U}\mathbf{Q}_0(\eta, \phi)\mathbf{U}^\dagger \\ &= \frac{1}{2\eta'}\,\partial_s \log \mathbf{T}_s^{\mathrm{sc}}(u, \beta, \phi', \eta')|_{s=(\ell_2-1)/2,\beta=0,u=-\eta/2}\,,\end{aligned} \tag{H.7}$$

satisfying the same algebraic relations after applying the unitary gauge transformation $\mathbf{U}$. Similar relations for $\mathbf{Q}_1^{\pm}$ can be inferred.

In this case $-\frac{\eta}{2} = \frac{\eta'}{2} - \frac{\mathrm{i}\pi}{2}$, indicating (7.30). We have used the value of u_0 defined in (7.30) to numerically verify the conjectures in Sec. 7.3. For instance, for the cases of $\eta = 2\mathrm{i}\pi/3$, $2\mathrm{i}\pi/5$ and $4\mathrm{i}\pi/5$, the conjectures remain true with system size N up to 12.

Bibliography

[1] O. Gamayun, Y. Miao and E. Ilievski, *Domain-wall dynamics in the Landau-Lifshitz magnet and the classical-quantum correspondence for spin transport*, Phys. Rev. B **99**, 140301 (2019), doi:10.1103/PhysRevB.99.140301.

[2] Y. Miao, E. Ilievski and O. Gamayun, *Semi-classical quantisation of magnetic solitons in the anisotropic Heisenberg quantum chain*, SciPost Phys. **10**, 86 (2021), doi:10.21468/SciPostPhys.10.4.086.

[3] Y. Miao, *An exact solution to asymptotic Bethe equation*, J. Phys. A **54**(19), 194001 (2020), doi:10.1088/1751-8121/abf1ad.

[4] Y. Miao, J. Lamers and V. Pasquier, *On the Q operator and the spectrum of the XXZ model at root of unity*, arXiv preprint arXiv:2012.10224 (2020).

[5] Y. Miao, *Conjectures on Hidden Onsager Algebra Symmetries in Interacting Quantum Lattice Models*, arXiv preprint arXiv:2103.14569 (2020).

[6] Y. Miao, E. Ilievski and O. Gamayun, *Interplay of solitons and radiation in one-dimensional Bose gases*, Phys. Rev. A **99**, 023605 (2019), doi:10.1103/PhysRevA.99.023605.

[7] V. B. Bulchandani, *On classical integrability of the hydrodynamics of quantum integrable systems*, J. Phys. A **50**(43), 435203 (2017), doi:10.1088/1751-8121/aa8c62.

[8] B. Doyon, T. Yoshimura and J.-S. Caux, *Soliton gases and generalized hydrodynamics*, Phys. Rev. Lett. **120**, 045301 (2018), doi:10.1103/PhysRevLett.120.045301.

[9] L. D. Faddeev and L. A. Takhtajan, *Hamiltonian Methods in the Theory of Solitons*, Springer Berlin Heidelberg, doi:10.1007/978-3-540-69969-9 (1987).

[10] S. Novikov, S. Manakov, L. Pitaevskii and V. Zakharov, *Theory of solitons: the inverse scattering method*, Springer Science & Business Media (1984).

[11] O. Babelon, D. Bernard and M. Talon, *Introduction to Classical Integrable Systems*, Cambridge Monographs on Mathematical Physics. Cambridge University Press, doi:10.1017/CBO9780511535024 (2003).

[12] J. A. Minahan and K. Zarembo, *The Bethe-ansatz for $\mathcal{N} = 4$ super Yang-Mills*, J. High Energy Phys. **2003**(03), 013 (2003), doi:10.1088/1126-6708/2003/03/013.

[13] V. A. Kazakov, A. Marshakov, J. A. Minahan and K. Zarembo, *Classical/quantum integrability in AdS/CFT*, J. High Energy Phys. **2004**(05), 024 (2004), doi:10.1088/1126-6708/2004/05/024.

[14] A. Marshakov, *Seiberg-Witten theory and extended Toda hierarchy*, J. High Energy Phys. **2008**(03), 055 (2008), doi:10.1088/1126-6708/2008/03/055.

[15] A. Fokas, A. Its, A. Kapaev and V. Novokshenov, *Painlevé Transcendents*, American Mathematical Society, doi:10.1090/surv/128 (2006).

[16] O. Gamayun, N. Iorgov and O. Lisovyy, *How instanton combinatorics solves Painlevé VI, V and IIIs*, J. Phys. A **46**(33), 335203 (2013), doi:10.1088/1751-8113/46/33/335203.

[17] C. A. Tracy and H. Widom, *Level-spacing distributions and the Airy kernel*, Commun. Math. Phys. **159**(1), 151 (1994), doi:10.1007/bf02100489.

[18] H. A. Bethe, *Zur Theorie der Metalle. i. Eigenwerte und Eigenfunktionen der linearen Atomkette*, Zeit. für Physik **71**, 205 (1931), doi:10.1007/BF01341708.

[19] R. Baxter, *Exactly solved models in statistical mechanics*, ISBN 978-0-486-46271-4 (1982).

[20] M. Gaudin, *The Bethe Wavefunction*, Cambridge University Press (2014).

[21] E. H. Lieb, *Exact Solution of the Problem of the Entropy of Two-Dimensional Ice*, Phys. Rev. Lett. **18**, 692 (1967), doi:10.1103/PhysRevLett.18.692.

[22] B. Sutherland, *Exact Solution of a Two-Dimensional Model for Hydrogen-Bonded Crystals*, Phys. Rev. Lett. **19**, 103 (1967), doi:10.1103/PhysRevLett.19.103.

[23] M. T. Batchelor and A. Foerster, *Yang-Baxter integrable models in experiments: from condensed matter to ultracold atoms*, J. Phys. A **49**(17), 173001 (2016), doi:10.1088/1751-8113/49/17/173001.

[24] L. Khaykovich, F. Schreck, G. Ferrari, T. Bourdel, J. Cubizolles, L. Carr, Y. Castin and C. Salomon, *Formation of a matter-wave bright soliton*, Science **296**(5571), 1290 (2002), doi:10.1126/science.1071021.

[25] T. Kinoshita, T. Wenger and D. S. Weiss, *A quantum Newton's cradle*, Nature **440**, 900 (2006), doi:10.1038/nature04693.

[26] E. H. Lieb and W. Liniger, *Exact Analysis of an Interacting Bose Gas. I. The General Solution and the Ground State*, Phys. Rev. **130**, 1605 (1963), doi:10.1103/PhysRev.130.1605.

[27] P. Calabrese and J. Cardy, *Time dependence of correlation functions following a quantum quench*, Phys. Rev. Lett. **96**, 136801 (2006), doi:10.1103/PhysRevLett.96.136801.

[28] F. H. L. Essler and M. Fagotti, *Quench dynamics and relaxation in isolated integrable quantum spin chains*, J. Stat. Mech. **2016**(6), 064002 (2016), doi:10.1088/1742-5468/2016/06/064002.

[29] J.-S. Caux and F. H. L. Essler, *Time Evolution of Local Observables After Quenching to an Integrable Model*, Phys. Rev. Lett. **110**, 257203 (2013), doi:10.1103/PhysRevLett.110.257203.

[30] J.-S. Caux, *The Quench Action*, J. Stat. Mech. **2016**(6), 064006 (2016), doi:10.1088/1742-5468/2016/06/064006.

[31] J. De Nardis, B. Wouters, M. Brockmann and J.-S. Caux, *Solution for an interaction quench in the Lieb-Liniger Bose gas*, Phys. Rev. A **89**, 033601 (2014), doi:10.1103/PhysRevA.89.033601.

[32] B. Wouters, J. De Nardis, M. Brockmann, D. Fioretto, M. Rigol and J.-S. Caux, *Quenching the Anisotropic Heisenberg Chain: Exact Solution and Generalized Gibbs Ensemble Predictions*, Phys. Rev. Lett. **113**, 117202 (2014), doi:10.1103/PhysRevLett.113.117202.

[33] M. Brockmann, J. De Nardis, B. Wouters and J.-S. Caux, *Néel-XXZ state overlaps: odd particle numbers and Lieb-Liniger scaling limit*, J. Phys. A **47**(34), 345003 (2014), doi:10.1088/1751-8113/47/34/345003.

[34] E. Ilievski, J. De Nardis, B. Wouters, J.-S. Caux, F. H. L. Essler and T. Prosen, *Complete Generalized Gibbs Ensembles in an Interacting Theory*, Phys. Rev. Lett. **115**, 157201 (2015), doi:10.1103/PhysRevLett.115.157201.

[35] O. A. Castro-Alvaredo, B. Doyon and T. Yoshimura, *Emergent Hydrodynamics in Integrable Quantum Systems Out of Equilibrium*, Phys. Rev. X **6**, 041065 (2016), doi:10.1103/PhysRevX.6.041065.

[36] B. Bertini, M. Collura, J. De Nardis and M. Fagotti, *Transport in Out-of-Equilibrium XXZ Chains: Exact Profiles of Charges and Currents*, Phys. Rev. Lett. **117**, 207201 (2016), doi:10.1103/PhysRevLett.117.207201.

[37] B. Doyon, *Exact large-scale correlations in integrable systems out of equilibrium*, SciPost Phys. **5**, 54 (2018), doi:10.21468/SciPostPhys.5.5.054.

[38] B. Doyon, *Hydrodynamic projections and the emergence of linearised Euler equations in one-dimensional isolated systems*, arXiv preprint arXiv:2011.00611 (2020).

[39] M. Schemmer, I. Bouchoule, B. Doyon and J. Dubail, *Generalized Hydrodynamics on an Atom Chip*, Phys. Rev. Lett. **122**, 090601 (2019), doi:10.1103/PhysRevLett.122.090601.

[40] E. Ilievski and J. De Nardis, *Microscopic Origin of Ideal Conductivity in Integrable Quantum Models*, Phys. Rev. Lett. **119**, 020602 (2017), doi:10.1103/PhysRevLett.119.020602.

[41] E. Ilievski and J. De Nardis, *Ballistic transport in the one-dimensional Hubbard model: The hydrodynamic approach*, Phys. Rev. B **96**, 081118 (2017), doi:10.1103/PhysRevB.96.081118.

[42] J. De Nardis, D. Bernard and B. Doyon, *Hydrodynamic Diffusion in Integrable Systems*, Phys. Rev. Lett. **121**, 160603 (2018), doi:10.1103/PhysRevLett.121.160603.

[43] E. Ilievski, J. De Nardis, M. Medenjak and T. Prosen, *Superdiffusion in one-dimensional quantum lattice models*, Phys. Rev. Lett. **121**, 230602 (2018), doi:10.1103/PhysRevLett.121.230602.

[44] S. Gopalakrishnan and R. Vasseur, *Kinetic Theory of Spin Diffusion and Superdiffusion in XXZ Spin Chains*, Phys. Rev. Lett. **122**, 127202 (2019), doi:10.1103/PhysRevLett.122.127202.

[45] J. De Nardis, S. Gopalakrishnan, E. Ilievski and R. Vasseur, *Superdiffusion from Emergent Classical Solitons in Quantum Spin*

Chains, Phys. Rev. Lett. **125**, 070601 (2020), doi:10.1103/PhysRevLett.125.070601.

[46] B. A. Dubrovin, *Inverse problem for periodic finite zoned potentials in the theory of scattering*, Funct. Anal. its Appl. **9**(1), 61 (1975), doi:10.1007/bf01078183.

[47] A. R. Its and V. B. Matveev, *Schrödinger operators with finite-gap spectrum and N-soliton solutions of the Korteweg-de Vries equation*, Theor. Math. Phys. **23**(1), 343 (1975), doi:10.1007/bf01038218.

[48] B. A. Dubrovin, *Theta functions and non-linear equations*, Russ. Math. Surv. **36**(2), 11 (1981), doi:10.1070/rm1981v036n02abeh002596.

[49] V. E. Korepin, N. M. Bogoliubov and A. G. Izergin, *Quantum Inverse Scattering Method and Correlation Functions*, Cambridge Monographs on Mathematical Physics. Cambridge University Press, doi:10.1017/CBO9780511628832 (1993).

[50] E. Fradkin, *Field Theories of Condensed Matter Physics*, Cambridge University Press, doi:10.1017/cbo9781139015509 (2013).

[51] T. Prosen and E. Ilievski, *Families of quasilocal conservation laws and quantum spin transport*, Phys. Rev. Lett. **111**, 057203 (2013), doi:10.1103/PhysRevLett.111.057203.

[52] T. Prosen, *Quasilocal conservation laws in XXZ spin-1/2 chains: Open, periodic and twisted boundary conditions*, Nucl. Phys. B **886**, 1177 (2014), doi:10.1016/j.nuclphysb.2014.07.024.

[53] E. Ilievski, M. Medenjak, T. Prosen and L. Zadnik, *Quasilocal charges in integrable lattice systems*, J. Stat. Mech. **2016**(6), 064008 (2016), doi:10.1088/1742-5468/2016/06/064008.

[54] M. Lakshmanan, T. Ruijgrok and C. Thompson, *On the dynamics of a continuum spin system*, Phys. A **84**(3), 577 (1976), doi:10.1016/0378-4371(76)90106-0.

[55] S. Gutiérrez, J. Rivas and L. Vega, *Formation of Singularities and Self-Similar Vortex Motion Under the Localized Induction Approximation*, Comm. Part. Differ. Equat. **28**(5-6), 927 (2003), doi: 10.1081/pde-120021181.

[56] O. Gamayun and O. Lisovyy, *On self-similar solutions of the vortex filament equation*, J. Math. Phys. **60**(8), 083510 (2019), doi:10. 1063/1.5096170.

[57] A. Kosevich, B. Ivanov and A. Kovalev, *Magnetic Solitons*, Phys. Rep. **194**(3-4), 117 (1990), doi:10.1016/0370-1573(90)90130-t.

[58] M. M. Bogdan and A. S. Kovalev, *Exact multisoliton solution of one-dimensional Landau-Lifshitz equations for an anisotropic ferromagnet*, JETP Lett. **31**(8), 424 (1980).

[59] M. Svendsen and H. C. Fogedby, *Phase shift analysis of the Landau-Lifshitz equation*, J. Phys. A **26**(7), 1717 (1993), doi:10.1088/ 0305-4470/26/7/026.

[60] R. F. Bikbaev, A. I. Bobenko and A. R. Its, *Landau-Lifshitz equation, uniaxial anisotropy case: Theory of exact solutions*, Theor. Math. Phys. **178**(2), 143 (2014), doi:10.1007/s11232-014-0135-4.

[61] H. Segur, *Wobbling kinks in $\varphi 4$ and sine-Gordon theory*, J. Math. Phys. **24**(6), 1439 (1983), doi:10.1063/1.525867.

[62] A. De Rossi, C. Conti and S. Trillo, *Stability, Multistability, and Wobbling of Optical Gap Solitons*, Phys. Rev. Lett. **81**, 85 (1998), doi:10.1103/PhysRevLett.81.85.

[63] G Kälbermann, *The sine-Gordon wobble*, J. Phys. A **37**(48), 11603 (2004), doi:10.1088/0305-4470/37/48/006.

[64] L. A. Ferreira, B. Piette and W. J. Zakrzewski, *Wobbles and other kink-breather solutions of the sine-gordon model*, Phys. Rev. E **77**, 036613 (2008), doi:10.1103/PhysRevE.77.036613.

[65] D. Gobert, C. Kollath, U. Schollwöck and G. Schütz, *Real-time dynamics in spin-$\frac{1}{2}$ chains with adaptive time-dependent density matrix renormalization group*, Phys. Rev. E **71**, 036102 (2005), doi:10.1103/PhysRevE.71.036102.

[66] J. Mossel and J.-S. Caux, *Relaxation dynamics in the gapped XXZ spin-1/2 chain*, New J. Phys. **12**(5), 055028 (2010), doi:10.1088/1367-2630/12/5/055028.

[67] M. Collura, A. De Luca and J. Viti, *Analytic solution of the domain-wall nonequilibrium stationary state*, Phys. Rev. B **97**, 081111 (2018), doi:10.1103/PhysRevB.97.081111.

[68] M. Ljubotina, M. Žnidarič and T. Prosen, *Spin diffusion from an inhomogeneous quench in an integrable system*, Nat. Commun. **8**, 16117 (2017), doi:10.1038/ncomms16117.

[69] G. Misguich, K. Mallick and P. L. Krapivsky, *Dynamics of the spin-$\frac{1}{2}$ Heisenberg chain initialized in a domain-wall state*, Phys. Rev. B **96**, 195151 (2017), doi:10.1103/PhysRevB.96.195151.

[70] M. Ljubotina, M. Žnidarič and T. Prosen, *A class of states supporting diffusive spin dynamics in the isotropic Heisenberg model*, J. Phys. A **50**(47), 475002 (2017), doi:10.1088/1751-8121/aa8bdc.

[71] M. Takahashi, *One-Dimensional Heisenberg Model at Finite Temperature*, Prog. Theor. Phys. **46**(2), 401 (1971), doi:10.1143/ptp.46.401.

[72] M. Takahashi and M. Suzuki, *One-Dimensional Anisotropic Heisenberg Model at Finite Temperatures*, Prog. Theor. Phys. **48**(6), 2187 (1972), doi:10.1143/ptp.48.2187.

[73] B. Sutherland, *Low-Lying Eigenstates of the One-Dimensional Heisenberg Ferromagnet for any Magnetization and Momentum*, Phys. Rev. Lett. **74**, 816 (1995), doi:10.1103/PhysRevLett.74.816.

[74] A. Dhar and B. Sriram Shastry, *Bloch Walls and Macroscopic String States in Bethe's Solution of the Heisenberg Ferromagnetic Linear*

Chain, Phys. Rev. Lett. **85**, 2813 (2000), doi:10.1103/PhysRevLett.85.2813.

[75] T. Bargheer, N. Beisert and N. Gromov, *Quantum stability for the Heisenberg ferromagnet*, New J. Phys. **10**(10), 103023 (2008), doi:10.1088/1367-2630/10/10/103023.

[76] F. C. Alcaraz, S. R. Salinas and W. F. Wreszinski, *Anisotropic ferromagnetic quantum domains*, Phys. Rev. Lett. **75**, 930 (1995), doi:10.1103/PhysRevLett.75.930.

[77] T. Koma and B. Nachtergaele, *The Spectral Gap of the Ferromagnetic XXZ Chain*, Lett. Math. Phys. **40**(1), 1 (1997), doi:10.1023/a:1007351803403.

[78] R. Dijkgraaf, D. Orlando and S. Reffert, *Quantum crystals and spin chains*, Nucl. Phys. B. **811**(3), 463 (2009), doi:10.1016/j.nuclphysb.2008.11.027.

[79] R. Dijkgraaf, D. Orlando and S. Reffert, *Relating field theories via stochastic quantization*, Nucl. Phys. B. **824**(3), 365 (2010), doi:10.1016/j.nuclphysb.2009.07.018.

[80] J.-M. Stéphan, *Return probability after a quench from a domain wall initial state in the spin-1/2 XXZ chain*, J. Stat. Mech. **2017**(10), 103108 (2017), doi:10.1088/1742-5468/aa8c19.

[81] Prosen, Tomaž and Žunkovič, Bojan, *Macroscopic diffusive transport in a microscopically integrable hamiltonian system*, Phys. Rev. Lett. **111**, 040602 (2013), doi:10.1103/PhysRevLett.111.040602.

[82] E. Ilievski and T. Prosen, *Thermodyamic Bounds on Drude Weights in Terms of Almost-conserved Quantities*, Commun. Math. Phys. **318**(3), 809 (2012), doi:10.1007/s00220-012-1599-4.

[83] B. Sutherland, *A Brief History of the Quantum Soliton with New Results on the Quantization of the Toda Lattice*, Rocky Mt. J. Math. **8**(1/2), 413 (1978).

[84] B. S. Shastry and A. Dhar, *Solution of a generalized Stieltjes problem*, J. Phys. A **34**(31), 6197 (2001), doi:10.1088/0305-4470/34/31/313.

[85] N. Beisert, A. A. Tseytlin and K. Zarembo, *Matching quantum strings to quantum spins: One-loop vs. finite-size corrections*, Nucl. Phys. B. **715**(1-2), 190 (2005), doi:10.1016/j.nuclphysb.2005.03.030.

[86] N. Beisert, M. Staudacher, J. A. Minahan and K. Zarembo, *Stringing spins and spinning strings*, J. High Energy Phys. **2003**(09), 1 (2003), doi:10.1088/1126-6708/2003/09/010.

[87] M. G. Forest and J.-E. Lee, *Geometry and Modulation Theory for the Periodic Nonlinear Schrodinger Equation*, In C. Dafermos, J. L. Ericksen, D. Kinderlehrer and M. Slemrod, eds., *Oscillation Theory, Computation, and Methods of Compensated Compactness*, pp. 35–69. Springer New York, New York, NY, ISBN 978-1-4613-8689-6 (1986).

[88] E. Brézin and V. Kazakov, *Universality of Correlations of Levels with Discrete Statistics*, Commun. Math. Phys. **214**(1), 233 (2000), doi:10.1007/s002200000259.

[89] D. J. Gross and E. Witten, *Possible third-order phase transition in the large-N lattice gauge theory*, Phys. Rev. D **21**, 446 (1980), doi:10.1103/PhysRevD.21.446.

[90] S. R. Wadia, $N = \infty$ *phase transition in a class of exactly soluble model lattice gauge theories*, Phys. Lett. B **93**(4), 403 (1980), doi:10.1016/0370-2693(80)90353-6.

[91] M. R. Douglas and V. A. Kazakov, *Large N phase transition in continuum QCD2*, Phys. Lett. B **319**(1-3), 219 (1993), doi:10.1016/0370-2693(93)90806-s.

[92] P. Zinn-Justin, *Six-vertex model with domain wall boundary conditions and one-matrix model*, Phys. Rev. E **62**, 3411 (2000), doi:10.1103/PhysRevE.62.3411.

[93] F. Colomo and A. G. Pronko, *Third-order phase transition in random tilings*, Phys. Rev. E **88**, 042125 (2013), doi:10.1103/PhysRevE.88.042125.

[94] D. Flassig, A. Franca and A. Pritzel, *Large-N ground state of the Lieb-Liniger model and Yang-Mills theory on a two-sphere*, Phys. Rev. A **93**, 013627 (2016), doi:10.1103/PhysRevA.93.013627.

[95] L. Piroli and E. Vernier, *Quasi-local conserved charges and spin transport in spin-1 integrable chains*, J. Stat. Mech. **2016**(5), 053106 (2016), doi:10.1088/1742-5468/2016/05/053106.

[96] N. Gromov, A. Sever and P. Vieira, *Tailoring three-point functions and integrability III. Classical tunneling*, J. High Energy Phys. **2012**(7) (2012), doi:10.1007/jhep07(2012)044.

[97] G. Misguich, N. Pavloff and V. Pasquier, *Domain wall problem in the quantum XXZ chain and semiclassical behavior close to the isotropic point*, SciPost Phys. **7**, 25 (2019), doi:10.21468/SciPostPhys.7.2.025.

[98] R. Hagemans and J.-S. Caux, *Deformed strings in the Heisenberg model*, J. Phys. A **40**(49), 14605 (2007), doi:10.1088/1751-8113/40/49/001.

[99] C. Marboe and D. Volin, *Fast analytic solver of rational Bethe equations*, J. Phys. A **50**(20), 204002 (2017), doi:10.1088/1751-8121/aa6b88.

[100] I. Kostov, *Classical Limit of the Three-Point Function of $N = 4$ Supersymmetric Yang-Mills Theory from Integrability*, Phys. Rev. Lett. **108**, 261604 (2012), doi:10.1103/PhysRevLett.108.261604.

[101] I. Kostov, *Three-point function of semiclassical states at weak coupling*, J. Phys. A **45**(49), 494018 (2012), doi:10.1088/1751-8113/45/49/494018.

[102] Y. Jiang and J. Brunekreef, *On the semi-classical limit of scalar products of the XXZ spin chain*, J. High Energy Phys. **2017**(3) (2017), doi:10.1007/jhep03(2017)012.

[103] C. Babenko, *Semiclassical expansion of the Bethe scalar products in the XXZ spin chain*, arXiv preprint arXiv:1703.01123 (2017).

[104] R. Siddharthan, *Singularities in the Bethe solution of the XXX and XXZ Heisenberg spin chains*, arXiv preprint arXiv:cond-mat/9804210 (1998).

[105] K. Fabricius and B. M. McCoy, *Bethe's Equation Is Incomplete for the XXZ Model at Roots of Unity*, J. Stat. Phys. **103**, 647 (2001), doi:10.1023/A:1010380116927.

[106] R. J. Baxter, *Completeness of the Bethe Ansatz for the Six and Eight-Vertex Models*, J. Stat. Phys. **108**, 1 (2002), doi:10.1023/A:1015437118218.

[107] T. Deguchi, K. Fabricius and B. M. McCoy, *The sl2 Loop Algebra Symmetry of the Six-Vertex Model at Roots of Unity*, J. Stat. Phys. **102**, 701 (2001), doi:10.1023/A:1004894701900.

[108] K. Fabricius and B. M. McCoy, *Completing Bethe's Equations at Roots of Unity*, J. Stat. Phys. **104**, 573 (2001), doi:10.1023/A:1010372504158.

[109] R. Baxter, *Eight-vertex model in lattice statistics and one-dimensional anisotropic heisenberg chain. III. Eigenvectors of the transfer matrix and hamiltonian*, Ann. Phys. (N. Y.) **76**(1), 48 (1973), doi:10.1016/0003-4916(73)90441-7.

[110] T. Prosen and E. Ilievski, *Families of Quasilocal Conservation Laws and Quantum Spin Transport*, Phys. Rev. Lett. **111**, 057203 (2013), doi:10.1103/PhysRevLett.111.057203.

[111] R. G. Pereira, V. Pasquier, J. Sirker and I. Affleck, *Exactly conserved quasilocal operators for the XXZ spin chain*, J. Stat. Mech. **2014**(9), P09037 (2014), doi:10.1088/1742-5468/2014/09/p09037.

[112] I. Krichever, O. Lipan, P. Wiegmann and A. Zabrodin, *Quantum Integrable Models and Discrete Classical Hirota Equations*, Commun. Math. Phys. **188**(2), 267 (1997), doi:10.1007/s002200050165.

[113] P. Wiegmann, *Bethe Ansatz and Classical Hirota Equation*, Int. J. Mod. Phys. B **11**(01n02), 75 (1997), doi:10.1142/s0217979297000101.

[114] R. Baxter, *Eight-vertex model in lattice statistics and one-dimensional anisotropic heisenberg chain. I. Some fundamental eigenvectors*, Ann. Phys. (N. Y.) **76**(1), 1 (1973), doi:10.1016/0003-4916(73)90439-9.

[115] R. Baxter, *Eight-vertex model in lattice statistics and one-dimensional anisotropic heisenberg chain. II. Equivalence to a generalized ice-type lattice model*, Ann. Phys. (N. Y.) **76**(1), 25 (1973), doi:10.1016/0003-4916(73)90440-5.

[116] A. Lazarescu and V. Pasquier, *Bethe ansatz and Q-operator for the open ASEP*, J. Phys. A **47**(29), 295202 (2014), doi:10.1088/1751-8113/47/29/295202.

[117] K. Fabricius and B. M. McCoy, *Evaluation parameters and Bethe roots for the six vertex model at roots of unity*, arXiv preprint arXiv:cond-mat/0108057 (2001).

[118] C. Korff, *Auxiliary matrices for the six-vertex model at $q^N = 1$: II. Bethe roots, complete strings and the Drinfeld polynomial*, J. Phys. A **37**(2), 385 (2003), doi:10.1088/0305-4470/37/2/009.

[119] A. De Luca, M. Collura and J. De Nardis, *Nonequilibrium spin transport in integrable spin chains: Persistent currents and emergence of magnetic domains*, Phys. Rev. B **96**, 020403 (2017), doi:10.1103/PhysRevB.96.020403.

[120] O. Babelon, K. K. Kozlowski and V. Pasquier, *Baxter Operator and Baxter Equation for q-Toda and Toda$_2$ Chains*, Rev. Math. Phys. **30**(06), 1840003 (2018), doi:10.1142/s0129055x18400032.

[121] D. Chicherin, S. Derkachov, D. Karakhanyan and R. Kirschner, *Baxter operators with deformed symmetry*, Nucl. Phys. B. **868**(3), 652 (2013), doi:10.1016/j.nuclphysb.2012.12.002.

[122] P. P. Kulish, N. Y. Reshetikhin and E. K. Sklyanin, *Yang-Baxter equation and representation theory: I*, Lett. Math. Phys. **5**(5), 393 (1981), doi:10.1007/bf02285311.

[123] A. Klümper and P. A. Pearce, *Conformal weights of RSOS lattice models and their fusion hierarchies*, Physica A **183**(3), 304 (1992), doi:10.1016/0378-4371(92)90149-k.

[124] A. Kuniba, T. Nakanishi and J. Suzuki, *T-systems and Y-systems in integrable systems*, J. Phys. A **44**(10), 103001 (2011), doi:10.1088/1751-8113/44/10/103001.

[125] G. P. Pronko and Y. G. Stroganov, *Bethe equations on the 'wrong side of the equator'*, J. Phys. A **32**(12), 2333 (1999), doi:10.1088/0305-4470/32/12/007.

[126] Z. Bajnok, E. Granet, J. L. Jacobsen and R. I. Nepomechie, *On generalized Q-systems*, J. High Energy Phys. **2020**(3), 177 (2020), doi:10.1007/jhep03(2020)177.

[127] E. Vernier, E. O'Brien and P. Fendley, *Onsager symmetries in $U(1)$ -invariant clock models*, J. Stat. Mech. **2019**(4), 043107 (2019), doi:10.1088/1742-5468/ab11c0.

[128] C. Korff, *Auxiliary matrices on both sides of the equator*, J. Phys. A **38**(1), 47 (2004), doi:10.1088/0305-4470/38/1/003.

[129] A. V. Razumov and Y. G. Stroganov, *Spin chains and combinatorics*, J. Phys. A **34**(14), 3185 (2001), doi:10.1088/0305-4470/34/14/322.

[130] L. Cantini and A. Sportiello, *Proof of the Razumov-Stroganov conjecture*, J. Comb. Theory Ser. A. **118**(5), 1549 (2011), doi:10.1016/j.jcta.2011.01.007.

[131] P. Fendley, K. Schoutens and J. de Boer, *Lattice Models with $\mathcal{N} = 2$ Supersymmetry*, Phys. Rev. Lett. **90**, 120402 (2003), doi:10.1103/PhysRevLett.90.120402.

[132] P. Fendley, B. Nienhuis and K. Schoutens, *Lattice fermion models with supersymmetry*, J. Phys. A **36**(50), 12399 (2003), doi:10.1088/0305-4470/36/50/004.

[133] L. Zadnik, M. Medenjak and T. Prosen, *Quasilocal conservation laws from semicyclic irreducible representations of $U_q(\mathfrak{sl}_2)$in XXZ spin-1/2 chains*, Nucl. Phys. B **902**, 339 (2016), doi:10.1016/j.nuclphysb.2015.11.023.

[134] M. Takahashi, *Thermodynamics of One-Dimensional Solvable Models*, Cambridge University Press (1999).

[135] E. Ilievski, E. Quinn, J. De Nardis and M. Brockmann, *String-charge duality in integrable lattice models*, J. Stat. Mech. **2016**(6), 063101 (2016), doi:10.1088/1742-5468/2016/06/063101.

[136] E. Ilievski, E. Quinn and J.-S. Caux, *From interacting particles to equilibrium statistical ensembles*, Phys. Rev. B **95**, 115128 (2017), doi:10.1103/PhysRevB.95.115128.

[137] L. Onsager, *Crystal statistics. i. a two-dimensional model with an order-disorder transition*, Phys. Rev. **65**, 117 (1944), doi:10.1103/PhysRev.65.117.

[138] S. Howes, L. P. Kadanoff and M. Den Nijs, *Quantum model for commensurate-incommensurate transitions*, Nucl. Phys. B. **215**(2), 169 (1983), doi:10.1016/0550-3213(83)90212-2.

[139] G. von Gehlen and V. Rittenberg, *z_n-symmetric quantum chains with an infinite set of conserved charges and z_n zero modes*, Nucl. Phys. B. **257**, 351 (1985), doi:10.1016/0550-3213(85)90350-5.

[140] R. J. Baxter, J. H. H. Perk and H. Au-Yang, *New solutions of the star-triangle relations for the chiral potts model*, Phys. Lett. A **128**(3-4), 138 (1988), doi:10.1016/0375-9601(88)90896-1.

[141] H. Au-Yang, B. M. McCoy, J. H. H. Perk and S. Tang, *Solvable Models in Statistical Mechanics and Riemann Surfaces of Genus Greater than One*, In *Algebraic Analysis*, pp. 29–39. Elsevier, doi:10.1016/b978-0-12-400465-8.50014-6 (1988).

[142] J. H. H. Perk, *The early history of the integrable chiral potts model and the odd-even problem*, J. Phys. A **49**(15), 153001 (2016), doi: 10.1088/1751-8113/49/15/153001.

[143] H. A. Kramers and G. H. Wannier, *Statistics of the two-dimensional ferromagnet. part i*, Phys. Rev. **60**, 252 (1941), doi:10.1103/ PhysRev.60.252.

[144] L. Dolan and M. Grady, *Conserved charges from self-duality*, Phys. Rev. D **25**, 1587 (1982), doi:10.1103/PhysRevD.25.1587.

[145] Jacques H. H. Perk, *Star-triangle equations, quantum Lax pairs, and higher genus curves*, In *Proceedings of Symposia in Pure Mathematics* (1989).

[146] B. Davies, *Onsager's algebra and superintegrability*, J. Phys. A **23**(12), 2245 (1990), doi:10.1088/0305-4470/23/12/010.

[147] E. Date and S. Roan, *The algebraic structure of the Onsager algebra*, Czechoslovak J. Phys. **50**, 37 (2000), doi:10.1023/A:1022812728907.

[148] E. Date and S. Roan, *The structure of quotients of the Onsager algebra by closed ideals*, J. Phys. A **33**(16), 3275 (2000), doi:10. 1088/0305-4470/33/16/316.

[149] J. H. H. Perk, *Onsager algebra and cluster XY-models in a transverse magnetic field*, arXiv preprint arXiv:1710.03384 (2017).

[150] C. El-Chaâr, *The Onsager algebra*, arXiv preprint arXiv:1205.5989 (2012).

[151] O. Lychkovskiy, *Closed hierarchy of Heisenberg equations in integrable models with Onsager algebra*, arXiv preprint arXiv:2012.00388 (2020).

[152] N. Shibata, N. Yoshioka and H. Katsura, *Onsager's scars in disordered spin chains*, Phys. Rev. Lett. **124**, 180604 (2020), doi: 10.1103/PhysRevLett.124.180604.

[153] R. Orbach, *Linear Antiferromagnetic Chain with Anisotropic Coupling*, Phys. Rev. **112**, 309 (1958), doi:10.1103/PhysRev.112.309.

[154] E. K. Sklyanin, *Separation of Variables: New Trends*, Prog. Theor. Phys. Supp. **118**, 35–60 (1995), doi:10.1143/PTPS.118.35.

[155] A. Cavaglià, N. Gromov and F. Levkovich-Maslyuk, *Separation of variables and scalar products at any rank*, J. High Energy Phys. **2019**(9) (2019), doi:10.1007/jhep09(2019)052.

[156] N. Gromov, F. Levkovich-Maslyuk, P. Ryan and D. Volin, *Dual separated variables and scalar products*, Phys. Lett. B **806**, 135494 (2020), doi:10.1016/j.physletb.2020.135494.

[157] M. Medenjak, B. Buča and D. Jaksch, *Isolated heisenberg magnet as a quantum time crystal*, Phys. Rev. B **102**, 041117 (2020), doi:10.1103/PhysRevB.102.041117.

[158] M. Medenjak, T. Prosen and L. Zadnik, *Rigorous bounds on dynamical response functions and time-translation symmetry breaking*, SciPost Phys. **9**, 3 (2020), doi:10.21468/SciPostPhys.9.1.003.

[159] R. Hernández, E. López, Á. Periáñez and G. Sierra, *Finite size effects in ferromagnetic spin chains and quantum corrections to classical strings*, J. High Energy Phys. **2005**(06), 011 (2005), doi:10.1088/1126-6708/2005/06/011.

[160] N. I. Akhiezer, *Elements of the Theory of Elliptic Functions*, American Mathematical Society (1990).

[161] H. McKean and V. Moll, *Elliptic Curves: Function Theory, Geometry, Arithmetic*, Cambridge University Press, doi:10.1017/CBO9781139174879 (1997).

[162] V. Pasquier and H. Saleur, *Common structures between finite systems and conformal field theories through quantum groups*, Nucl. Phys. B. **330**(2-3), 523 (1990), doi:10.1016/0550-3213(90)90122-t.

[163] M. Jimbo, *Topics from representations of $U_q(\mathfrak{g})$ – an introductory guide to physicists*, pp. 1–61, Nankai lectures on mathematical physics. World Scientific, Ge, M. L. (Ed.) (1992).

Summary

In recent years, the advance of ultracold atom experiments boosted theoretical endeavours on the quantum many-body systems out of equilibrium. However, due to the large number of degrees of freedom and the interacting nature, there are few exact results on the non-equilibrium properties of quantum many-body systems. With the aid of classical and quantum integrability, we are able to obtain several exact results that are presented in this thesis.

The physical systems that we consider are integrable models. Due to the exact solvability, we have a plethora of mathematically accurate techniques that apply to integrable models. We use those techniques to study a specific type of non-equilibrium scenario, quantum quench. Quantum quench is an adequate theoretical approximation of many ultracold atom experiments. For example, we study the transport properties of an inhomogeneous quench, the semi-classical limit of quantum eigenstates and the full spectra of quantum integrable lattice models.

Domain-wall quench of classical Landau–Lifshitz model

We study the inhomogeneous quench problem of a domain-wall initial profile in classical Landau–Lifshitz model, the semi-classical (long-wavelength) limit of quantum spin-1/2 XXZ model with weak anisotropy. Using classical inverse scattering method, we find three different regimes of spin transport: ballistic transport in easy-plane regime, solved by hydrodynamic approximation; superdiffusion in isotropic limit; domain-wall

frozen phenomenon in easy-axis regime. Comparing to the results in the quantum counterpart, we summarise the classical-quantum correspondence of spin transport for domain-wall quench.

Semi-classical quantisation of finite-gap solutions

In order to shed light on the relation between the classical and quantum domain-wall frozen phenomena, we study the semi-classical quantisation of finite-gap solutions in classical Landau–Lifshitz model. In the classical regime, a bion solution causes the domain-wall frozen phenomenon, becoming a static kink in the soliton limit. We quantise the classical bion solution to obtain Bethe root distribution of the quantum semi-classical eigenstate, which is responsible for the quantum domain-wall frozen phenomenon. We construct the semi-classical quantisation theory, and it leads to a more quantitative description of the classical-quantum correspondence.

Full spectrum of quantum XXZ model at root of unity

In order to study the quantum quench problem in XXZ model, we would like to investigate its full spectrum. Full spectrum gives us access to quantities such as correlation functions and entanglement entropy. We are able to obtain the full spectrum by constructing Baxter's Q operator, which contains the information of every eigenstate. Using the properties of transfer matrices, we obtain the full spectrum as eigenvalues of Q operator in XXZ model at root of unity. From the full spectrum, it is elucidated the exponential degeneracies. We further use the full spectrum to explain the results of out-of-equilibrium properties in the thermodynamic limit.

Hidden Onsager algebra symmetry in XXZ model at root of unity

The full spectrum of XXZ model at root of unity also reveals a possible hidden Onsager algebra symmetry, motivated by known results for XX model, i.e. XXZ model with anisotropic parameter $\Delta = 0$. We conjecture the relations between the Onsager algebra and the (quasi-)local conserved charges derived from different transfer matrices.

Samenvatting

Gedurende de afgelopen jaren heeft de vooruitgang van experimenten met ultrakoude atomen veel theoretische werken op het gebied van kwantum veel-deeltjes-systemen geïnspireerd. Door het grote aantal vrijheidsgraden en de van nature aanwezige interacties in deze systemen zijn er echter weinig exacte resultaten beschikbaar voor de eigenschappen van deze systemen buiten evenwicht. Met behulp van klassieke- en kwantum integreerbaarheid zijn wij er in geslaagd enkele exacte resultaten te behalen die in deze scriptie gepresenteerd worden.

De fysische systemen die we beschouwen zijn integreerbare modellen. Door de exacte oplosbaarheid is er een veelvoud van wiskundige technieken die van toepassing zijn op integreerbare modellen. Wij gebruiken deze technieken om een specifiek scenario te beschouwen waar het kwantumsysteem niet in evenwicht is: een kwantum *quench*. Een kwantum *quench* is een adequate theoretische benadering van veel experimenten met ultrakoude atomen. Wij bestuderen bijvoorbeeld de transporteigenschappen van een inhomogene *quench*, de semi-klassieke limiet van kwantum eigentoestanden en het volledige spectrum van kwantum integreerbare roostermodellen.

Domeinmuur *quench* van het klassieke Landau-Lifschitz model

We bestuderen de inhomogene *quench* van het klassieke Landau-Lifschitz model, de semi-klassieke (lange golflengte) limiet van het kwantum spin-1/2 XXZ model met zwakke anisotropie, met een domeinmuur in de be-

gintoestand. Door gebruik te maken van de klassieke inverse verstrooiingsmethode vinden we drie verschillende regimes van spintransport: ballistisch transport in het *easy-plane* regime, opgelost door middel van een hydrodynamische benadering; superdiffusie in de isotropische limiet; het domeinmuur bevroren fenomeen in het *easy-axis* regime. Door de resultaten te vergelijken met die voor het kwantum equivalent, vatten we de klassiek-kwantum correspondentie van het spintransport voor de domeinmuur *quench* samen.

Semi-klassieke kwantisatie van *finite-gap* oplossingen

Om licht te werpen op de relatie tussen het klassieke en het kwantum domeinmuur bevroren fenomeen, bestuderen wij de semi-klassieke kwantisatie van van *finite-gap* oplossingen in het klassieke Landau-Lifschitz model. In het klassieke regime veroorzaakt een bion-oplossing het bevroren domeinmuur fenomeen en wordt een statische kink in de solitonlimiet. Wij kwantiseren de klassieke bion-oplossing om een Bethe wortelverdeling van de kwantum semi-klassieke eigentoestand te verkrijgen, die verantwoordelijk is voor het kwantum bevroren domeinmuur fenomeen. Wij construeren de semi-klassieke kwantisatietheorie wat leidt tot een meer kwantitatieve beschrijving van de klassiek-kwantum correspondentie.

Het volledige spectrum van het XXZ-model bij een eenheidswortel

Om het kwantum *quench* probleem in het XXZ-model te bestuderen willen we het volledige spectrum van XXZ onderzoeken. Het volledige spectrum geeft ons toegang tot grootheden zoals de correlatiefuncties en de verstrengelingsentropie. Wij zijn in staat het volledige spectrum te verkrijgen door Baxter's Q-operator te construeren, die de informatie over elke eigentoestand bevat. Door gebruik te maken van de eigenschappen van *transfer* matrices verkrijgen we het volledige spectrum als eigenwaardes van de Q-operator in het XXZ-model bij een eenheidswortel. Het volledige spectrum geeft inzicht in de oorsprong van de exponentiële hoeveelheid ontaardingen. Verder gebruiken wij het volledige spectrum om resultaten voor eigenschappen van het systeem buiten evenwicht te verklaren in de thermodynamische limiet.

Verborgen Onsager algebra symmetrie in het XXZ-model bij een eenheidswortel

Het volledige spectrum van het XXZ-model bij een eenheidswortel onthult ook een mogelijk verborgen Onsager algebra symmetrie, gemotiveerd door bekende resultaten voor het XX-model. d.w.z. het XXZ-model waar de anisotropie gelijk is aan 0. Wij formuleren een vermoeden voor de relaties tussen de Onsager algebra en de quasi-lokale behouden grootheden afgeleid van verschillende *transfer* matrices.

Acknowledgments

First of all, I would like to thank my PhD supervisor, Prof. Jean-Sébastien Caux, for offering me the opportunity to pursue my PhD study in your group (the "Gang") and giving me the freedom to work on subjects that interest me. J-S, your taste on various subjects around quantum integrability and your persistence on pursuing the mathematical exactness have influenced me enormously. I would like to thank Prof. Kareljan Schoutens for being my co-supervisor and having numerous discussions on physics, which always provide me with new perspectives. I would like to thank Prof. Benjamin Doyon, Prof. Paul Fendley, Prof. Japser Stokman, Prof. Jan de Boer, Dr. Philippe Corboz Dr. Vladimir Gritsev, and Dr. Enej Ilievski for agreeing to be in my committee. Ben, thank you very much for helping me with the fellowship applications. Paul, thanks a lot for the discussions which are forged into my recent research. I have to admit that I enjoyed almost every paper of yours.

I would like to thank my collaborators who help me enormously and tolerate me for being stubborn sometimes. Sasha and Enej, I would like to thank both of you for helping me at the beginning of my PhD, and showing me how to be a researcher. I cherish our endless discussions back in the days and I hope that we could keep on working together in the future, despite being further away. Jules and Vincent, thank you very much for working on the nice project together, which I am proud of. I have benefited a lot from the mathematical rigour that both of you have shown me. I would like to thank other collaborators of mine,

Eric, Lenart, Marko and Neil, for teaching me many different aspects of theoretical physics.

During the four years of my PhD, I have attended several schools, workshops and conferences. Especially, I would like to thank the organisers of École de Physique des Houches, GGI in Firenze, IHP in Paris and IIP in Natal, where I have met many good friends and colleagues. I would like to thank all of them. Another "big" event for me personally is the Student Workshop on Integrability. I am honoured to be the best speaker of the second edition and I hope it could continue to bring researchers in integrability together. Among the organisers, I own special thanks to Giuseppe Mussardo, who is always the polymath I look up to.

I would like to thank the J-S "Gang" members throughout my PhD: Alvi, Vincenzo, Sasha, Neil, Enej, Eoin, Bart (dK), Sergio, Rebekka and Daniel. Special thanks to Alvi for the physics discussions and gym time. Many thanks to Bart for helping me translate the summary into Dutch. And Eyzo, thanks for teaching me fusion and hanging around during the pandemics. I would like to thank the CMT group: Kareljan, Vladimir, Jasper, Philippe, Jiří, Bart (vV), Schelto, Boris, Wouter, Jans, Ana, Corentin, Natalia, Patrick, and Ward. Big thanks to Jiří who is always open for various discussions. I have made several friends in the big family of IoP: Dr. Barbé :), Sheng, Sheng, Francesca, Rodrigo, Carla, Beatrix, Chiara, Antonio, Greg, Horng-Sheng and Bahman. Thank you all! And Dr. Barbé, thanks for numerous intriguing evenings at Foeders. I would like to thank the supporting staff too, Joost, Anne-Marieke, Jiřina, Astrid and Klaartje.

Last but not the least, I would like to thank my friends and family in China and Germany. Without your help, I would have never achieved so much. My parents and grandparents are always supportive for me to study abroad for so long. My most sincere thanks to my family, who always loves me.

Amsterdam 2021, Yuan Miao